COMPARISON BETWEEN PAVEMENT MECHANISTIC-EMPIRICAL DESIGN APPROACHES FOR RUBBLIZED PAVEMENTS IN MICHIGAN

By

Faizan Ahmad Lali

A THESIS

Submitted to
Michigan State University
in partial fulfillment of the requirements
for the degree of

Civil Engineering - Master of Science

2023

ABSTRACT

The pavement mechanistic-empirical design (PMED) is a modern approach to designing new and rehabilitated pavements. MDOT uses the American Association of Highway and Transportation Officials (AASHTO) 1993 design methodology for rehabilitation pavement designs. MDOT designs hot mix asphalt (HMA) overlay over rubblized plain cement concrete (PCC) pavements as new flexible pavement, modeling rubblized PCC layer as an unbound aggregate base with a modulus of 70,000 psi. The PMED offers an alternative design option [HMA overlay over fractured jointed plain cement concrete (JPCP)] for rubblized pavement. This study analyzes the most optimum design approach and HMA input level for rubblized pavements in Michigan.

The study compared the predicted performance using global and locally calibrated models for new and overlay designs for rubblized pavements at all three hierarchical input levels. The global performance predictions at input Levels 1 and 3 showed negligible differences in new and overlay design options. Local calibration of new and overlay design at input Level 1 produced better results with minimum standard error of estimate (SEE) and bias. However, local calibration results at input Level 3, where Level 1 data is unavailable, are also acceptable.

The study evaluated the impact of local calibration on the new and overlay design by designing 11 pavement sections with variable traffic data. An overlay design resulted in 1.5-inch thinner pavements than AASHTO93 and 0.4-inch thinner than the new design using PMED. The difference between new and overlay designs is not significant based on available data. Therefore, a new design (MDOT's existing practice) using input Level 1 (if data are available) is recommended for rubblized pavement in Michigan. Finally, the study documented the sensitivity of the calibration coefficients using scaled sensitivity coefficient analysis and compared SSCs-based ranking with normalized sensitivity index (NSI) ranking.

I dedicate this thesis to my parents, beloved son, and wife, who have been my unwavering source of love, inspiration, and motivation. Thank you for being my constant pillars of strength and sharing in this journey's joys and challenge.

ACKNOWLEDGMENTS

First and foremost, I express my deepest gratitude to Allah, the Most Merciful and Most Compassionate, for His guidance, wisdom, and blessings that have sustained me throughout this academic journey.

I am deeply thankful to my thesis advisor, Dr. Syed Waqar Haider, for his unwavering support, guidance, and invaluable mentorship throughout this journey. His expertise, patience, and encouragement have been instrumental in shaping the direction of this research. I am thankful for his time and support in writing this thesis.

I am also indebted to the committee members, Dr. Karim Chatti and Dr. M. Emin Kutay, whose collective wisdom and academic insights enriched my understanding of the subject matter. I am thankful for the lessons they taught me during my graduate studies, who helped me in my research. I always found them helpful and encouraging.

I thank my family for their enduring encouragement and love, which motivated me to persevere during challenging times.

Furthermore, I am also incredibly thankful to all of my friends for their unwavering support and companionship throughout this academic endeavor.

TABLE OF CONTENTS

CHAPTER 1 INTRODUCTION

The American Association of State Highway and Transportation Officials (AASHTO) Guide for Design of Pavement Structures (AASHTO, 1993) and the related DARWin software have been used by most state highway agencies (SHAs) to design new and rehabilitated pavement structures. This design method is based on the empirical relations developed from the American Association of State Highway Officials (AASHO) Road Test conducted in Ottawa, Illinois, in the 1950s (1). Many SHAs still use the AASHTO 93 guide to design the pavement structure; this guide still holds the state of the practice design procedures and some material inputs; however, it lacks the principles of engineering mechanics. The AASHTO Joint Task Force on Pavements (JTFP) developed Mechanistic-Empirical Pavement Design Guide (PMED) and its associated software Pavement-ME under National Cooperative Highway Research Program (NHCRP) project 1-37A in 2004 to incorporate mechanistic design principles in pavement analysis and design (2). The PMED takes a significant number of inputs compared to the AASHTO 93 design approach, and pavement performance is assessed based on principles of engineering mechanics (3). The PMED uses a mechanistic approach to estimate pavement's principle responses (stress, strain, and deflections) based on material inputs, i.e., traffic, climate, and martial inputs; it computes incremental damage over time to predict surface distress through transfer functions (4). The PMED performance prediction models were calibrated initially using relevant data inputs extracted from the National Long Term Pavement Performance (LTPP) database, which warrants re-calibration of these models according to local state conditions and inputs (5).

Many SHAs across the United States have implemented or are in the process of implementing the PMED in pavement design and analysis. According to a report about Pavement-ME User Group meetings, 18 SHAs have implemented and are working on further reviews, and 24 SHAs plan to implement PMED in pavement design (6). Most of the SHAs implemented PMED to design new flexible and rigid pavements; however, no comprehensive efforts have been reported for rehabilitation pavement design; either the same coefficients of the new design are used for rehabilitation design, or most of the rehabilitated pavements have been modeled as new or reconstructed pavements in PMED. The PMED analysis and design procedure has been implemented in Michigan to design new pavements. Several studies were

performed in the recent past to characterize climate, traffic, material properties, and calibration of the performance models to address the local conditions, materials, and construction practices in the Pavement-ME procedure. Moreover, the Michigan Department of Transportation (MDOT) recently started a research project collaborating with the Michigan State University (MSU) research team to implement PMED for rehabilitation pavement design.

1.1 Background

The empirical-based AASHTO designed equations were improved over time with several updated publications of AASHTO design guides, with AASHTO 98 being the most recent updated design guide. All these guides have served as vital tools for pavement design. However, significant weaknesses observed in the plan were over-designed thicknesses or premature failures of the pavements. The NHCRP program by the National Academy of Science developed mechanistic-empirical (M-E) based design for new and rehabilitated flexible and rigid pavements incorporating local climate, material inputs, and real-time traffic distribution by considering axle load spectra (2). The first comprehensive M-E design guide was developed under project 1-40. Since its inception, the M-E design has undergone many improvements (versions) to address the challenges and difficulties faced by the agencies implementing PMED for pavement designs. The AASHTO recently released the latest version, 3.0 of PMED; however, version 2.6.2.2 is used for this study. The significant aspects of the M-E design approach are:

a. Real-time characterization of pavement materials based on principles of mechanics.
b. Modeling temperature, moisture, and their interaction with the pavement material.
c. Simulated real-time traffic distribution based on axle load spectra and forecasted traffic growth. Mechanistic calculation of Pavement response due to traffic loading for various climatic conditions.
d. Characterization of time and climate-dependent material properties.
e. Incremental damage accumulates over time, and empirical relations are used to predict the development of surface distresses and their progression through transfer functions.
f. Various new and rehabilitated pavement designs achieve the desired performance criteria for a specific reliability level.

The distress and IRI prediction models of PMED were calibrated initially using data from hundreds of flexible, rigid, and composite in-service pavements across the US in the LTPP database under the Federal Highway Administration (FHWA) and other national databases, such as MnRoad. The reliability of performance prediction models depends on the accuracy of the transfer functions, which is achieved through calibration and subsequent validation with observed pavement condition data. A satisfactory correlation between measured and predicted performance indicators increases the viability, acceptance, and usage of the PMED procedures of pavement analysis and design.

The calibration is a mathematical method to minimize the difference between predicted performance and field-measured surface distresses and IRI. Cross-validation refers to a process that evaluates the performance of mathematical models to independent or global datasets (i.e., data that are not used for model development). As initial calibration of the performance prediction models was carried out based on the selected pavement sections across the US, these are referred to as "global" calibrated models. Since it does not reflect the local conditions of any specific state or location, NHCRP 1-40B provides the guidelines for local calibration of performance prediction models in new and rehabilitated pavements to accommodate the impacts due to these regional differences (7). The bias and standard error of estimates (S_e) are used for calibrating pavement performance prediction models. The S_e is a statistical measure used to assess the accuracy of the predictions made by a regression model. It measures the average deviation of the predicted values from field-measured values. The bias can be related to the accuracy and reliability of the estimating function or measurements. Simply put, it can be defined as the consistent tendency of an estimator to over-predict or under-predict the responses. Figure 1-1 shows the different combinations of bias and S_e.

The implementation of PMED in new and rehabilitation design poses practical challenges to SHAs, which include:

a. Complexity involved in PMED software.

b. Damage characterization of existing pavement layers.

c. Resource constraints on data collection techniques.

d. Identifying the most significant input variables.

e. Establishing data requirements and developing historical roadway conditions and management database for continuous calibration of the performance models

f. Calibrating the pavement performance prediction model considering the local traffic, weather, and material properties.

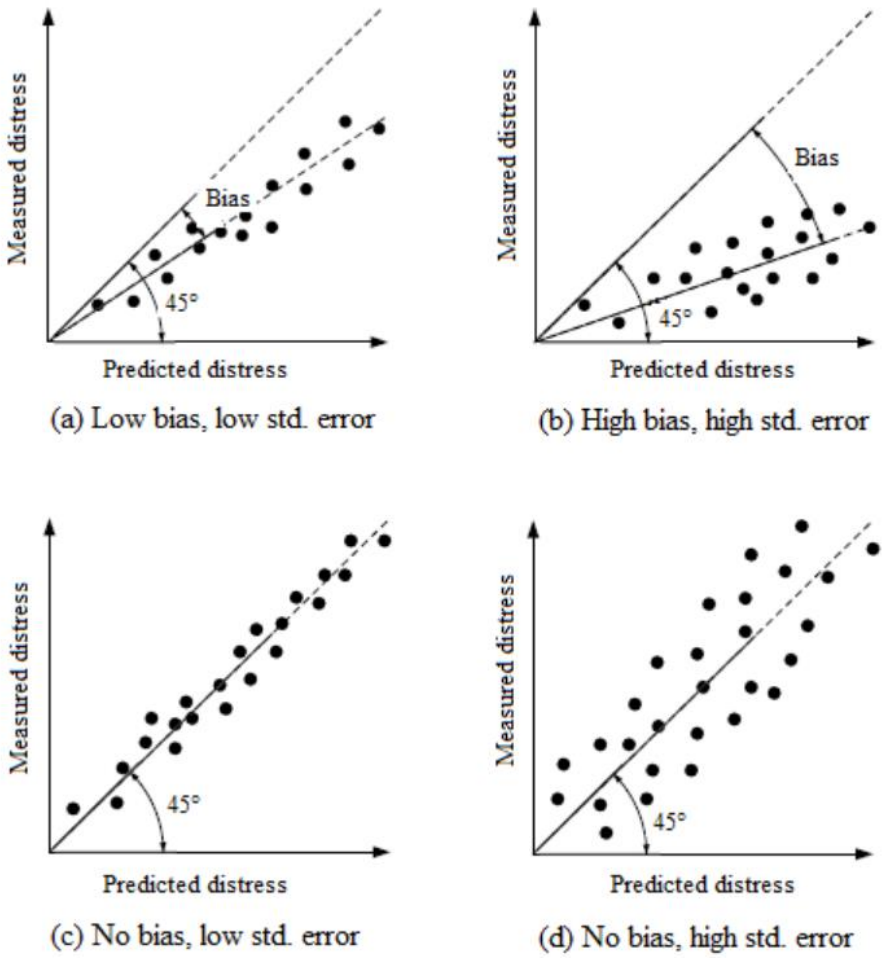

Figure 1-1: S_e and bias for calibration (5)

1.2 Problem Statement

Most older roads and highways in Michigan need rehabilitation and repair. The Michigan Department of Transportation (MDOT) uses the AASHTO 1993 Guide for the Design of Pavement Structures (AASHTO 1993) to design various structural rehabilitation treatments. The AASHTO 1993 method has proven to be an essential tool for several decades; however, its empirical approach limits its effectiveness as a modern pavement design method compared to the

new AASHTO Mechanistic-Empirical Pavement Design Guide (PMED). The PMED uses site-specific traffic, climate, material properties, and existing pavement surface conditions for analyzing the final design. While several design inputs are identical for both new and rehabilitation design processes, there are variations in how some inputs are selected for rehabilitation design. The material properties that characterize the existing pavement play a vital role in the PMED rehabilitation analysis and design process. MDOT is undergoing the full implementation of the PMED and its associated software. MDOT has implemented the PMED for new and reconstruction pavement designs for flexible and rigid pavements; however, the rehabilitation analysis and design process needs more careful evaluation for local adoption. The PMED rehabilitation pavement design is more complex and requires the characterization of existing materials and their thicknesses; however, MDOT records for older existing pavements may be incomplete or missing altogether. Furthermore, past projects included various types of hot mix asphalt (HMA) that are no longer used or have been adjusted (such as air voids or gradations requirements). Therefore, due to these added complexities, extensive investigations are needed to standardize or provide guidelines related to PMED rehabilitation design based on practically available records.

In a recent study by MDOT for the implementation of PMED for new and reconstructed pavements, the HMA overlay over rubblized PCC is analyzed as new flexible pavement. The rubblized layer is modeled as an unbonded aggregate base having a resilient modulus of 70,000 psi. This research aims to design an HMA overlay over rubblized PCC, an overlay design with a modeling option of HMA overlay over fractured JPCP. Figure 2 shows the disparities between both design approaches.

1.3 Research Objectives

The objectives of the study are:

a. Using the global model, compare and evaluate the impact of three hierarchical input levels of HMA mechanical properties (E*, G*, and creep compliance) on the performance predictions of rubblized pavement design approaches, i.e., new and overlay.

b. Recommend a suitable design approach and hierarchical input level for MDOT design practices after local calibration of the transfer function coefficients.

c. Sensitivity analysis of the transfer function coefficients over the entire range of sections and independent variables using scaled sensitivity coefficients (SSCs).

d. Compare SSCs-based ranking with NSI values from the literature.

1.4 Study Outline

Chapter 2 discusses and summarizes the review of several studies related to rehabilitated pavement design adopted by other SHAs. The national and local calibration efforts are discussed in this chapter, along with a comparison of calibration coefficients for different rehabilitation designs. It also covers the PMED performance prediction models used in the local calibration of HMA overlay over rubblized PCC. Chapter 3 covers the efforts to collect data and make it ready to be used in PMED for calibration. This chapter will briefly discuss data acquisition and compatibility with PMED, project selection criteria, review/ analysis of measured performance data, pavement cross-section information, traffic, construction materials, and climate inputs. Chapter 4 briefly discusses the concept of scaled sensitivity coefficients (SSCs) and its application to rank the transfer function coefficients based on SSCs ranking. Moreover, this chapter also covers the SSCs organizing comparison with literature-based normalized sensitivity index (NSI) values for new flexible pavement design only. Chapter 5 covers the different sampling techniques and their application in the local calibration of PMED performance prediction models. This chapter briefly explains the various sampling techniques, i.e., bootstrapping and maximum likelihood (MLE) for calibration of PMED models. Chapter 6 summarizes the results and analysis of the study. The comparison is drawn between new and overlay designs of rubblized pavements. This chapter reports the performance prediction results at three hierarchical input levels for HMA mechanical properties, i.e., E*, G*, and creep compliance. Further, the impact of local calibration on the design of rubblized pavement has been studied in this Chapter.

Finally, the conclusions and recommendations for future improvement in the modeling and calibration of HMA overlays over rubblized PCC are provided in Chapter 7.

CHAPTER 2 LITERATURE REVIEW

The Mechanistic-Empirical Pavement Design Guide (PMED) was developed under the National Cooperative Highway Research Program (NCHRP) Project 1-37A to provide a state-of-the-art pavement design tool to the highway community *(8)*. Many state agencies adopted or are implementing the PMED to design new or rehabilitated pavements, replacing entirely or partly the old empirical design approach from the AASHTO 1993 design guide. The PMED approach uses pavement mechanistic responses (stresses and strains) to compute damage accumulation based on various distress evolution mechanisms by considering axle load levels and climate variation. Subsequently, this damage is used to estimate field-observed pavement distresses through transfer functions for performance prediction.

The use of PMED models in pavement engineering has increased over the past few years. However, performance prediction models used in PMED software are designed for the general conditions and calibrated nationally, necessitating the local calibration of these models per locally available materials, traffic, and climatic conditions for any specific state. Since its inception, several state highway agencies (SHA) have implemented or are implementing the PMED. To date, 17 SHAs have implemented PMED as a primary design method, and 20 SHAs use PMED with other ways to design new asphalt and concrete pavements and overlays, respectively. With the advancement of calibration tools and techniques, these efforts have become more vigorous. Haider et al. (2018) used resampling methods (bootstrapping and repeated sampling) to calibrate transverse cracking and the International Roughness Index (IRI) in Michigan *(9)*. Tabesh and Sakhaeifar (2021) calibrated Oklahoma's bottom-up, top-down, rutting, transverse cracking, and IRI models using a narrow-down iterative approach to minimize the standard error *(10)*.

The MDOT has been using PMED software since 2014 in conjunction with the AASHTO 1993 method, allowing for a thickness deviation of ± 1 inch from the software for all new/reconstruction projects *(11)*. To reach this implementation stage of the PMED approach, MDOT has sponsored several research efforts in the past *(5, 11-17)*.

2.1 MDOT Existing Design Practices – AASHTO93

The MDOT is currently using the AASHTO 1993 design methodology for rehabilitation designs. AASHTO93 design approach yields the overlay thickness to improve the structural deficiency of

the existing pavement to sustain design traffic (1). Figure 2-1 represents the decrease in structural capacity (SC) and serviceability of any pavement type with increased load repetitions (N). The SC is expressed by structural number (SN) and PCC slab thickness (D) for flexible and rigid pavement, respectively. At initial serviceability (P1), the pavement has a structural capacity of SC_o and reaches SC_{eff} at acceptable serviceability (P2) due to load repetitions (N_p). Additional structural (SC_{OL}) is required as an overlay to upgrade the pavement's structural capacity to the serviceability conditions at the time of construction. Equation 2-1 represents the general overlay design equation.

$$(SC_{OL})^n = (SC_f)^n + (SC_{eff})^n \qquad (2\text{-}1)$$

where;

SC_{OL} = Additional structural capacity of the overlay; SC_{eff} = Existing structural capacity of the pavement; SC_f = Structural capacity of newly designed pavement for projected future overlay traffic N_f; n = constant; n=2 for unbonded rigid overlays over rigid; n=1 for all other pavement types.

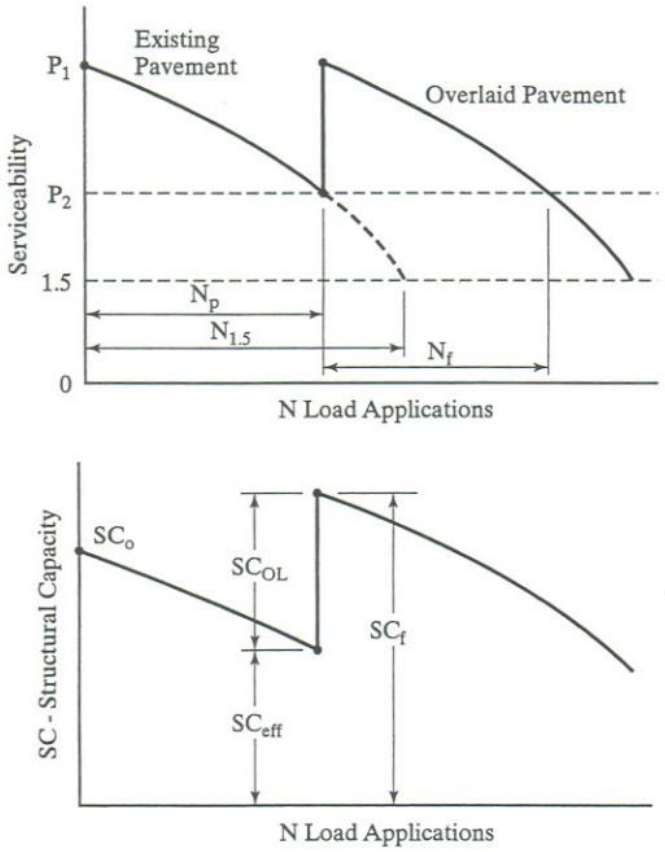

Figure 2-1: Effect of traffic on serviceability and structural capacity (4)

2.2 HMA Overlays - Effective Structural Capacity of Existing Pavement

In overlay design, it is vital to accurately evaluate the pavement's effective structural capacity (SNeff). Three methods are used to estimate $SN_{eff:}$ visual survey and material testing, non-destructive deflection testing, and remaining life from fatigue damage by traffic (1). MDOT uses DARWin software for overlay design, which operates based on the condition survey method to characterize existing layer damage and obtain the effective structural capacity of the existing HMA layer and the effective thickness of the existing concrete slab (4). The following paragraphs will explain the visual survey and materials testing method outlined by the AASHTO93 guide and the textbook "Pavement Analysis and Design" by Yang H. Haung (1).

2.2.1 Visual Survey and Materials Testing

A visual pavement survey includes a detailed review of pavement design, construction procedure, maintenance habits, identification of distress type, source, location, and severity of distress. Material testing demands a detailed testing protocol, including coring, to identify and verify causes of surface distress in the pavement. There are different approaches for flexible and rigid pavements to identify effective structural capacity and slab thickness, respectively (1). The following paras explain these approaches and the range of inputs MDOT uses for these design methodologies.

2.2.1.1 Flexible Pavements

The effective structural capacity of flexible pavements from the condition survey method can be obtained using Equation 2-2, which involves component analysis using a structural number equation for new pavement design (1).

$$SN_{eff} = a_1 D_1 + a_2 m_2 D_2 + a_3 m_3 D_3 \qquad (2\text{-}2)$$

where;

a_1, a_2, a_3 = Layer coefficients; depends upon type and amount of deterioration in pavement layers; m_1, m_2 = Drainage coefficients; D_1, D_2, D_3 = Corresponding layer thicknesses.

Over the years, MDOT developed specific standards and inputs for pavement design using AASHTO93. MDOT typically uses 15-20 years as the design life of the pavement overlays to calculate the number of equivalent single axle load (ESALs) repetitions, which is a crucial input for any pavement design (4). Tables 2-1 and 2-2 list the MDOT recommended values of layer coefficients and drainage coefficients, respectively, for flexible pavements; moreover, MDOT uses the following input values for all types of pavements.

a. Initial serviceability – 4.5
b. Terminal serviceability – 2.5
c. Reliability Level – 95%
d. Subgrade resilient modulus ranges from 3000 – 5000 psi.

Table 2-1: MDOT recommended drainage coefficients per layer

Layer	Drainage coefficient
HMA top and levelling course	1
HMA base course	1
ASCRL	1
Cement stabilized base	1.1
Asphalt/ emulsion stabilized base	1
Crushed & shaped HMA	1
Rubblized concrete	1
Aggregate base (open and dense)	1
Sand subbase	1
16-inches of open-graded drainage course	1.1
< 16-inches of open-graded drainage course	1 – 1.05
Existing HMA	1*
Existing aggregate base	1*
Existing sand subbase	1*

* Use drainage coefficient =1 for each base/subbase layer unless there is a known moisture problem.

Each pavement layer behaves differently under repeated loads over its design life. Elastic modulus is the check of layer stiffness and its resistance to elastic deformation and is related to the structural layer coefficient. Table 2-3 lists the recommended values of the elastic modulus of different layers by MDOT.

Table 2-2: MDOT recommended values of structural coefficients per layer

Layer	Structural coefficient
HMA top and levelling course	0.42
HMA base course	0.36
ASCRL	0.30
Cement stabilized base	0.26
Asphalt/ emulsion stabilized base	0.22
Crush and shaped HMA	0.20
Rubblized concrete	0.18
Dense-graded aggregate base	0.14
Open-graded drainage course	0.13
Sand subbase	0.10

Table 2-2 (cont'd)

Existing HMA**	Excellent condition – little or no alligator cracking and/ or low-severity transverse cracking	0.36
	Good condition • < 10% low-severity alligator cracking and/or • < 5% medium and high-severity transverse cracking	0.30
	Fair condition • 10% low-severity alligator cracking and/or • < 10% medium-severity alligator cracking and/ or • 5-10% medium and high severity transverse cracking	0.24
	Poor condition • 10% medium-severity alligator cracking and/or • < 10% high-severity alligator cracking and/or • > 10% medium and high severity transverse cracking	0.17
	Very poor condition • 10% high-severity alligator cracking and/or • > 10% high severity transverse cracking	0.12
Existing aggregate base	No evidence of pumping, degradation, or contamination by fines	0.13
	Evidence of pumping, degradation, or contamination by fines	0.06
Existing sand subbase	No evidence of pumping, degradation, or contamination by fines	0.09
	Evidence of pumping, degradation, or contamination by fines	0.04

** The existing HMA can be represented by multiple layers, but one layer is sufficient. The existing HMA structural coefficient should represent the material after milling or repair(s), (to be overlaid).

2.2.1.2 Rigid Pavements

MDOT construction practices for concrete pavements include JPCP reconstruction, HMA over existing concrete/ composite, HMA ASCRL over existing concrete/ composite, and standard concrete overlays (6 inches thick or more) over existing concrete/ composite pavements (4). Equation 2-3 is used to compute the effective thickness (D_{eff}) of the existing slab in overlay design (1).

$$D_{eff} = (F_{jc})(F_{dur})(F_{fat})(D) \quad (2\text{-}3)$$

where:

F_{jc} = Joints and crack adjustment factor.

F_{dur} = Durability adjustment factor.

F_{fat} = Fatigue damage adjustment factor.

D = Existing slab thickness.

MDOT recommends following generic values for concrete pavement design (4).

a. 28 – days mean PCC modulus of rupture = 670 psi.
b. 28 – days mean elastic modulus of slab = 4,200,000 psi.
c. Mean effective k-value typical range = 100 – 200 psi/in (use AASHTO charts).
d. Load transfer coefficient (J)
    1) Tied shoulder or widened slab (14 ft) = 2.70.
    2) Untied shoulders = 3.20.
e. Overall drainage coefficient
    1) Typical cross-section and subgrade = 1 – 1.05.
    2) 16 – inches of open-graded drainage course = 1.10.

Table 2-3: MDOT recommended elastic modulus values per layer

Layer	Elastic modulus (psi)
HMA top and leveling course	390,000 – 410,000
HMA base course	275,000 – 320,000
ASCRL	210,000
Cement stabilized base	1,000,000
Asphalt/ emulsion stabilized base	160,000
Crush and shaped HMA	100,000 – 150,000
Rubblized concrete	45,000 – 55,000
Dense-graded aggregate base	30,000
Open-graded drainage course	24,000
Sand subbase	13,500
Existing aggregate base	15,000** – 28,000*
Existing sand subbase	7,500** – 12,500*

* No evidence of pumping, degradation, or contamination by fines.
** Evidence of pumping, degradation, or contamination by fines.

As per Equation 2-3, the effective thickness is a function of the existing slab thickness three adjustment factors: joints and crack adjustment factor, durability adjustment factor, and fatigue damage adjustment factor. Tables 2-4 and 2-5 present the MDOT's recommended values of these adjustment factors for durability and fatigue damage.

Table 2-4: Concrete/ composite durability adjustment factor

Existing pavement condition	F_{dur}
No evidence or history of PCC durability problem	1.0
Durability cracking exists or is suspended, but no spalling due to "D" cracking or localized failures is visible	0.98
Substantial durability cracking and some spalling due to "D" cracking with visible localized failures	0.92
Extensive durability cracking and severe spalling due to "D" cracking with visible localized failures	0.85

The joints and crack adjustment factor is related to unrepaired deteriorated joints and cracks other than "D" cracking, and it is a sum of all unrepaired deteriorated joints, cracks, punch outs, expansion joints, wide joints (>1"), and HMA full depth patches per mile (4). Table 2-6 shows the MDOT suggested range for overlay design; however, the number of joints and cracks can be obtained after a detailed condition survey and according to the project scope. After getting a summation of these joints and cracks, the adjustment factor can be obtained by the AASHTO93 chart shown in Figure 2-2 (4).

MDOT recommends an additional factor as a quality adjustment factor for existing HMA layers shown in Table 2-7, compensating for any defects or deformations in the existing HMA pavements that surface milling cannot address (4).

Table 2-5: Concrete fatigue damage adjustment factor

Existing pavement condition	F_{fat}
Few transverse cracks/ punch outs exist (none caused by "D" cracking) • JPCP: < 5% of slabs cracked • JRCP: < 25 cracks/mi (working cracks) • CRCP: < 4 punch outs/mi	1.0
A significant number of transverse cracks/ punch outs exist • JPCP: 5 – 15% slabs cracked • JRCP: 25 – 75 cracks/mi (working cracks) • CRCP: 4 – 12 punch outs/mi	0.96
Several transverse cracks/ punch outs exist • JPCP: > 15% of slabs cracked • JRCP: > 75 cracks/mi (working cracks) • CRCP: > 12 punch outs/mi	0.93

Table 2-6: MDOT suggested range of unrepaired joints and cracks for overlay design

Unrepaired condition	Typical number per mile
Unrepaired deteriorated joints*	20 – 40
Unrepaired deteriorated cracks	20 – 40
Unrepaired punch outs**	5 – 10
Expansion joints, wide joints (>1"), or HMA full-depth patches	5 – 10

* Not needed if HMA overlay of existing composite pavements.

** Punch outs are commonly associated with CRCP, possible occurrence in JPCP/JRCP.

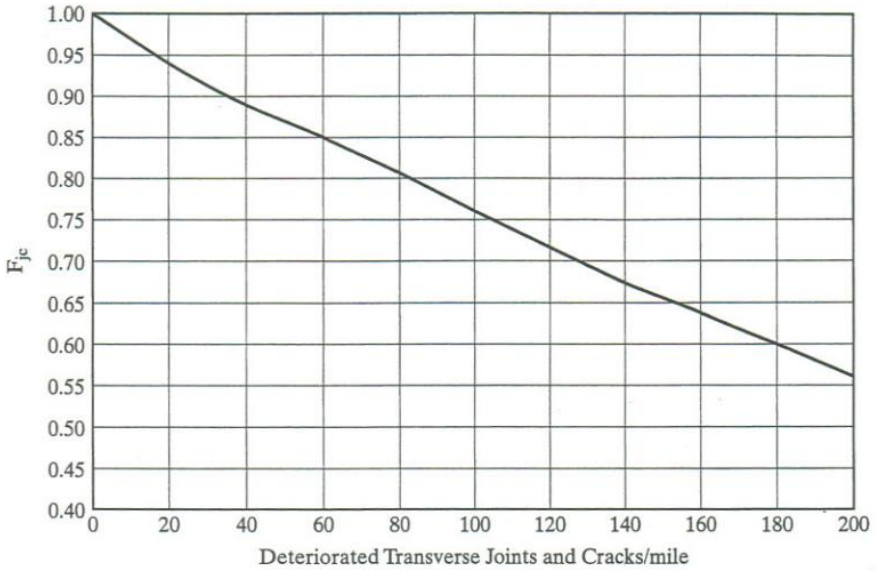

Figure 2-2: Joints and cracks adjustment factor F_{jc} (4)

2.3 Concrete Overlays

MDOT uses the Corps of Engineers design method to design thin (< 6 inches) over any pavement type and unbonded concrete overlays over full-depth HMA pavements.

Table 2-7: HMA AC quality adjustment factor, F_{ac}

Existing pavement condition	F_{ac}
No HMA pavement material distress	1.0
Minor HMA material distress (weathering or raveling) not corrected by milling	0.96
Significant HMA material distress (rutting, stripping, and/ or shoving)	0.93
Severe HMA material distress (rutting, stripping, and/ or shoving)	0.85

2.3.1 Thin Concrete Overlays (< 6")

MDOT recommends using concrete equivalent single axle load (CESAL) value at a design life of 15 years, commercial annual daily traffic (CADT), and a separator layer if overlying existing concrete pavement. The method uses the following empirical equation to find the overlay thickness (4).

$$D_{OL} = \sqrt{D_N^2 - C(D_E)^2} \quad (2\text{-}4)$$

where:

D_{OL} = Required PCC overlay thickness.

D_N = Required new PCC pavement thickness to carry future traffic.

D_E = Thickness of existing pavement.

C = Coefficient depends upon structural condition of pavement.

Table 2-8 shows the MDOT suggested design matrix for thin concrete overlay thicknesses.

Table 2-8: The MDOT's recommended concrete overlay thickness matrix

Design lane CADT	CADT (2-way)	CESAL	Overlay thickness on existing PCC (inches)				Overlay thickness on existing HMA (inches)			
			C Factor							
			0.80	**0.75**	**0.70**	**0.65**	**0.42**	**0.38**	**0.34**	**0.30**
100	≤ 220	650,000	4	4	4	4	4	4	4	4.5
150	330	970,000	4	4	4	4	4	4.5	4.5	5
200	440	1,300,000	4	4	4	4	4.5	5	5	5.5
250	550	1,630,000	4	4	4	4	5	5.5	5.5	
300	650	1,950,000	4	4	4	4	5.5	5.5		
350	760	2,270,000	4	4	4	4	5.5			
400	870	2,590,000	4	4	4	4.5				
450	980	2,900,000	4	4	4.5	5				
500	1090	3,230,000	4	4.5	4.5	5				
600	1310	3,900,000	4.5	5	5	5.5				
700	1525	4,500,000	5	5	5.5					
800	1750	5,200,000	5	5.5						
900	1950	5,800,000	5.5							
1000	2000	6,450,000	5.5							

The C factor value depends on the existing pavement conditions. Tables 2-9 and 2-10 show the MDOT's recommended C factor concrete overlay values on existing concrete/ composite and concrete overlay of existing HMA pavements, respectively (4).

Table 2-9: C-factor for structural condition of existing concrete/ composite pavements

Existing pavement condition	C – factor
Fair overall condition with minimum cracking	0.75 – 0.80
Mid–slab and D cracking, with adequate load transfer	0.65 – 0.70

Table 2-10: C-factor for the structural condition of existing HMA pavements

Existing pavement condition	C – factor
Fair overall condition with uniform support • Alligator cracking, transverse cracking, and rutting are minimal	0.38 – 0.42
Has an adequate structural condition • Alligator cracking and high-severity transverse cracking are minimal • Rutting (after milling) is greater than 0.1 inch	0.30 – 0.34

2.3.2 Concrete Overlays (6 inches or more)

As explained above, the Corps of Engineers approach is used to develop a catalog to estimate the design thickness of a concrete overlay. MDOT uses Table 2-8 for concrete overlay of existing concrete pavements with similar inputs as explained above; however, it developed a separate design matrix for concrete overlay (6 inches or more) of existing HMA pavements. Table 2-11 shows the MDOT's recommended values of overlay thickness of existing HMA pavement (4). The C-factors are shown in Table 2-10.

2.4 Mechanistic-Empirical (ME) Design Philosophy

In ME design, the engineering mechanics approach is used to compute the pavement responses; pavement distresses are predicted based on these responses and from field performance data (8). The iterative design and analysis procedure used by the PMED software is represented in Figure 2-3. In rehabilitation design, the PMED software allows users to select any rehabilitation design strategy and other critical inputs, including traffic, climate, and layer properties. As mentioned above, the nationally calibrated models predict pavement distress. Locally calibrated transfer functions are used to predict field performances for state-specific conditions. The M-E design approach has the following advantages over the traditional empirical approach (4):

a. Each state is allowed to have its design criteria.
b. Material characterization to reflect pavement performance.
c. Ability to assess the extent of damage resulting from specific loading configurations .
d. Incorporating the impacts of seasonal variations.
e. Ability to explore alternative design strategies and additional design features.

Table 2-11: MDOT's recommended concrete overlay (6" or more) thickness matrix

Design lane CADT	CADT (2-way)	CESAL	Overlay thickness on existing HMA (inches)			
			C Factor			
			0.42	**0.38**	**0.34**	**0.30**
250	550	2,210,000				6
300	650	2,650,000			6	6
350	760	3,090,000		6	6	6.5
400	870	3,540,000	6	6	6.5	6.5
450	980	3,980,000	6	6.5	6.5	7
500	1090	4,420,000	6.5	6.5	7	7
600	1310	5,300,000	6.5	7	7	7.5
700	1525	6,190,000	7	7.5	7.5	7.5
800	1750	7,070,000	7.5	7.5	7.5	8
900	1950	7,960,000	7.5	7.5	8	8
1000	2000	8,840,000	7.5	8	8	8.5
1100	2400	9,720,000	8	8	8.5	8.5
1200	2600	10,610,000	8	8.5	8.5	8.5
1400	3050	12,380,000	8.5	8.5	8.5	9
1600	3500	14,150,000	8.5	9	9	9
1800	3925	15,910,000	9	9	9	9.5
2000	4350	17,680,000	9	9	9.5	9.5
2500	5450	22,100,000	9.5	9.5	10	10
3000	6550	26,520,000	10	10	10	10.5
3500	7625	30,940,000	10	10.5	10.5	10.5
4000	8700	35,360,000	10.5	10.5	10.5	11
4500	9800	39,780,000	10.5	11	11	11
5000	10,900	44,200,000	11	11	11	11.5
5500	12,000	48,620,000	11	11	11.5	11.5
6000	13,075	53,040,000	11.5	11.5	11.5	11.5

2.5 Rehabilitation Design Strategy

Every design, no matter how well and efficiently, does not perform to the 100 percent desired results; similarly, in the case of pavement, the combined effect of traffic loadings, climatic effects, and other material-related deficiencies cause pavements to deteriorate before their design life. Pavement rehabilitation can be defined as restoring existing pavement to prevent further deterioration. Different rehabilitation strategies developed consensus among designers over time, which are listed in the PMED user manual as *(8)*:

a. Reconstruction without lane addition.
b. Reconstruction with lane addition.
c. Structural overlays.

d. Nonstructural overlays.
e. Reconstruction without overlays.

The selection procedure of any rehabilitation design strategy demands detailed analysis and thorough engineering judgment of the problem. The flow chart shown in Figure 2-4 reflects the steps outlined by the PMED user manual *(8)*. Reconstruction can be applied to all types of payments; however, some criteria should be considered while deciding the most appropriate rehabilitation strategy. High severity load-related distresses in flexible pavements and a high percentage of cracked slabs, deteriorated joints, inadequate foundation support, and D cracking in rigid are candidates for reconstruction *(8)*. Structural overlays are used when routine pavement maintenance does not address the cause of distress and can reoccur quickly. As per the PMED user guide, structural overlays are characterized into the following categories:

a. HMAC overlay over an existing flexible pavement.
b. HMAC overlay over an existing rigid pavement.
c. HMAC overlay over an existing composite pavement.
d. Bonded or un-bonded JPCP and CRCP over an existing rigid or composite pavement.
e. PCC overlay over an existing flexible pavement.

The most common practice across the US is placing an HMAC overlay over existing asphalt or PCC pavement to provide a new wearing surface and substantially use existing pavements' remaining fatigue life and structural capacity. MDOT's rehabilitation work significantly involves placing an HMAC overlay over existing AC, JPCP, or composite pavements. Figure 2-5 shows the variety of overlay design options offered by PMED software. MDOT is currently using the AASHTO93 method for all rehabilitation designs. Although AASHTO93 has proved to be a simple and powerful pavement design tool for several decades, its empirical nature limits its applicability as a modern design method compared to PMED. The PMED approach is more rational as it uses site-specific inputs and the existing pavement conditions for pavement rehabilitation analysis and design.

MDOT sponsored a sensitivity study to evaluate the PMED pavement design procedure for local construction, materials, and design practices. The PMED approach can design new and rehabilitated pavements; however, some differences exist in how the damage is calculated in the pavement layers *(11)*. These differences include (a) location within the pavement layer where

damage is calculated for flexible rehabilitation options, (b) age hardening of the existing HMA layers, and (c) characterization of the existing pavement damage.

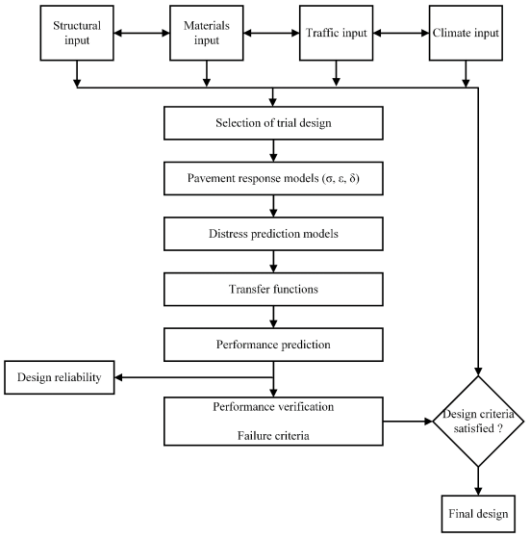

Figure 2-3: Flowchart of the AASHTOWare Pavement-ME design process

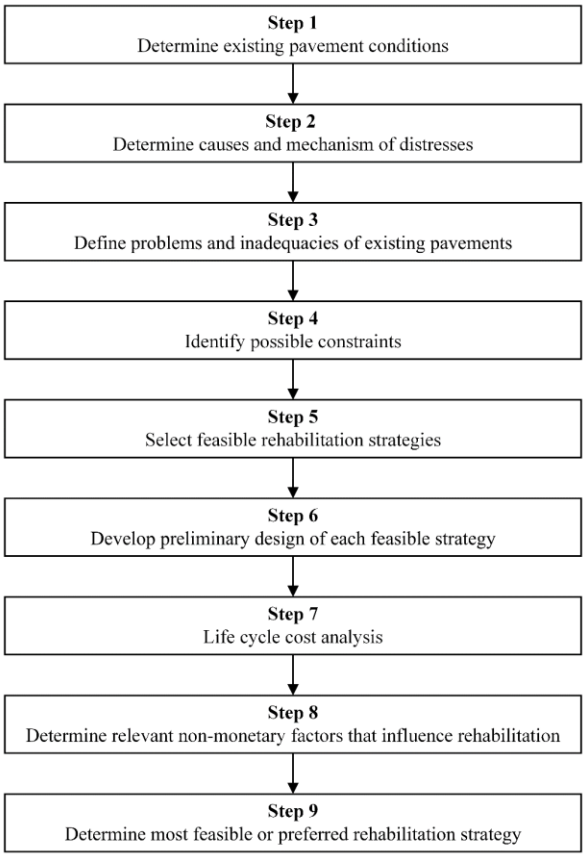

Figure 2-4: Procedure for selecting preferred rehabilitation strategy

The difference in the location and reduction of modulus may impact the percent alligator cracking, rutting, longitudinal cracking, and IRI for the rehabilitation options. Rehabilitation options also consider reflective cracking. While the AASHTO93 method requires limited data information for the structural design of pavements, the PMED requires many design inputs. Thus, it is crucial to know the impact of the different design inputs on the predicted pavement performance measures for the various rehabilitation options. Table 2-12 summarizes the sensitivity analyses of the multiple inputs reflecting Michigan practices on the PMED rehabilitation options *(11, 18-20).*

Table 2-12: Impact of input variables on PMED rehabilitation options *(11, 18-20)*

Fatigue cracking	Longitudinal cracking	Transverse cracking	Rutting	IRI
HMA thickness HMA effective binder content HMA air voids Base material type Subbase material type	HMA thickness HMA air voids HMA effective binder content Base material Subbase material Subgrade material	HMA binder grade HMA thickness HMA effective binder content HMA air voids HMA aggregate gradation	HMA thickness Subgrade material Subgrade modulus HMA effective binder content HMA air voids Base material Subbase material Base thickness Subbase thickness	HMA thickness HMA aggregate gradation HMA effective binder content HMA air voids Base material type Subbase thickness Subbase material type Subgrade material type

Interaction between the overlay HMA air voids and existing HMA thickness significantly impacts all performance measures among flexible rehabilitation options. The overlay thickness and the existing PCC layer modulus interaction significantly affect un-bonded overlay performance predictions. A study determined the sensitive inputs for the pavement rehabilitation options (11). The rankings of essential information for each rehabilitation option are summarized below (Tables 2-13 to 2-16):

Table 2-13: List of significant inputs — Composite pavement

Inputs	Ranking (NSI)
Overlay air voids	1 (9)
Overlay thickness	2 (2)
Existing PCC thickness	3 (1)

Table 2-14: List of significant inputs — HMA over HMA

Input variables	Ranking (NSI)
Overlay air voids	1 (6)
Existing thickness	2 (5)
Overlay thickness	3 (4)
Existing pavement condition rating	4 (4)
Overlay effective binder	5 (2)
Subgrade modulus	6 (2)
Subbase modulus	7 (1)

Note: NSI = Normalized sensitivity index

Table 2-15: List of significant inputs — Rubblized PCC pavement

Inputs	Ranking (NSI)
Overlay air voids	1 (6)
Overlay effective binder	2 (2)
Overlay thickness	3 (1)

Table 2-16: List of significant inputs — Un-bonded PCC overlay

Design inputs	Ranking (NSI)
Overlay PCC thickness	1 (23)
Overlay PCC coefficient of thermal expansion (CTE)	2 (12)
Overlay PCC modulus of rupture (MOR)	3 (8)
Overlay joint spacing	4 (5)
Existing PCC elastic modulus	6 (1)
Climate	7 (1)

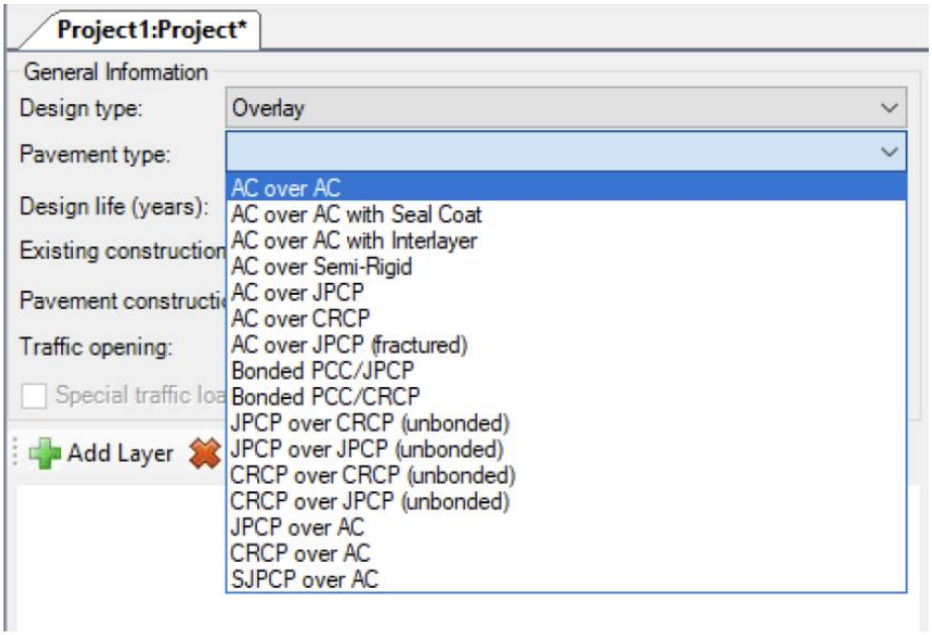

Figure 2-5: Overlay modeling options available in the Pavement-ME

The following sections explain the process of damage characterization of existing pavement layers of flexible and rigid pavements.

2.6 Characterization of Existing Pavement Layers

The PMED can design new and rehabilitated pavements with some key differences. The characterization of the existing layer is a critical step in rehabilitation design. Damage accumulated in the existing layer is a crucial factor for the future deterioration rate in the overlaid layers, as PMED considers the distressed development of AC overlays and the propagation of damage in the existing pavement layers *(8)*. First and foremost, the step in rehabilitation design is to assess the overall condition of the existing pavement; Levels 1, 2, or 3 data can be used to evaluate the overall pavement condition. The following eight categories of data required for the assessment of existing pavement condition are recommended by the PMED user manual 2015 *(8)*:

a. Structural adequacy.
b. Functional adequacy.
c. Subsurface drainage accuracy.
d. Material durability.
e. Shoulder profile adequacy.
f. Variability in condition or performance of existing pavement.
g. Miscellaneous activities (maintenance activities performed in the past, etc.).
h. Constraints (Bridge clearance, lateral clearance, etc.).

The following sections describe the primary characterization process for flexible and rigid pavement.

2.6.1 Existing HMA Layer Characterization

Accurate damage assessment in existing pavements and in-situ material properties are the most challenging in the characterization process. Damage modulus (mechanical property) is one of the critical factors in characterizing the existing pavement condition at the time of overlay *(8)*; volumetric properties, including percent air voids, effective binder content, Poisson's ratio, and unit weight of AC mixture are also vital in characterizing the existing HMAC layers. Three different hierarchical levels of inputs in the PMED software are used to represent the existing HMA layer.

2.6.1.1 Input Level 1

FWD deflections are used to backcalculate the layer moduli of the existing layer; these backcalculated moduli, along with pavement temperature, age, and FWD load frequency, are used to characterize the existing AC layer by developing a damaged modulus master curve. Equation 2-5 represents the undamaged modulus master curve $|E^*|$ *(8, 21)*.

$$|log\, E^*| = \delta + \frac{\alpha}{1 + e^{\beta+\gamma\, log\, t_r}} \quad (2\text{-}5)$$

where;

E^* = AC modulus, psi; δ = Regression parameter (10^{δ} = minimum modulus); α = Range; t_r = reduced time, seconds; β & ɣ = Regression parameters.

The undamaged modulus master curve is adjusted for pre-overlay damage. Figure 2-6 explains the vertical shift of the undamaged modulus master curve to the amount where the undamaged master curve passes through the in situ backcalulated modulus from the FWD test value E_{NDT}. Equation 2-6 represents the damaged modulus master curve.

$$E^*_{dam} = 10^{\delta} + \frac{E^* - 10^{\delta}}{1 + e^{-0.3+5\, log(d_{AC})}} \quad (2\text{-}6)$$

where:

E^*_{dam}= Damaged modulus, psi; δ = Regression parameter; E^*= Undamaged modulus for a specific reduced time; d_{AC} = Fatigue damage in the HMA layer.

After knowing the damaged and undamaged modulus, Equation 2-6 is used to compute fatigue damage d_{AC} in the AC layer.

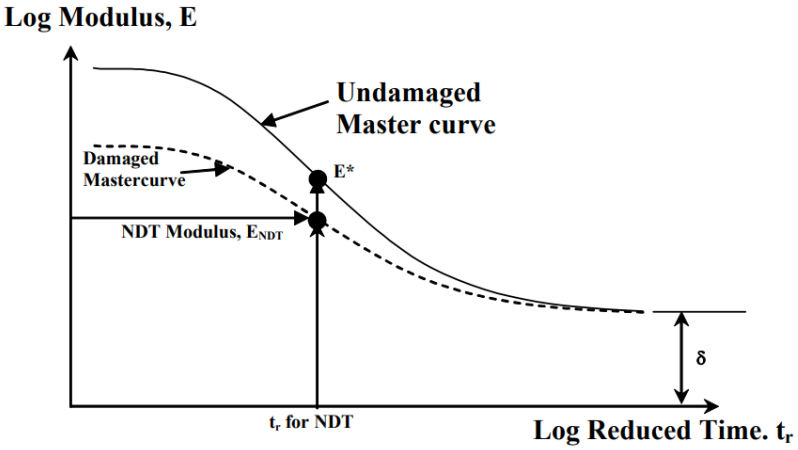

Figure 2-6: HMAC layer damage computation for input Level 1 *(8)*

2.6.1.2 Input Level 2

At input Level 2, the damage is predicted by the amount of fatigue cracking exhibited by the existing AC layer. Field investigation, including pavement condition surveys and coring, is used to measure the fatigue damage on AC pavement. Field cores are used to obtain the undamaged master curve of the AC layer. Damage is predicted by the PMED software using the empirical transfer function represented by Equation 2-7 *(8)*.

$$FC_{AC} = \left(\frac{1}{60}\right) + \frac{C_4}{1 + e^{C_1 C_1^* - C_2 C_2^* log(DI_{AC})}} \quad (2\text{-}7)$$

where:

FC_{AC} = Fatigue cracking (in the percentage of area); DI_{AC} = cumulative damage at the bottom of the AC layer; C_1, C_2, C_4 = Transfer function coefficients where C2 is a function of HMA thickness between 5 and 12 inches.

C_1* and C_2* can be determined using Equations 2-8 and 2-9.

$$C_1^* = -2C_2^* \quad (2\text{-}8)$$

$$C_2^* = -2.40874 - 39.748(1 + H_{HMA})^{-2.856} \quad (2\text{-}9)$$

2.6.1.3 Input Level 3

Likewise input Level 1, the undamaged modulus master curve is obtained using HMA volumetric and binder properties; however, the general condition rating of pavement is sued to assess the current damage in the existing pavement. Table 2-17 represents the damage values corresponding to the pavement's general condition ratings *(8)*. With undamaged modulus and current damage known, Equation 2-6 is used to predict damaged modulus.

Table 2-17: HMA damage based on pavement condition rating

Category	Damage
Excellent	0.00 – 0.20
Good	0.20 – 0.40
Fair	0.40 – 0.80
Poor	0.80 – 1.20
Very poor	> 1.20

Table 2-18 summarizes the methods for characterization of the existing HMA layer recommended by PMED user guide (8).

Table 2-18: Recommended methods for characterizing existing HMA pavement layers

Layer Material	Input	Hierarchical Levels		
		1	2	3
Subgrade	Modulus	NDT	Simple test correlations	Soil classification
	Initial ε_p	Trench data	User input	User input
Unbound base or subbase	Modulus	NDT	Simple test correlations	Soil classification
	Initial ε_p	Trench data	User input	User input
Chemically stabilized materials	Damaged modulus	NDT	Estimated from undamaged modulus	Estimated from undamaged modulus
	Undamaged modulus	Compressive strength of field cores	Estimated from compressive strength of field cores	Estimated from typical compressive strength
	Fatigue damage	% Alligator cracking	% Alligator cracking	Pavement rating
Existing asphalt layers	Damaged modulus	NDT	Estimated from undamaged modulus	Estimated from undamaged modulus
	Undamaged modulus	HMA dynamic modulus model with project-specific inputs	HMA dynamic modulus model with project-specific inputs	HMA dynamic modulus model with agency historical inputs
	Fatigue damage	% Alligator cracking from visual condition surveys	% Alligator cracking from visual condition surveys	Pavement rating
	Initial ε_p	Trench data	User input	User input

2.6.2 Existing PCC Layer Characterization

The following section explains the different approaches adopted by other states to characterize the exisiting pavements.

2.6.2.1 Input Levels 1

For damage analysis of existing JPCP and CRCP pavement layers, an estimate of existing damage in PCC is required as the damage continues to develop but at a slower rate after the overlay placement. The characterization of damage in the HMA overlaid PCC pavement is done based on a detailed condition survey of the pavements. Tables 2-19 to 2-21 show the recommended initial values for damage in JPCP and the number of punch-outs in CRCP pavements and the values of factor C based on pavement condition *(8)*. FWD testing of the

existing pavement is used to compute the elastic modulus E_{TEST} and then adjusted for the pavement condition factor C to get E_c required to be used as design input *(8, 21)*.

$$E_c = C * E_{TEST} \quad (2\text{-}10)$$

Table 2-19: Initial cracking damage estimates

Distress (%slab cracked)	Damage
0	0.100 – 0.250[1]
10	0.270
20	0.438
30	0.604
40	0.786
50	1.00

Table 2-20: Recommended condition factor "C" Values

Pavement condition	Recommended C value
Good	0.42 – 0.75
Moderate	0.22 – 0.42
Severe	0.042 – 0.22

Table 2-21: Initial punchout and associated damage estimates

Number of punchouts per mile	Damage
0	0.10 – 0.150[2]
2	0.22
4	0.34
6	0.44
8	0.53
10	0.62
> 10	> 0.62

2.6.2.2 Input Levels 2

For Level 2, compressive strength correlation is used to estimate the elastic modulus and modulus of rupture. In situ, compressive strength f_c' is measured from the cores, and PMED calculates E_{TEST} internally using in-situ f_c' using Equation 2-11 *(8, 21)*:

$$E_c = 33\rho^{3/2}(f_c')^{1/2} \quad (2\text{-}11)$$

Where;

[1] Assumed default value.
[2] Assumed default value.

E_c = PCC elastic modulus, psi; ρ = unit weight of concrete lb/ft^3; f_c'= compressive strength of PCC, psi; E_c can be found using equation 2-10 as explained in Input level 1 above.

2.6.2.3 Input Level 3

For Level 3 characterization, a general condition rating of the pavement is used to estimate current damage. Table 2-22 shows the recommended criteria by the PMED user guide for damage estimation based on general condition rating *(8)*. Moreover, in situ, E_c is estimated as a function of pavement condition using Table 2-23. f_c' or 28-day MOR is computed from historical data or local practices in place; f_c' is converted to MOR internally by PMED using the following relationship *(8, 21)*:

$$MR = 9.5 * (f_c')^{0.5} \quad (2\text{-}12)$$

Table 2-22: Damage for JPCP and CRCP based upon general condition rating

Category	Damage
Excellent	0.10 – 0.250
Good	0.50 – 0.67
Fair	1.00
Poor	>1.00
Very Poor	>1.00

Table 2-23: Recommended condition factor values to adjust moduli of intact slab

Pavement condition	Typical modulus range
Adequate	3 – 4 x 10^6
Marginal	1 – 3 x 10^6
Inadequate	0.3 – 1 x 10^6

Table 2-24 summarizes the methods for characterizing HMA overlays of PCC Pavements recommended by the PMED user guide (8).

Table 2-24: Summary of existing layer characterization for HMA overlays of PCC pavements

Layer Material	Input	Hierarchical Level		
		1	2	3
Subgrade	Modulus	NDT	Simple test correlations	Soil classification
Existing unbound base or subbase	Modulus	NDT	Simple test correlations	Soil classification

Table 2-24: (cont'd)

Existing asphalt base or subbase	Dynamic modulus	NDT	HMA dynamic modulus model with project specific inputs	HMA dynamic modulus model with agency historical inputs
JPCP	Elastic modulus for PCC	Field cores (lab testing) or backcalculated FWD (adjusted)	Estimated from compressive strength of field cores	Estimated from historical compressive strength data
	Modulus of rupture	Field beam (lab testing)	Estimated from compressive strength of field cores	Estimated from historical compressive strength data
	Past fatigue damage	% Slab Cracked	% Slab cracked	Pavement rating
CRCP	Elastic modulus for PCC	Field cores (lab testing) or backcalculated FWD (adjusted)	Estimated from compressive strength of field cores	Estimated from historical compressive strength data
	Modulus of rupture	Field beam (lab testing)	Estimated from compressive strength of field cores	Estimated from historical compressive strength data
	Past fatigue damage	Punchouts and repairs /mile	Punchouts and repairs /mile	Pavement rating
JRCP	Elastic modulus for PCC	Field cores (lab testing) or backcalculated FWD (adjusted)	Estimated from compressive strength of field cores	Estimated from historical compressive strength data

2.7 Characterization of Existing Pavement Layers by Other States

The following section explains the different approaches adopted by other states to characterize the exisiting pavements.

2.7.1 Kansas

Islam et al. 2023 conducted a recent study to implement PMED to design rehabilitated pavements in Kansas to focus on the AC over AC and AC over JPCP sections (21). This study characterizes the existing layer as per the procedure explained above. The team collected data at the time of construction for overlay layers where possible, and in situ material properties were assumed after reviewing the construction management system (CMS) database of the Kansas Department of Transportation (KDOT). This study takes 7% as constructed air voids for all HMA mixes, and effective binder content (by volume) was obtained by the difference of voids in mineral aggregate (VMA) and target air voids. In rehabilitation design, characterizing existing pavement is the most critical step; efforts were made to collect the maximum data required to

characterize the existing pavement layers. The unit weight (128 pcf to 150 pcf) and percent air voids were taken from the KDOT CMS database, and the poison ratio for all mixes was assumed as 0.35. For level 1 rehabilitation input, FWD backcalculated moduli were used. The study used pre-overlay FWD data for 16 AC over AC sections; however, KDOT does not conduct pre-overlay FWD for AC over JPCP pavements. EVERCALC version 5 was used to backcalculate the layer moduli for each drop at a 9000 lb load level. Any calculated value with a root mean square error of more than 5% was neglected. As FWD testing data were not available for 9 projects, level 2 inputs were used for their analysis. Distress data was collected by Laser Crack Measurement System (LCMS) and manual condition survey of the pavements. For pre-overlay condition data, all load-related cracking was considered top-down because KDOT PMIS does not differentiate between top-down and bottom-up cracking. For JPCP mix inputs, the data for 7-, 14-, 28-, and 90-day PCC elastic modulus and modulus of rupture (MOR) were unavailable for Level 1 inputs; instead, Levels 2 and 3 mix properties were used. For Level 2 inputs, PCC compressive strength at 7-, 14-, 28-, and 90-days and a ratio of 20-yr to 28-day compressive strength were predicted using the following models developed under FHWA (2012):

$$f_{ct} = 6358.60655 + 3.53012 * CMC - 34.24312 * \frac{w}{c} * uw + 633.3489 * ln(t) \quad (2\text{-}13)$$

where:

f_{ct} = Compressive strength at age t years, psi; CMC = Cementitious materials content, lb/yd3; w/c = Water to cement ratio; uw = Unit weight, lb/yd3; and t = Short-term age up to 1 year.

$$f_{c,LT} = -3467.3508 + 3.63452 * CMC + 0.42362 * uw^2 \quad (2\text{-}14)$$

where:

$f_{c,LT}$ = Compressive strength at age t (variable up to 20 years), psi; CMC = Cementitious materials content, lb/yd3; and uw = Unit weight, lb/yd3.

The 28-day MOR and elastic modulus E_c required for Level 3 input analysis, and those were estimated using the following equations:

$$E_c = 57000\sqrt{f_c'} \quad (2\text{-}15)$$

$$MOR = 9.5\sqrt{f_c'} \quad (2\text{-}16)$$

For existing JPCP characterization, KDOT does not collect data on transverse slab cracking and transverse joint load transfer efficiency (LTE) for AC over JPCP. However, this study considered a constant value of 3% for slab cracking as a trigger value for JPCP

rehabilitation. LTE was estimated based on faulting values, and Table 2-25 represents LTE guidelines to estimate LTE used by KDOT for this study.

Table 2-25: KDOT recommended guidelines for estimating LTE

Functional class of the roadway	Faulting criteria (in.)	Recommended LTE (%)
Interstate	< 0.1 in.	80%
	0.1–0.15 in.	65%
	> 0.15 in.	50%
Principal arterials	< 0.125 in.	80%
	0.125–0.20 in.	65%
	> 0.20 in.	50%
Local roads	< 0.15 in.	80%
	0.15–0.30 in.	65%
	> 0.30 in.	50%

2.7.2 Virginia

Virginia (VDOT) adopted the PMED for the new/reconstruction of interstate and primary routes on January 1, 2018 (22). However, like MDOT, the VDOT uses AASHTO 1993 method for rehabilitation designs and expects to implement PMED for the most common rehabilitation treatments. One of the objectives of this study was to compare Levels 1 and 2 input results for AC rehabilitation. For characterization of the existing HMA layer, FWD testing was performed for the Level 1 rehabilitation option, the resilient modulus was measured in the laboratory for Level 2, and a pavement condition survey was done for the Level 3 rehabilitation design. However, it is recommended by pavement experts to use only Levels 1 and 2 input data (FHWA Pavement ME User Group, 2020). VDOT used performance grade and volumetric properties of VDOT's base mixer and state-level average values of new AC mixtures for overlay layers. Layer thickness data were estimated using GPR and coring on specific locations to compare the results with GPR analysis. Data collected from GPR and coring was also used to estimate the crack damage in the existing layers. GPR images were processed to mark the AC and base layer interfaces; however, due to the large thickness of the AC layer (8-13 inches), the bottom of the base layer (depth > 20 inches) could not be seen and marked from GPR images. Table 2-26 represents the HMA and base thickness comparisons obtained from GPR and coring for VDOT. The study recommended that Level 1 data is necessary for accurate and reliable estimates of

existing HMA layers; Level 2 data provides unrealistic estimates for the damage modulus master curve.

Table 2-26: HMA and base thicknesses comparison from GPR and coring

Site	Coring average AC thickness (in)	GPR average AC thickness (in)	Core average base thickness (in)	GPR average base thickness (in)
1	12	11.3	8	7
2	7.5	7	4 to 8	8
3	11.6	10.8	4 to 8	7.1

2.7.3 Oregon

The Oregon Department of Transportation (ODOT) conducted a study in 2013 to implement a PMED design approach for new and rehabilitation pavement designs (23). The FWD data were unavailable to characterize the existing layer in rehabilitation design, so rehabilitation Level 3 was selected, assuming pavement rating as fair and a total rut depth of 0 inches. Asphalt binder dynamic modulus data were available at Levels 1 and 2; however, for creep compliance and indirect tensile strength input, Level 3 was chosen in this study. The team conducted field distress surveys to assess the condition of existing pavements. The condition survey results are (1) average rut depth varies from 0.044 inches to 0.3 inches, (2) Coast and valley region showed zero thermal cracking; however, sites in the eastern region showed the presence of thermal cracking, (3) weighting function represented by Equation 2-17 was used, to sum up, the low, medium, and high-intensity thermal cracking (TC) by using following equation ARA-2004 *(24)*.

$$TC = \frac{LowseverityTC + 3 * MediumseverityTC + 5 * HighseverityTC}{9} \qquad (2\text{-}17)$$

2.7.4 Missouri

Missouri Department of Transportation (MoDOT) conducted a recent study to recalibrate the pavement distresses and IRI prediction models for new and rehabilitated flexible and rigid pavements in Missouri using PMED version 2.5.5 (25). FWD testing was performed only for flexible pavement sections, and deflection data were used to backcalculate the resilient modulus. FWD was conducted as per standard procedures of LTPP FWD testing protocols. Four load levels (6000, 9000, 12,000, and 16,000 lb) were used as target load levels, and 16 drops were made at each site, having four replicates for each load level. The integral backcalculation tool "EVERCAL™" was used to backcalculate the resilient modulus of subgrade material; it was found that a deflection basin of 9000 lb and 12,000 lb yielded acceptable results. The researchers

also collected loose HMA material and field cores to test HMA martial inputs. Asphalt Mixture Performance Tester (AMPT) was used to measure the dynamic modulus E^* of HMA mixtures and then converted Level 1 input compatible with PMED. Tests were conducted to get and maintain the material input library of creep compliance and tensile strength of HMA for Missouri as per AASHTO T322 laid down procedures. The team found that tensile strength increased with an increase in air voids, and the reverse is true for creep compliance. Mallela et al. 2009 conducted a study to develop the PCC input database *(26)*. Time series data were obtained from PMS and LTTP projects for distress and smoothness performance models. Table 2-27 shows the mix of hierarchical input levels used for this study.

2.7.5 Louisiana

Louisiana has conducted few studies focusing on new and full-depth rehabilitated flexible pavements (27). Only 33 sections of AC overlay over existing flexible pavement were considered. To characterize the existing layer's damage, rehabilitation Level 3 used total rutting in the pavement surface and pavement condition rating as standards in the Manual of Practice(8). These standards assessed the pre-overlay pavement condition rating based on the quantity of distress measured in the existing pavement. Louisiana Department of Transportation maintains a database as a project management system (PMS), which was used to get the average rutting for each available project for missing sections the pavement condition rating was assumed poor, and a total rutting value of 0.25 inches was considered.

2.7.6 Colorado

Colorado Department of Transportation (CDOT) carried out a study in 2013 to implement PMED design to calibrate performance prediction models for new and rehabilitated pavements in Colorado using PMED version 1 (28). The study's primary objectives were to address routine design problems for new and rehabilitated pavements and conduct forensic analysis to obtain and assemble a database encompassing guidelines of the new PMED user guide. A total of 126 pavement projects of new and rehabilitated pavements were selected for this study from LTPP and Colorado DOT's PMIS database. CDOT performed FWD testing to backcalculate the layer moduli of existing JPCC and composite pavements; for HMA pavements, FWD was performed at 25 ft intervals, and for JPCP, it was performed at the center, transverse joints, and corners of the slab. To characterize PMED input, researchers reviewed traffic, climate, and other relevant

data records; laboratory testing and conducting field surveys, including destructive and non-destructive testing, also became part of the study.

Table 2-27: Input data levels for MoDOT

Input Type	Input Data Elements	Hierarchical Level
Traffic	Truck volume distribution and vehicle class distribution	Level 1project specific data from MoDOT
	Axle load distributions	Level 1 or 2 site-specific computed using MoDOT WIM data or national defaults when data is not available
	Monthly adjustment factors	Level 1 when available, or default
	All others	Level 3 Pavement-ME defaults
Climate	Temperature, wind speed, percent sunshine, precipitation, and relative humidity	AASHTOWare procedure; MERRA data for flexible pavements and NARR data for rigid pavements. Not associated with hierarchical level.
AC materials	HMA dynamic modulus	Level 1 Laboratory testing (for PMS sections) Level 2 computed (for LTPP sections)
	Air voids	Level 1 field air void data from MoDOT and LTPP database
	Binder	Level 1 for PMS sections; Level 3 defaults for LTPP sections
	HMA creep compliance & indirect tensile strength	Level 1 laboratory test data for PMS sections; Level 2 computed data for LTPP sections
	Other inputs	Level 3 Pavement-ME defaults
PCC materials	Strength over time and mix design inputs	Level 1 strength data from previous laboratory test results for different MoDOT specification gradations. Levels 2 and 3 for CTE and other inputs.
Unbound base and subgrade	Resilient modulus Atterberg limits, & gradation	Level 1 backcalculated data and field test data for PMS sections, and Level 3 data from the LTPP database for LTPP sections.
Performance	Distress & smoothness	Level 1: Field measured

2.7.7 Utah

Utah DOT uses Level 3 inputs for existing pavement characterization (29). A condition survey is required to determine the percent of alligator cracking (all severity levels) and an overall pavement rating to estimate the HMA dynamic modulus (|E*|). For the HMA overlays and concrete pavement restoration of an existing JPCP and unbonded JPCP overlays, the elastic

modulus of the slab is estimated using cores or 28-day modulus and multiplying by 1.2 to approximate long-term modulus. For constructing an HMA overlay of rubblized JPCP, a modulus of 60,000 psi is used while limiting the unbound base resilient modulus value to 2 to 3 times that of the subgrade. However, falling weight deflectometer (FWD) testing and backcalculation are recommended to estimate subgrade modulus for unbonded JPCP overlays of existing JPCP.

2.7.8 Maryland

The Maryland Department of Transportation conducted a study to develop a significant and fundamental input database required by the PMED design methodology (30). Level 3 approach was used for characterization. A few other inputs needed for the HMA rehabilitation design, including thermal conductivity, heat capacity, unit weight, and poison ratio, were assumed to be the same as in the new pavement design.

***Summary*:** Table 2-28 summarizes the rehabilitation levels used to characterize damage in existing pavement layers by other SHAs.

Table 2-28: Summary of existing HMA layer damage characterization

State	Damage characterization		
	Level 1	Level 2	Level 3
Kansas	Y	Y	N
Virginia	Y	Y	N
Oregon	N	N	Y
Missouri	N	N	Y
Louisiana	N	N	Y
Colorado	N	Y	Y
Maryland	N	N	Y
Utah	N	N	Y

Y = Yes; N = No

2.8 Local Calibration Efforts And Challenges

Many SHAs have been working on implementing the PMED design approach to design new and reconstructed pavements. However, very few states worked on rehabilitation design that too with a limited number of pavement sections and data input variables. Rehabilitation design poses almost similar challenges as new design, which is listed below:

a. Project selection: identify the available sections with performance data.
b. Existing layer characterization: unavailability of different data collection techniques (FWD, GPR, etc.) for the existing layer's characterization.

c. Pavement-ME inputs: the data might not be available with the required information and assumptions.
d. Performance data: measured data might not be available in the database for the Pavement-ME compatible units. Necessary assumptions must be made for conversion.
e. Local calibration techniques: identify mathematical tools/processes for local calibration.

The Pavement-ME models are nationally calibrated based on pavement material properties, structure, climate, truck loading conditions, and data from the Long-term Pavement Performance (LTPP) program *(31),* which demands local calibration of performance prediction models per state-specific conditions. The local calibration process ensures precision and accuracy in performance prediction. Many SHAs have been working on calibrating the PMED models by adopting different calibration techniques while reducing the standard error of estimates (SEE) and bias in the predictions. The local calibration guide, 2010 *(32)* and 2015 *(8)* outlined the following steps for local calibration.

a. Step 1: Selection of input levels.
b. Step 2: Develop an experimental plan and sampling strategy.
c. Step 3: Assess the adequate sample size for each distress.
d. Step 4: Selection of pavement sections.
e. Step 5: Get Pavement-ME inputs and measured distress data.
f. Step 6: Conduct field and forensic investigation.
g. Step 7: Validation of global model coefficients to local conditions.
h. Step 8: Eliminate the local bias for Pavement-ME models.
i. Step 9: Estimate the standard error of the estimate.
j. Step 10: Eliminate the standard error of the estimate.
k. Step 11: Assessment of the calibration process.

The PMED was updated with time as many national and state-level studies have been conducted to implement the new Mechanistic-Empirical design approach for pavement design. Mainly, these studies centered on sensitivity analysis to determine the impact of inputs on distress prediction, development of a database for state DOT, calibration and validation of PMED performance prediction models, and implementation of these calibrated models to design new and rehabilitated pavements. As part of the initial implementation, most states focused on

new or reconstructed pavement designs; however, few states worked on selective models of overlay design with limited input data available. These states include:

a. Iowa
b. Colorado
c. Kansas
d. Pennsylvania
e. Maryland
f. Virginia
g. Utah
h. Oregon

The following sections summarize the local calibration efforts of rehabilitation models for several SHAs.

2.8.1 Local Calibration Efforts for Flexible Pavement Overlays

The following section summarizes the local calibration of performance prediction models for flexible pavement overlays by other states.

2.8.1.1 Kansas

In February 2023, KDOT conducted a research study to implement the PMED design of rehabilitated pavements for state-managed roads in Kansas, New Jersey, and Maine (21). Local calibration for AC over AC and AC over JPCP pavements models was carried out using PMED version 2.5, and results were verified using PMED version 2.6.2.2. Standard error of estimates (S_e) and bias were used as criteria for model verification. About 25 sections of AC over AC were used for calibration in this study. The hierarchical level of inputs directly impacts the performance prediction of PMED model. Hence, a comprehensive study was conducted to select the best available input level for traffic, climate, material properties, and existing pavement conditions. The research team tried to model AC over AC within the limitations of the maximum number of HMA layers over the existing pavement layers as specified by the PMED user guide *(8)*. The team aimed to collect the as-constructed material properties of the new layer at the time of overlay construction from the KDOT construction management system (CMS) database and by reviewing the QC/QA spreadsheets. Permanent deformation, transverse (thermal + reflection) cracking, load-related cracking (bottom-up + top-down), and IRI models for AC over AC were calibrated in this study. The PMED did not predict thermal cracking for KDOT conditions, so only reflection cracking model coefficients were calibrated, and all load-related cracking was modeled as top-down cracking for AC over AC pavement sections. An automated calibration technique with three types of resampling approaches (traditional split sampling, jackknife, and bootstrap) was adopted to calibrate the PMED performance prediction models using Python

software. The limitations of the automated technique mentioned by the researcher team are that (a) it cannot be implemented for parameters that need multiple runs of PMED software, i.e., β_{2r} and β_{3r} coefficients of permanent deformation model, and (b) identification of bounds of model coefficients.

Local calibration improved the prediction accuracy of the rutting, transverse cracking, load-related cracking, and IRI models for AC over AC pavement sections. However, local calibration of the transverse cracking model for both rehabilitation types resulted in higher S_e because AC thermal cracking model was calibrated at global values, as KDOT does not distinguish between reflection and thermal cracking. Compared to globally calibrated values, the top-down cracking model showed high accuracy with minimum bias and S_e. However, S_e was high due to variability in data collection. Distress data on all sections overlaid before 2013 were collected manually, which made it responsible for high data variability; moreover, KDOT considers all load-related cracking as top-down, so it was considered another factor towards high S_e. The research team also compared calibration results from PMED versions 2.5 and 2.6.2.2, which showed slightly higher distress prediction for AC total fatigue cracking, especially for AC bottom-up fatigue cracking; the rest of all predicted distress values remained unchanged. The study has the following important recommendations:

a. Accurate data collection for pavement layer properties.
b. Collection of cores to distinguish between top-down and bottom-up fatigue cracking.
c. Creep compliance test and indirect tensile strength test for AC overlay mix to characterize low-temperature cracking.
d. Efforts to reduce measurement errors in distress measurement and data collection to improve the accuracy of local calibration.
e. Rutting in each layer is to be incorporated to achieve better results from local calibration of the rutting model.

2.8.1.2 Iowa

A handful of studies have been conducted by Iowa DOT for calibration of PMED models and to implement PMED design type in Iowa (33-35). The initial study in 2009 focused on HMA rutting and the IRI model's evaluation with national calibration coefficients, and bias was reported for these models. In 2013, overall efforts were made to calibrate the PMED performance models with the local conditions of Iowa. A total of 35 sections of new HMA and

60 of HMA over JPCP (composite) were selected for the study. This study concluded that rutting and top-down cracking for new HMA and composite pavement sections yielded acceptable predictions locally. Bottom-up cracking for New HMA pavements provides acceptable predictions at nationally calibrated values. Both nationally and locally calibrated models for alligator cracking provide acceptable predictions for composite sections. Iowa DOT PMIS does not differentiate between thermal and reflection cracking for composite pavements. Iowa DOT conducted a recalibration study in 2015 with the same sections as used in 2013 but with upgraded AASHTOWare PMED version 2.1.24 to compare results of national and previous calibrations of PMED performance prediction models and, if deemed necessary, recalibrate the performance models for local conditions of Iowa. The researchers came up with the following conclusions:

a. Recalibration of rutting and IRI models for HMA over JPCP at local conditions of Iowa significantly increased the prediction accuracy as compared to national and previous calibration efforts.
b. The accuracy of longitudinal (top-down) cracking improved due to recalibration efforts for local conditions.
c. Iowa DOT could calibrate the thermal cracking model with acceptable accuracy, as they considered measured transverse cracking data as thermal cracking only.

2.8.1.3 Missouri

Missouri started implementing PMED design in early 2009, making them one of the earliest adopters of AASHTOware pavement ME design in pavement design procedures. The MoDOT conducted two studies in 2009 to imply and calibrate the performance prediction models per Missouri's local conditions *(26, 36)* using PMED version 1.0. These studies focused on developing a database for MoDOT by collecting field/ laboratory data and calibrating the PMED performance prediction designs for new pavements. The findings of this study were (a) overprediction of rutting by PMED, (b) most of the sections exhibit alligator cracking less than 5%, so a nationally calibrated model was used for this study, (c) predictions on locally calibrated models were acceptable for newly constructed sections; however, higher reliability was recommended for pavements older than 15 years. In continuation of the efforts mentioned above, MoDOT conducted a recent study to recalibrate the pavement distresses and IRI prediction models for new and rehabilitated flexible and rigid pavements in Missouri using PMED version

2.5.5. MoDOT used PMS and LTPP database to consider new AC, AC over AC, and AC over JPCP for flexible pavements. All five models for flexible pavement were calibrated. MoDOT used recycled material, and material testing capacity enhancement was done before the study to get maximum Level 1 input for Pavement-ME. The traffic data was obtained from weight-in-motion (WIM) data collection sites, and a detailed analysis was carried out to decide the usage of hierarchal data input levels in the Pavement-ME. The goodness of fit and bias are used as part of the model verification methodology. Statistical parameter R^2 and hypothesis testing were used to check the goodness of fit and bias. This study carried out the sensitivity analysis and local calibration of the abovementioned models, except for the top-down cracking model. The researchers recommended calibrating the fatigue and reflection cracking simultaneously, as it is difficult to differentiate between both distress types in the field. Local calibration of the rutting model slightly improved the R^2 value from 0.26 to 0.34, which was considered reasonable due to noise in the rutting measurement in the field. This study concluded with the following results:

a. Significant results were achieved by the local calibration of all flexible pavement models; however, a significant variation was noted in the rutting model, which was considered due to field measurement noise.
b. Alligator cracking, rutting, and the transverse thermal cracking of flexible pavements decreased with increased AC layer thickness; however, the opposite is true for increasing air voids.
c. Warmer region pavements showed more rutting and alligator cracking and colder regions had more low-temperature cracking.

2.8.1.4 Michigan

Calibration for new flexible and rehabilitated pavements for Michigan was conducted in a research study by Haider et al. (2014). A total of 129 reconstructed flexible sections and 40 rehabilitated sections were selected for this project. The Pavement-ME inputs were obtained from the Michigan Department of Transportation (MDOT) Pavement Management System (PMS) database, construction records, and previous studies conducted in Michigan. Models were calibrated outside the Pavement-ME using no sampling and bootstrapping resampling techniques. For validation of these models, traditional and repeated split sampling were used, with 70% of the sections used for calibration and the remaining 30% for validation. Bootstrapping and repeated split sampling provide a distribution of calibration coefficients and

error terms instead of single-point estimates. Standard deviation equations for all performance models were calibrated to incorporate reliability using local performance and prediction data (5).

2.8.1.5 Oregon

The Oregon Department of Transportation (ODOT) conducted a study in 2013 to implement PMED for the overlay design of existing pavements (23). Forty-four pavement sections were selected from all over Oregon with three different climate regions (a) Coastal, (b) valley, and (c) eastern. Rutting, alligator (bottom-up) cracking, longitudinal (top-down) cracking, and thermal cracking models for HMA overlays of existing pavements were calibrated according to Oregon state's local conditions. Essential traffic and climatic input values were available to be used in pavement ME; however, material input properties were missing due to the non-availability of complete data. The researcher used default values at input level 3 for indirect tensile strength and creep compliance of the HMA layer. Sensitivity analysis was carried out to observe the effect of HMA properties on the distress predictions by PMED. For sensitivity analysis, HMA material properties like HMA overlay thickness, unbound layers' thickness, air voids, and effective binder content were varied within a limit defined by the researcher team, and distress predictions were evaluated for all four prediction models as described earlier. Researchers found that thermal and bottom-up cracking models are insensitive to overlay properties. Local calibration was performed using PMED software Darwin M-E (Version 1.1). Standard error of estimates (SSE) and bias were used as criteria for calibration, and the nonlinear approach using the Microsoft Excel solver function was used to minimize both criteria. The results of the study are the following:

a. The Drawin M-E overpredicted rutting, whereas alligator cracking and transverse cracking were underestimated compared to measured cracking values, while longitudinal cracking showed high variability.
b. Alligator cracking, longitudinal cracking, and rutting yielded acceptable results from local calibration; however, thermal cracking and longitudinal cracking showed high variability between measured and predicted distresses.
c. Due to the error in measurements, the delineation between alligator and longitudinal cracking remained a challenge.

d. Researchers recommended additional sites for calibration and more input data availability, especially Level 1, to reduce the input error, substantially improving the calibration results.

2.8.1.6 Colorado

Colorado DOT and the Colorado Asphalt Pavement Association (CAPA) initiated a project in 2001 to make a road map for implementing PMED in Colorado (28). CDOT carried out a study in 2013 to implement PMED for calibration of performance prediction models for new and rehabilitated pavements in Colorado using PMED version 1.0. The study's primary objectives were to address routine design problems for new and rehabilitated pavements and conduct forensic analysis to obtain and assemble a database encompassing guidelines of the new PMED user guide. A total of 126 pavement projects of new and rehabilitated pavements were selected for this study from LTPP and Colorado DOT's PMIS database; however, all sections were analyzed as new or reconstructed pavements instead of rehabilitation design. This study calibrated all four models (alligator cracking, rutting, transverse cracking, and IRI) for new and rehabilitated flexible pavements. The goodness of fit and bias are used as the criteria for verification of local calibration. R^2 and standard error of estimates (S_e) were used to decide reasonable goodness of fit, and the absence of bias was determined based on hypothesis testing. A detailed sensitivity analysis was performed using the One-at-a-time (OAT) approach to appraise the impact of the input's variation in the calibration/ validation process of PMED performance prediction models. The sensitivity analysis concluded that PMED calibration predicted reasonable distress and smoothness for both flexible and JPCP designs. The study also included comparing two design methodologies: the 1993 AASHTO Pavement Design Guide/1998 Rigid Pavement Supplemental Guide and the new locally calibrated PMED design. Seven projects with low traffic volumes were selected for the subject comparison, for which results showed acceptable correlations between both design methodologies with a variation of $\pm$1 inch; however, a significant difference was observed for high traffic volumes.

2.8.1.7 Virginia

VDOT recently conducted a PMED implementation study to design overlays over flexible, rigid, and composite pavements (22, 37). The study evaluated different input levels along with the need for separate local calibration factors for three types of rehabilitation options: (a) HMA over HMA, (b) HMA over jointed plain concrete pavement (JPCP), and (c) HMA over continuously

reinforced concrete pavement (CRCP) using the PMED software v2.2.6. Standard error of estimates (Se) and bias were used as criteria to evaluate the goodness of fit for the calibrated model. The conclusions of the study are the following:

a. The study emphasized the overall condition assessment of the existing pavement for the rehabilitation designs.
b. The backcalculated modulus (Level 1) predicted higher distresses than Level 2 inputs, mainly due to higher damage prediction of the AC layer using backcalculated damage modulus than damage prediction by fatigue cracking (%).
c. Coring is recommended for assessing the damage in the existing HMA layers and a detailed forensic evaluation as part of the rehabilitation design for restorative maintenance projects.
d. This study also recommended that the reflection cracking issue for the AC overlay of JPCP be addressed outside of the Pavement-ME design.
e. Further assessment is required for bottom-up and reflection cracking models as the reflection cracking model predicts very high early cracking compared to measured cracking values.

2.8.1.8 Louisiana

Louisiana conducted its first research study in 2012 to implement PMED as designing software, which focused on only new and full-depth rehabilitated flexible pavements, followed by another study in 2016 (27, 38, 39). A total of 162 pavement sections were selected for this study, including flexible pavements with AC base, rubblized PCC base, crushed stone base, soil cement base, and stabilized base; rigid pavements with unbound granular base, stabilized base, and asphalt mixture blanket and HMA overlay on top of existing flexible pavements. Only 33 sections of AC overlay over existing flexible pavement were considered, as in Louisiana AC over existing flexible layer is the most common pavement rehabilitation technique. The rehabilitation projects included AC over soil cement, AC over AC over unbound base, and AC over AC over PCC. AC over rubblized PCC pavements were designed as new pavements. Since limited data sites from Louisiana were included in the development of PMED by the NCHRP study, it was deemed necessary to develop its design criterion for distress and IRI for local calibration of PMED models per Louisiana conditions. Table 2-29 shows the recommended

criteria. Sensitivity analysis was also conducted to observe and evaluate the impact of inputs on predicted distress and IRI.

Bottom-up fatigue cracking and rutting models were calibrated for new flexible pavements; however, only the reflective cracking model was calibrated for rehabilitation, and calibration coefficients of new flexible pavements were applied to overlay design in Louisiana. The calibration and verification process of models showed that PMED under-predicts the fatigue cracking and over-predicts the rutting and IRI for flexible pavements.

Table 2-29: Recommended design criteria of ME pavement design for Louisiana

Pavement Type	Distress	Interstate	Primary	Secondary
New AC and AC overlay	Reliability Level, %[a]	95	90	80
	Alligator cracking, %	15	25	35
	Total rutting, in.	0.40	0.50	0.65
	AC rutting, in.[b]	0.40	0.50	0.65
	Transverse cracking, ft/mi	500	700	700
	Reflective cracking, %	15	25	35
	IRI, in./mi.	160	200	200

Note: a. Reliability level does not apply to reflective cracking; b. AC rutting uses the same criteria as total rutting.

For overlay design, transverse cracking was considered reflective cracking instead of thermal cracking and was over-predicted. Overall calibration worked reasonably for all selected projects; however, it was noted that predicted rutting in overlay design was mainly due to overlay AC layer rutting; it was assumed that stable settlement conditions had prevailed for the underlying subgrade. The study concluded that PMED over-predicts the rutting and under-predicts fatigue cracking for overlay design similar to the new flexible design. Reflective cracking was over-predicted. Due to a software bug, the cement soil layer in the rehabilitation design was modeled as a crushed stone layer with a modulus of 25,000 psi. The study also found that design thickness for overlay design was comparable with the 1993 AASHTO design guide with $\pm$0.5 inches of variability.

2.8.1.9 Tennessee

The Tennessee Department of Transportation validated the PMED models using their typical pavement designs and compared measured and predicted pavement performances (40-42). The validation effort included 19 pavement sections with HMA overlays of PCC and HMA pavements; however, all sections were analyzed as new or reconstructed pavements instead of

rehabilitation designs. The study observed that Level 1 inputs gave reasonable rutting predictions but over-predicted base and subbase rutting with Level 3 inputs. In a recent study, Tennessee DOT locally calibrated the distresses and roughness models using measured distresses, maintenance activities, and traffic data for interstate roads. Using the PMED flexible pavement rehabilitation analyses, reflective cracking was observed as the primary contributor to the total predicted cracking, irrespective of the thickness of the pavement structure and traffic level. A pavement with more than two overlays becomes very thick, resulting in extremely low alligator cracking prediction despite a large amount of cracking observed in the field. It was suggested that a procedure that considers the loss in thickness according to the age and structural condition of the pavements could help improve the alligator cracking predictions.

The following section presents the formulation of transfer functions for flexible pavement models and the local calibration coefficients for different states.

2.8.1.10 Fatigue Bottom-up cracking

Bottom-up cracking is a load-related distress resulting from repeated axle loads. It originates at the bottom of the asphalt concrete (AC) layer and progresses upward to the surface. The total cumulative damage (DI) can be estimated by summing up the cumulative damage computed using Miner's law (43), as shown in Equation 2-18.

$$DI = \sum(\Delta DI)_{j,m,l,p,T} = \sum\left(\frac{n}{N_{f-HMA}}\right)_{j,m,l,p,T} \quad (2\text{-}18)$$

where,

n = number of actual axle load applications within a specific time period; j = axle load-interval; m = axle type (single, tandem, tridem, quad); l = truck type classified in the PMED; p = month; T = median temperature for five temperature quintiles used in PMED; $N_{f\text{-}HMA}$ = the allowable number of axle load applications, can be computed using Equation 2-19.

$$N_{f-HMA} = C \times k_1 \times C_H \times \beta_{f1}(\varepsilon_t)^{-k_2\beta_{f2}}(E_{HMA})^{-k_3\beta_{f3}} \quad (2\text{-}19)$$

where,

ε_t = tensile strain at critical AC locations; E_{HMA} = dynamic modulus (E*) of the Hot mix asphalt (HMA), psi; *k1, k2, k3* = laboratory regression coefficients, and β_{f1}, β_{f2}, β_{f3} = local or field calibration constants; C = Adjustment factor (laboratory to the field) as shown in Equation 2-20 and Equation 2-21.

$$C = 10^{M} \tag{2-20}$$

$$M = 4.84\left(\frac{v_{be}}{V_a + V_{be}} - 0.69\right) \tag{2-21}$$

where,

V_{be} = effective binder content by volume, percent; V_a = In-situ air voids in the HMA mixture (%); C_H = thickness correction factor for bottom-up cracking as shown in Equation 2-22.

$$C_H = \frac{1}{0.000398 + \frac{0.003602}{1 + e^{(11.02 - 3.49H_{HMA})}}} \tag{2-22}$$

where,

H_{HMA} = AC layer thickness

Once the cumulative damage is calculated, the bottom-up fatigue cracking (%) can be estimated using the transfer function given in Equation 2-23.

$$FC_{\text{Bottom}} = \left(\frac{1}{60}\right)\left(\frac{C_4}{1 + e^{C_1 C_1^* + C_2 C_2^* \log(DI_{\text{Bottom}} \cdot 100)}}\right) \tag{2-23}$$

where,

FC_{Bottom} = Bottom-up fatigue cracking (in the percentage of area); DI_{Bottom} = cumulative damage at the bottom of the AC layer; C_1, C_2, C_4 = Transfer function coefficients where C_2 is a function of thickness for HMA thickness between 5 and 12 inches.

C_1* and C_2* can be determined using Equation 2-24 and Equation 2-25.

$$C_1^* = -2C_2^* \tag{2-24}$$

$$C_2^* = -2.40874 - 39.748(1 + H_{HMA})^{-2.856} \tag{2-25}$$

Table 2-30 summarizes the local calibration coefficients among several states.

2.8.1.11 Top-down cracking

Top-down or longitudinal cracking is a load-related distress where the crack initiates at the pavement surface and propagates downwards due to repeated axle loads. It appears in the form of cracks parallel to the wheel path and starts at the surface of the AC layer.

Old model: The damage calculation for top-down cracking is the same as bottom-up cracking for the old model except for the thickness correction factor and the transfer function, as shown in Equations 2-26 and 2-27.

$$C_H = \frac{1}{0.01 + \frac{12.00}{1 + e^{(15.676 - 2.8186H_{\text{HMA}})}}} \tag{2-26}$$

$$FC_{\text{Top}} = 10.56\left(\frac{C_3}{1+e^{C_1-C_2Log(DI_{\text{Top}})}}\right) \quad (2\text{-}27)$$

where,

FC_{Top} = Top-down fatigue cracking (in ft/mile); DI_{Top} = cumulative damage at the top of the AC layer; C_1, C_2, C_3 = Transfer function coefficients.

Table 2-30: Local calibration coefficients for bottom-up cracking

States	C_1	C_2	C_4
Kansas (R)	-	-	-
Iowa (N)*	2.44	0.18	6000
Missouri (N)**	-0.31	hac<5: 1.367 5<hac<12: 0.867+0.1*h_{ac} Hac>12: 2.067	6000
Michigan (R)	0.67	0.56	6000
Oregon (R)	0.56	0.225	6000
Colorado (N)**	0.07	2.35	6000
Virginia (R)	-	-	-
Louisiana (R)	0.892	0.892	6000
Tennessee (N)**	1.023	0.045	6000
Pavement-ME v2.6	1.31	hac<5: 2.1585 5<hac<12: (0.867+0.2583*h_{ac})*1 Hac>12: 3.9666	6000

N = New; R = Rehabilitation;

* = HMA over JPCP designed as new; ** = HMA over HMA designed as new

New model: The top-down cracking model is based on fracture mechanics concepts (44). It is expressed in percentage rather than ft./mile. The model involves crack initiation and propagation [based on Paris' law (45)]. Crack initiation is a crack length of 7.5mm (0.3 inches). Equation 2-28 shows the time to crack initiation formulated using regression over longitudinal and alligator cracking data from the LTPP database.

$$t_0 = \frac{\mathrm{K}_{L1}}{1+e^{\mathrm{K}_{L2}\times 100\times(\mathrm{a}_0/2\mathrm{A}_0)+\mathrm{K}_{L3}\times \mathrm{HT}+\mathrm{K}_{L4}\times LT+K_{L5}\times \log_{10}\mathrm{AADTT}}} \quad (2\text{-}28)$$

where,

t_0 = Time to crack initiation, days; H_T = Annual number of days above 32°C; L_T = Annual number of days below 0°C; *AADTT* = Annual average daily truck traffic (initial year); K_{L1}, K_{L2}, K_{L3}, K_{L4}, K_{L5}= Calibration coefficients for time to crack initiation; $a_0/2A_0$ = Energy parameter that can be calculated by Equation 2-29.

$$\frac{a_0}{2A_0} = 0.1796 + 1.5\text{x}10^{-5}E_1 - 0.69m - 7.1691.5\text{x}10^{-4}H_a \quad (2\text{-}29)$$

where,

E_1 and m = Relaxation modulus parameters; H_a = HMA thickness;

The top-down cracking is expressed in percentage using the transfer function, as shown in Equation 2-30.

$$L(t) = L_{MAX}e^{-\left(\frac{C_1\rho}{t-C_3t_0}\right)^{C_2\beta}} \quad (2\text{-}30)$$

where,

$L(t)$ = Top-down cracking expressed as total lane area (%); L_{MAX} = Maximum area of top-down cracking (%) – a value of 58% is assumed; t = Analysis month in days; ρ = Scale parameter for the top-down cracking curve as shown in Equation 2-31.

$$\rho = \alpha_1 + \alpha_2 \times \text{ Month} \quad (2\text{-}31)$$

β = Shape parameter for the top-down cracking curve as shown in Equation 2-32.

$$\beta = 0.7319 \times (\log_{10} \text{ Month })^{-1.2801} \quad (2\text{-}32)$$

where,

α_1 and α_2 are functions of the climatic zone (wet freeze, wet non-freeze, dry freeze, dry non-freeze).

Table 2-31 Summarizes the local calibration coefficient of the top-down cracking model.

Table 2-31: Local calibration coefficients for top-down cracking

States	C_1	C_2	C_3
Kansas (R)	1.87	0.12	1000
Iowa (N)*	2.2	2.0	36000
Missouri (N)**	-	-	-
Michigan (R)	2.97	1.2	1000
Oregon (R)	1.435	0.097	1000
Colorado (N)**	-	-	-
Virginia (R)	-	-	-
Tennessee (N)**	6.44	0.27	204.54
Pavement-ME	7	3.5	1000

N = New; R = Rehabilitation;

* = HMA over JPCP designed as new; ** = HMA over HMA designed as new

2.8.1.12 Transverse (thermal) cracking model

Thermal cracking is caused by surface temperature fluctuations leading to the contraction of Hot Mix Asphalt (HMA) material. This contraction causes volume changes and stresses

development, resulting in thermal cracks under constrained conditions. A thermal crack forms when the tensile stresses within the HMA layers reach or exceed the material's tensile strength. These initial cracks propagate through the HMA layer with each subsequent thermal cycle. The amount of crack propagation induced by a given thermal cooling cycle is predicted using the Paris law of crack propagation. Experimental results indicate that reasonable estimates of *A* and *n* can be obtained from the indirect tensile creep-compliance and tensile strength of the HMA per Equations 2-33 and 2-34.

$$\Delta C = A(\Delta K)^n \quad (2\text{-}33)$$

where;

ΔC = Change in the crack depth due to a cooling cycle

ΔK = Change in the stress intensity factor due to a cooling cycle

A, n = Fracture parameters for the HMA mixture

$$A = k_t \beta_t 10^{[4.389 - 2.52 Log(E_{HMA} \sigma_m \eta)]} \quad (2\text{-}34)$$

where;

η = $0.8\left[1 + \frac{1}{m}\right]$

k_t = Regression coefficient determined through field calibration

E_{HMA} = HMA indirect tensile modulus, psi

σ_m = Mixture tensile strength, psi

m = The m-value derived from the indirect tensile creep compliance curve measured in the laboratory

β_t = Local or mixture calibration factor

The stress intensity factor, *K*, has been incorporated in the Pavement-ME through a simplified equation developed from theoretical finite element studies using the model shown in Equation 2-35.

$$K = \sigma_{tip}(0.45 + 1.99(C_0)^{0.56}) \quad (2\text{-}35)$$

where;

σ_{tip} = Far-field stress from pavement response model at a depth of crack tip, psi

C_o = Current crack length, feet

Equation 2-36 shows the transfer function for transverse cracking in the Pavement-ME.

$$TC = \beta_{t1} N(z) \left[\frac{1}{\sigma_d} \log \left(\frac{C_d}{H_{HMA}} \right) \right] \quad (2\text{-}36)$$

where,

TC = Observed amount of thermal cracking, ft/500ft

β_{t1} = Regression coefficient determined through global calibration (400)

N[z] = Standard normal distribution evaluated at [z]

σ_d = The standard deviation of the log of the depth of cracks in the pavement (0.769), in

C_d = Crack depth, in;

H_{HMA} = The thickness of HMA layers, inches

Table 2-32 summarizes the modified local calibration coefficients for the various States.

Table 2-32: Local calibration coefficients for the thermal cracking model

Calibration coefficient	Level 1 (K)	Level 2 (K)	Level 3 (K)
Missouri (N)**	0.61	-	-
Oregon (R)	-	-	10
Colorado (N)**	7.5	-	-
Michigan (R)	0.75	-	-
Iowa (N)*	-	-	2.7
Pavement-ME	$3 \times 10^{-7} \times MAAT^{4.0319}$	$3 \times 10^{-7} \times MAAT^{4.0319}$	$3 \times 10^{-7} \times MAAT^{4.0319}$

N = New; R = Rehabilitation;

* = HMA over JPCP designed as new; ** = HMA over HMA designed as new

2.8.1.13 Rutting model

Due to axle loads, rutting is the total accumulated plastic strain in different pavement layers (AC, base/sub-base, and subgrade). It is calculated by summing up the plastic strains at the mid-depth of individual layers accumulated for each time increment. Equation 2-37 shows the permanent plastic strain for the AC layer.

$$\Delta_{p(HMA)} = \varepsilon_{p(HMA)} h_{HMA} = \beta_{1r} k_z \varepsilon_{r(HMA)} 10^{k_{1r}} T^{k_{2r}\beta_{2r}} N^{k_{3r}\beta_{3r}} \quad (2\text{-}37)$$

where,

$\Delta_{p(HMA)}$ = permanent plastic deformation in the AC layer; $\varepsilon_{p(HMA)}$ = accumulated permanent or plastic axial strain in the AC layer/sublayer; $\varepsilon_{r(HMA)}$ = resilient or elastic strain calculated by the structural response model at the mid-depth of each AC sublayer; $h_{(HMA)}$ = thickness of the AC layer/sublayer; N = number of axle load repetitions; T =Pavement temperature; k_z = depth confinement factor; k_{1r}, k_{2r}, k_{3r} = global field calibration parameters; β_{1r}, β_{2r}, β_{3r}, = local or mixture field calibration constants.

The permanent plastic strain can be expressed for the unbound layers, as shown in Equation 2-38.

$$\Delta_{p(soil)} = \beta_{s1} k_{s1} \varepsilon_v h_{soil} \left(\frac{\varepsilon_o}{\varepsilon_r}\right) e^{-\left(\frac{\rho}{n}\right)^{\beta}} \quad (2\text{-}38)$$

where;

$\Delta_{p(Soil)}$ = permanent plastic deformation for the unbound layer/sublayer; ε_o = intercept determined from laboratory repeated load permanent deformation tests; n = number of axle load applications; ε_r = resilient strain imposed in laboratory tests to obtain material properties ε_o, β, and ρ; ε_v = average vertical resilient or elastic strain in the layer/sublayer and calculated by the structural response model; h_{soil} = unbound layer thickness; k_{s1} = global calibration coefficients (different for granular and fine-grained material); β_{s1} = local calibration constant for rutting in the unbound layers (base or subgrade).

The total rutting is calculated based on Equation 2-39 below:

$$Rut\ Depth_{Total} = \Delta_{HMA} + \Delta_{Base/subbase} + \Delta_{Subgrade} \quad (2\text{-}39)$$

The summary of the local calibration coefficients for total rutting model for the different states is presented below.

Table 2-33: Local calibration coefficients for the rutting model

States	β_{1r}	β_{2r}	β_{3r}	β_{gb}	β_{sg}
Kansas (R)	0.36	-	-	-	-
Iowa (N)*	1	1.01	1	0.001	-
Missouri (N)**	0.899	-	-	1.0798	0.9779
Michigan (R)	0.9453	1.3	0.7	0.0985	0.0367
Oregon (R)	1.48	1	0.9	0	0
Colorado (N)**	1.34	1	1	0.4	0.84
Lousiana (R)	0.8	-	0.85	-	0.4
Pavement-ME v2.6	0.4	0.52	1.36	1	1

N = New; R = Rehabilitation;

* = HMA over JPCP designed as new; ** = HMA over HMA designed as new

2.8.1.14 IRI model (flexible pavements)

IRI is a measure of ride quality provided by a pavement surface and affects the vehicle operation cost, safety, and comfort of the driver. The IRI model is based on findings from multiple studies showing that IRI at any age is a function of the initial construction ride quality and the development of different distresses over time that impacts the ride quality. IRI can be formulated

using the initial IRI and distresses (fatigue cracking, transverse cracking, and rutting), as shown in Equation 2-40.

$$IRI = IRI_o + C1(RD) + C2(FC_{\text{Total}}) + C3(TC) + C4(SF) \quad (2\text{-}40)$$

where,

IRI_o = initial IRI at construction; FC_{Total} = percent area of alligator, longitudinal, and reflection cracking in the wheel path; TC = length of transverse cracking (including the reflection of transverse cracks in existing AC pavements); RD = average rut depth; $C1$, $C2$, $C3$, $C4$ = Calibration coefficients; SF = site factor, which can be expressed as shown in Equation 2-41 to Equation 2-43.

$$SF = (\text{Frost} + \text{Swell}) \times Age^{1.5} \quad (2\text{-}41)$$

$$\text{Frost} = \text{Ln}[(\text{Rain} + 1) \times (FI + 1) \times P_4] \quad (2\text{-}42)$$

$$\text{Swell} = \text{Ln}[(\text{Rain} + 1) \times (FI + 1) \times P_{200}] \quad (2\text{-}43)$$

where,

SF = Site factor; Age = Pavement age (years); FI = Freezing index; $Rain$ = Mean annual rainfall; P_4 = Percent subgrade material passing No. 4 sieve; P_{200} = Percent subgrade material passing No. 200 sieve.

Table 2-34 presents the adjusted calibration coefficients in different states.

Table 2-34: Local calibration coefficients for the IRI model

States	C1	C2	C3	C4
Kansas (R)	40.5 – 43.5	0.34 – 0.41	0.0074 – 0.0082	0.001 – 0.002
Iowa (N)*	25	0.4	0.008	0.019
Missouri (N)**	58.9	0.3	0.0072	0.0129
Michigan (R)	50.3720	0.4102	0.0066	0.0068
Colorado (N)**	35	0.3	0.02	0.019
Louisiana (R)	40	0.4	0.008	0.015
Pavement-ME v2.6	40	0.4	0.008	0.015

N = New; R = Rehabilitation;

* = HMA over JPCP designed as new; ** = HMA over HMA designed as new

2.8.1.15 Reflective Cracking model

Old model: The transverse reflection cracking model originally was empirical in nature. The percentage of the area of cracks is predicted by the empirical equation as a function of time using a sigmoidal function represented by Equation 2-44.

$$RC = \frac{1}{1 + e^{a(c) + bt(d)}} \quad (2\text{-}44)$$

where,

RC = Percent of cracks reflected; *t* = Time (years); *a,b* = Regression fitting parameters defined through the calibration process and depend upon effective HMA thickness as shown in Equations 2-45 and 2-46; *c,d* = User-defined cracking progression parameter.

$$a = 3.5 + 0.75\left(H_{eff}\right) \tag{2-45}$$

$$b = -0.688684 - 3.37302\left(H_{eff}\right)^{-0.915469} \tag{2-46}$$

H_{eff} = Effective HMA overlay thickness.

New model: The new mechanistic-based transverse reflection cracking model, developed under the NCHRP 1-41 project, replaced the empirical reflection cracking model and has recently been integrated into the PMED software *(46)*. The new mechanistic model combines finite element and fracture mechanics approaches based on the Paris Law *(47)*. The newly developed reflection cracking model also considers incremental crack growth due to flexure, shear, and thermal stress in the overlaid AC layer. Equations 2-47 to 2-53 show the transverse reflective crack model.

$$\Delta C = k_1 * \Delta_{Bending} + k_2 * \Delta_{Shearing} + k_3 * \Delta_{Thermal} \tag{2-47}$$

$$\Delta_{Bending} = A(SIF)_B^n \tag{2-48}$$

$$\Delta_{Shearing} = A(SIF)_S^n \tag{2-49}$$

$$\Delta_{Thermal} = A(SIF)_T^n \tag{2-50}$$

$$\Delta D = \frac{c_1 k_1 * bending + c_2 k_2 * shearing + c_3 k_3 * thermal}{h_{OL}} \tag{2-51}$$

$$D = \sum_{i=1}^{N} \Delta D \tag{2-52}$$

$$RCR = \left(\frac{100}{C_4 + e^{C_5 \log D}}\right) * EX_{CRK} \tag{2-53}$$

where,

ΔC = Crack length increment, in; ΔD = Increment damage ratio; $\Delta_{Bending}$, $\Delta_{Shearing}$, $\Delta_{Thermal}$, = Crack length increment due to bending, shearing, and thermal loading; k_1,k_2,k_3,c_1,c_2,c_3 = Calibration factors; *A, n* = HMA material fracture properties; *N* = Total number of days; $(SIF)_B$, $(SIF)_S$, $(SIF)_T$ = Stress intensity factor due to bending, shearing, and thermal loading; *D* = Damage ratio; h_{OL} = Overlay thickness, in; *RCR* = Cracks in underlying layers, reflected, %;

EX_{CRK} = Transverse cracks in underlying layers ft/mile (transverse cracking); Alligator cracking in underlying layers, % lane area (alligator cracking).

Table 2-35 presents the adjusted calibration coefficients in different states.

Table 2-35: Summary of design thresholds for flexible pavements

States	Old Model		New Model	
	c	d	C_4	C_5
Missouri (N)**	-	-	254.4	-261.6
Colorado (N)**	2.5489	1.2341	-	-
Arizona (N)	2.7 if h_{eff} < 3-in. 4.0 if h_{eff} > 3-in.	1	-	-
Kansas (R)	-	-	251-253	(-2.45) – (-2.58)
Louisiana (R)	0.72	0.30	-	-

N = New; R = Rehabilitation;

* = HMA over JPCP designed as new; ** = HMA over HMA designed as new

2.8.2 Local Calibration Efforts for Rigid Pavement Overlays

The following section shows the calibration efforts by other states.

2.8.2.1 Iowa

The local calibration effort for the Pavement-ME models in Iowa was conducted using PMED version 1.1. Faulting was under-predicted, and transverse cracking and IRI were over-predicted using the national coefficients. Multiple runs calibrated faulting and fatigue cracking in Pavement-ME, whereas transverse cracking and IRI were calibrated using MS Excel Solver. Predictions for all models were significantly improved after calibration.

In 2013, overall efforts were made to calibrate the PMED performance models with the local conditions of Iowa (34). A total of 35 sections of new JPCP and 60 of HMA over JPCP (composite) were selected for the study. This study concluded that locally calibrated transverse cracking, faulting, and IRI models yielded better predictions than global models for JPCP pavements. Iowa DOT PMIS does not differentiate between thermal and reflection cracking for composite pavements. Iowa DOT conducted a recalibration study in 2015 with the same sections as used in 2013 but with upgraded AASHTOWare PMED version 2.1.24 to compare results of national and previous calibrations of PMED performance models (35). The study concluded that mean joint faulting, transverse cracking, and IRI models for JPCP pavements yielded improved predictions compared to global and previously calibrated predictions. Iowa DOT could calibrate the thermal cracking model with acceptable accuracy, as they considered measured transverse cracking data as thermal cracking only.

2.8.2.2 Missouri

The MoDOT conducted two studies in 2009 to imply and calibrate the PMED designs per Missouri's local conditions *(26, 36)* using PMED version 1.0. In continuation of the efforts, MoDOT conducted a recent study to recalibrate the pavement distresses and IRI prediction models for new and rehabilitated flexible and rigid pavements in Missouri using PMED version 2.5.5. All three models for rigid pavement were calibrated.

The thermal cracking model for MAAT<57℉ and the transverse reflection cracking models were also calibrated simultaneously. As 80% of the projects reported have zero percent transverse slab cracking, a non-regression approach was used to verify the model's accuracy. The study recommended that comprehensive calibration and validation is only possible once measured damage values are in the range of 0.01 to 1.0, so the creation of a confusion matrix represented in Table 2-36 based upon predicted and measured cracking was used to validate the accuracy of models by Equation 2-54.

$$Accuracy = \frac{TP + TN}{TP + TN + FP + FN} \quad (2\text{-}54)$$

where:

TP = true positive, that is, observation is greater than or equal to 1 percent, and the predicted is greater than or equal to 1 percent; FN = false negative; observation is greater than or equal to 1 percent but is predicted as less than 1 percent; TN = true negative, observation is less than 1 percent, and the predicted is less than 1 percent; FP = false positive, observation is less than 1 percent but predicted is greater than or equal to 1 percent.

Table 2-36: Comparisons matrix for new JPCP and unbonded overlays

Predicted transverse cracking	Measured cracking		
	< 1 percent	>= 1 percent	
< 1 percent	22	5	
>= 1 percent	0	0	
Predicted transverse faulting	H (Faulting > 0.005)	L (Faulting < 0.005)	Total
H (faulting > 0.005)	9	5	14
L (faulting < 0.005)	13	27	40
Total	22	32	54

The conclusions of the study were:

a. Due to the absence of significant distress in rigid pavements, model accuracy was assessed with a non-regression classification approach.

b. Reduction in slab cracking was noted with an increase in PCC thickness and flexural strength of PCC, reducing Coefficient of Thermal Expansion (CTE), and adding edge support.
c. Larger dowel diameter values and lower CTE values yielded lower joint faulting.
d. The widened slab also reduced the distresses and IRI for JPCP, an un-bonded overlay of JPCP.
e. The team recommended using Level 1 input data as maximum as possible.

2.8.2.3 Michigan

Haider et al. conducted a study to calibrate the Pavement-ME models for new JPCP and un-bonded overlay over JPCP pavements in Michigan (5). A total of 29 reconstructed JPCP sections and 16 un-bonded overlays over JPCP sections were selected for this project. For transverse cracking and IRI models, the calibration was performed outside the Pavement ME and for the joint faulting model, the Pavement-ME was run every time by changing the coefficient (Only C1 was optimized by keeping other coefficients fixed to the global value).

2.8.2.4 Kansas

As mentioned earlier, KDOT published a research study for the implementation of PMED approach to design rehabilitated pavements (21). Eighteen sections of AC over JPCP were used for calibration in this study. The research team tried to model AC over JPCP within the limitations of the maximum number of HMA layers over the existing pavement layers as specified by the PMED user guide (8). AC rutting, transverse cracking (thermal + reflection), load-related cracking, and IRI models for AC over JPCP were calibrated in this study. PMED does not predict any thermal cracking for KDOT conditions, so only reflection cracking model coefficients were calibrated, and all load-related cracking was modeled as top-down cracking for AC over JPCP pavement sections.

Local calibration improved the prediction accuracy of the rutting, transverse cracking, load-related cracking, and IRI models for AC over the JPCP pavement section. However, local calibration of the transverse cracking model for both rehabilitation types resulted in higher S_e because AC thermal cracking model was calibrated at global values, as KDOT does not distinguish between reflection and thermal cracking. The top-down cracking model showed high accuracy with minimum bias and S_e compared to globally calibrated values; however, S_e was high due to variability in data collection. Distress data on all sections overlaid before 2013 were

collected manually, which made it responsible for high data variability. Moreover, KDOT considers all load-related cracking as top-down, so it was considered another factor toward high S_e. The study has the following important recommendations:

a. Accurate data collection for pavement layer properties.
b. Collection of cores to distinguish between top-down and bottom-up fatigue cracking.
c. Efforts to reduce measurement errors in distress measurement and data collection to improve the accuracy of local calibration.
d. Rutting in each layer is to be incorporated to achieve better results from local calibration of the rutting model.

2.8.2.5 Louisiana

Louisiana state conducted its first research study in 2012 to implement PMED as designing software, which focused on only new and full-depth rehabilitated flexible pavements, followed by another study in 2016 (27, 38, 39). A total of 162 pavement sections were selected for this study, including flexible pavements with AC base, rubblized PCC base, crushed stone base, soil cement base, and stabilized base; rigid pavements with unbound granular base, stabilized base, and asphalt mixture blanket and HMA overlay on top of existing flexible pavements. AC over rubblized PCC pavements were designed as new pavements, and the resilient modulus for rubblized PCC was taken as 200 ksi. Since limited data sites from Louisiana were included in the development of PMED by the NCHRP study, it was deemed necessary to develop its design criterion for distress and IRI for local calibration of PMED models as per Louisiana conditions. Sensitivity analysis was also conducted to observe and evaluate the impact of inputs on predicted distress and IRI. The key findings of sensitivity analysis are:

a. Coefficient of thermal expansion (CTE), PCC slab thickness, joint spacing, climate location, and PCC strength are critical factors for JPCP performance.
b. Base thickness, base modulus, and subgrade modulus were found to be insignificant for rigid pavements.
c. Total cracking is only sensitive to existing pavement conditions for overlay design.
d. Overlay thickness, existing rutting, subgrade modulus, and overlay AC properties are major influencers of rutting and IRI models for overlay design.

The transverse cracking, joint faulting, and IRI models for new rigid pavements were calibrated; however, only the reflective cracking model was calibrated for rehabilitation, and

calibration coefficients of new flexible pavements were applied to overlay design in Louisiana. As Louisiana state rarely uses PCC overlays, this study was carried out for only AC overlay, and local calibration was done for the new PCC design. The calibration and verification process of models showed that PMED over-predicted transverse slab cracking and IRI and under-predicted faulting.

The following is a summary of transfer functions for the Pavement-ME models applicable to rigid pavements and a review of local calibration coefficients for various states.

2.8.2.6 Transverse Cracking Model

Transverse slab cracking in the Pavement-ME is calculated as the percentage of slabs cracked, including all severity levels. The mechanism involves independently predicting the bottom-up and top-down cracking and utilizing a probabilistic relationship to combine both, eliminating the possibility of both co-occurring. The fatigue damage for both bottom-up and top-down is defined using Miner's law as given in Equation 2-55.

$$DI_F = \sum \frac{n_{i,j,k,l,m,n,o}}{N_{i,j,k,l,m,n,o}} \quad (2\text{-}55)$$

where,

DI_F = total fatigue damage (bottom-up or top-down); $n_{i,j,k,l,m,n,o}$ = actual load applications applied at an age *i*, month *j*, axle type *k*, load level *l*, the equivalent temperature difference between top and bottom PCC surfaces *m*, traffic offset path *n*, and hourly truck traffic fraction *o;* $N_{i,j,k,l,m,n,o}$ = allowable number of load applications applied at an age *i*, month *j*, axle type *k*, load level *l*, the equivalent temperature difference between top and bottom PCC surfaces *m*, traffic offset path *n*, and hourly truck traffic fraction *o.*

The allowable number of load applications is a function of PCC strength and applied stress and is calculated based on Equation 2-56.

$$\log\left(N_{i,j,k,l,m,n,o}\right) = C_1 \cdot \left(\frac{MR_i}{\sigma_{i,j,k,l,m,n,o}}\right)^{C_2} \quad (2\text{-}56)$$

where,

MR_i = Modulus of rupture of the PCC slab at the age *i;* $\sigma_{i,j,k,l,m,n}$ = applied stress at the age *i*, month *j*, axle type *k*, load level *l*, the equivalent temperature difference between top and bottom PCC surface *m*, traffic offset path *n*, and hourly truck traffic fraction *o;* C_1, C_2 = fatigue life calibration coefficients.

The fraction of slabs cracked is predicted using Equation 2-57 for both bottom-up and top-down cracking.

$$CRK = \frac{1}{1 + C_4(DI_F)^{C_5}} \quad (2\text{-}57)$$

where,

CRK = predicted fraction of bottom-up or top-down cracking.

Once the bottom-up and top-down cracking is estimated, the percentage of slabs cracked is calculated using Equation 2-58.

$$TCRACK = \left(CRK_{\text{Bottom-up}} + CRK_{\text{Top-down}} - CRK_{\text{Bottom-up}} \cdot CRK_{\text{Top-down}}\right) \cdot 100 \quad (2\text{-}58)$$

where,

TCRACK = total transverse cracking (percentage of slabs cracked with all severities); $CRK_{Bottom\text{-}up}$ = predicted fraction of bottom-up transverse cracking; $CRK_{Top\text{-}down}$ = predicted fraction of top-down transverse cracking.

Table 2-37 summarizes the transverse cracking model local calibration coefficients in different states. As discussed earlier, 80% of the projects showed zero percent measured transverse slab cracking, so a non-regression approach was used to calibrate the transverse cracking model using Equation 2-53. The equation resulted in 81.4% model accuracy for the transverse cracking model.

Table 2-37: Local calibration coefficients for the rigid transverse cracking model

States	C1	C2	C4	C5
Michigan (R)	-	-	0.23	-1.80
Missouri (N)	2	1.22	0.52	-2.17
Iowa (N)	2.17	1.32	1.08	-1.81
Louisiana (N)	2.75	1.22	1.16	-1.73
Colorado (N)#	-	-	1	-1.98
Minnesota (N)	-	-	0.9	-2.61
Pavement-ME v2.6 (N,R)	2	1.22	0.52	-2.17

N = New; R = Rehabilitation;
# = JPCP over JPCP or unbonded overlays over JPCP

2.8.2.7 Joint Faulting Model

The transverse joint faulting is calculated monthly in the Pavement-ME using the material properties, climatic conditions, present faulting level, pavement design properties, and axle loads

applied. Total faulting is the sum of faulting increments from previous months and is predicted using Equations 2-59 to 2-62 below.

$$\text{Fault}_m = \sum_{i=1}^{m} \Delta\text{Fault}_i \tag{2-59}$$

$$\Delta\ \text{Fault}_i = C_{34} \times (\ \text{FAULTMAX}_{i-1} - \ \text{Fault}_{i-1})^2 \times\ \text{DE}_i \tag{2-60}$$

$$FAULTMAX_i = FAULTMAX_0 + C_7 \times \sum_{j=1}^{m} DE_j \times \log(1 + C_5 \times 5.0^{EROD})^{C_6} \tag{2-61}$$

$$\begin{aligned}\text{FAULTMAX X}_0 &= \text{C}_{12} \times \delta_{\text{curling}} \\ &\times \left[\log(1 + \text{C}_5 \times 5.0^{\text{EROD}}) \times \log\left(\frac{\text{P}_{200} \times\ \text{WetDays}}{\text{P}_\text{s}}\right)\right]^{\text{C}_6}\end{aligned} \tag{2-62}$$

where,

$Fault_m$ = mean joint faulting at the end of month m; $\Delta Fault_i$ = incremental change (monthly) in mean transverse joint faulting during the month i; $FAULTMAXi$ = maximum mean transverse joint faulting for a month i; $FAULTMAX_0$ = initial maximum mean transverse joint faulting; $EROD$ = erodibility factor for base/subbase; DE_i = differential deformation energy of subgrade deformation accumulated during the month I; $\delta_{curling}$ = maximum mean monthly slab corner upward deflection PCC due to temperature curling and moisture warping; P_S = overburden pressure on the subgrade; P_{200} = percent subgrade soil material passing No. 200 sieve; $WetDays$ = average annual number of wet days (greater than 0.1 in rainfall); $C1,2,3,4,5,6,7,12,34$ = calibration coefficients; C_{12} and C_{34} are defined by Equation 2-63 and Equation 2-64.

$$\text{C}_{12} = \text{C}_1 + \text{C}_2 \times FR^{0.25} \tag{2-63}$$

$$\text{C}_{34} = \text{C}_3 + \text{C}_4 \times FR^{0.25} \tag{2-64}$$

FR = base freezing index defined as the percentage of time (in hours) the top base temperature is below freezing (32 °F) temperature to the total number of hours in design life.

Damage in a dowel joint for the current month is estimated using Equation 2-65.

$$\Delta DOWDAM_{tot} = \sum_{j=1}^{N} C_8 \times F_j \frac{n_j}{10^6 df_c^*} \tag{2-65}$$

where,

$\Delta DOWDAM_{tot}$ = cumulative dowel damage for the current month; n_j = number of axle load applications for the current increment and load group j for the current month; N = number of load categories; fc^* = estimated PCC compressive stress; d = dowel diameter; C_8 = calibration constant; F_j = effective dowel shear force induced by axle loading of load category j.

The faulting model local calibration results for several states are summarized in Table 2-38. As discussed earlier, 80% of the projects showed zero percent measured transverse slab cracking, so a non-regression approach was used to calibrate the transverse cracking model using Equation 2-54. The equation resulted in 66.6% model accuracy for the transverse cracking model.

Table 2-38: Local calibration coefficients for the faulting model

States	C1	C2	C3	C4	C5	C6	C7	C8
Michigan (R)	0.4	-	-	-	-	-	-	-
Missouri (N)	0.595	1.636	0.00217	0.00444	250	0.47	7.3	400
Iowa (N)	2.0427	1.8384	0.00438	0.00177	-	0.8	-	-
Louisiana (N)	1.5276	-	0.00262	-	-	0.55	-	-
Pavement-ME v2.6 (N,R)	0.595	1.636	0.00217	0.00444	250	0.47	7.3	400

N = New; R = Rehabilitation;

2.8.2.8 IRI Model

IRI in the Pavement-ME is a linear relationship between the IRI at construction and change in other distresses (transverse cracking, joint faulting, and joint spalling) over time. IRI, as a linear relationship of these factors, can be expressed by Equation 2-66.

$$IRI = IRI_I + C1 \times CRK + C2 \times SPALL + C3 \times TFAULT + C4 \times SF \quad (2\text{-}66)$$

where,

IRI = Predicted IRI; IRI_I = Initial IRI at the time of construction; CRK = Percent slabs with transverse cracking (all severities); $SPALL$ = Percentage of joints with spalling (medium and high severities); $TFAULT$ = Total joint faulting cumulated per mi; C_1, C_2, C_3, C_4 = Calibration coefficients; SF = Site factor, which can be calculated as shown in Equation 2-67.

$$SF = AGE(1 + 0.5556 \times FI)(1 + P_{200}) \times 10^{-6} \quad (2\text{-}67)$$

where,

AGE = Pavement age; FI = Freezing index, °F-days; $P200$ = Percent subgrade material passing No. 200 sieve.

The joint faulting and transverse cracking for IRI calculation are obtained using the models described previously. The joint spalling is calculated as shown in Equation 2-68.

$$SPALL = \left[\frac{AGE}{AGE + 0.01}\right]\left[\frac{100}{1 + 1.005(-12 \times AGE + SCF)}\right] \quad (2\text{-}68)$$

where,

SPALL = percentage joints spalled (medium- and high-severities); *AGE* = pavement age since construction.

SCF = scaling factor based on site-, design-, and climate-related variables, which is estimated as given in Equation 2-69.

$$SCF = -1400 + 350 \times ACPCC \times (0.5 + PREFORM) + 3.4f_c'^{0.4} - 0.2(\text{FTcycles} \times AGE) + 43h_{PCC} - 536WC_{PCC} \quad (2\text{-}69)$$

where,

ACPCC = PCC air content; *AGE* = time since construction; *PREFORM* = 1 if the preformed sealant is present; 0 if not; f'_c = PCC compressive strength; *FTcycles* = average annual number of freeze-thaw cycles; h_{PCC} = PCC slab thickness; WC_{PCC} = PCC water/cement ratio.

The IRI local calibration coefficients for various states are summarized in Table 2-39.

Table 2-39: Local calibration coefficients for rigid IRI model

States	C1	C2	C3	C4
Michigan (R)	1.198	3.570	1.4929	25.24
Missouri (N)	0.8203	0.4417	1.4929	25.24
Iowa (N)	0.04	0.04	0.07	1.17
Louisiana (N)	0.8203	0.4417	1.4929	25.24
Ohio (N)	0.82	3.7	1.711	-
Colorado (N)[#]	0.82	0.442	1.493	-
Pavement-ME v2.6	0.8203	0.4417	1.4929	25.24

N = New; R = Rehabilitation;
# = JPCP over JPCP or unbonded overlays over JPCP

CHAPTER 3 DATA SYNTHESIS

The local calibration of PMED models is a challenging task that requires a minimum number of pavement sections to represent the pavement conditions in certain areas. The first step in this regard is data acquisition for selected sections, including material properties, traffic data, climatic data, types of fixes applied to pavement in the past, and pavement performance data. The reliability of predicted performance depends upon the accuracy of the data used for calibration. The PMED allows users to input layer properties and traffic data at three hierarchical levels, which provides substantial flexibility in obtaining input data based on available resources. Since the inception of PMED, SHAs have developed their databases for all hierarchical input levels based on available data acquisition resources. However, all these efforts were mainly for new or reconstructed pavement design. The rehabilitation design has almost similar data input requirements, except for the characterization of existing pavement, which is a vital step in rehabilitation design; PMED assumes pre-overlay damage as a starting point. The characterization of existing pavement requires different data input at three different rehabilitation levels for HMA overlay over HMA only. Since this study is about the calibration of HMA overlay over rubblized PCC, no rehabilitation levels can be specified in the PMED. This chapter outlines the process for selecting pavement sections for local calibration of rubblized rehabilitated pavements and the steps in obtaining the required information for each pavement section.

The previous local calibration effort used 108 flexible and 20 JPCP pavement projects (5). The focus was on identifying and reviewing all these projects in the MDOT database to determine the availability of additional distress data. In this process, the time-series trends of all distress types were evaluated considering any significant maintenance activities over time, which helped later in decision-making—i.e., whether an existing project should be regarded as a reconstructed or rehabilitated overlay project. The PMED inputs to these sections were also reviewed to obtain more current or higher levels of inputs.

Another objective was to identify and select new potential candidate projects. For this task, all available sections of rubblized pavements were reviewed from the MDOT databases for their performance and data availability. The project selection process, getting the PMED input,

and performance data analysis have been summarized in this chapter. The following topics are discussed:

a. Data acquisition and its compatibility with PMED.
b. Project selection criteria.
c. Review/ analysis of measured performance data.
d. Pavement cross-section information.
e. Traffic inputs.
f. Construction materials inputs.
g. Climate input.

3.1 Data Acquisition and its Compatibility with PMED

The Pavement Management System (PMS), construction records, and QA/QC sources were reviewed to extract pavement performance data and the PMED inputs. The following data was obtained after a thorough evaluation:

a. The compatibility of the measured data was evaluated; if necessary, measured data was converted to the PMED-compatible units.
b. The material properties and pavement cross-sectional details were obtained from construction records, plans, job-mix formula (JMF), and other data sources. Any unavailable data was acquired from MDOT, or MDOT provided test results for the best possible estimates.
c. Traffic data was collected from the construction records and MDOT Transportation Data Management System (TDMS). Level 2 data was used for traffic data based on road type, number of lanes, and vehicle class 9 traffic percentage.
d. For asphalt concrete (AC) mix and binder properties, DYNAMOD software, which is based on laboratory tests for Michigan mixes, was used. The most common construction materials in Michigan were used for base, subbase, and subgrade properties.
e. For climatic data, the updated NARR files for Michigan have been used (5).

3.1.1 Selected Distresses

The MDOT PMS and sensor database were carefully analyzed, and relevant data were extracted to obtain the required distress information. The current distress Manual of MDOT PMS was referred to determine all the principal distress corresponding to the predicted distresses in the

PMED. The earlier versions of the PMS manual were also reviewed to ensure accurate data extraction for all the years. The necessary steps for PMS data extraction include:

a. Identify the stresses that correspond to the PMED predicted distresses.
b. Convert (if necessary) MDOT-measured distresses to the PMED compatible with the units.
c. Extract sensor data for each project.
d. Summarize time-series data for each project and each distress type.

The significant distress for HMA overlay over rubblized PCC is similar to the new flexible pavement design. The identified and extracted pavement distresses and conditions for rubblized pavements are summarized in Tables 3-1. This section also discusses converting measured distresses to PMED-compatible units for HMA overlay over rubblized pavements.

Table 3-1: Major pavement distresses

Distress/ roughness	MDOT units	PMED units	Conversion needed?
IRI	in/mile	in/mile	No
Top-down cracking	miles	% area	Yes
Bottom-up cracking	miles	% area	Yes
Thermal cracking	No. of occurrences	ft/mile	Yes
Rutting	in	in	No

3.1.2 Distress Unit Conversion for HMA Overlay of Rubblized PCC

It is worth mentioning that only distress types predicted by the PMED were considered for the local calibration. The corresponding MDOT's measured distresses were extracted from the PMS database and compared with distress types predicted by the PMED to verify if any conversions were necessary. The subsequent paragraphs explain the conversion process (where necessary) for all distress types.

IRI: The IRI measurements in the MDOT sensor database are compatible with those in the PMED. Therefore, no conversion or adjustments were needed, and data can be used directly.

Top-down cracking: Top-down cracking is load-related longitudinal cracking in the wheel path. The distresses in the MDOT PMS database, which has not developed an alligator cracking pattern, were assumed to correspond to top-down cracking. These cracks could develop due to fatigue and are called bottom-up cracking. Therefore, it took much work to differentiate between bottom-up and top-down crackings based on the PMS data as it records the data in miles. The PMS data was converted into the percent of the total area cracked using Equation 3-1, and then,

based on the thickness threshold, it was grouped into bottom-up or top-down crackings. The lane width was assumed to be 12 ft. The typical wheel path width of 3 feet was taken as recommended by the LTPP distress identification manual (5). Table 3-2 presents the threshold thicknesses of top-down cracking for each surface type.

$$\%\, AC_{top-down} = feet\ length \times 100 \quad (3\text{-}1)$$

Table 3-2: Threshold thicknesses for top-down cracking

Surface type	Threshold thickness (in)
Bituminous overlay on rubblized concrete	6
Composite overlay	6
Crush and shape	4
HMA over HMA overlay	6

Bottom-up cracking: Bottom-up cracking is defined as alligator cracking in the wheel path. The PMS database also records the bottom-up cracking in miles; these values were converted to percent of the total area using Equation 3-1. The values achieved were compared to threshold limits for each pavement type given in Table 3-3 to obtain bottom-up cracking.

Thermal cracking: Thermal cracking corresponds to transverse cracking in the top HMA surface of the HMA overlay of rubblized JPCP. The transverse cracking is recorded as the number of occurrences, but the PMED predicts thermal cracking in feet/mile. The number of occurrences was multiplied by lane width (12 ft) to get the length of the crack. All transverse crack lengths were summed up and divided by the project length to get feet/mile, as shown in Equation 3-2.

$$TC = \frac{\sum \text{No. of Occurrences} \times \text{Lane Width (ft)}}{\text{Project Length (miles)}} \quad (3\text{-}2)$$

Thermal cracking predictions in the Pavement-ME are restricted to a maximum value of 2112 ft/mile due to a minimum crack spacing limit of 30 feet. This means that PMED predictions at 50% reliability cannot go beyond 2112 ft/mile. Due to this limitation, any measured data above the 2112 ft/mile cut-off value was removed from the dataset.

Rutting: This is the total amount of surface rutting all the pavement layers contribute. The average rutting (left-right wheel paths) was determined for the entire project length. No conversion was necessary. It is assumed that the measured rutting corresponds to the total surface rutting predicted by the PMED.

Reflective cracking: MDOT does not differentiate between thermal and reflective cracking, as it is difficult to segregate a thermal and a reflective crack at the surface. Therefore, the total transverse cracking observed is compared to the total combined thermal and reflective cracking. Moreover, it is worth noting that rubblization of existing PCC warrants control of reflective cracking in overlaid HMA layer.

3.2 Project Selection Criteria

The selection criteria for reliable local calibration demands a representative number of pavement sections based on Michigan's pavement design, construction practices, and performance. Project selection criteria were established to guarantee that the chosen pavement sections would adhere to the necessary standards and effectively depict Michigan's pavement network. The selected project may have more than one section, which could be due to the location of the sample within the chosen project, so the number of sections will be more than the selected projects. The selection criteria are discussed in subsequent paragraphs.

3.2.1 Minimum Number of Required Pavement Sections

The PMED local calibration guide provides guidelines to determine the minimum required sections for each distress type. The minimum number of pavement sections required for local calibration of each distress are summarized in Table 3-3. The following relationship is used to determine the minimum number of sections needed.

$$n = \left(\frac{Z_{\alpha/2} \times \sigma}{e_t}\right)^2 \qquad (3\text{-}3)$$

Where:

$Z_{\alpha/2}$ = The z-value from a standard normal distribution
n = Minimum number of pavement sections
σ = Performance threshold
e_t = Tolerable bias $Z_{\alpha/2} \times SEE$
SEE = Standard error of the estimate

Table 3-3: Minimum number of sections for local calibration

Performance Model	*N* (required number of sections)	Number of sections used
Bottom-up cracking (%)	16	12
Top-down cracking (ft/mile)	12	17
Transverse “thermal” cracking	30	22
Rutting (in)	22	38
IRI (in/mile)	83	32

N= minimum number of samples required for a 90% confidence level

3.2.2 Initial Projects Selection

MDOT maintains an exhaustive database encompassing all construction projects executed within Michigan. As the first step, a meticulous evaluation was conducted on all prior projects, including 140 flexible pavements and 28 JPCP projects previously utilized in calibration endeavors. In addition, the supplementary projects that could serve as viable candidates for our ongoing local calibration initiative were identified. The PMS data extraction was completed for all required distress types in a compatible format with the PMED software. The time series for each pavement section's performance measures were plotted and analyzed to finalize the preliminary list of new potential candidate projects. The criteria used to identify additional performance data and the selection of new potential pavement projects include:

a. The pavement section must have at least three measured data points over time. There are some exceptions to this criterion. Bottom-up cracking has relatively fewer data points; some sections with even two points have been included, considering further data points will be collected in the future.
b. At least one of the distresses should have an increasing trend. Any section with decreasing and no or flat trends over time was excluded from the list.
c. The previous maintenance history for all pavement sections was reviewed to explain any decrease or flat trend observed in the time series plot. If there were any major rehabilitation or reconstruction activities, the measured data from the year traffic opened initially to the very last year until the major repair took place are considered.
d. The last recorded point should have a Distress Index (DI) of at least 5.

Figures 3-1 show the example distress progressions for the HMA overlay over rubblized JPCP. The top-down cracking for the initial project selection was evaluated in feet/mile and later converted to a percentage. The vertical dashed red line is the last reported construction, whereas the dotted blue line in the DI plot indicates reported maintenance activities.

The performance data for these initially selected sections is the average for the entire section length. This data is calculated by averaging the performance for every 0.1-mile segment in the project length. The cutoff value of 2112 ft/mile was adopted for thermal cracking. The data seems reasonable for other performance measures, and no further filtering/investigation is required.

3.2.3 Summary of the Selected Projects

The initially selected projects were further refined based on performance, availability of inputs, and initial IRI. Tables 3-4 summarize the HMA over rubblized PCC projects. It is worth mentioning that in previous calibration efforts of MDOT, HMA over rubblized PCC projects were analyzed as new pavements. Additionally, Tables 3-5 outline the selected projects based on the design matrix for HMA over rubblized PCC projects.

Table 3-4: Number of new construction projects by pavement type & region

Pavement type	MDOT region	Number of projects
HMA over rubblized PCC	Bay	3
	Grand	2
	North	9
	Southwest	1
	University	7

Table 3-5: Selection matrix displaying selected projects (sections)

Road type	Traffic level*	Thickness level*	Age Level			Total
			<10	10-15	>15	
HMA over rubblized PCC	1	1				
		2		4	16	20
		3		2	4	6
	2	1				
		2		9	3	12
		3				
	3	1				
		2			7	7
		3			4	4

*Levels	1	2	3
Traffic (AADTT)	<1000	1000-3000	>3000
Thickness (in)	<3	3-7	>7

These sections were selected based on performance trends to accommodate various inputs, including layer thicknesses, traffic, region, etc. Figures 3-2 show the geographical location of the finally selected projects. Tables 3-6 summarize the selected projects along with the year of construction and two-way AADTT.

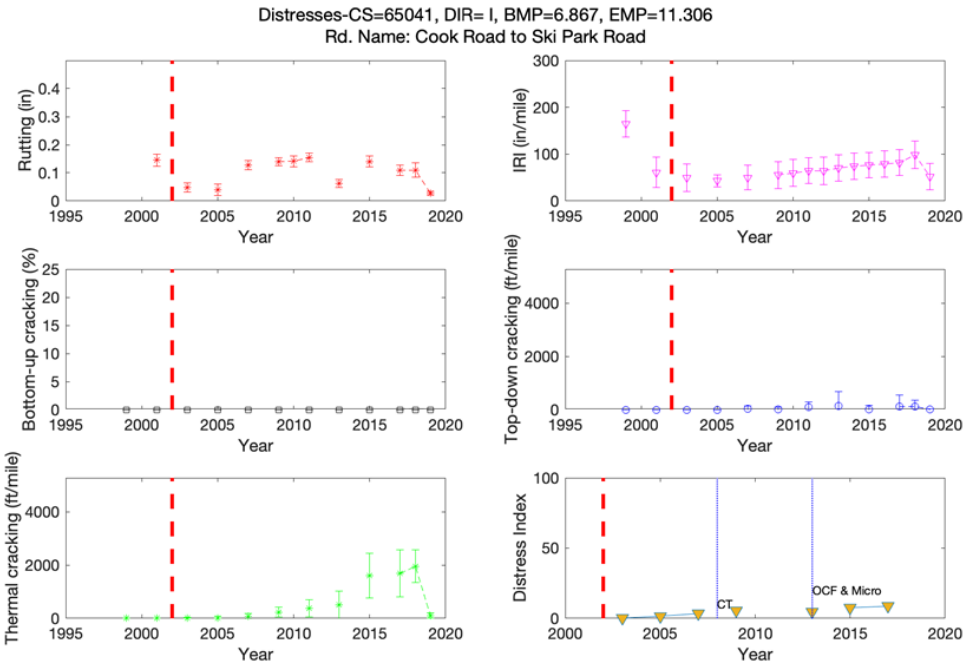

(a) Freeway

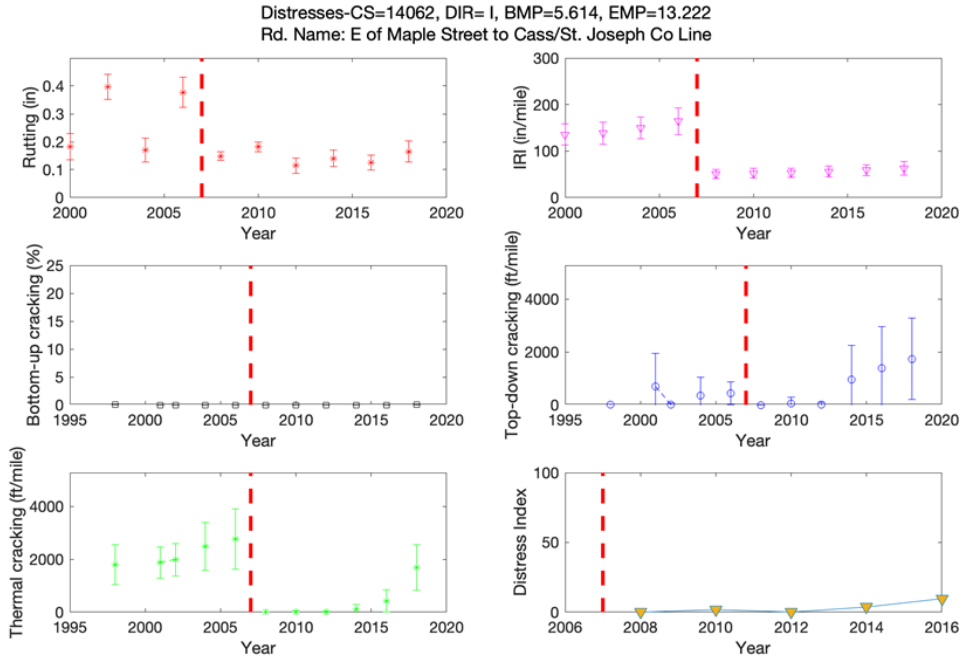

(b) Non-freeway

Figure 3-1: Examples of selected sections for bituminous overlay on rubblized PCC

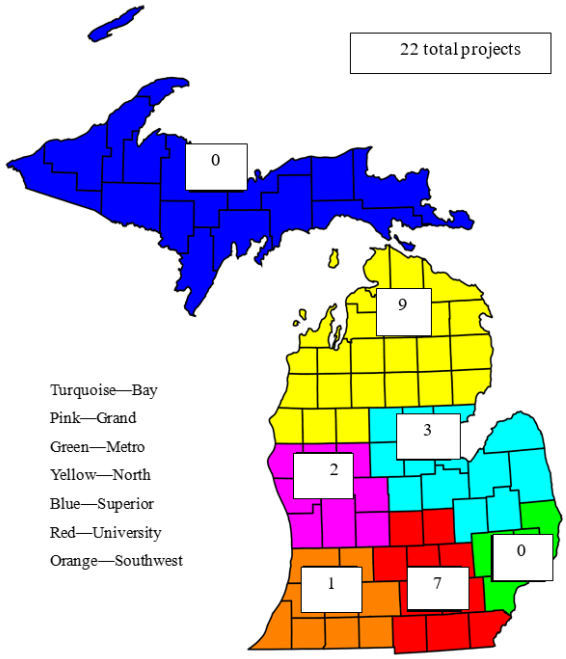

Figure 3-2: Geographical location of selected rubblize projects

Table 3-6: Summary of selected projects

No.	Job Number	Control Section	Type	Route	Region	AADTT	Year of construction
1	28115	34031	Existing	M-66	Grand	490	1989
2		34032				340	
3	29768	47013		US-23 N	University	3390	1992
4				US-23 S			
5		47014		US-23 N			
6				US-23 S			
7				US-23 N			
8				US-23 S			
9				US-23 N			
10				US-23 S			
11	29670	13033		I-194 N	Southwest	856	1993
12				I-194 S			

Table 3-6 (cont'd)

13	29581	33084		I-96 E	University	3707	1994
14				I-96 W			
15		33083		I-96 E			1993
16				I-96 W			
17	29729	74012		M-53	Bay	370	1993
18	45053	67021		US-10	North	675	1999
19		67022					
20	44109	5011		US-31	North	279	1999
21	38190	41033		M-37	Grand	575	2000
22		61171					
23	32388	46082		M-50	University	455	1997
24							
25							1998
26	45865	65041	New	I-75 N	North	1500	2002
27				I-75 S		1081	
28	75774	18021		US-10 W	Bay	1284	2004
29		18024		US-10 E			
30	53288	16092		I-75 N	North	847	2005
31				I-75 S			
32	60540	33031		US-127 S	University	2492	2005
33	59468	16091		I-75 N	North	1398	2007
34				I-75 S			
35	60433	56044		US-10 E	Bay	2619	2008
36				US-10 W		1764	
37				US-10 E		2844	
38				US-10 W		1917	
39	90279	16091		I-75 N	North	972	2008
40	43521	46071		M-52	University	715	2005
41	57104	46071			University	318	2005
42	45676	46074			University	675	2007
43	48458	51012		US-31	North	399	2002
44							
45	48556	71072		US-23	North	173	2003
46	48517	10031		US-31	North	399	2003
47							
48							

3.3 Review/Analysis of Measured Performance Data

The comparison of predicted and measured performance for each project is vital for the calibration process. To have a robust local calibration, the levels of distress must fall within a reasonable range (i.e., above and below threshold limits for each type of distress). Therefore, the distress levels for all projects were compiled and analyzed to determine their respective ranges. A total of 48 HMA over rubblized PCC sections were considered in the local calibration. The selected sections' time series and age distribution are shown in Figures 3-3 to 3-7. The following can be inferred from the results:

a. Bottom-up fatigue cracking: The selected sections exhibited low-value bottom-up cracking, while only one section reached the threshold of 20%. The age varies from 6 to 20 years.
b. Longitudinal/top-down fatigue cracking: Top-down is measured in the percent area cracked, but the MDOT has not defined its threshold. However, top-down fatigue cracking is observed more frequently than bottom-up cracking.
c. Transverse (thermal) cracking: The thermal cracking for the HMA overlay over rubblized PCC projects was significant, with two sections exceeding the 2112 ft/mile threshold. The age varies from 9 to 18 years. Superpave (PG) binder sections have been used for thermal cracking calibration. It is worth noting that rubblization minimizes the reflection cracking, so only thermal cracking prediction from PMED is used for local calibration.
d. Rutting: Rutting does not seem to be a dominating problem, as seen in Figures 3-5, where only one section exceeds the threshold of 0.5 inches. At the same time, most of the sections exhibit significantly low amount of rutting. The age distribution ranged from 3 to 18 years.
e. IRI: The IRI time series is usually flat, with no sections exceeding the 172 in/mile threshold. The age at maximum IRI ranged from 10 to 20 years. It is worth noting that only sections with an initial IRI less than or equal to 82 in/mile were selected to calibrate the IRI model.

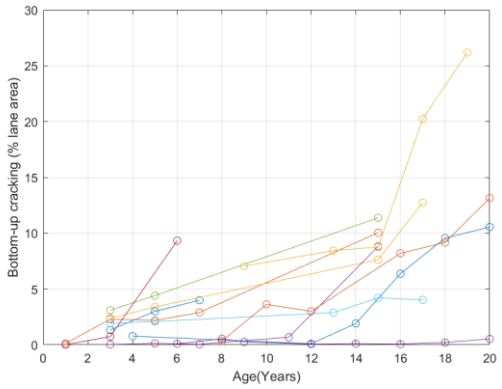

(a) Time series

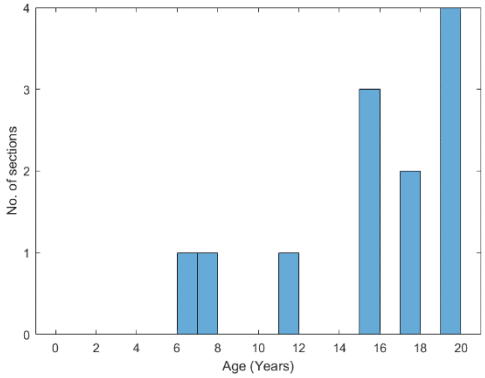

(b) Age distribution

Figure 3-3: Selected HMA over rubblized PCC sections — Bottom-up cracking

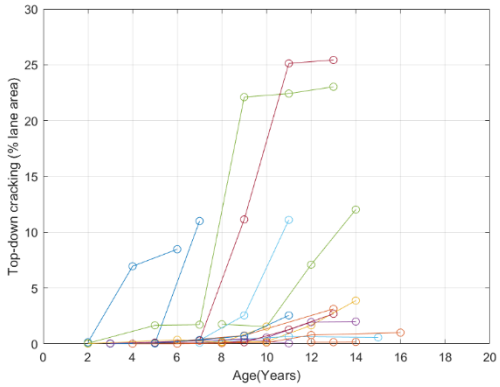

(a) Time series

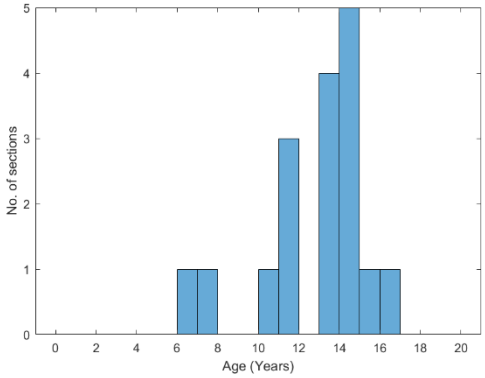

(b) Age distribution

Figure 3-4: Selected HMA over rubblized PCC sections — Top-down cracking

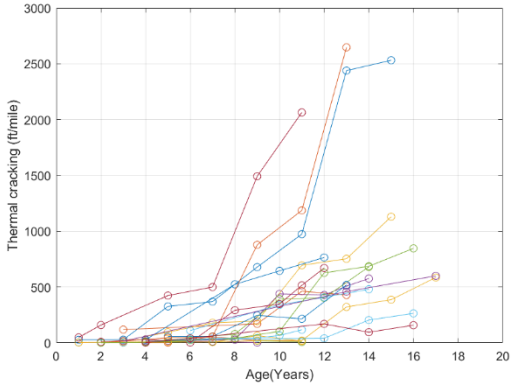

(a) Time series

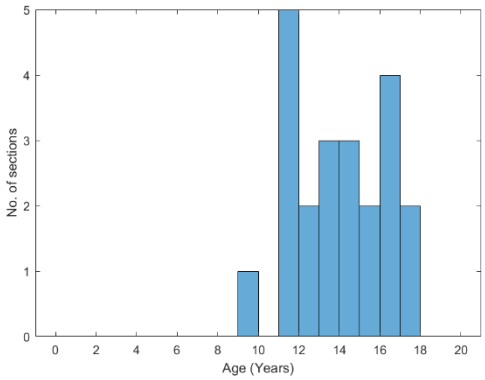

(b) Age distribution

Figure 3-5: Selected HMA over rubblized PCC sections — Transverse (thermal) cracking

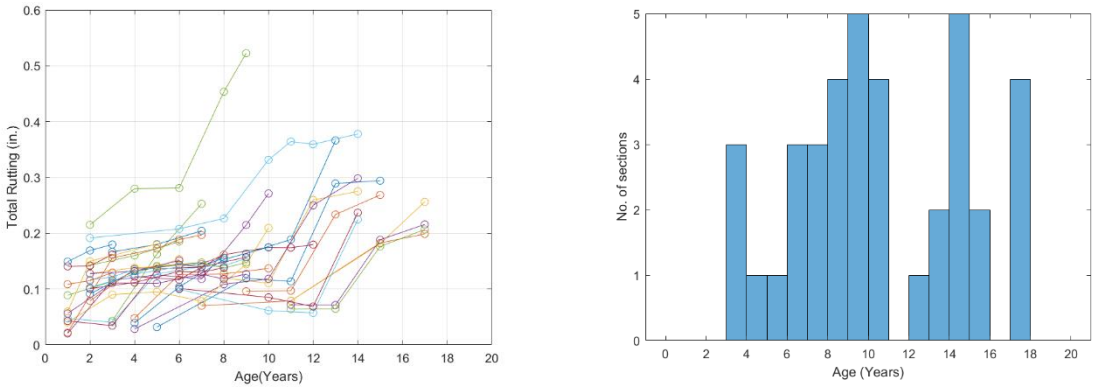

(a) Time series (b) Age distribution

Figure 3-6: Selected HMA over rubblized PCC sections — Total rutting

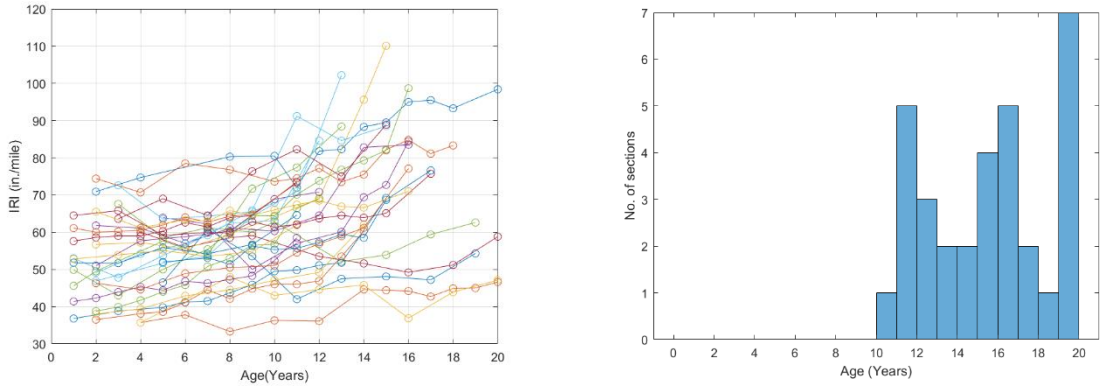

(a) Time series (b) Age distribution

Figure 3-7: Selected HMA over rubblized PCC sections — IRI

3.4 PMED Input Data for Selected Projects

Accurate calibration of the PMED models directly relies on the pavement cross-sectional, traffic, climate, material inputs, and performance data. Moreover, an appropriate hierarchical level of inputs must be selected for most of the critical inputs to characterize the existing pavements (5). Data collection for each hierarchical input level is a challenging task as PMED requires many data inputs to characterize pavements. Many studies have been conducted to highlight the sensitivity of an input to the PMED performance prediction. Selecting hierarchical input is vital for PMED performance prediction, as any wrong selection can result in over-designed or under-designed pavements (5). The following section explains the process of collecting as-constructed input data, including pavement cross-section details, traffic, layer materials, and climate input data. All three hierarchical input level data were used for calibration, and PMED performance prediction was compared at each level.

3.4.1 Pavement Cross-Section Inputs

The pavement cross-sectional information is necessary to characterize the layer thicknesses of the various layers for modeling in PMED software. The construction records were utilized to obtain the cross-sectional information for new sections. The thickness, mix type, traffic, and unbound layer information were extracted from the construction drawings. For the sections used for the previous calibration effort (5), the Pavement-ME inputs data sheet was used to extract design inputs. The missing information was obtained from MDOT in case construction plans were unavailable. Typically, HMA overlays are laid in three layers, and the drawings typically provided the asphalt application rate of the HMA layers, which was used to determine the HMA lift thicknesses. A summary of the design thicknesses for selected pavement projects is shown in Tables 3-7.

Table 3-7: Average HMA thicknesses

Layer	Average thickness (in.)
HMA top course	2.9
HMA leveling course	2.1
HMA base course	3.1
Fractured PCC	8.8
Base	3.8
Subbase	10.8

3.4.2 Traffic Inputs

The traffic input is one of the vital inputs for pavement design and analysis. The PMED requires traffic load spectra to represent loads from all mixed traffic types. The MDOT's developed spreadsheet extracted all sections' Level 2 traffic data. This spreadsheet with traffic distribution tables was used to extract the following data:

a. Vehicle class distribution.
b. Monthly adjustment factor.
c. Number of axles per truck.
d. Single axle load spectra.
e. Tandem axle load spectra.
f. Tridem axle load spectra.
g. Quad axle load spectra.

The inputs (with input categories) required to obtain these tables are summarized in Table 3-8.

Table 3-8: Traffic inputs used to extract traffic data from MDOT spreadsheets

Inputs	Categories
Percentage of vehicle class 9	• Less than 45 • 45 to 70 • Above 70
Region type	• Rural • Urban
COHS type	• National • Regional • Statewide
Number of lanes	• 2 • 3 • 4+

The number of lanes was identified from the plans. Wherever the number of lanes was unavailable, they were visually estimated utilizing Google Maps coordinates. The COHS type was estimated using each project's PR number and beginning and ending milepost. The percentage of class 9 vehicles was calculated for each section using the MDOT Transportation Data Management System (TDMS) website from the following URL: https://mdot.public.ms2soft.com/tcds/tsearch.asp?loc=mdot. For sections where the traffic data was unavailable at the exact location, nearby locations in the same section were used. The range and average two-way AADTT values for all selected projects are summarized in Table 3-9.

Table 3-9: Ranges of AADTT for all rubblized projects

AADTT	Quantity
Min	173
Max	3707
Average	1160

3.4.3 As-Constructed Material Inputs

The as-constructed material inputs were obtained from the construction records, JMFs, and other test records. Ideally, these inputs are to be recorded at the time of construction. These inputs range between project-specific and statewide average values. The details of material properties for each pavement structural layer are discussed in this section.

3.4.3.1 HMA Layer Inputs

All inputs were collected at the highest hierarchy level; however, the needed data were unavailable for all pavement sections. In that case, the data was collected using other correlations/sources. Data collection for each HMA layer input is as follows:

a. Dynamic modulus (E*): E* was obtained from the DYNAMOD software developed in a study at Michigan State University (17). E* for the Superpave mixes was directly obtained from the database. For older mixes (marshal mixes), the volumetric, binder, and gradation information was used to predict the E* using DYNAMOD's Artificial Neural Networks (ANNs). E* was obtained at Level 1 from DYNAMOD; however, E* was used at all hierarchical levels.
b. Binder (G*): G* was also obtained from the DYNAMOD database using the region and binder information. G* was obtained at Level 1; however, all hierarchical levels were used for calibration.
c. Creep compliance (D(t)): D(t) was obtained from the DYNAMOD database. D(t) was obtained at Level. Creep compliance at Level 2 (at mid temperature @14^{o}F) was also extracted from DYNAMOD's Level 1 creep compliance data. Default values of Level 3 were also used to compare the results at each hierarchical level.
d. Indirect tensile strength (IDT): IDT was obtained from the DYNAMOD database at Level 2.
e. AC layer thickness: These were obtained from construction records. Usually, the application rate in lbs/yards^2 is available, which can be utilized to obtain the layer thickness.
f. Air voids and binder content: As constructed, air voids and binder content were obtained from construction records. Table 3-10 summarizes the average as-constructed air voids for the top HMA layer. Historical test records were used for unavailable data to obtain an average value based on mix type, as shown in Table 3-15.
g. Aggregate gradation: Gradation was obtained from JMFs. Tables 3-11 summarize the average gradation for the top, leveling, and base layers for HMA overlay over rubblized PCC pavement. Historical test records were used for unavailable data to obtain an average value based on mix type, as shown in Table 3-25.

It is important to note that Level 1 G* and Level 2 IDT data were used to calibrate the thermal cracking model. For the thermal cracking model, mixes with PG binder type were used. Since G* and IDT predictions from DYNAMOD were possible for the Superpave mixes only, for all other sections, G* and IDT were kept at Level 3.

Table 3-10: As-constructed percent air voids for HMA top course

HMA layer	Average as-constructed air voids (%)
Top	6.8
Leveling	6.4
Base	5.8

Table 3-11: HMA top course average aggregate gradation

Item	HMA layers		
	Top	Leveling	Base
Effective AC binder content	11.9	11.2	10.6
3/4	99.4	100.0	99.3
3/8	89.8	87.0	78.9
#4	67.3	67.8	59.9
#200	5.9	5.2	4.8

3.4.3.2 Fractured PCC Layer Inputs

The existing JPCP is fractured to control reflection cracks in the HMA overlaid layer. A recent study by MDOT is underway in which HMA over rubblized sections were designed as new flexible pavement in PMED; modeling fractured JPCP as an unbonded aggregate base with MDOT's recommended 70,000 psi elastic modulus. This study modeled HMA over rubblized PCC as an overlay design with HMA over fractured JPCP option in PMED. MDOT recommends an elastic modulus value of 70,000 for rubblized JPCP; however, PMED doesn't allow users to use elastic modulus for fractured JPCP less than 150,000 psi. FWD is used to characterize the existing pavement layers moduli. Due to the unavailability of FWD data for the selected sections, an elastic modulus of 150,000 psi was selected based on the minimum threshold value of PMED software. Besides, the elastic modulus of fractured JPCP, the crack spacing of fractured slab, and load transfer efficiency (LTE) are essential inputs in overlay design. As this data was also unavailable from the field, default values were selected. Table 3-12 summarizes the inputs for the fractured PCC layer.

Table 3-12: Fractured PCC inputs

Input	Value
Elastic modulus	150,000 psi
Crack spacing	3 ft
LTE	50%
Poisson's ratio	0.2

3.4.3.3 Aggregate Base/Subbase and Subgrade Input Values

The aggregate base/subbase and subgrade input values were obtained from the following sources:

a. Backcalculation of unbound granular layer moduli *(16).*
b. Pavement subgrade MR design values for Michigan's seasonal changes *(15).*

The resilient modulus (MR) values for the base and subbase material were selected based on the results from previous MDOT studies. The typical backcalculated values for base and subbase MR is 33,000 psi and 20,000 psi, respectively. For base/subbase layers, the software default to "Modify input values by temperature/moisture" was selected. The subgrade material type and resilient modulus were selected using the Subgrade MR study *(15, 16)*. The study outlined the location of specific soil types and their MR values across the entire State. Annual representative values for subgrade MR were used in PMED. The recommended design MR value corresponding to the soil type is shown in Table 3-13.

3.4.4 Climate Inputs

The Enhanced Integrated Climatic Model (EICM) in Pavement-ME requires hourly climatic data. This data includes air temperature, precipitation, relative humidity, percent sunshine, and wind speed. The improved MDOT NARR climatic files created under a previous research study were used for climatic inputs *(48)*. The files were downloaded as .hcd files, which can be read directly in Pavement-ME. The closest weather station to each selected project was used. For rigid sections, these files were directly used, and for flexible sections, custom stations were formed using these files. Table 3-14 summarizes the climatic files used for calibration.

Table 3-13: Average roadbed soil MR values

Roadbed Type		Average MR			
USCS	AASHTO	Laboratory determined (psi)	Back-calculated (psi)	Design value (psi)	Recommended design MR value (psi)
SM	A-2-4, A-4	17,028	24,764	5,290	5,200
SP1	A-1-a, A-3	28,942	27,739	7,100	7,000
SP2	A-1-b, A-3	25,685	25,113	6,500	6,500
SP-SM	A-1-b,A-2-4, A-3	21,147	20,400	7,000	7,000
SC-SM	A-2-4, A-4	23,258	20,314	5,100	5,000
SC	A-2-6, A-6,A-7-6	18,756	21,647	4,430	4,400
CL	A-4, A-6, A-7-6	37,225	15,176	4,430	4,400
ML	A-4	24,578	15,976	4,430	4,400
SC/CL/ML	A-2-6, A-4, A-6, A-7-6	26,853	17,600	4,430	4,400

Table 3-14: Michigan climate station information

HCD filename	City/Location	Climate identifier	Latitude	Longitude
4847	Adrian	Adrian Lenawee County Arpt	41.868	-84.079
94849	Alpena	Alpena Co Rgnl Airport	45.072	-83.581
94889	Ann Arbor	Ann Arbor Municipal Arpt	42.224	-83.74
14815	Battle Creek	W K Kellogg Airport	42.308	-85.251
94871	Benton Harbor	Sw Michigan Regional Arpt	42.129	-86.422
14822	Detroit	Detroit City Airport	42.409	-83.01
94847	Detroit	Detroit Metro Wayne Co Apt	42.215	-83.349
14853	Detroit	Willow Run Airport	42.237	-83.526
14826	Flint	Bishop International Arpt	42.967	-83.749
4854	Gaylord	Otsego County Airport	45.013	-84.701
94860	Grand Rapids	Gerald R. Ford Intl Airport	42.882	-85.523
14858	Hancock	Houghton County Memo Arpt	47.169	-88.506
4839	Holland	Tulip City Airport	42.746	-86.097
94814	Houghton Lake	Roscommon County Airport	44.368	-84.691
94893	Iron Mountain/Kingsford	Ford Airport	45.818	-88.114
14833	Jackson	Jackson Co-RynoldsReynoldspt	42.26	-84.459
94815	Kalamazoo	Klmazo/Btl Creek Intl Arpt	42.235	-85.552
14836	Lansing	Capital City Airport	42.78	-84.579
14840	Muskegon	Muskegon County Airport	43.171	-86.237
14841	Pellston	Pton Rgl Ap Of Emmet Co Ap	45.571	-84.796
94817	Pontiac	Oakland Co. Intnl Airport	42.665	-83.418
14845	Saginaw	Mbs International Airport	43.533	-84.08
14847	Sault Ste Marie	Su Ste Mre Muni/Sasn Fl Ap	46.467	-84.367
14850	Traverse City	Cherry Capital Airport	44.741	-85.583
AMN	Alma	Gratiot Community Airport	43.322	-84.688
BAX	Bad Axe	Huron County Memorial Airport	43.78	-82.985
CFS	Caro	Tuscola Area Airport	43.459	-83.445
ERY	Newberry	Luce County Airport	46.311	-85.4572
ESC	Escanaba	Delta County Airport	45.723	-87.094
FKS	Frankfort	Frankfort Dow Memorial Field Airport	44.625	-86.201
IRS	Sturgis	Kirsch Municipal Airport	41.813	-85.439
ISQ	Manistique	Schoolcraft County Airport	45.975	-86.172
IWD	Ironwood	Gogebic Iron County Airport	46.527	-90.131
LDM	Ludington	Mason County Airport	43.962	-86.408
MOP	Mount Pleasant	Mount Pleasant Municipal Airport	43.622	-84.737
OSC	Oscoda	Oscoda Wurtsmith Airport	44.452	-83.394
PHN	Port Huron	Saint Clair County Intnl Airport	42.911	-82.529
RQB	Big Rapids	Robin Hood Airport	43.723	-85.504
SAW	Gwinn	Sawyer International Airport	46.354	-87.39

Table 3-15: MDOT recommended values volumetric and gradation

Mix type	Air voids (%)	Effective binder content (%)	% Passing 3/4" Sieve	% Passing 3/8" Sieve	% Passing # 4Sieve	% Passing #200 Sieve
3E1	5.8	10.8	99.85	80.44	62.94	4.40
4E1	6.1	11.5	100.00	87.24	70.43	5.11
5E1	6	12.6	100.00	97.14	78.23	5.63
2E3	4.8	9.7	92.65	68.70	53.95	4.40
3E3	5.8	10.8	99.63	77.88	60.33	4.56
4E3	6.1	11.5	100.00	86.91	68.66	4.92
5E3	6	12.6	100.00	97.86	79.81	5.49
2E10	4.8	9.7	94.55	73.50	59.70	4.50
3E10	5.8	10.8	99.78	80.27	62.78	4.84
4E10	6.1	11.5	100.00	87.65	70.06	5.26
5E10	6	12.6	100.00	98.30	81.27	5.67
2E30	4.8	9.7	99.00	71.80	60.60	4.20
3E30	5.8	10.8	99.95	79.20	59.82	4.40
4E30	6.1	11.5	100.00	88.63	66.90	4.33
5E30	6	12.6	100.00	99.00	81.24	5.68

3.5 Summary

The steps for data collection, project selection, and obtaining the PMED inputs have been outlined in this chapter. Details about each input, source, and possible estimates in case of unavailable data have also been discussed. The number of projects for each performance type and pavement type has also been summarized. Tables 3-16 and 3-17 summarize the inputs and corresponding levels for traffic and material characterization data used for the local calibration.

Table 3-16: Summary of fixed input levels

Input			Input Level	Input source
Traffic	Vehicle class distribution		2	MDOT specified traffic level-2 data
	Monthly adjustment factor		2	
	Number of axles per truck		2	
	single, tandem, tridem, quad axle load distribution		2	
	AADTT		1	From design drawings
	Vehicle class 9 percentage		1	MDOT TDMS website
Cross-section (new and existing)	HMA thickness		1	Project-specific HMA thicknesses based on design drawings
	PCC thickness		1	Project-specific PCC thicknesses based on design drawings
	Base thickness		1	Project specific base thicknesses based on design drawings
	Subbase thickness		1	Project-specific subbase thicknesses based on design drawings
Construction materials	Base/sub-base	MR	2	Recommendations from MDOT unbound material study
	Subgrade	MR	2	Soil-specific MR values - MDOT subgrade soil study
		Soil type	1	Location-based soil type - MDOT subgrade soil study
Climate			1	Closest available climate station

Note:

Level 1 is project-specific data, pseudo level 1 means that the inputs are not project-specific, but the material properties (lab measured) correspond to similar materials used in the project.

Level 2 inputs are based on regional averages in Michigan.

Level 3 inputs are based on statewide averages in Michigan.

Table 3-17: Level of inputs used for HMA mechanical properties

	Input	Level 1	Level 2	Level 3
HMA	Binder type (G*)	1	2	3
	Creep Compliance	1	2	3
	Mixture property (E*)	1	2	3
	IDT	2	2	3

CHAPTER 4 SENSITIVITY ANALYSIS

The PMED approach uses pavement mechanistic responses (stresses and strains) to compute damage accumulation based on various distress evolution mechanisms by considering axle load levels and climate variation. Subsequently, this damage is used to estimate field-observed pavement distresses through transfer functions for performance prediction (8). The performance prediction models used in PMED software are designed for the general conditions and calibrated nationally, necessitating the local calibration of these models per locally available materials, traffic, and climatic conditions for any specific state. Most states started using PMED for flexible and rigid pavement designing purposes, making it vital to calibrate the transfer functions accurately for better and definite performance predictions.

PMED requires more data inputs for comprehensive design. This challenges many state highway agencies (SHAs) to identify the most critical data input and the most sensitive transfer function coefficient affecting the local calibration authenticity. Many studies have been conducted to determine the sensitivity of material inputs over performance predictions of PMED models (20, 49-53), while very few studies have covered the sensitivity of transfer function coefficients. However, all these studies used a one-at-a-time (OAT) approach for sensitivity analysis by comparing the performance prediction with input change. Kim et al. and Dong et al. conducted a sensitivity study for all models of flexible and rigid pavements in Iowa and JPCP pavements in Ontario, respectively (54, 55). Both studies used the OAT approach for sensitivity analysis by varying each transfer function coefficient from 20% to 50% of its global value. The results ranked significant input variables based on normalized sensitivity index (NSI).

The NSI involves scaling of sensitivity index values by a range of calibration coefficients, making it possible to compare the impacts of different calibration coefficient values on the performance prediction of PMED models. NSI can be defined as "percent variation in predicted distress due to percent change in calibration coefficient." Equation 4-1 is used to calculate the NSI.

$$NSI = S_{ijk}^{DL} = \frac{\Delta Y_{ji}}{\Delta X_{ki}} \frac{X_{ki}}{Y_j} \quad (4\text{-}1)$$

where;

NSI = normalized sensitivity index; S_{ijk}^{DL} = sensitivity index for input *k*, distress *j*, and at point, *i* concerning a given global prediction; ΔY_{ji} = change in distress *j* around point *i* $\left(Y_{j,i+1} - Y_{j,i-1}\right)$;

X_{ki} = value of input X_k at point i; ΔX_{ki} = change in input X_k around point i $\left(X_{k,i+1} - X_{k,i-1}\right)$; Y_j = global prediction for distress j.

The NSI values explain the sensitivity of any input or transfer function coefficients; however, they do not give any information on the accuracy of coefficient estimation. Moreover, the NSI is calculated based on predicted distress data, so NSI ranking is affected by the magnitude of the predicted data (55).

4.1 Scaled Sensitivity Coefficients (SSCs)

Parameter estimation is a fundamental concept in mathematics, statistics, and many other engineering fields. It involves finding a suitable value of parameters in the model using observed data to ensure that the model fits accurately to the observed and predicted data. According to Beck and Arnold, parameter estimation is "a discipline that provides tools for the efficient use of data in the estimation of constants that appear in mathematical models and for aiding in modeling phenomena" (56). Parameter estimation without reporting relative error in parameters is similar to curve fitting, but relative errors can be computed if a sensitivity matrix is formulated (57). As per Dolan, the sensitivity matrix or Jacobian (J) is a matrix of the first derivatives of the model for each parameter and has the dimensions of n-by-p, where n and p are the numbers of data points and parameters, respectively (58).

SSCs are needed to determine whether parameters can be estimated and which will have the smallest relative error. Linear dependence can also be examined graphically by plotting sensitivity coefficients versus an independent variable (58). Consider a model $\eta = (x, \beta)$, where x is the independent variable, and β is the actual true parameter vector. The i^{th} sensitivity coefficient can be computed as $X_i = \partial\eta/\partial\beta_i$. To scale the sensitivity coefficient, it is multiplied by its parameter and called the scaled sensitivity coefficient, as shown by Equation 4-2.

$$X_i' = \beta_i \frac{\partial \eta}{\partial \beta_i} \qquad (4\text{-}2)$$

where;

X_i' = Scaled sensitivity coefficient of the parameter I; β_i = Estimate of the ith parameter; $\frac{\partial \eta}{\partial \beta_i}$ = ith sensitivity coefficient of the model w.r.t β_i.

The scaled sensitivity coefficients have the same units as the model η and can be compared directly to η. The SSCs indicate the magnitude of change of the response due to perturbations in the parameters (56). Computing the derivative analytically of the non-linear

function is a complex problem; however, it can be derived using the numerical approach to avoid errors in the analytical approach. If a model η(x,β) has two parameters, β_1 and β_2, then sensitivity coefficients (X_i) and SSC (X_i') w.r.t. both the parameters are estimated using Equations 4-3 to 4-6.

$$X_1 = \frac{\partial \eta}{\partial \beta_1} \approx \frac{\eta\left((1.001 * \beta_1)_{,}\, \beta_2\right) - \eta\left(\beta_{1,}\, \beta_2\right)}{0.001 * \beta_1} \tag{4-3}$$

$$X_1' = \beta_1 \frac{\partial \eta}{\partial \beta_1} \approx \frac{\eta\left((1.001 * \beta_1)_{,}\, \beta_2\right) - \eta\left(\beta_{1,}\, \beta_2\right)}{0.001} \tag{4-4}$$

$$X_2 = \frac{\partial \eta}{\partial \beta_2} \approx \frac{\eta\left(\beta_1, (1.001 * \beta_2)_{,}\,\right) - \eta\left(\beta_{1,}\, \beta_2\right)}{0.001 * \beta_2} \tag{4-5}$$

$$X_2' = \beta_2 \frac{\partial \eta}{\partial \beta_2} \approx \frac{\eta\left(\beta_1, (1.001 * \beta_2)_{,}\,\right) - \eta\left(\beta_{1,}\, \beta_2\right)}{0.001 * \beta_2} \tag{4-6}$$

As per Dolan, the sensitivity coefficients matrix (Jacobian) "J" can be obtained using a nonlinear regression algorithm in MATLAB to estimate the parameters β_i. No, the matrix of β and "J" can be used to get an approximation of SSCs using the following equations.

$$X_1' \approx \beta_1 * J(:,1) \tag{4-7}$$

$$X_2' \approx \beta_2 * J(:,2) \tag{4-8}$$

Scaled sensitivity coefficients $\boldsymbol{X_i'}$ to be large enough (the maximum value of SSC should be at least 10% of the most significant value of the dependent variable) with η and uncorrelated with each other. The larger the $\boldsymbol{X_i'}$, the greater the response and the more easily parameter $\boldsymbol{\beta_i}$ can be estimated. If any $\boldsymbol{X_i'}$ are correlated, meaning one is a linear function of another $\boldsymbol{X_j'}$, those parameters cannot be evaluated separately because the response η to both will be identical (58).

4.2 Methodology

The sensitivity of the PMED transfer function coefficients is crucial in estimating the impact of each coefficient on the overall performance predictions. It is often not viable to calibrate all coefficients; therefore, only the sensitive ones can be estimated if the sensitivity of each coefficient is known. The sensitivity of the PMED transfer function coefficients for all performance prediction models was obtained using the concept of SSCs. Moreover, ranking based on SSCs was compared to the NSI values from the literature *(54)*. Four performance prediction models similar to new flexible pavements, bottom-up cracking, top-down cracking, total rutting, and IRI, were used for sensitivity analysis using SSCs.

The SSC for a particular coefficient (say β_i) is calculated by differentiating the function w.r.t. β_i and multiplying it by β_i (as shown in Equation 2). Other coefficients except β_i are held constant. A similar approach is used to calculate SSCs for all different coefficients. The mathematical model (transfer function) can often be significantly complicated when differentiating the process. In that case, the SSCs can be approximated numerically to avoid errors in the analytical derivation. An example of the estimation of SSCs using the fatigue cracking (bottom-up) model (shown in Equation 4-9) for HMA overlay over rubblized PCC.

$$FC_{\text{Bottom}} = \left(\frac{1}{60}\right)\left(\frac{C_4}{1 + e^{C_1 C_1^* + C_2 C_2^* \log(DI_{\text{Bottom}} \cdot 100)}}\right) \quad (4\text{-}9)$$

where,

FC_{Bottom} = Bottom-up fatigue cracking (in the percentage of area); DI_{Bottom} = cumulative damage at the bottom of the AC layer; C_1, C_2, C_4 = Transfer function coefficients where C_2 is a function of thickness for HMA thickness between 5 and 12 inches; C_1* and C_2* can be determined using Equation 4-10 and Equation 4-11.

$$C_1^* = -2C_2^* \quad (4\text{-}10)$$

$$C_2^* = -2.40874 - 39.748(1 + H_{HMA})^{-2.856} \quad (4\text{-}11)$$

Denoting fatigue bottom-up cracking as a function of DI_B, C_1, and C_2 [$FC(DI_B, C_1, C_2)$], the sensitivity coefficient for C_1 (X_{C_1}) can be approximated as shown in Equation 4-12.

$$\frac{\partial FC}{\partial C_1} = X_{C_1} \approx \frac{FC(DI_B, C_1 + \delta, C_2) - FC(DI_B, C_1, C_2)}{\delta \times C_1} \quad (4\text{-}12)$$

Where δ is a small quantity (a value of 0.001 is used), the SSC for C_1 (X'_{C_1}) can be approximated as shown in Equation 4-13.

$$C_1 \frac{\partial FC}{\partial C_1} = X'_{C_1} \approx \frac{C_1}{} \frac{FC(DI_B, C_1 + \delta, C_2) - FC(DI_B, C_1, C_2)}{\delta \times C_1} = \frac{FC(DI_B, C_1 + \delta, C_2) - FC(DI_B, C_1, C_2)}{\delta} \quad (4\text{-}13)$$

The coefficient C_1 is changed by δ to get the first term of the numerator. The second term of the numerator is the fatigue bottom-up cracking at global values. These terms are evaluated at a continuous range of DI_B from 0 to 1. This provides a continuous set of X'_{C_1} for each value of DI_B. SSCs for C_2 (X_{C_2}) are calculated as shown in Equation 4-14. SSCs for each coefficient are plotted with DI_B on the same plot. A similar process was used for all other transfer functions.

$$C_2 \frac{\partial FC}{\partial C_2} = X'_{C_2} \approx \frac{FC(DI_B, C_1, C_2 + \delta) - FC(DI_B, C_1, C_2)}{\delta \times C_2} = \frac{FC(DI_B, C_1, C_2 + \delta) - FC(DI_B, C_1, C_2)}{\delta} \quad (4\text{-}14)$$

Table 4-1 summarizes the transfer functions for HMA overlay over rubblized PCC pavements used in this study. The sensitivity for the coefficients in red is estimated. The details of these transfer functions can be found in Chapter 2.

4.3 Sensitivity Results

The Pavement-ME V2.6 has been used for this study. No literature is available for the rehabilitated pavement model coefficients' sensitivity, so a comparison is made between the new flexible pavement design and HMA overlay over rubblized concrete. The SSCs were calculated and plotted using MATLAB codes, considering one coefficient at a time and others as constant. A wide range of independent variables have been used since calculating SSCs is a forward problem without data. Subsequent paragraphs explain and summarize the results of sensitivity based on SSCs for transfer functions.

Table 4-1: Summary of PMED transfer functions for rubblized pavements

Performance prediction model		Model transfer functions
Bottom up cracking		$FC_{Bottom} = \left(\frac{1}{60}\right)\left(\frac{6000}{1+e^{C_1 C_1^* + C_2 C_2^* Log(DI_{Bottom} \times 100)}}\right)$
Top-down cracking		$t_0 = \frac{K_{L1}}{1 + e^{K_{L2} \times 100 \times (a_0/2A_0) + K_{L3} \times HT + K_{L4} \times LT + K_{L5} \times log_{10} AADTT}}$ $L(t) = L_{MAX} e^{-\left(\frac{C_1 \rho}{t - C_3 t_0}\right)^{C_2 \beta}}$
Rutting	HMA	$\Delta_{p(HMA)} = \varepsilon_{p(HMA)} h_{HMA} = \beta_{1r} k_z \varepsilon_{r(HMA)} 10^{k_{1r}} n^{k_{2r} \beta_{2r}} T^{k_{3r} \beta_{3r}}$
	Base/ subgrade	$\Delta_{p(soil)} = \beta_{s1} k_{s1} \varepsilon_v h_{soil} \left(\frac{\varepsilon_o}{\varepsilon_r}\right) e^{-\left(\frac{\rho}{n}\right)^{\beta}}$
IRI		$IRI = IRI_o + C_1(RD) + C_2(FC_{Total}) + C_3(TC) + C_4(SF)$

4.3.1 Fatigue Bottom-up Cracking

For a wide range of damage, as shown in Figure 4 – 1 (a), C_1 is more sensitive than C_2, and C_1 and C_2 are not correlated. Moreover, both C_1 and C_2 are large enough to be confidently estimated. However, for a narrow range of damage, the sensitivity of the calibration coefficients is similar, i.e., C_2 is as sensitive as C_1 if the damage is less than 18 %. After 18%, the sensitivity

of the coefficients changes, and C_1 becomes more sensitive, as indicated by the Figure 4 – 1 (b). Coefficients with negative SSCs suggest that an increase in the coefficient will decrease predicted performance. Therefore, an increase in C_1 or C_2 will reduce bottom-up cracking. Figure 4 – 1 shows the SSCs for the fatigue bottom-up cracking model.

4.3.2 Top-down Cracking

The sensitivity of coefficients changes with the independent variables, which are t (analysis time in days) and t_0 (time to crack initiation). Overall, C_3 is the most sensitive coefficient, followed by C_2, and C_1 is the least sensitive coefficient. C_1 and C_2 correlate, indicating that only one can be confidently estimated. All coefficients are estimable based on the magnitude of SSCs, and an increase in any of the coefficients will reduce the predicted top-down cracking.

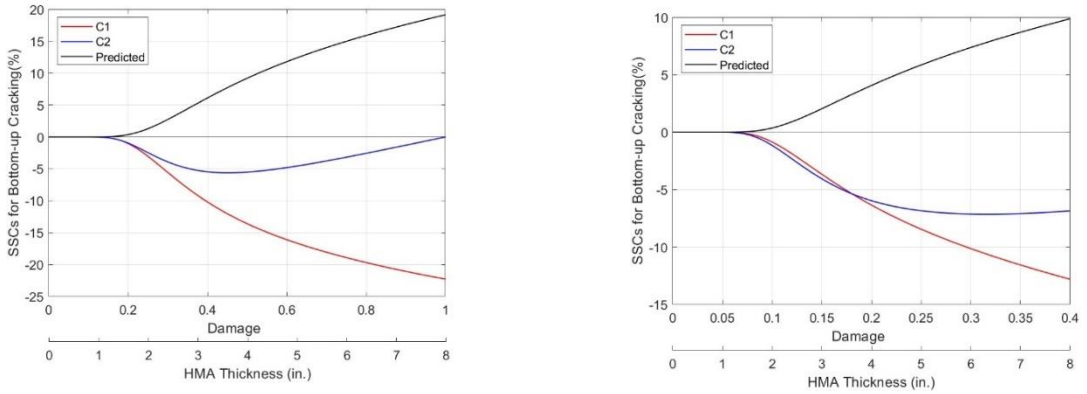

(a) Wide range damage (b) Narrow range damage

Figure 4-1: SSCs for fatigue bottom-up cracking

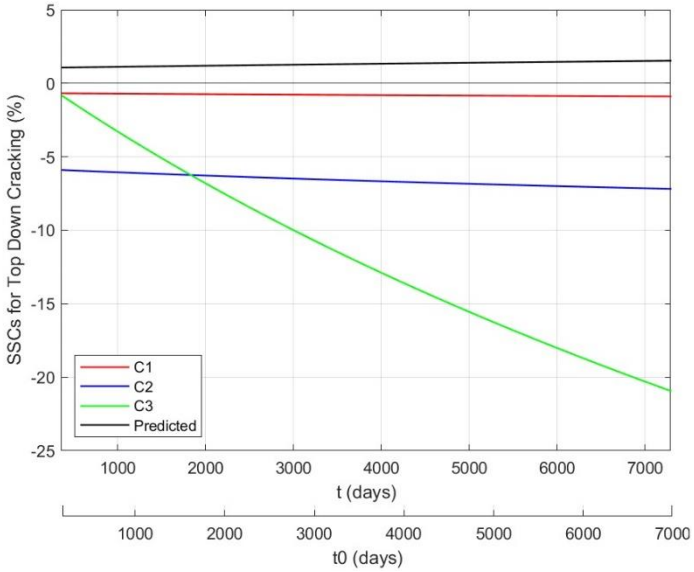

Figure 4-2: SSCs for top-down cracking

4.3.3 Total Rutting

Total rutting is a linear model between the individual layer rutting. Subgrade rutting coefficient (β_{sg1}) is the most sensitive, followed by asphalt concrete (AC) rutting coefficient (β_{1r}). The base rutting coefficient (β_{s1}) is the least sensitive. SSCs for all coefficients are large enough to be estimable and positive.

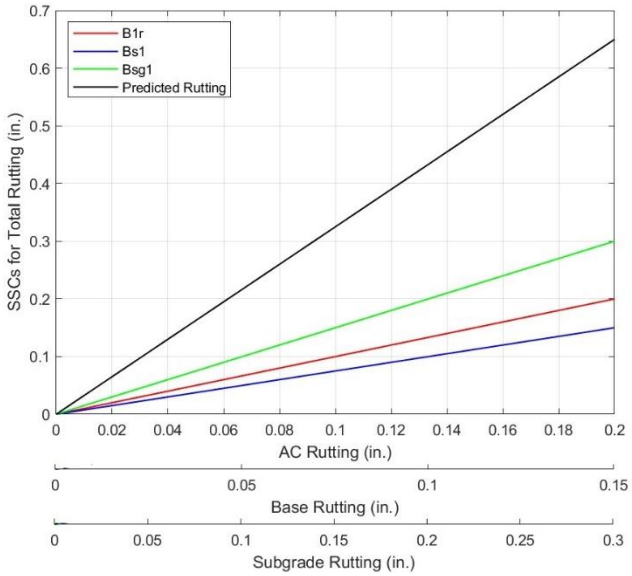

Figure 4-3: SSCs for total rutting

4.3.4 IRI

IRI is a linear relationship between IRI at the time of construction (initial IRI) and other distress (cracking, rutting, etc.). The site factor coefficient is the most sensitive, followed by the total rutting coefficient. The thermal cracking coefficient is the following sensitive input, while the fatigue cracking coefficient is the least sensitive. All coefficients have positive values for SSCs, which means that with an increase in coefficient value, the predicted performance for IRI will increase.

4.4 Summary

The sensitivity of the calibration coefficients of the performance prediction models has a direct impact on the performance prediction. The sensitivity of the model's coefficients is also helpful in deciding the importance and its calibration order when all coefficients cannot be estimated at one time. SSCs provide a convenient visual representation of the sensitivity of different transfer function coefficients over a continuous range of independent variables, unlike NSI, which is a point estimate. SSCs for fatigue bottom-up cracking show that the

sensitivity changes at different ranges of the independent variable “damage.” It also indicates any correlations between different coefficients and confidence in estimation.

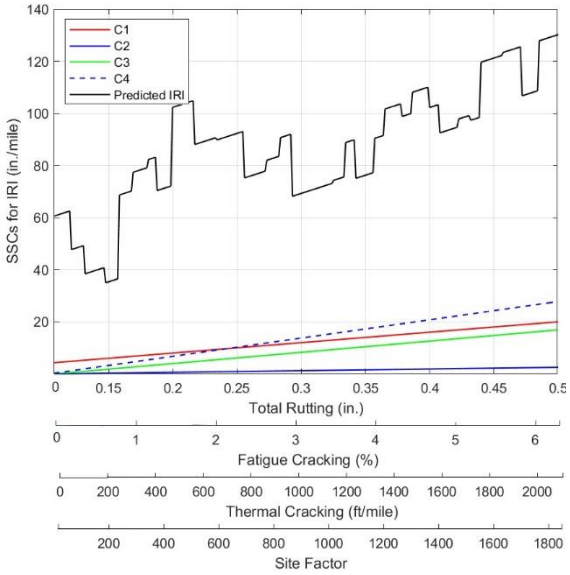

Figure 4-4: SSCs for IRI

The calculation of SSCs is a forward problem and does not require any input data. Therefore, a user only needs a mathematical model (the transfer functions) and can calculate SSCs on any range of independent variables. Table 4 -2 summarizes the sensitivity ranking for transfer functions of HMA overlay over rubblized PCC based on SSCs. The sensitivity order using SSCs is based on the overall sensitivity in the entire range of independent variables. Coefficients with the same NSI values have been ranked the same. For example, all rutting coefficients in Kim et al.'s (2014) study have been rated as one as they all have the same NSI values. Bottom-up cracking models have similar rankings using both methods, whereas others, e.g., IRI, total rutting, and top-down cracking models, have significant differences. These differences make it challenging to estimate the most sensitive coefficients. Therefore, SSCs can be helpful to obtain a continuous range of sensitivity rather than a point estimate.

Table 4-2: Sensitivity ranking comparison based upon SSCs and NSI values

Performance model	Coefficient	SSCs	Kim et al. (2014) *(54)*
Bottom-up cracking	C_1	1	1
	C_2	2	2
Top-down cracking	C_1	3	NA
	C_2	2	NA
	C_3	1	NA
Total rutting	β_{1r}	2	1
	β_{s1}	3	1
	β_{sg1}	1	1
IRI	C_1	2	2
	C_2	4	3
	C_3	3	3
	C_4	1	1

CHAPTER 5 CALIBRATION METHODOLOGY

The MEPDG was developed under the NCHRP project 1-37A to overcome the limitations of the AASHTO 1993 method (2). It is an advanced pavement design tool for new and rehabilitated pavements. MEPDG incorporates material properties, traffic, and climate to estimate the incremental damage using mechanical responses of the pavement. The cumulative damage is empirically used to predict the field distress using transfer functions. The transfer functions used in PMED have been calibrated using the Long-term Pavement Performance (LTPP) pavement sections at the national level *(3)*. Although the nationally calibrated models provide a fair performance prediction for the entire US road network, these may not represent the construction practices, materials, and climatic conditions of a particular state/region. Therefore, nationally calibrated models may under-predict or over-predict the pavement performance in specific states/regions. Re-calibration of these models has been recommended for local conditions in the local calibration guide *(32)*. Several studies have been conducted to recalibrate the transfer function coefficients locally for new and rehabilitated pavement sections; this study outlines the local calibration HMA overlay over rubblized PCC pavements. The critical performance distress in the PMED includes bottom-up cracking (percentage), top-down cracking (percentage), rutting (inches), thermal (transverse) cracking (feet/mile), and IRI (inches/mile) for rubblized pavements. This chapter briefly highlights the calibration methods and approaches for each model.

5.1 Calibration Approaches

Local calibration of the PMED models aims to optimize the model coefficients to minimize bias and standard error. The aim is achieved by matching the predicted and measured distress. Bias in the predictions signifies if there is a systematic over- or under-prediction, whereas standard error shows the scatter and variability. Figure 1-2 shows a representation of bias and standard error. Genetic Algorithm (GA) has been used to optimize transfer function coefficients using MATLAB program. GA involves the following operations:

a. Initialization: GA generates solutions by randomly selecting a subset inside the allowed search space called the population.
b. Selection: The generated solutions are selected based on the value of the objective function.

c. Generation of offspring: New solutions are created using the selected solutions or populations (offspring) based on mainly two processes: mutation and crossover.
d. Termination: This process continues till the termination criteria for the given population or the number of generations is reached.

The empirical transfer functions can be of two types: (a) model that directly calculates the magnitude of surface distress, and (b) model that calculates the cumulative damage index rather than actual distress magnitude. Based on the model, two different calibration approaches have been followed.

Approach 1: For specific models (e.g., fatigue cracking, rutting, transverse cracking, and IRI), damage is directly obtained from PMED outputs. The transfer functions predict distress from the damage and have been calibrated using the MATLAB program outside the PMED. Different resampling techniques have been used to calibrate these functions.

Approach 2: The Calibration Assistance Tool (CAT) calibrates the thermal cracking model where the damage is not obtained from PMED outputs. These models predict distress by calculating cumulative damage over time.

Table 5-1 summarizes the transfer functions and the coefficients calibrated during the study.

Table 5-1: Model transfer functions and calibration coefficients for rubblized pavements

Models		Approach I	Approach II	Model transfer functions
Fatigue cracking – bottom up.		✓		$FC_{\text{Bottom}} = \left(\frac{1}{60}\right)\left(\frac{C_4}{1+e^{C_1C_1^*+C_2C_2^*\log(DI_{\text{Bottom}}\cdot 100)}}\right)$
Fatigue cracking – top down.		✓		$t_0 = \frac{K_{L1}}{1+e^{K_{L2}\times 100\times(a_0/2A_0)+K_{L3}\times HT+K_{L4}\times LT+K_{L5}\times \log_{10} AADTT}}$ $L(t) = L_{MAX}e^{-\left(\frac{C_1\rho}{t-C_3t_0}\right)^{C_2\beta}}$
Rutting	HMA	✓	✓	$\Delta_{p(HMA)} = \varepsilon_{p(HMA)}h_{HMA} = \beta_{1r}k_z\varepsilon_{r(HMA)}10^{k_{1r}}T^{k_{2r}\beta_{2r}}N^{k_{3r}\beta_{3r}}$
	Base/subgrade	✓		$\Delta_{p(soil)} = \beta_{s1}k_{s1}\varepsilon_v h_{soil}\left(\frac{\varepsilon_o}{\varepsilon_r}\right)e^{-\left(\frac{\rho}{n}\right)^{\beta}}$
Thermal cracking			✓	$A = k_t\beta_t 10^{[4.389-2.52Log(E_{HMA}\sigma_m\eta)]}$
IRI		✓		$IRI = IRI_o + C1(RD) + C2(FC_{\text{Total}}) + C3(TC) + C4(SF)$

*Red font indicates coefficients being calibrated in this study

5.2 Calibration Techniques

This section discusses the various calibration techniques, their advantages, and limitations. These techniques include (a) traditional split sampling approach, (b) bootstrapping, and (c) Maximum likelihood estimation (MLE). These techniques are briefly discussed below.

5.2.1 Traditional Approach

The NCHRP Project 1-40B and local calibration guide provides recommended practices for local calibration of the PMED performance models. The traditional approach includes no resampling and is based on a random split into the calibration and validation subsets. The calibration-validation process depends on the number of selected sections, and two different calibration approaches may be needed depending on the distress predicted through the transfer function. The first approach (Approach 1) is used for models directly calculating the magnitude of surface distress. In contrast, the second approach (Approach 2) is used for models that calculate cumulative damage over time and related damage to distress. Data collected from in-service pavements are used to establish calibration coefficients that minimize the overall standard error of the estimate between the predicted and measured distress. The validation process demonstrates that the calibrated model can produce accurate predictions for sections other than those used for calibration. An efficient validation is determined by the bias in the predicted values and standard error of the estimate. Statistical hypothesis tests determine if a significant difference exists between the calibrated model and the model validation.

5.2.2 Bootstrapping

Bootstrap resampling is a statistical technique widely used in many research fields, including statistics, economics, finance, and computer science. This method allows researchers to estimate a statistic's sampling distribution and construct confidence intervals for a population parameter, even when the underlying population distribution is unknown. The basic idea of bootstrap resampling is to draw many bootstrap samples from the original sample with replacement. Each bootstrap sample resamples the original data with the same sample size but may contain some duplicate observations. The bootstrapped resampling can be performed using different methods: (a) resampling randomly or (b) resampling based on the residuals. The type of resampling approach for bootstrapping depends on the data structure. The statistic of interest is calculated for each bootstrap sample, and the statistic distribution is estimated using the bootstrap sample statistics. The general steps involved in the bootstrap resampling method are as follows:

a. Draw a random sample of size *n* with a replacement from the original data set.
b. Calculate the statistic of interest for the sample. For calibration, this can be the estimation of calibration coefficients.
c. Repeat steps 1 and 2 B times to obtain B bootstrap samples. The team used 1000 bootstrap resamples for calibration.
d. Calculate the statistic's standard error and confidence interval using the bootstrap samples.

In practice, the number of bootstrap samples B is often large, such as 1,000 or 10,000, to ensure accurate estimates of the standard error and confidence interval. The standard error of a statistic estimated using bootstrap resampling can be calculated using Equation 5-1.

$$\mathrm{SE} = \sqrt{\frac{1}{B-1}\sum(\theta_b - \theta^*)^2} \qquad (5\text{-}1)$$

where;

SE = estimated standard error of the statistic; B = number of bootstrap samples; θ_b = value of the statistic for the b_{th} bootstrap sample; θ^* = mean of the B bootstrap sample values.

The confidence interval for the statistic can be calculated using the percentile method, which involves ranking the B bootstrap sample values and taking the 2.5th and 97.5th percentiles as the lower and upper bounds of the confidence interval, as shown in Equation 5-2.

$$\mathrm{CI} = (\theta^* - \theta_{\frac{\alpha}{2}}, \theta^* + \theta_{\frac{\alpha}{2}}) \qquad (5\text{-}2)$$

where;

CI = bootstrap confidence interval; θ^* = mean of the B bootstrap sample values; $\theta_{\frac{\alpha}{2}}$ = $\frac{\alpha}{2}$th percentile of the bootstrap sample values.

Bootstrap resampling has several advantages over other statistical methods. First, it does not require population distribution or sample size assumptions. This is particularly useful when the sample size is small or the population distribution is unknown or not normal. Second, it allows researchers to estimate the variability of a statistic and construct confidence intervals without resorting to complex mathematical formulas or asymptotic approximations. Third, it can be easily implemented using standard statistical software packages like R, Python, or SAS. However, bootstrap resampling also has some limitations and potential pitfalls. First, it can be computationally intensive, especially when the number of bootstrap samples or the original

sample size is large. Second, the bootstrap samples may not accurately reflect the true population distribution, especially if the original sample is biased or contains outliers. Third, the results may be sensitive to the choice of the statistic and the resampling method.

5.2.3 Maximum Likelihood Estimation (MLE)

MLE is a powerful statistical technique for parameter estimation in various fields, including biology, physics, economics, and engineering. In the traditional calibration approach, the error term is assumed to be normally distributed. This might not be the case for all distress types. MLE seeks to estimate the parameters of a probability distribution that best describes the observed data based on the likelihood function. The likelihood function measures the probability of observing the data given a particular set of model parameters. MLE finds the set of model parameters that maximize the likelihood function, resulting in the most likely estimates of the parameters. Consider a dataset X = [x1, x2, ..., xn], that is assumed to be generated by a probability distribution with parameters θ. The likelihood function L(θ|X) is defined as the joint probability density function of the observed data, given the model parameters as shown in Equation 5-3.

$$\mathrm{L}(\theta|\mathrm{X}) = \mathrm{P}(\mathrm{X}|\theta) = \mathrm{P}(\mathrm{x1}, \mathrm{x2}, \ldots., \mathrm{xn}|\theta) \tag{5-3}$$

Where *P* denotes the probability density function, the likelihood function measures the probability of observing the data *X* given the model parameters θ. The goal of MLE is to find the set of model parameters θ that maximize the likelihood function. In practice, it is often easier to work with the log-likelihood function, which is the natural logarithm of the likelihood function. The log-likelihood function is given by Equation 5-4.

$$l(\theta|\mathrm{X}) = \log \mathrm{L}(\theta|\mathrm{X}) = \log \mathrm{P}(\mathrm{X}|\theta) = \log \prod \mathrm{P}(xi|\theta) = \sum \log \mathrm{P}(xi|\theta) \tag{5-4}$$

where;

Π = product operator; Σ = summation operator.

Taking the logarithm of the likelihood function simplifies the computation of the derivative, which is required for optimization. The optimization problem can be solved by finding the values of θ that maximize the log-likelihood function. This can be done using numerical optimization algorithms, such as gradient descent, Newton's, or quasi-Newton methods. These algorithms require the derivative of the log-likelihood function for the model parameters.

Numerical optimization algorithms iteratively update the values of the model parameters based on the score function to maximize the log-likelihood function. The optimization process continues until the algorithm converges to a maximum of the log-likelihood function. The MLEs obtained from the optimization process represent the most likely estimates of the model parameters that can explain the observed data. These estimates can be used for parameter inference, hypothesis testing, and model selection.

One of the main advantages of MLE is that it provides a robust and rigorous approach to parameter estimation. The MLEs are derived from a well-defined likelihood function based on the data's underlying probability distribution. This ensures that the estimates are statistically valid and can be interpreted meaningfully. Another advantage of MLE is that it is a computationally efficient optimization method. The likelihood function can often be evaluated using standard probability distributions, and the optimization problem can be solved using numerical optimization algorithms that are widely available. This makes MLE a practical and scalable method for parameter estimation, even in high-dimensional and complex models. MLE is beneficial when the complex model contains multiple parameters that are difficult to estimate using other methods. For example, in machine learning, MLE is used to estimate the parameters of probabilistic models, such as hidden Markov models and Bayesian networks.

Three distributions were used for this analysis: gamma, log-normal, and exponential. These distributions' probability density function (pdf)/ probability mass function (pmf) is shown in Equations 5-5 to 5-7, respectively.

a. Gamma distribution

$$f(y) = \frac{y^{\alpha-1}e^{-y/\beta}}{\beta^{\alpha}\Gamma(\alpha)} \tag{5-5}$$

b. Log-normal distribution

$$f(x) = \frac{e^{-\left(\left(\ln((x-\theta)(m))^2/(2\sigma^2)\right)\right)}}{(x-\theta)\sigma\sqrt{2\pi}}\, x > \theta; m, \sigma > 0 \tag{5-6}$$

c. Exponential distribution

$$f(\mathrm{x}) = \lambda \mathrm{e}^{-\lambda \mathrm{x}} \tag{5-7}$$

The selection of the best distribution is based on the SEE, bias, Negative Log Likelihood (NLL), Akaike Information Criterion (AIC), and Bayesian Information Criterion (BIC)

5.2.4 Summary of Resampling Techniques

Traditional no-sampling or split sampling technique provides a convenient approach to selecting pavement sections from the calibration database. Though these techniques are easy to implement and can be used for any PMED model, they might impose some limitations. Resampling techniques have several advantages over traditional approaches. Since these are non-parametric techniques, the model parameters can be estimated without making assumptions about the data distribution. The distribution of the model coefficients and error parameters can be estimated instead of the point estimate. This can give a better estimation of parameters within desired confidence intervals. Since a new sample is created every time, the outliers or sections controlling the calibration process can be identified. Though these resampling techniques have several advantages over traditional approaches, there are also certain limitations. Bootstrapping cannot be used for small datasets or when the independence assumption is unmet. Resampling techniques also require higher computing power and time and can be used only for those performance models where the damage and other inputs are available from PMED. Table 5-2 summarizes the advantages and limitations of all calibration techniques.

Table 5-2: Summary of calibration techniques

Technique	Advantages	Limitations
No sampling	• Computationally efficient • Applicable even for small sample size	• Provides point estimates • It may not be suitable for non-normally distributed data
Split sampling	• Computationally efficient • Provides validation	• Provides point estimates • It may not be suitable for non-normally distributed data
Bootstrapping	• Provides confidence intervals • Identifies outliers • Distribution assumption is not required	• Computationally time-consuming • It cannot be used for smaller sample size • It may not be suitable for non-normally distributed data
MLE	• Suitable for non-normally distributed data • Identifies outliers • Can be used with resampling techniques and for validation	• Distribution assumption is required • Computationally time-consuming and requires prior knowledge of the concept of maximum likelihood

5.3 Procedure for Calibration of Performance Models

The details for input data, performance data, and project selection have already been discussed in Chapter 3. Once the data is extracted, it can run the PMED files (.dgpx files) and generate outputs (structural responses). The process for local calibration is summarized below:

a. Run PMED (using global model coefficients) and extract critical responses and predicted distresses.
b. Compare the predicted distress with measured distress.
c. Based on the results from step 2, test the accuracy of the global models and the need for local calibration.
d. If predictions using global models are satisfactory, local calibration is not required, and global models can be accepted. If the global model has significant bias and standard error, local calibration is required.
e. Check your calibration results by validating them on an independent set of sections not used for calibration.

5.3.1 Sampling Techniques Used

The following techniques have been used to calibrate the PMED models. All these methods have been used for models calibrated using Approach I. For models calibrated using Approach II, only no sampling and traditional split sampling have been used in the CAT tool.

a. No sampling (include all data).
b. Traditional split sampling.
c. Bootstrapping.

The entire dataset (all available data points) is considered in no sampling. Bootstrapping has been used by considering 1000 bootstrap resamples with replacement. Both of these techniques have been used for calibration. For calibration validation, a split of 70%-30% has been used where 70% of the data goes to the calibration set, whereas 30% goes to the validation set.

5.4 Rubblized Pavement Model Coefficients

The critical performance distress in the PMED includes bottom-up cracking, top-down cracking, rutting, thermal (transverse) cracking, and IRI. The following section discusses the calibration of each model and the specific coefficients.

5.4.1 Bottom-up Cracking Model

The fatigue cracking (bottom-up) model was calibrated by optimizing the C_1 and C_2 coefficients (see Table 5-1). In PMED v2.6, coefficient C_1 is a single value, whereas coefficient C_2 has three different values depending on the total HMA thickness. Table 5-3 shows the global values for C_1 and C_2.

Table 5-3: Global values for bottom-up cracking model coefficients

Calibration coefficient	Global values
C_1	1.31
C_2	H_{ac} < 5 in. : 2.1585
	5 in. <= H_{ac} <=12 in.: (0.867 + 0.2583 × H_{ac}) ×1
	H_{ac} > 12 in.: 3.9666

H_{ac}: Total HMA thickness in inches

Notably, no selected section for the bottom-up calibration had a total HMA thickness of more than 12 inches, so the coefficient C_2 was calibrated separately for the thickness ranges less than 5 inches and 5 to 12 inches, respectively. For a thickness range of 5 to 12 inches, only the multiplying factor 1 (marked in bold here: (0.867 + 0.2583 × Hac) ×1) was calibrated while other values (0.867 and 0.2583) were kept at global values.

5.4.2 Top-down Cracking Model

The top-down cracking model has been modified in the PMED v2.6. The model consists of a crack initiation function that calculates the time to crack initiation and a crack propagation function that calculates the percent lane area cracked. This makes it a total of 8 coefficients combined from both functions. Since the actual crack initiation time is not known, it was not possible to calibrate the crack initiation model separately. So, a single function was used by substituting the crack initiation function with the crack propagation function. Initially, an attempt was made to change all eight coefficients simultaneously. This approach had some challenges.

a. The model has some mathematical limitations. High values for C_3 give mathematical errors when using it in PMED.
b. There is no current literature available for the top-down cracking model calibration. Therefore, estimating the range for each coefficient to be used in optimization was difficult.
c. The model has many coefficients with coefficient values ranging from 0.011 to 64271618. This makes the optimization challenging to converge.

Finally, four coefficients from the crack initiation function (*kL2, kL3, kL4, kL5)* and two coefficients from the crack propagation function (C_1, C_2) have been calibrated.

5.4.3 Rutting Model

Due to axle loads, rutting is the total accumulated plastic strain in different pavement layers (HMA, base/sub-base, and subgrade). It is calculated by summing up the plastic strains at the mid-depth of individual layers accumulated for each time increment. In the PMED, rutting is predicted separately for the different layers (AC, base, and subgrade). The total rutting is the sum of rutting from all layers. The AC rutting model has three coefficients (β_{1r}, β_{2r}, β_{3r}). β_{1r} is a direct multiplier and can be calibrated using optimization outside the PMED. In the AC rutting model, β_{2r} and β_{3r} are powers to the pavement temperature and the number of axle load repetitions. Calibration of β_{2r} and β_{3r} cannot be done outside of the PMED and requires running the PMED multiple times or optimizing these in the CAT tool. So, β_{2r} and β_{3r} were kept at global values, and β_{1r} was calibrated.

The unbound layers (base and subgrade) rutting model have one calibration coefficient each (β_{s1}). Since β_{s1} is a direct multiplier, it can be calibrated using optimization outside the PMED without running the software or CAT tool. Since both base and subgrade have the same model and calibration coefficient, the base calibration coefficient is referred to as $\beta_{s1,}$ and the subgrade coefficient is referred to as β_{sg1} to avoid confusion. The total measured rutting was calibrated against the sum of individual predicted rutting (i.e., β_{1r}, $\beta_{s1,}$ and β_{sg1} were calibrated simultaneously).

5.4.4 Thermal Cracking Model

The thermal cracking model in the PMED has three different levels for the calibration coefficient. These levels are based on the level of HMA input, i.e., *G** and IDT. Table 5-4 shows the input matrix used for the thermal cracking coefficient at three hierarchical levels. Both *G** and IDT values were obtained from the DYNAMOD software database. In the DYNAMOD database, *G** and IDT values are available only for sections with Performance grade (PG) binder type. Therefore, sections with PG binder type have been used to calibrate the thermal cracking model. In the PMED v2.6, the calibration coefficient k_t is originally a mean annual air temperature (MAAT) function. So, the following approaches can be used for calibration.

a. Using the CAT tool, an initial attempt was made to calibrate kt (using the original equation as a function of MATT).

b. A second attempt was made to calibrate k_t by running the PMED multiple times with different k_t values. This time, single values for k_t, which were not a function of MAAT, were used.

Due to the limitation of the CAT tool at the time of calibration, the k_t value based on the second approach was adopted. It is important to note that for this calibration, the average thermal cracking for a section was cut at 2112 ft/mile.

Table 5-4: HMA properties matrix used for thermal cracking coefficient

Hierarchical Levels	HMA properties (G*, IDT)		
	Level 1	Level 2	Level 3
1	G*	IDT	
2		G*, IDT	
3			G*, IDT

5.4.5 IRI Model

IRI is a linear function of initial IRI, rut depth, total fatigue cracking, transverse cracking, and site factor, as shown in Equation 5-8. The initial IRI was obtained from linear back casting based on the time series trend for each section. The fatigue cracking, rutting, and transverse cracking models were calibrated before calibrating the IRI model. Since all inputs to the IRI model could be obtained, it was calibrated outside the PMED without rerunning it or using the CAT tool.

$$\mathrm{IRI} = \mathrm{IRI_o} + 40.0(\mathrm{RD}) + 0.400(\mathrm{FC_{Total}}) + 0.0080(\mathrm{TC}) + 0.0150(\mathrm{SF}) \quad (5\text{-}8)$$

where;

IRI_o = Initial IRI after construction, in/mi.

SF = Site factor

FC_{Total} = Area of fatigue cracking (combined bottom-up, top-down, and reflection cracking in the wheel path), percent of total lane area.

TC = Length of transverse cracking (including the reflection of transverse cracks in existing HMA pavements), ft/mi.

RD = Average rut depth, in.

5.5 Design Reliability

The PMED estimates the performance of a pavement using mechanistic models and transfer functions. Although these estimates are rational for pavement design purposes, the actual field measurements may show variability. This variability may come from the uncertainties in estimating the future traffic, material, and construction variability, measurement error,

uncertainties due to the use of level 2 and 3 inputs, and errors associated with the model predictions. To incorporate all these variabilities, PMED uses a reliability-based design. Reliability for any prediction can be defined as the probability of getting a prediction lower than the threshold prediction over the design life, as shown in Equation 5-9.

$$\text{Reliability} = \text{P}[\text{distress at the end of design life} < \text{Critical distress}] \quad (5\text{-}9)$$

If 100 sections have been designed at 90% reliability, on average, ten of them may fail before the end of design life. Design reliability levels may vary by distress type and IRI or may remain constant for each. It is recommended, however, that the same reliability be used for all performance indicators *(8)*. Except for IRI, reliability for all other models is estimated using a relationship between the standard deviation of measured distress as the dependent variable and mean predicted distress as the independent variable. The basic assumption implies that the error in predicting the distress is normally distributed on the upper side of the prediction (not on the lower side or near zero values). Figure 5-1 shows an example of IRI prediction at 50% reliability (mean prediction), prediction at any desired reliability *R*, and are associated with the probability of failure. For 90 percent design reliability, the dashed curve at reliability *R* should not cross the IRI at the threshold criteria throughout the design analysis period. Failing to do so may lead to a modified design.

A step-by-step approach to estimating the reliability of bottom-up cracking for an overlay design at input Level 1 is shown below. A similar approach is used for the reliability of all other models except IRI in the PMED.

Step 1: All predicted and measured data points are grouped by creating bins on the predicted cracking. The number of data points in each group should be equivalent to provide fair weightage to each group.

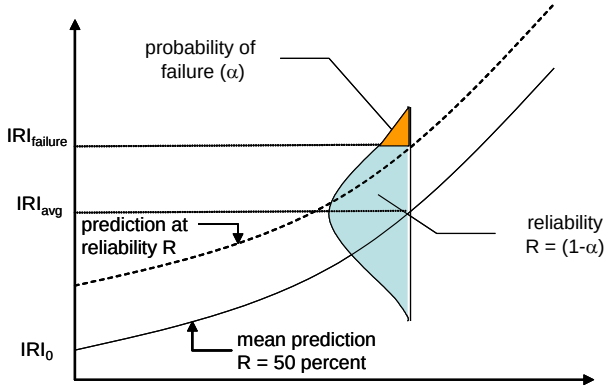

Figure 5-1: Design Reliability Concept for IRI (32)

Step 2: The average and standard deviation of measured and predicted cracking are computed for each group. Table 5-5 shows the number of data points, bin ranges, and descriptive statistics.

Table 5-5: Summary statistics for reliability analysis

Cracking range (%)	No. of data points	Average Measured Cracking	Average Predicted Cracking	Standard dev. of Measured Cracking	Standard dev. of Predicted Cracking
0-1.5	4309	2.309	2.060	2.707	0.283
1.5-2.5	7859	3.136	3.051	3.244	0.286
2.5-3.5	12096	3.421	4.017	3.386	0.286
3.5-4.5	6116	3.364	4.736	3.396	0.144
4.5-5.0	12292	4.343	6.345	3.477	1.282
5.0-100	1884	8.027	10.267	3.264	1.734

Step 3: A relationship is determined between the standard deviation of the measured cracking on the y-axis and the average predicted cracking on the x-axis. Figures 5-2 show the fit model to the grouped data in steps 1 and 2. Equation 5-10 shows the relationship between the standard deviation of the measured cracking and the average predicted cracking.

$$S_{e(Alligator)} = 1.0256 + \frac{2.4828}{1 + e^{0.0046 - 5.2091 \times log(D)}} \quad (5\text{-}10)$$

Step 4: Since the error term is assumed to be normally distributed, the predicted cracking can be adjusted to the desired reliability level using Equation 5-11.

$$\text{Crack}^{R}_{Bottom-up} = \text{Crack}_{Bottom-up} + S_{e(FC)} \times Z_{a/2} \quad (5\text{-}11)$$

where,

$\text{Crack}^{R}_{Bottom-up}$ = Predicted cracking at reliability *R* (%); $\text{Crack}_{Bottom-up}$ = Predicted cracking at 50% reliability; $S_{e(FC)}$ = Standard deviation of cracking, which can be estimated using Equation (5-10); $Z_{a/2}$ = Standardized normal deviate (mean = 0; standard deviation = 1) at reliability *R*.

Step 5: For the final step, the reasonableness of the model should be verified based on the actual measured data before using the reliability equation for design.

The reliability model for IRI is different from that of other models. Since a closed-form solution and the variances of different components of IRI are known, the reliability model for IRI is based on the variance-covariance analysis of its components. The basic assumption implies that the error in predicting IRI is roughly normally distributed. The reliability of the IRI model is

calculated internally in PMED; details can be found elsewhere (2). Table 5-6 shows the global standard error equations of the PMED models.

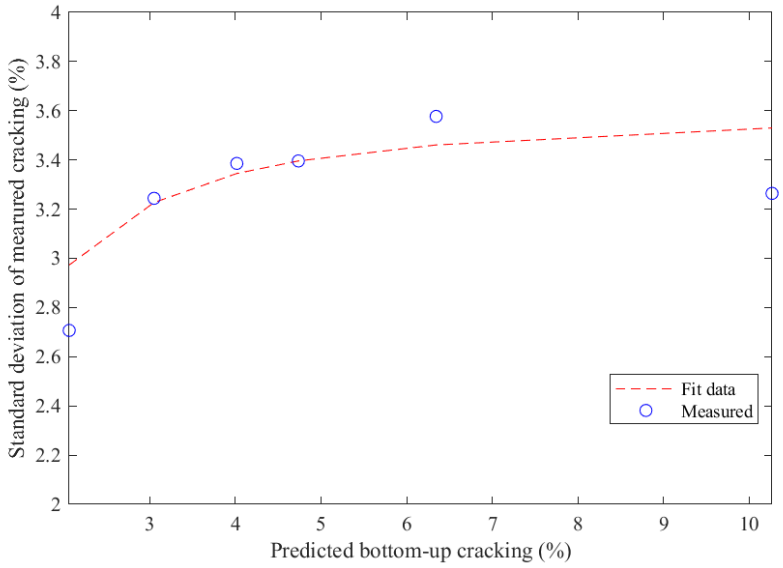

Figure 5-2: Fitting curve for the reliability of transverse cracking

5.6 Summary

This chapter discusses the calibration approach used for each transfer function. Transfer functions have been calibrated based on whether they calculate the distresses directly or calculate them based on cumulative damage. It also discusses the different calibration techniques, applications, and advantages of each. No sampling and bootstrapping have been used for calibration. The traditional split sampling approach is used for calibration and validation. Figure 5-3 illustrates the summary of calibration work done in this study.

Table 5-6: Global equations of standard errors for each distress and smoothness model

Performance prediction models		Standard error equation
Fatigue cracking (bottom-up)		$s_{e(FC)} = 1.13 + \frac{13}{1 + e^{7.57 - 15.5 \times log(D)}}$
Fatigue cracking (top-down)		$s_{e(Top-down)} = 0.3657 \times TOP + 3.6563$
Rutting		$s_{e(HMA)} = 0.24(Rut_{HMA})^{0.8026} + 0.001$
		$s_{e(base)} = 0.1477(Rut_{base})^{0.6711} + 0.001$
		$s_{e(subgrade)} = 0.1235\left(Rut_{subgrade}\right)^{0.5012} + 0.001$
Transverse cracking	Level 1	$s_e = 0.14(TC) + 168$
	Level 2	$s_e = 0.20(TC) + 168$
	Level 3	$s_e = 0.289(TC) + 168$
IRI		Estimated internally by the software

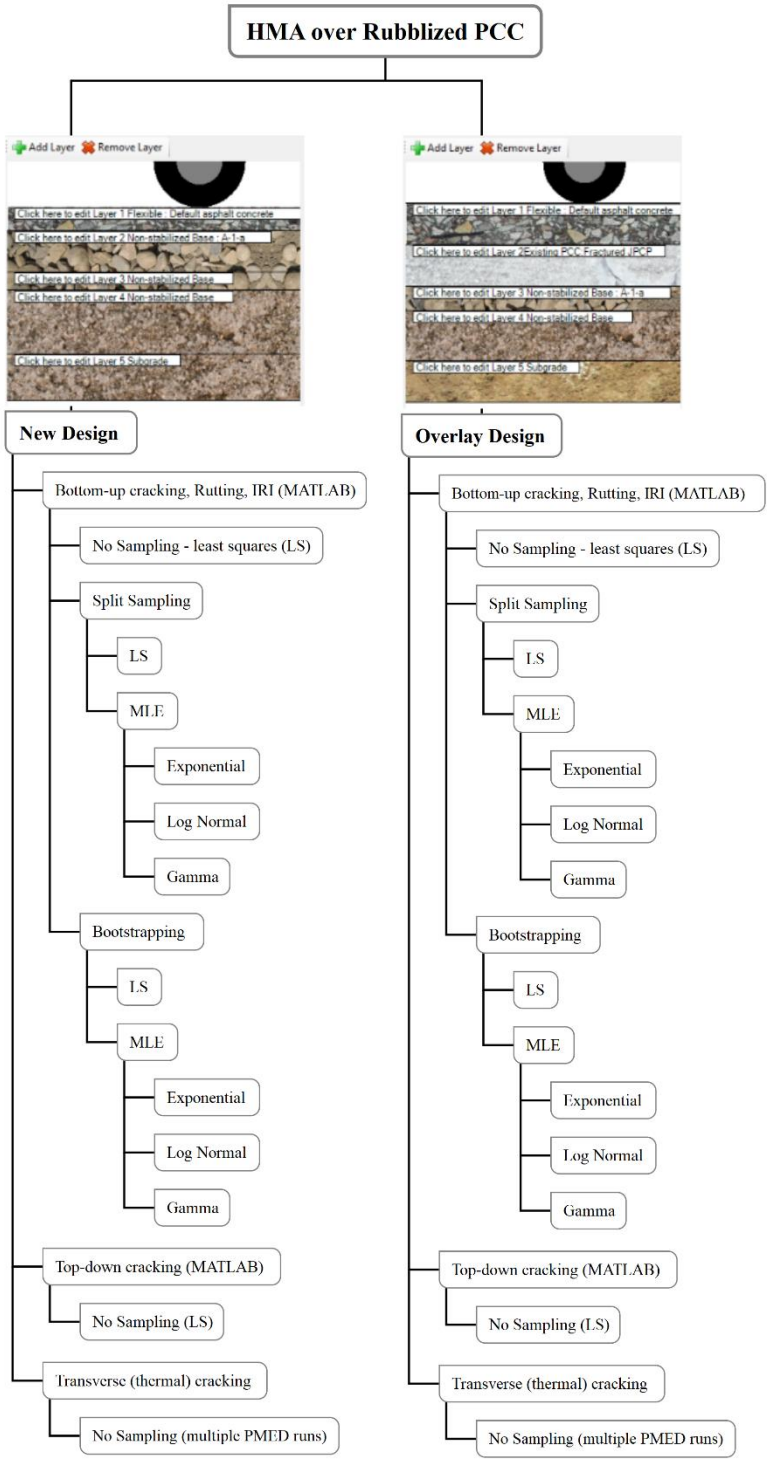

Figure 5-3: Calibration summary of rubblized pavement design

CHAPTER 6 LOCAL CALIBRATION

The PMED models' parameters are adjusted to match observed data for reliable performance predictions during calibration. The calibration process can be challenging because of the model's complexity and the many parameters involved. However, technological advancements and data collection methods have made the calibration process more efficient and effective. Automated data collection techniques, such as laser-based measurements (sensors), provide high-resolution data that can calibrate the PMED models accurately.

This chapter discusses the different options and the calibration results for each model. No sampling and bootstrapping approaches were used for calibration only, whereas traditional split sampling techniques were used for calibration and validation. The following models were recalibrated for both design approaches.

a. Fatigue bottom-up cracking.
b. Fatigue top-down cracking.
c. Total rutting.
d. Transverse (thermal) cracking.
e. IRI.

As already mentioned in Chapter 5, the thermal cracking model was calibrated using PMED. Multiple run analysis was done for thermal cracking sections using PMED by varying thermal cracking model coefficient "K". The PMED was initially used for other performance models to determine the damage with all available inputs (material, traffic, and climate). Then, the calibration approaches mentioned above were implemented using the outputs from the PMED program. A predicted vs. measured distress plot was generated for each model with a line of equality at 45 degrees. These plots can visually inspect a model's SEE and bias. For an ideal model, all the points should lie on equality. The calibration approach used the hypothesis tests outlined in the local calibration guide.

The local calibration results are presented for new and overlay design approaches among the different statistical techniques and the hierarchical input levels. Table 6-1 illustrates the hierarchical input levels and HMA properties used at each input level. It is pertinent that MLE analysis was done using three distributions, as discussed in Chapter 5. Only the results of the selected distribution of MLE are reported in this chapter.

The following section presents a detailed comparison of new and overlay designs of rubblized pavements and the local calibration of performance prediction models.

Table 6-1: Summary of input levels

Input			PMED input level	Input source
Layer materials	HMA	Mix properties	1,2, and 3	MDOT HMA mixture characterization study (DYNAMOD database)
		HMA mixture aggregate gradation	1	Project-specific mixture gradation data obtained from data collection or average statewide values
		Binder properties	1,2, and 3	MDOT HMA mixture characterization study (DYNAMOD database)
	Rubblized PCC	MR	1	Default value of PMED
		Crack spacing	1	Default value of PMED
		LTE	1	Default value of PMED
	Base/ subbase	MR	3	Recommendations from MDOT unbound material study
	Subgrade	MR	3	Soil-specific MR values per MDOT subgrade soil study
		Soil properties	A mix of all levels	Location-based soil type per MDOT subgrade soil study

6.1 Fatigue Bottom-Up Cracking Model

The bottom-up cracking model was recalibrated for both design approaches. The number of sections showing bottom-up cracking is relatively lower. Therefore, sections with even two measured points have been included in the calibration. Two different approaches were used to calibrate the bottom-up cracking model.

a. *Approach 1: Measured bottom-up cracking only*. Only 12 sections with measured bottom-up cracking were used for calibration.
b. *Approach 2: Measured bottom-up + top-down cracking*. It is difficult to differentiate visually between bottom-up and top-down cracking in the wheel path. The accurate way is to take cores on the crack and determine its initiation mechanism. Therefore, in this approach, measured bottom-up and top-down cracking in the wheel path was assumed as bottom-up cracking. A total of 24 sections were used to calibrate the bottom-up cracking in this approach.

6.1.1 Approach 1: Measured Bottom-up Cracking only

This approach only used measured bottom-up cracking for calibration. Local calibration was done using the following techniques.

6.1.1.1 No Sampling

In no sampling, the entire dataset was used for recalibration. The error was minimized between the predicted and measured fatigue cracking. Figures 6 1 and 6-2 show the predicted vs. measured bottom-up for the global and locally calibrated models at three hierarchical input levels for new and overlay designs, respectively. The global model under-predicts bottom-up cracking. Table 6-2 shows the local calibration results. Figure 6-3 shows the measured and locally predicted bottom-up cracking with time. These measured and predicted cracking values are for the same sections and at the same ages.

Table 6-2: Local calibration summary for bottom-up cracking (No sampling)

Parameter	Level 1				Level 2				Level 3			
	New		Overlay		New		Overlay		New		Overlay	
	Global	Local	Global	Local	Global	Local	Global	Local	Global	Local	Global	Local
C1	1.31	0.30	1.31	0.29	1.31	0.43	1.31	0.20	1.31	0.43	1.31	0.26
C2 < 5"	2.16	0.84	2.16	0.78	2.16	0.71	2.16	0.80	2.16	0.79	2.16	0.74
5"<C2<12"	2.16	0.29	2.16	0.25	2.16	0.25	2.16	0.20	2.16	0.25	2.16	0.29
SEE	7.16	6.05	7.16	6.20	7.16	5.26	7.17	6.21	7.16	5.26	7.16	6.64
Bias	-4.70	2.85	-4.70	3.26	-4.69	0.68	-4.71	0.19	-4.69	0.67	-4.70	3.93

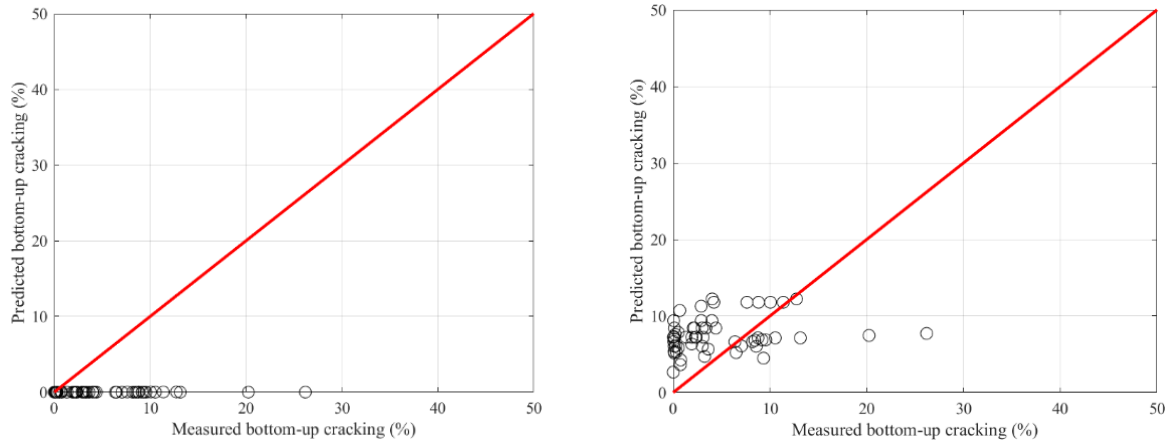

(a) Global model (level 1)

(b) Local model (level 1)

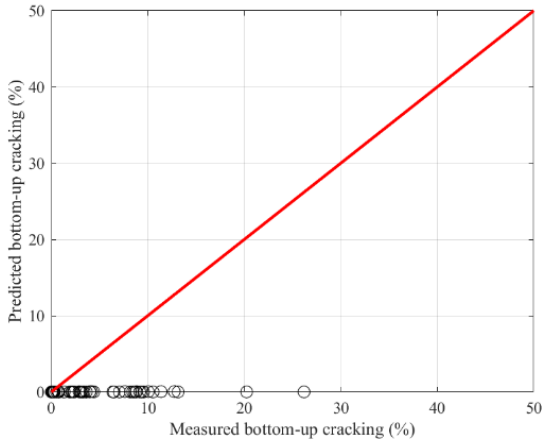

(c) Global model (level 2)

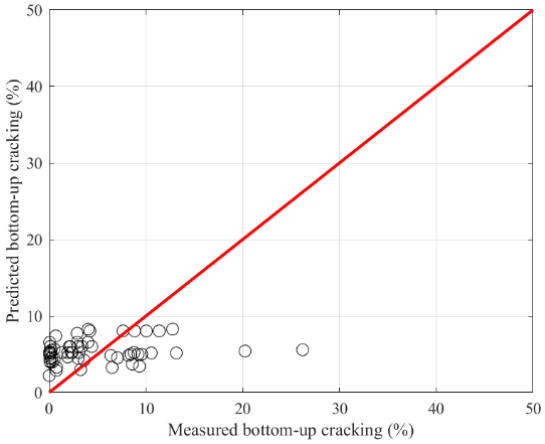

(d) Local model (level 2)

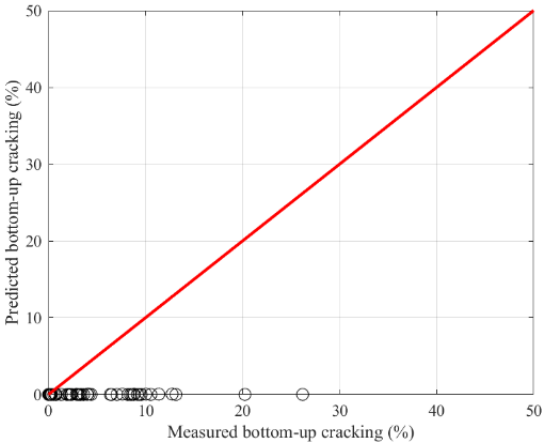

(e) Global model (level 3)

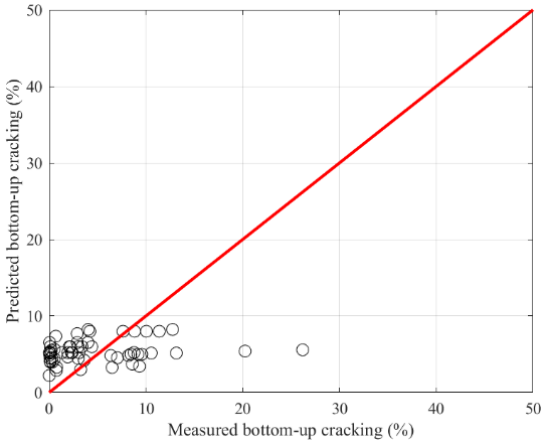

(f) Local model (level 3)

Figure 6-1: Predicted vs. measured bottom-up cracking (No sampling) – New design

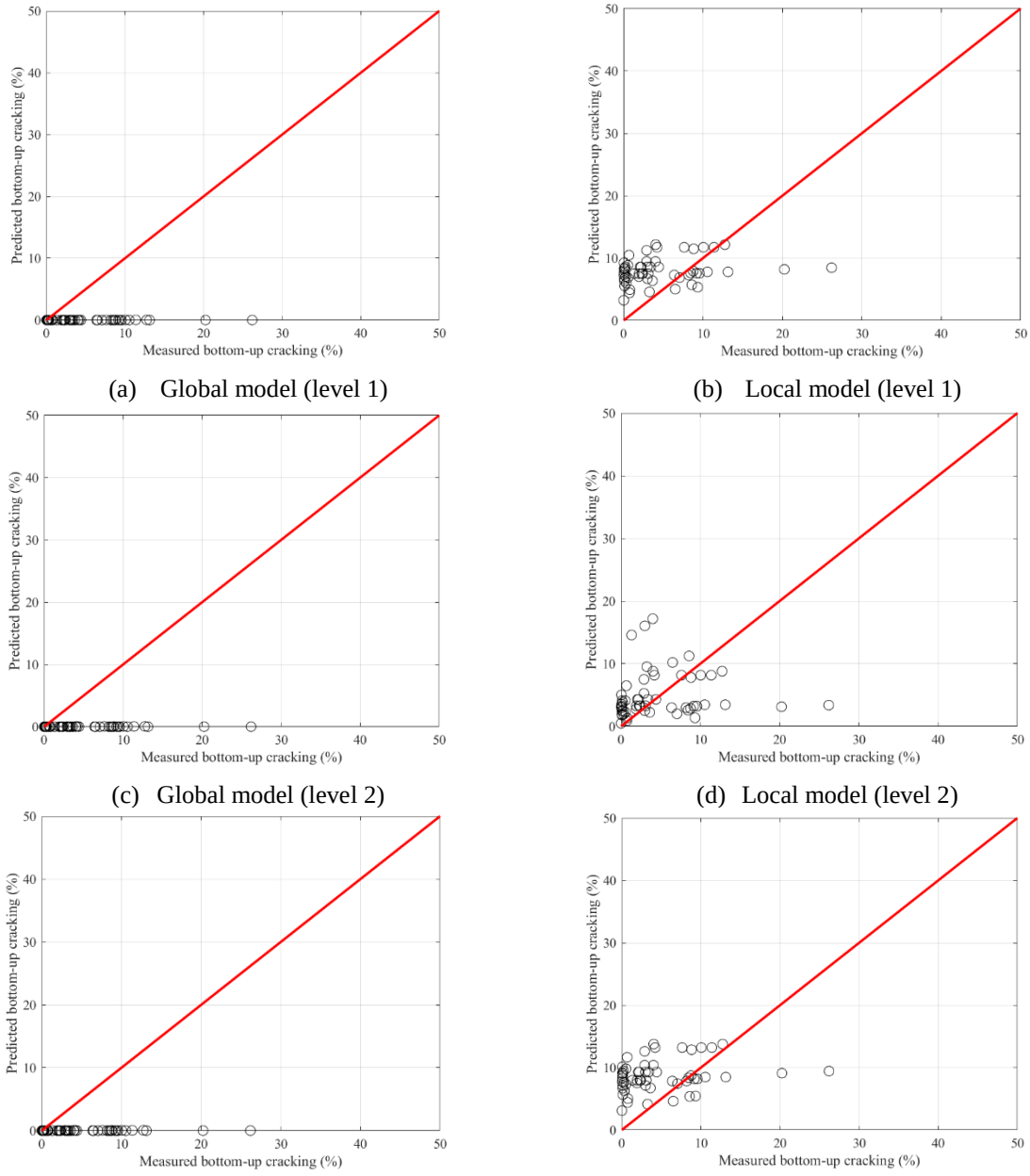

(a) Global model (level 1)

(b) Local model (level 1)

(c) Global model (level 2)

(d) Local model (level 2)

(e) Global model (level 3)

(f) Local model (level 3)

Figure 6-2: Predicted vs measured bottom-up cracking (No sampling) – Overlay design

6.1.1.2 Split Sampling

Split sampling was used with a random split of 70% sections for the calibration set and the rest 30% for the validation set. Figures 6-4 and 6-5 show the predicted vs. measured bottom-up cracking for the calibration and validation set. The validation set shows a similar trend as the calibration set. Tables 6-3 and 6-4 summarize the local calibration and validation results. Though

SEE is higher than the global model, bias is significantly improved from -4.54 to 0.7018 in the validation set. Overall, the validation results are satisfactory.

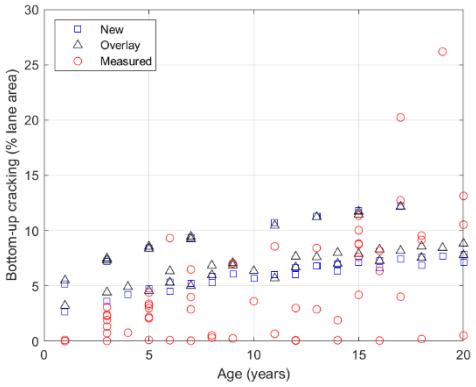

(a) New vs. overlay - level 1

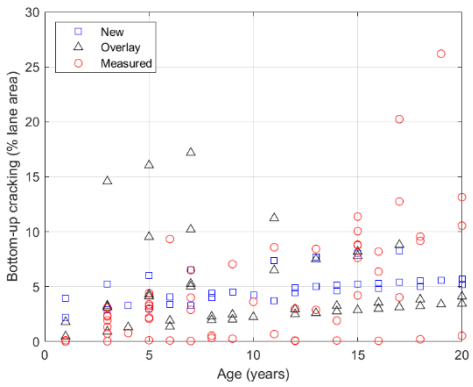

(b) New vs. overlay - level 2

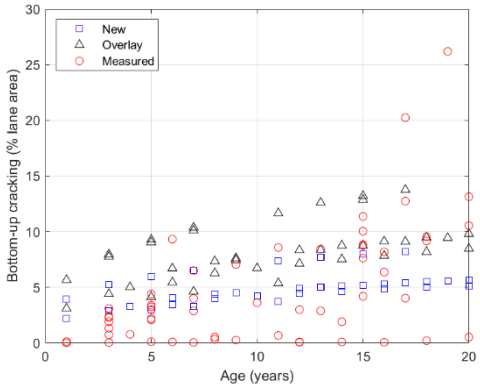

(c) New vs. overlay - level 3

Figure 6-3: Measured vs. predicted with time series for bottom-up cracking

Table 6-3: Local calibration summary for bottom-up cracking (calibration set)

Parameter	Level 1				Level 2				Level 3			
	New		Overlay		New		Overlay		New		Overlay	
	Global	Local	Global	Local	Global	Local	Global	Local	Global	Local	Global	Local
C1	1.31	0.15	1.31	0.29	1.31	0.54	1.31	0.53	1.31	0.48	1.31	0.53
C2 < 5"	2.16	1.61	2.16	1.76	2.16	0.59	2.16	1.05	2.16	1.09	2.16	1.05
5"<C2<12"	1.00	0.45	1.00	0.25	1.00	0.15	1.00	0.05	1.00	0.21	1.00	0.05
SEE	7.31	5.96	7.29	5.67	6.87	5.49	6.76	5.57	6.66	5.42	6.76	5.57
Bias	-4.68	-2.14	-4.75	-1.87	-4.48	-2.10	-4.17	-1.91	-3.99	-1.69	-4.17	-1.91

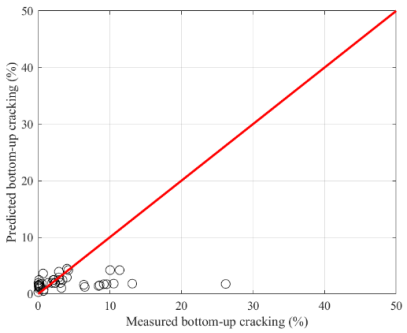

(a) Level 1 – local model (new design)

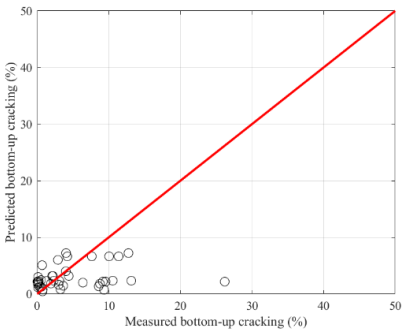

(b) Level 1 – local model (overlay design)

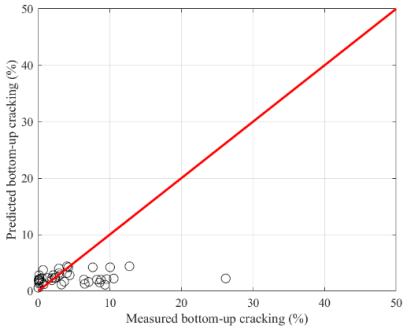

(c) Level 2 – local model (new design)

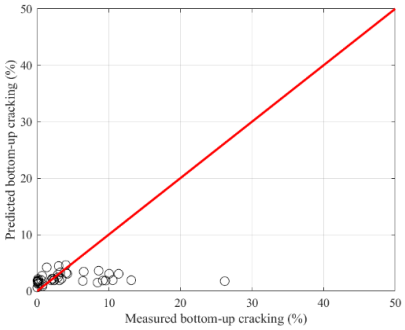

(d) Level 2 – local model (overlay design)

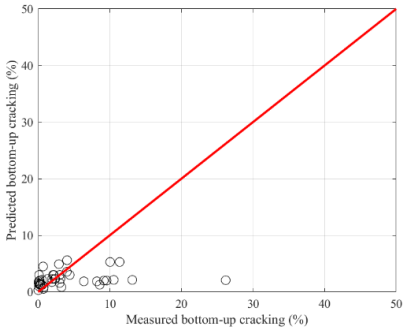

(e) Level 3 – local model (new design)

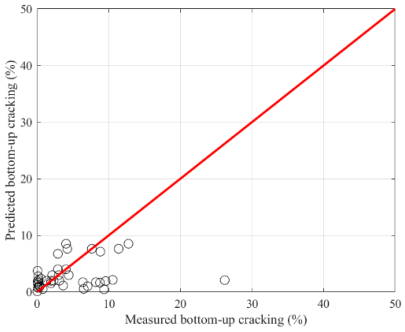

(f) Level 3 – local model (overlay design)

Figure 6-4: Predicted vs. measured bottom-up cracking (split sampling) – calibration set

Table 6-4: Local calibration summary for bottom-up cracking (validation set)

Parameter	Level 1				Level 2				Level 3			
	New		Overlay		New		Overlay		New		Overlay	
	Global	Local	Global	Local	Global	Local	Global	Local	Global	Local	Global	Local
C1	1.31	0.15	1.31	0.29	1.31	0.54	1.31	0.53	1.31	0.48	1.31	0.53
C2 < 5"	2.16	1.61	2.16	1.76	2.16	0.59	2.16	1.05	2.16	1.09	2.16	1.05
5"<C2<12"	1.00	0.45	1.00	0.25	1.00	0.15	1.00	0.05	1.00	0.21	1.00	0.05
SEE	7.27	6.83	7.35	6.03	8.37	6.75	8.60	7.10	8.80	6.88	8.60	7.10
Bias	-4.78	-2.79	-4.58	-2.27	-5.27	-2.92	-6.05	-4.14	-6.49	-3.65	-6.05	-4.14

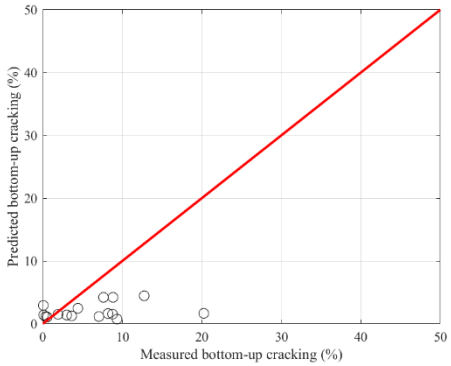

(a) Level 1 – local model (new design)

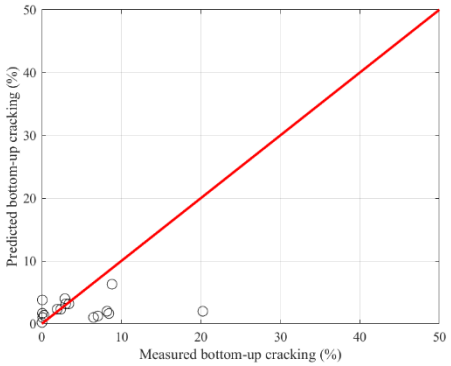

(b) Level 1 – local model (overlay design)

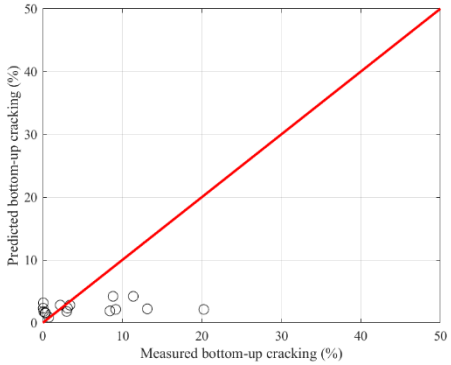

(c) Level 2 – local model (new design)

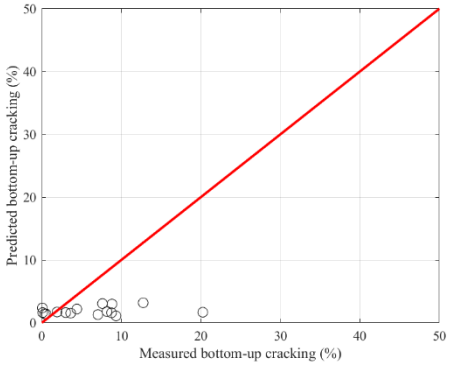

(d) Level 2 – local model (overlay design)

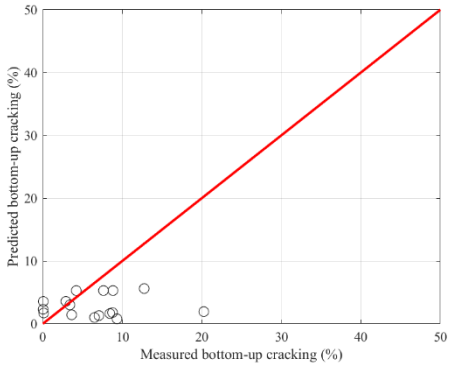

(e) Level 3 – local model (new design)

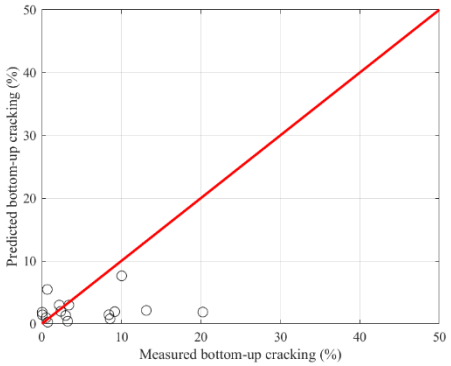

(f) Level 3 – local model (overlay design)

Figure 6-5: Predicted vs. measured bottom-up cracking (split sampling) – validation set

6.1.1.3 Bootstrapping

Bootstrapping was used as a resampling technique to calibrate the bottom-up cracking model. One thousand bootstrap samples were created, randomly sampling with replacement. Unlike split sampling, the entire dataset was used in bootstrap. Tables 6-5 and 6-6 summarize the parameters for global and local models, respectively. SEE and bias significantly improved after local

calibration. Figures 6-6 and 6-7 show the local model's measured versus predicted and residual distribution plots for the 1000 bootstrap samples, respectively.

Table 6-5: Bootstrapping global model summary

Parameters	Levels	1		2		3	
	Design	New	Overlay	New	Overlay	New	Overlay
C1	Mean	1.31					
	Median						
C2 < 5"	Mean	2.158					
	Median						
5"<C2<12"	Mean	1					
	Median						
SEE	Mean	7.08	7.06	7.09	7.06	7.11	7.17
	Median	6.99	7	7.01	7	7.11	7.12
Bias	Mean	-4.71	-4.68	-4.73	-4.68	-4.71	-4.77
	Median	-4.68	-4.64	-4.69	-4.64	-4.67	-4.75

Table 6-6: Bootstrapping local calibration results summary

Parameters	Levels	1		2		3	
	Design	New	Overlay	New	Overlay	New	Overlay
C1	Mean	0.27	0.26	0.29	0.25	0.29	0.26
	Median	0.3	0.27	0.3	0.2	0.3	0.28
C2 < 5"	Mean	1.35	1.35	1.36	1.21	1.34	1.35
	Median	1.34	1.36	1.35	1.14	1.35	1.36
5"<C2<12"	Mean	0.31	0.27	0.42	0.21	0.43	0.29
	Median	0.3	0.27	0.41	0.2	0.41	0.29
SEE	Mean	5.56	5.43	5.82	6.74	5.85	5.48
	Median	5.51	5.4	5.78	6.68	5.83	5.47
Bias	Mean	-1.89	-1.8	-2.11	-3.99	-2.1	-1.78
	Median	-1.86	-1.77	-2.06	-3.93	-2.06	-1.77

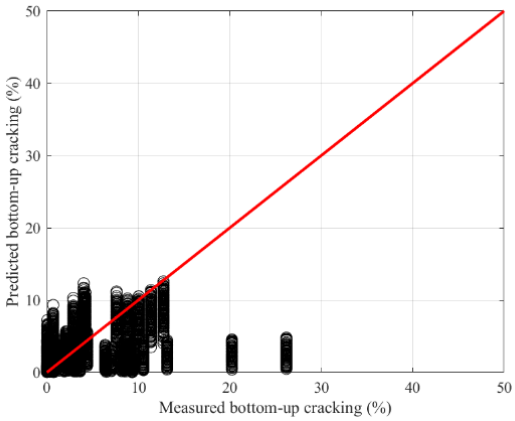

(a) Level 1 – local model (new design)

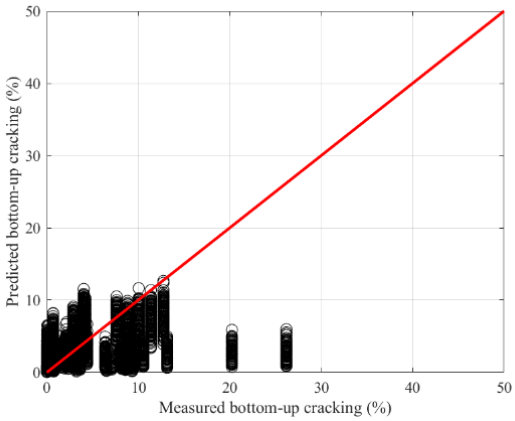

(b) Level 1 – local model (overlay design)

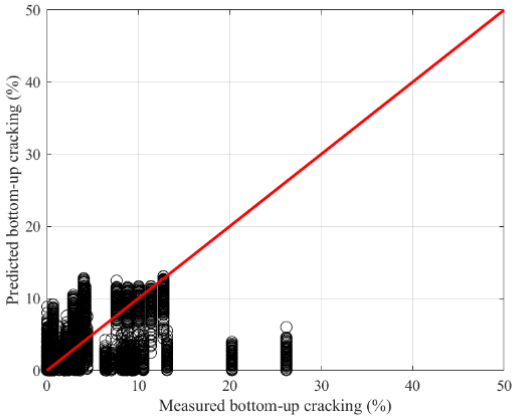

(c) Level 2 – local model (new design)

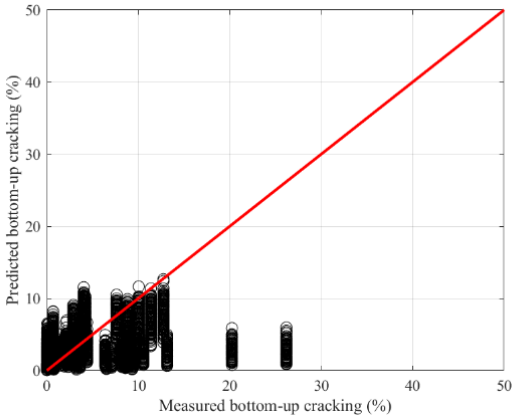

(d) Level 2 – local model (overlay design)

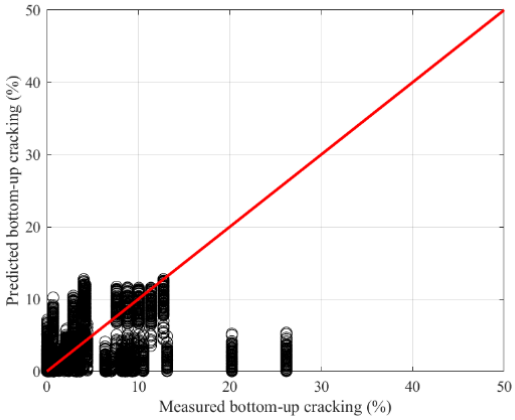

(e) Level 3 – local model (new design)

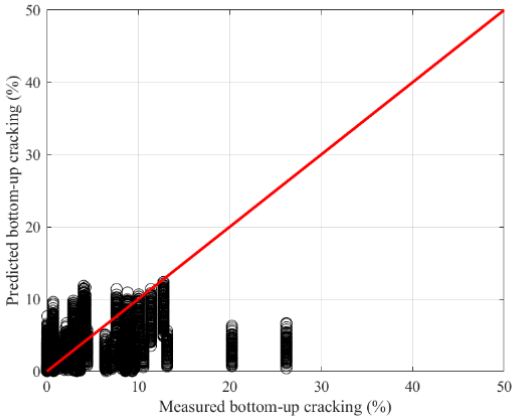

(f) Level 3 – local model (overlay design)

Figure 6-6: Measured vs. predicted for local model (bootstrapping)

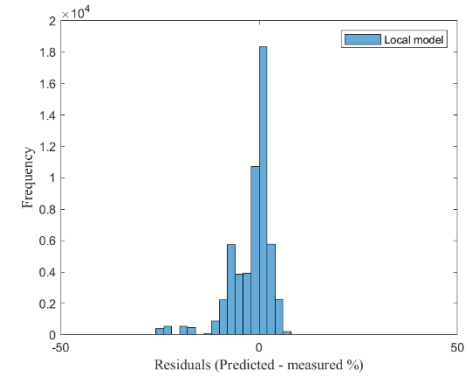

(a) Level 1 – local model (new design)

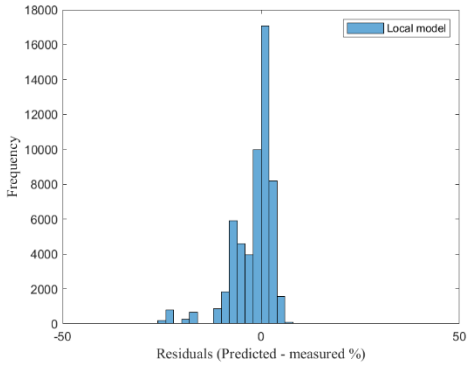

(b) Level 1 – local model (overlay design)

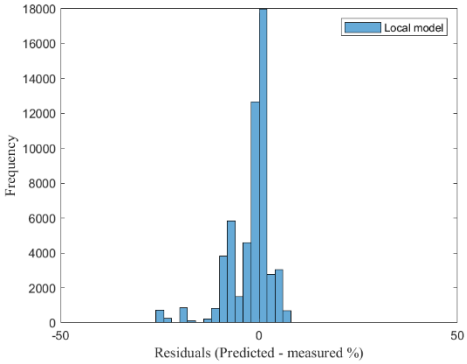

(c) Level 2 – local model (new design)

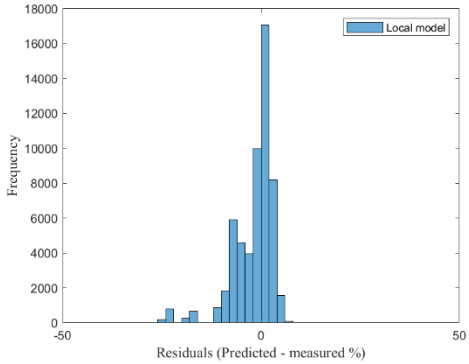

(d) Level 2 – local model (overlay design)

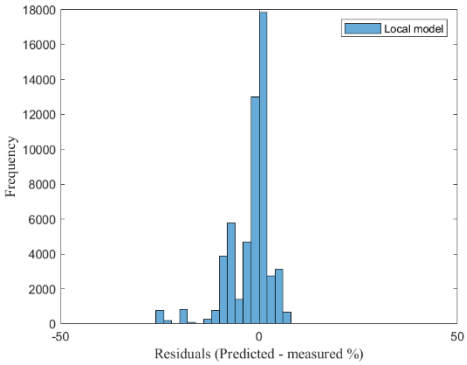

(e) Level 3 – local model (new design)

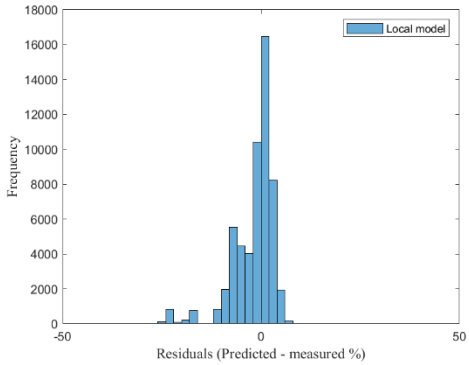

(f) Level 3 – local model (overlay design)

Figure 6-7: Residual distribution (bootstrapping)

6.1.1.4 Maximum Likelihood Estimation (MLE)

As discussed in Chapter 5, three distributions were used to calibrate the performance prediction models. The exponential distribution significantly improved the bias; however, a slight increase in SEE is noted. Tables 6-7 and 6-8 show the calibration summary results using exponential distribution. Figures 6-8 and 6-9 present the measured vs. predicted and residual distribution, respectively. Table 6-9 compares statistical parameters between least squares and MLE.

Table 6-7: Global model summary - bootstrapping using MLE (exponential distribution)

Parameters	Levels	1		2		3	
	Design	New	Overlay	New	Overlay	New	Overlay
C1	Mean	1.31					
	Median						
C2 < 5"	Mean	2.158					
	Median						
5"<C2<12"	Mean	1					
	Median						
SEE	Mean	7.08	7.06	7.09	7.06	7.11	7.17
	Median	6.99	7	7.01	7	7.11	7.12
Bias	Mean	-4.71	-4.68	-4.73	-4.68	-4.71	-4.77
	Median	-4.68	-4.64	-4.69	-4.64	-4.67	-4.75

Table 6-8: Local model summary – bootstrapping using MLE (exponential distribution)

Parameters	Levels	1		2		3	
	Design	New	Overlay	New	Overlay	New	Overlay
C1	Mean	0.2	0.27	0.24	0.25	0.24	0.25
	Median	0.19	0.26	0.21	0.23	0.21	0.24
C2 < 5"	Mean	1.07	1.07	1.06	1.05	1.07	1.08
	Median	1.09	1.07	1.04	1.05	1.09	1.07
5"<C2<12"	Mean	0.28	0.2	0.35	0.08	0.36	0.23
	Median	0.29	0.19	0.36	0.08	0.36	0.23
SEE	Mean	5.69	5.31	6.25	6.12	6.2	5.4
	Median	5.7	5.29	6.2	6.01	6.09	5.4
Bias	Mean	0	0	0	0	0	0
	Median	0	0	0	0	0	0

Table 6-9: Local model statistics

Levels	Design	Parameters					
		MLE (exponential distribution)			Least square		
		NLL	AIC	BIC	NLL	AIC	BIC
1	New	141.89	285.79	288.56	288.75	581.50	585.55
	Overlay	141.82	285.64	288.49	347.66	699.31	703.37
2	New	142.37	286.94	288.77	233.47	470.93	474.98
	Overlay	142.57	287.60	289.16	865.54	1735.07	1739.12
3	New	141.56	285.89	287.14	236.04	476.09	480.14
	Overlay	142.07	286.62	288.17	315.27	634.54	638.59

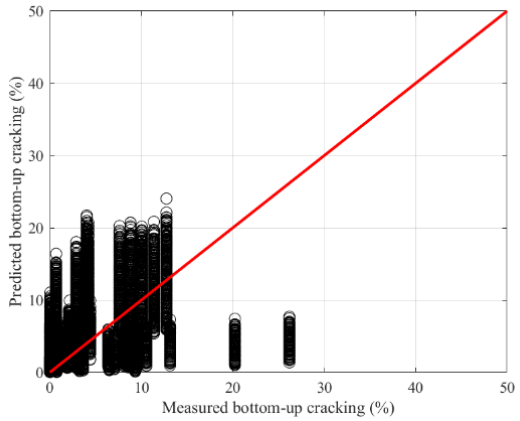

(a) Level 1 – local model (new design)

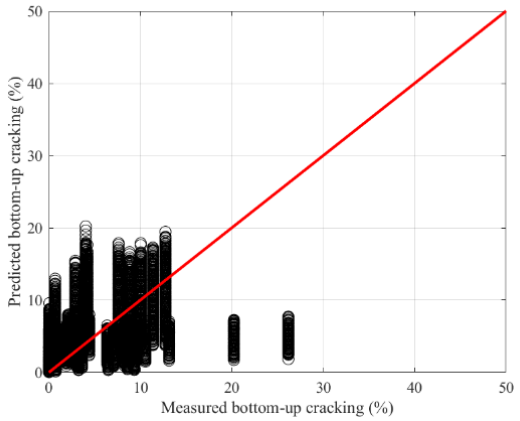

(b) Level 1 – local model (overlay design)

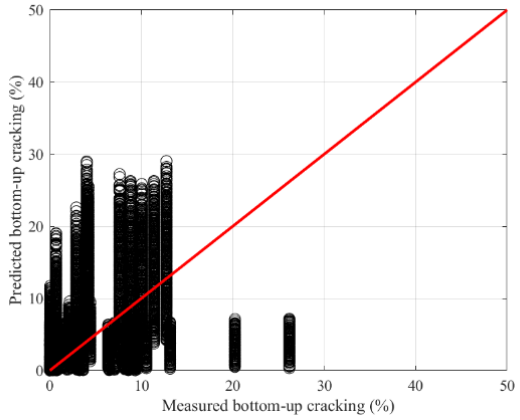

(c) Level 2 – local model (new design)

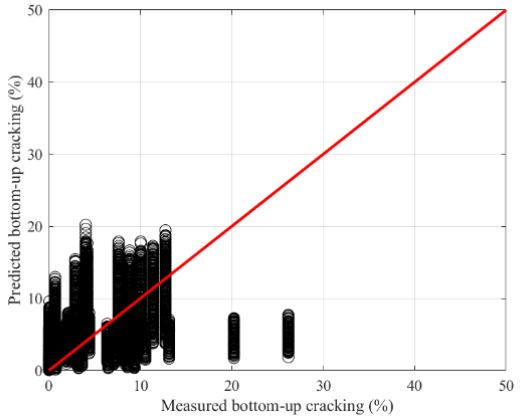

(d) Level 2 – local model (overlay design)

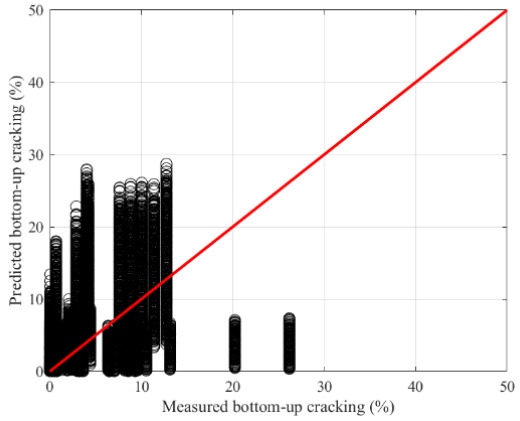

(e) Level 3 – local model (new design)

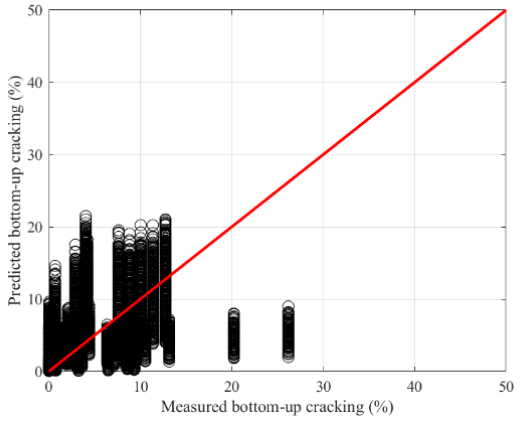

(f) Level 3 – local model (overlay design)

Figure 6-8: Measured vs. predicted for the local model using MLE (exponential distribution)

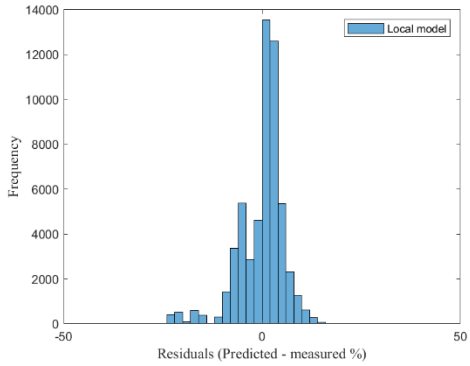

(a) Level 1 – local model (new design)

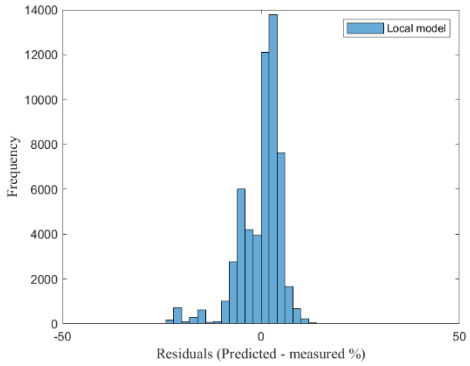

(b) Level 1 – local model (overlay design)

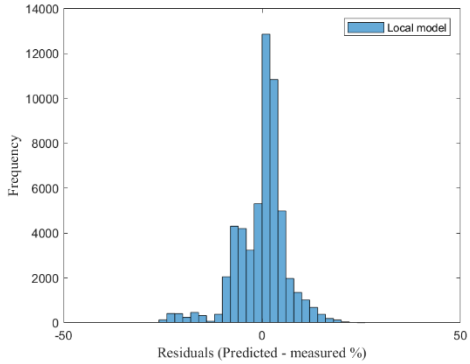

(c) Level 2 – local model (new design)

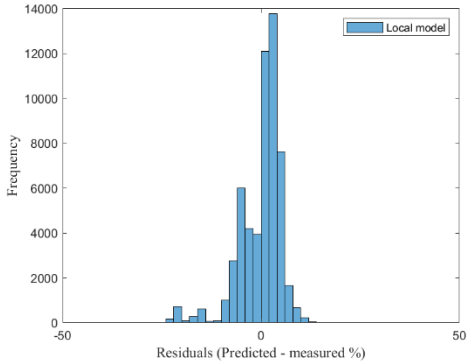

(d) Level 2 – local model (overlay design)

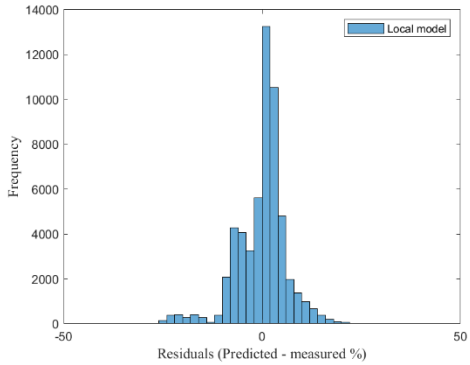

(e) Level 3 – local model (new design)

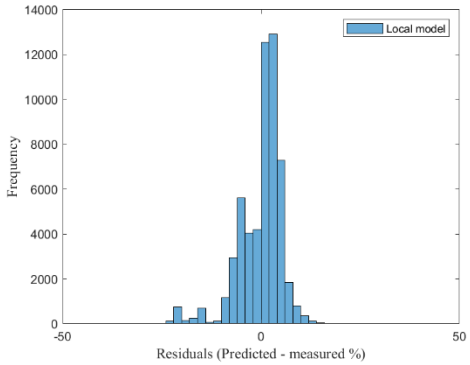

(f) Level 3 – local model (overlay design)

Figure 6-9: Residual distribution using MLE (exponential distribution)

6.1.1.5 Summary

All calibration approaches have significantly improved the bottom-up cracking model. Tables 6-10 and 6-11 show the calibration summary of the bottom-up cracking model for new and overlay designs, respectively. Figure 6-10 illustrates the SEE and bias comparison of all calibration techniques for both design approaches. An overlay design at input Level 1 produced better results with minimum SEE and bias.

Table 6-10: Summary of results for all sampling techniques (new design)

Levels	Sampling technique	SEE	Bias	C_1	*C2 (hac < 5 in.)*	*C2 (5 in. <= hac <=12 in.)*
1	No sampling (LS)	6.05	2.85	0.30	0.84	(0.867+0.2583* hac)*0.29
	Split sampling (LS)	5.96	-2.14	0.15	1.61	(0.867+0.2583* hac)*0.45
	Bootstrapping (LS)	5.56	-1.89	0.27	1.35	(0.867+0.2583* hac)*0.31
	Bootstrapping (MLE)	5.69	0.00	0.20	1.07	(0.867+0.2583* hac)*0.28
2	No sampling (LS)	5.26	0.68	0.43	0.71	(0.867+0.2583* hac)*0.25
	Split sampling (LS)	5.49	-2.10	0.54	0.59	(0.867+0.2583* hac)*0.15
	Bootstrapping (LS)	5.82	-2.11	0.29	1.36	(0.867+0.2583* hac)*0.42
	Bootstrapping (MLE)	6.25	0.00	0.24	1.06	(0.867+0.2583* hac)*0.35
3	No sampling (LS)	5.26	0.67	0.43	0.79	(0.867+0.2583* hac)*0.25
	Split sampling (LS)	5.42	-1.69	0.48	1.09	(0.867+0.2583* hac)*0.21
	Bootstrapping (LS)	5.85	-2.10	0.29	1.34	(0.867+0.2583* hac)*0.43
	Bootstrapping (MLE)	6.20	0.00	0.24	1.07	(0.867+0.2583* hac)*0.36

LS = least square

Table 6-11: Summary of results for all sampling techniques (overlay design)

Levels	Sampling technique	SEE	Bias	C_1	*C2 (hac < 5 in.)*	*C2 (5 in. <= hac <=12 in.)*
1	No sampling (LS)	6.20	3.26	0.29	0.78	(0.867+0.2583* hac)*0.25
	Split sampling (LS)	5.49	0.00	0.24	1.85	(0.867+0.2583* hac)*0.21
	Bootstrapping (LS)	5.43	-1.80	0.26	1.35	(0.867+0.2583* hac)*0.27
	Bootstrapping (MLE)	5.31	0.00	0.27	1.07	(0.867+0.2583* hac)*0.20
2	No sampling (LS)	6.21	0.19	0.20	0.80	(0.867+0.2583* hac)*0.20
	Split sampling (LS)	6.34	0.00	0.21	1.22	(0.867+0.2583* hac)*0.10
	Bootstrapping (LS)	6.74	-3.99	0.25	1.21	(0.867+0.2583* hac)*0.21
	Bootstrapping (MLE)	6.12	0.00	0.25	1.05	(0.867+0.2583* hac)*0.08
3	No sampling (LS)	6.64	3.93	0.26	0.74	(0.867+0.2583* hac)*0.29
	Split sampling (LS)	6.34	0.00	0.21	1.22	(0.867+0.2583* hac)*0.10
	Bootstrapping (LS)	5.48	-1.78	0.26	1.35	(0.867+0.2583* hac)*0.29
	Bootstrapping (MLE)	5.40	0.00	0.25	1.08	(0.867+0.2583* hac)*0.23

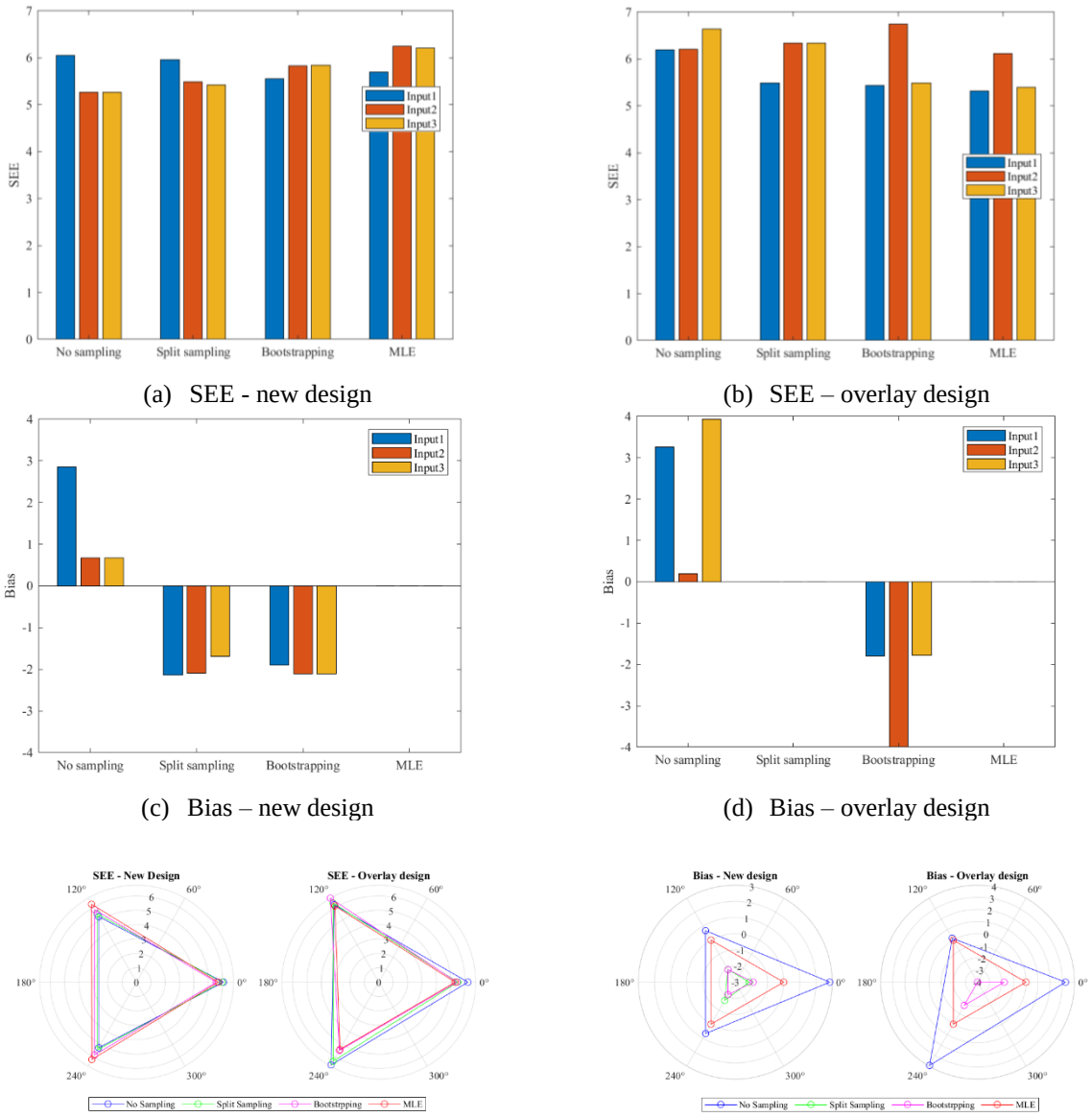

(a) SEE - new design

(b) SEE – overlay design

(c) Bias – new design

(d) Bias – overlay design

(e) SEE

(f) Bias

Figure 6-10: SEE and bias comparison of new vs. overlay design

6.1.2 Approach 2: Measured Bottom-up + Top-down Cracking

As discussed earlier, bottom-up and top-down cracking in the wheel path were combined to calibrate the fatigue bottom-up cracking model. The least square method was used for local calibration using no sampling, split sampling, and bootstrapping sampling techniques. Three MLE distributions (exponential, log-normal, and gamma) were used for local calibration; the exponential distribution produced better results than another least square method with minimum SEE and bias. Figures 6-11 and 6-12 show the measured versus predicted results for new and overlay designs at all three input levels and residuals distribution, respectively.

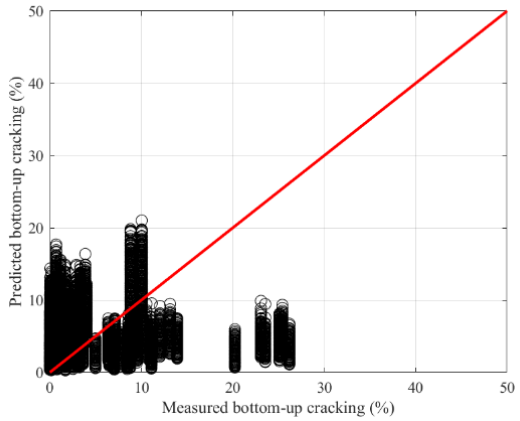

(a) Level 1 – local model (new design)

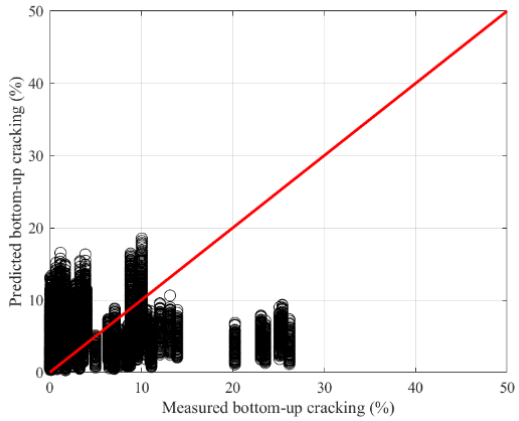

(b) Level 1 – local model (overlay design)

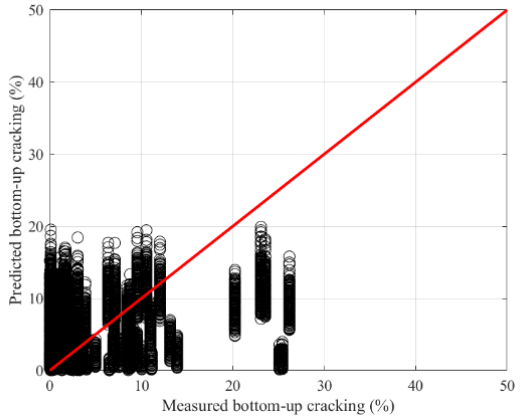

(c) Level 2 – local model (new design)

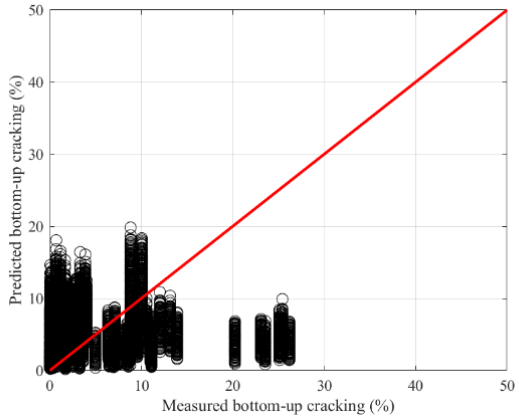

(d) Level 2 – local model (overlay design)

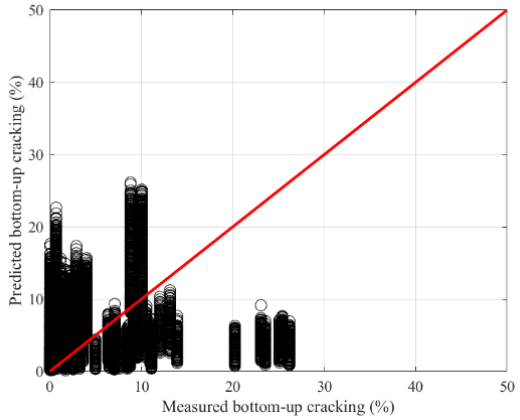

(e) Level 3 – local model (new design)

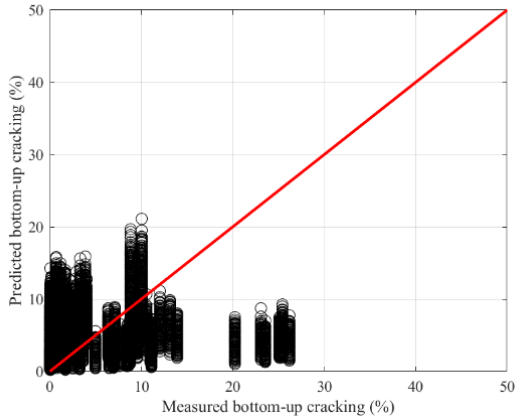

(f) Level 3 – local model (overlay design)

Figure 6-11: Measured vs. predicted for the local model using MLE (exponential distribution)

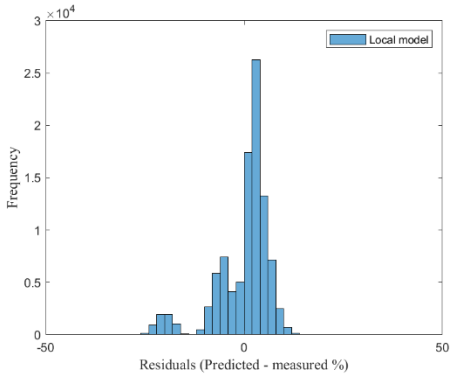

(a) Level 1 – local model (new design)

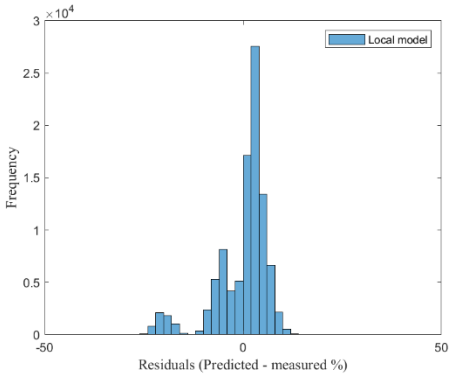

(b) Level 1 – local model (overlay design)

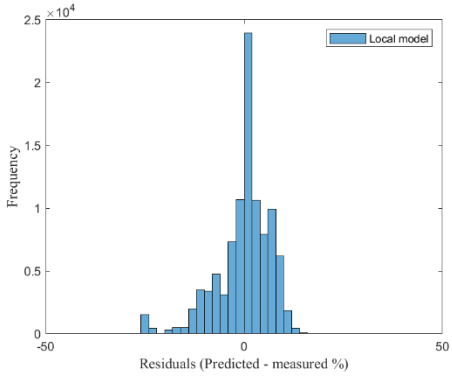

(c) Level 2 – local model (new design)

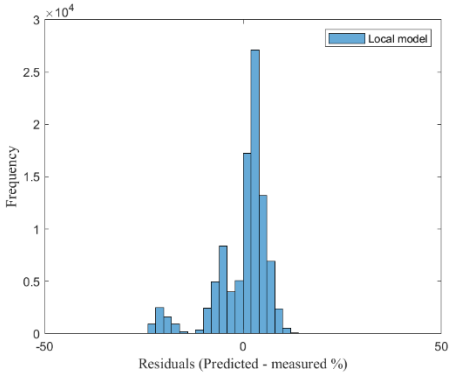

(d) Level 2 – local model (overlay design)

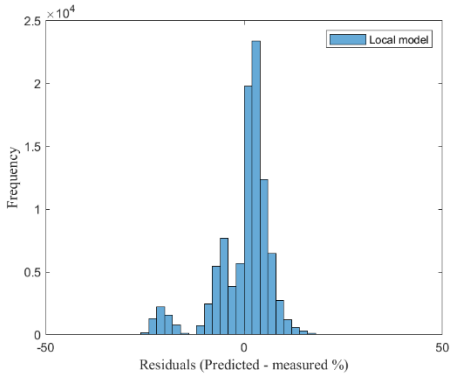

(e) Level 3 – local model (new design)

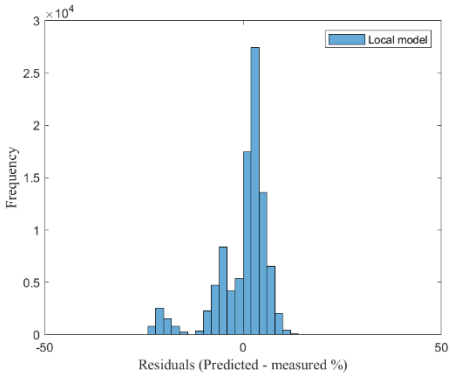

(f) Level 3 – local model (overlay design)

Figure 6-12: Residual distribution using MLE (exponential distribution)

6.1.2.1 Summary

All sampling techniques improved the local calibration. However, MLE using exponential distribution is the most effective calibration technique for the fatigue bottom-up cracking model. Tables 6-12 and 6-13 show the local calibration results for new and overlay designs. Figures 6-

13 show the comparison plots of SEE and bias. Overall, local calibration of an overlay design at input Level 1 and 3 produced better results with a minimum SEE and bias.

Table 6-12: Summary of results for all sampling techniques (new design)

Levels	Sampling technique	SEE	Bias	C_1	*C2 (hac < 5 in.)*	*C2 (5 in. <= hac <=12 in.)*
1	No sampling (LS)	6.79	1.72	0.31	0.53	(0.867+0.2583* hac)*0.31
	Split sampling (LS)	6.45	0.00	0.37	0.60	(0.867+0.2583* hac)*0.12
	Bootstrapping (LS)	7.03	-3.00	0.37	0.65	(0.867+0.2583* hac)*0.28
	Bootstrapping (MLE)	6.72	0.00	0.24	0.60	(0.867+0.2583* hac)*0.20
2	No sampling (LS)	7.16	0.46	0.28	0.61	(0.867+0.2583* hac)*0.35
	Split sampling (LS)	6.30	-1.81	0.38	0.82	(0.867+0.2583* hac)*0.39
	Bootstrapping (LS)	6.57	-1.47	0.40	0.63	(0.867+0.2583* hac)*0.35
	Bootstrapping (MLE)	6.78	0.00	0.34	0.60	(0.867+0.2583* hac)*0.31
3	No sampling (LS)	7.19	-2.80	0.28	0.53	(0.867+0.2583* hac)*0.32
	Split sampling (LS)	7.05	0.00	0.27	0.82	(0.867+0.2583* hac)*0.21
	Bootstrapping (LS)	7.06	-2.96	0.37	0.67	(0.867+0.2583* hac)*0.30
	Bootstrapping (MLE)	6.70	0.00	0.23	0.60	(0.867+0.2583* hac)*0.23

LS = least square

Table 6-13: Summary of results for all sampling techniques (overlay design)

Levels	Sampling technique	SEE	Bias	C_1	*C2 (hac < 5 in.)*	*C2 (5 in. <= hac <=12 in.)*
1	No sampling (LS)	7.18	-3.09	0.20	0.87	(0.867+0.2583* hac)*0.34
	Split sampling (LS)	6.49	0.00	0.33	0.80	(0.867+0.2583* hac)*0.12
	Bootstrapping (LS)	6.98	-3.01	0.36	0.65	(0.867+0.2583* hac)*0.25
	Bootstrapping (MLE)	6.58	0.00	0.23	0.65	(0.867+0.2583* hac)*0.18
2	No sampling (LS)	7.08	-2.94	0.32	0.56	(0.867+0.2583* hac)*0.27
	Split sampling (LS)	6.91	0.00	0.20	0.60	(0.867+0.2583* hac)*0.20
	Bootstrapping (LS)	7.05	-3.00	0.35	0.65	(0.867+0.2583* hac)*0.26
	Bootstrapping (MLE)	6.69	0.00	0.24	0.66	(0.867+0.2583* hac)*0.19
3	No sampling (LS)	7.09	-2.97	0.30	0.77	(0.867+0.2583* hac)*0.29
	Split sampling (LS)	6.89	0.00	0.20	0.72	(0.867+0.2583* hac)*0.20
	Bootstrapping (LS)	6.97	-2.94	0.34	0.66	(0.867+0.2583* hac)*0.27
	Bootstrapping (MLE)	6.49	0.00	0.24	0.65	(0.867+0.2583* hac)*0.19

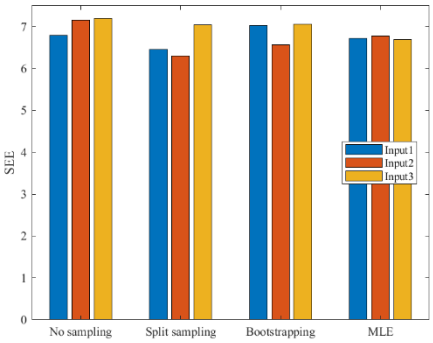

(a) SEE - new design

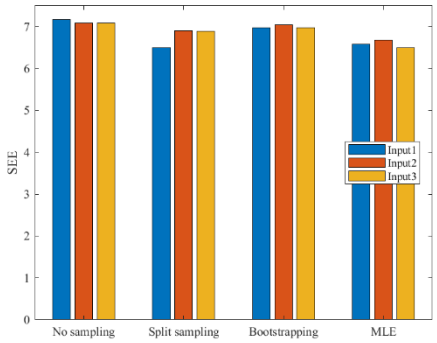

(b) SEE – overlay design

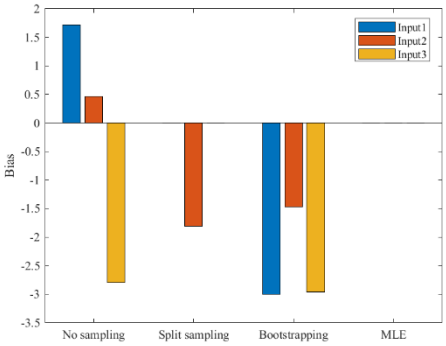

(c) Bias – new design

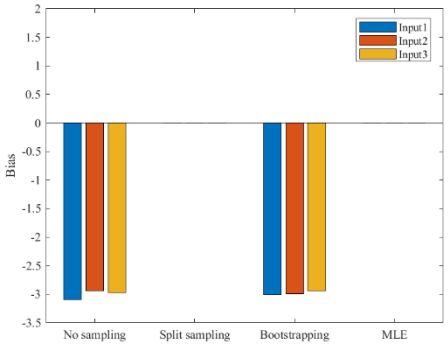

(d) Bias – overlay design

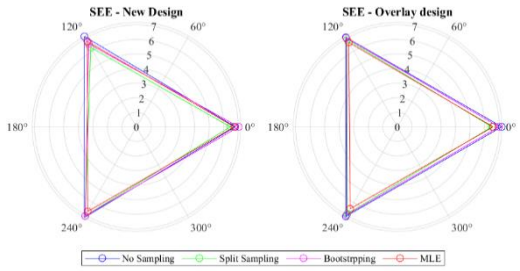

(e) SEE

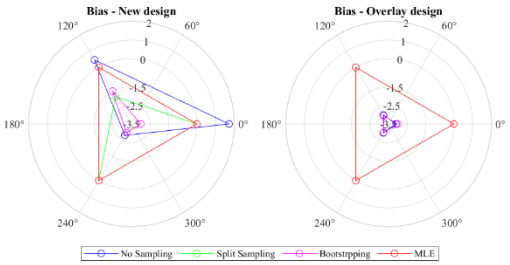

(f) Bias

Figure 6-13: SEE and bias comparison of new vs. overlay design

6.2 Fatigue Top-down Cracking Model

The following section shows the calibration of the top-down cracking model. The model contains crack initiation and crack propagation models. Since the actual crack initiation time is not known, it was not possible to calibrate the crack initiation model separately. So, a single function was used by substituting the crack initiation function with the crack propagation function. Four coefficients from the crack initiation function (kL2, kL3, kL4, kL5) and two from the crack propagation function (C1, C2) have been calibrated. Only no sampling method was used for this

calibration. The PMED predicted the same performance for new and overlay designs; only a single set of plots is reported for both design approaches. Measured vs. predicted plots are appended in Appendix A. Table 6-14 summarizes model parameters for both design approaches. The SEE and bias at input Level 1 are acceptable. Figure 6-14 compares SEE and bias at each level.

Table 6-14: Calibration results for top-down cracking

Parameters	Level 1		Level 2		Level 3	
	Global	Local	Global	Local	Global	Local
SEE	4.657	3.672	4.629	3.670	4.402	3.732
Bias	-1.097	0.000	-0.093	0.000	0.310	0.000
K_{L2}	0.286	0.657	0.286	1.529	0.286	0.915
K_{L3}	0.011	0.100	0.011	0.028	0.011	0.105
K_{L4}	0.015	0.092	0.015	0.086	0.015	0.081
K_{L5}	3.266	2.044	3.266	1.702	3.266	1.376
C_1	2.522	0.097	2.522	0.105	2.522	0.057
C_2	0.807	2.416	0.807	2.336	0.807	3.143

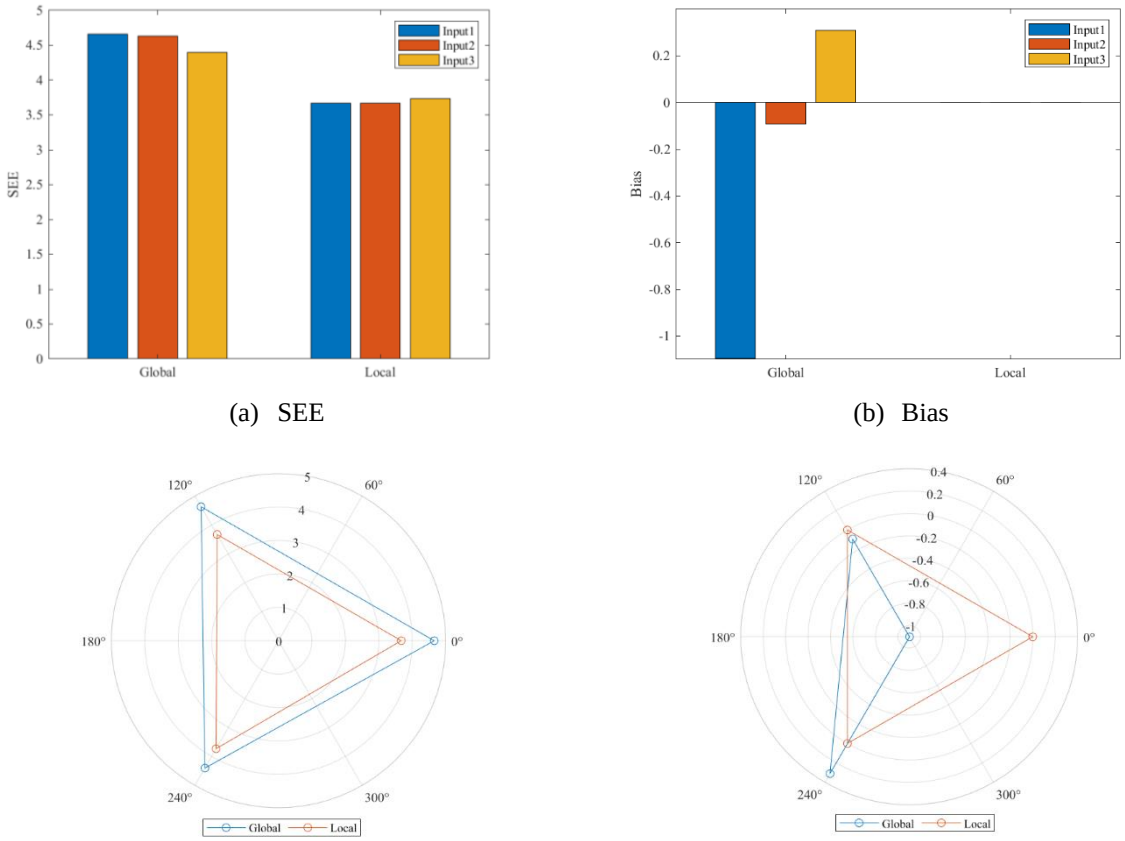

(a) SEE (b) Bias

(c) SEE (d) Bias

Figure 6-14: SEE and bias comparison of new vs. overlay design

6.3 Rutting Model

Rutting in the PMED is a sum of permanent deformations from individual layers. The total measured rutting was calibrated against the sum of individual predicted rutting where β1r, βs1, and βsg1 were calibrated simultaneously to match measured performance. No sampling, split sampling, and bootstrapping techniques were used for local calibration. The detailed results are appended as section A-2 in Appendix A.

6.3.1.1 Summary

The statistical results of all sampling techniques are summarized in Tables 6-15 and 6-16 for new and overlay designs, respectively. The SEE and bias improved for all calibration approaches. Based on the results, both design approaches at Level 1 input produce better results. Figures 6-26 illustrate the comparison of SEE and bias within each input level and calibration technique for new and overlay designs. The minimal SEE and bias were observed for an overlay calibration at Level 3.

Table 6-15: Summary of results for all sampling techniques (new design)

Levels	Sampling technique	SEE	Bias	Br1	Bs1	Bsg1
1	No sampling (LS)	0.079	-0.002	0.445	0.101	0.851
	Split sampling (LS)	0.079	0.000	0.150	0.362	0.905
	Bootstrapping (LS)	0.079	-0.001	0.598	0.536	0.647
	Bootstrapping (MLE)	0.079	0.000	0.576	0.569	0.659
2	No sampling (LS)	0.081	-0.004	0.057	2.173	0.200
	Split sampling (LS)	0.079	0.000	0.169	0.309	0.844
	Bootstrapping (LS)	0.079	-0.004	0.378	0.865	0.422
	Bootstrapping (MLE)	0.078	0.000	0.313	0.540	0.617
3	No sampling (LS)	0.077	-0.001	0.176	0.926	0.626
	Split sampling (LS)	0.079	0.017	0.129	0.326	0.959
	Bootstrapping (LS)	0.078	-0.003	0.413	0.894	0.471
	Bootstrapping (MLE)	0.077	0.000	0.779	0.519	0.391

LS = least square

Table 6-16: Summary of results for all sampling techniques (overlay design)

Levels	Sampling technique	SEE	Bias	Br1	Bs1	Bsg1
1	No sampling (LS)	0.082	-0.005	0.580	2.245	0.351
	Split sampling (LS)	0.080	0.000	0.331	0.297	0.953
	Bootstrapping (LS)	0.077	-0.002	0.361	0.504	0.510
	Bootstrapping (MLE)	0.077	0.000	0.359	0.542	0.552
2	No sampling (LS)	0.077	-0.001	0.233	0.930	0.676
	Split sampling (LS)	0.083	0.000	0.149	0.367	0.916
	Bootstrapping (LS)	0.079	-0.004	0.386	1.312	0.455
	Bootstrapping (MLE)	0.077	0.000	0.322	0.546	0.704
3	No sampling (LS)	0.076	-0.002	0.248	0.392	0.830
	Split sampling (LS)	0.081	0.000	0.129	0.326	0.959
	Bootstrapping (LS)	0.078	-0.003	0.463	1.270	0.489
	Bootstrapping (MLE)	0.076	0.000	0.816	0.258	0.520

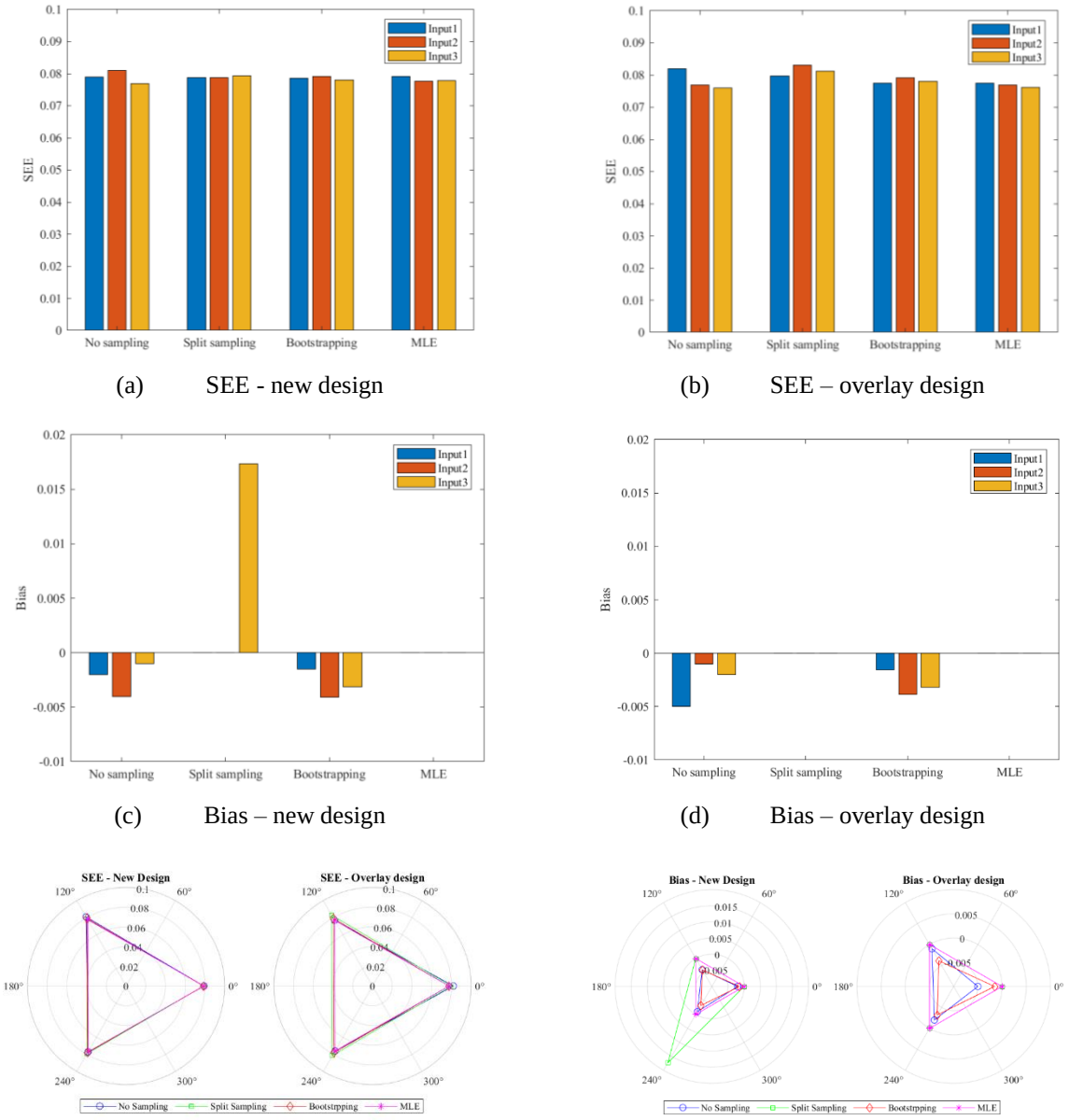

(a) SEE - new design (b) SEE – overlay design

(c) Bias – new design (d) Bias – overlay design

(e) SEE (f) Bias

Figure 6-15 SEE and bias (Rutting) comparison of new vs. overlay design

6.4 Transverse (Thermal) Cracking Model

The thermal cracking model was calibrated for all input levels in the PMED. The model calibration only considered sections with Performance Grade (PG) binder type. The thermal cracking model was calibrated as a single K-value by running PMED multiple times. Since reflective cracking is not critical distress in rubblized pavements, only the thermal cracking model was calibrated.

Although calibration coefficient K is a function of mean annual air temperature (MAAT), it was calibrated as a single value. For this purpose, the PMED was run at different K values for both designs. SEE and bias were determined for each value of K. Table 6-17 summarizes the SEE and bias for the global model and for different K values at each input level for both designs. Based on the SEE and bias, the recommended K-values for each design at each input level are marked in bold. Recalibration improved the SEE and bias, but thermal cracking predictions still show high variability. The predicted vs. measured plot can be found in Appendix A.

6.4.1 Summary

No sampling technique was used for calibration because all sections were run multiple times in PMED at different K-values. The SEE and bias improved for all calibration approaches. The results at level 1 and 2 are reasonable, but input Level 3 produced not acceptable K value as per MDOT's practices. Figures 6-16 illustrate the comparison of SEE and bias within each input level and calibration technique for new and overlay designs.

Table 6-17: Transverse thermal cracking results

Design	Level 1			Level 2			Level 3		
	K	SEE	Bias	K	SEE	Bias	K	SEE	Bias
New	Global	1517.62	-1323.93	Global	1785.53	-1670.69	Global	632.72	346.72
	0.6	635.25	255.12	0.45	620.40	309.58	0.85	633.19	347.22
	0.65	**704.48**	**145.38**	**0.55**	**705.21**	**136.94**	1.5	619.26	327.15
	0.75	915.93	-91.91	0.65	937.46	-163.12	**2**	**622.93**	**201.70**
	0.8	964.95	-183.89	0.7	990.04	-383.00	2.5	719.99	-170.60
	0.85	989.44	-300.45	0.75	1105.58	-606.38	3.5	961.45	-540.56
Overlay	Global	1463.21	-1136.94	Global	1672.05	-1504.65	Global	631.56	345.49
	0.65	654.62	227.81	0.55	643.02	239.04	0.85	633.24	347.28
	0.75	773.46	93.18	**0.65**	**723.88**	**30.88**	2.0	316.34	129.92
	0.85	**790.06**	**-96.98**	0.75	861.64	-292.61	**2.2**	**337.01**	**47.16**
	0.9	830.13	-196.71	0.8	1006.69	-459.63	2.5	445.43	-32.19
	1.25	1281.30	-823.02	0.85	1135.35	-594.81	3.5	818.48	-353.66

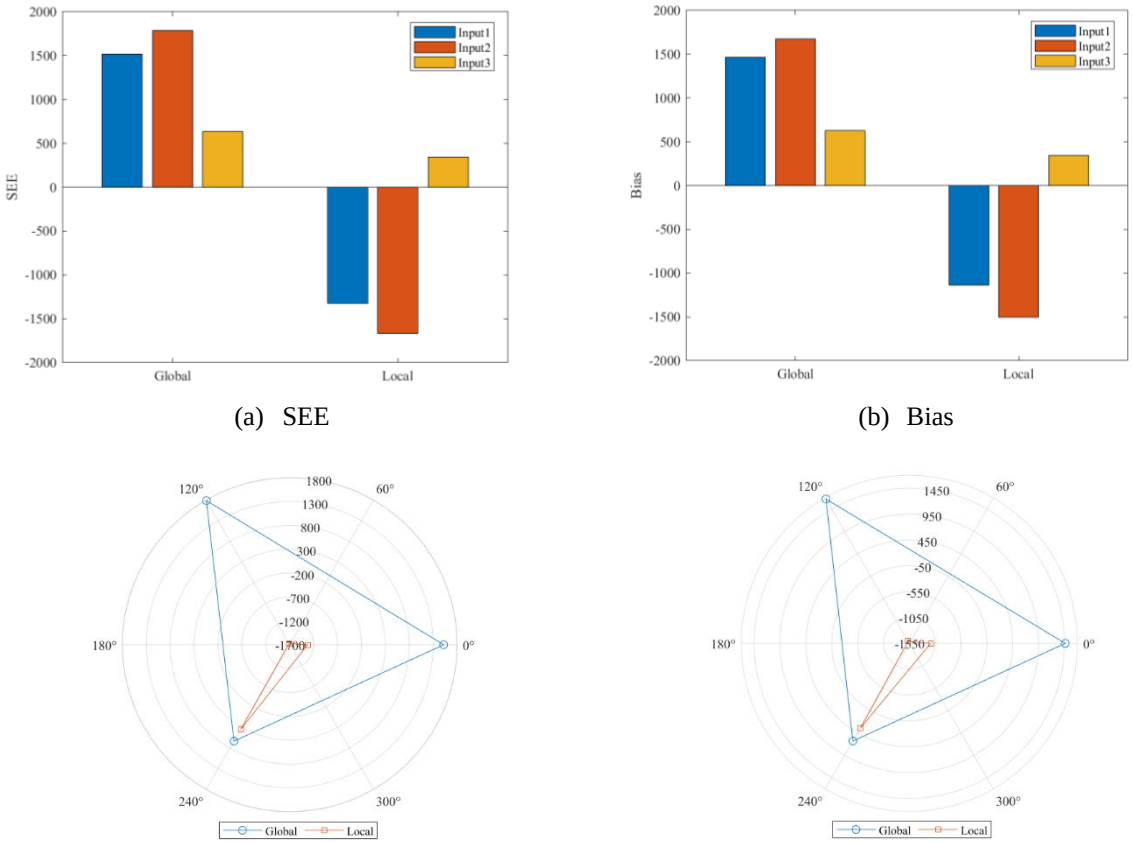

(a) SEE (b) Bias

(c) SEE (d) Bias

Figure 6-16: SEE and bias comparison of new vs. overlay design

6.5 IRI Model

IRI is a linear function of initial IRI, rut depth, total fatigue cracking, transverse cracking, and site factor. The IRI model was calibrated after the local calibration of the fatigue, transverse cracking, and rutting models.

6.5.1 Summary

The statistical results of all sampling techniques are summarized in Tables 6-18 and 6-19 for new and overlay designs, respectively. The SEE and bias improved for all calibration approaches. Based on the results, both designs at input Level 1 produced better results. Figure 6-17 compares the SEE and bias for each input level within both design approaches and using four calibration techniques. Overall, both design using input level 1 and 3 are acceptable.

Table 6-18: Summary of results for all sampling techniques (new design)

Levels	Sampling technique	SEE	Bias	C1	C2	C3	C4
1	No sampling (LS)	10.31	0.00	14.05	0.36	0.00	0.008
	Split sampling (LS)	9.34	0.00	10.22	0.42	0.00	0.002
	Bootstrapping (LS)	10.93	0.34	13.98	0.25	0.01	0.003
	Bootstrapping (MLE)	10.59	0.05	13.51	0.28	0.01	0.003
2	No sampling (LS)	10.02	0.00	9.86	1.93	0.00	0.003
	Split sampling (LS)	10.43	0.00	10.01	0.45	0.02	0.004
	Bootstrapping (LS)	12.99	0.02	12.68	0.33	0.02	0.004
	Bootstrapping (MLE)	10.61	0.27	14.33	0.51	0.01	0.003
3	No sampling (LS)	10.21	0.00	7.30	1.30	0.00	0.004
	Split sampling (LS)	10.03	0.43	19.39	0.32	0.01	0.003
	Bootstrapping (LS)	11.25	-0.08	13.15	0.32	0.01	0.003
	Bootstrapping (MLE)	10.52	0.00	19.56	0.44	0.01	0.003

LS = least square

Table 6-19: Summary of results for all sampling techniques (overlay design)

Levels	Sampling technique	SEE	Bias	C1	C2	C3	C4
1	No sampling (LS)	10.29	0.00	28.19	0.61	0.00	0.004
	Split sampling (LS)	9.99	0.00	12.59	0.20	0.00	0.006
	Bootstrapping (LS)	11.22	0.12	13.43	0.24	0.01	0.004
	Bootstrapping (MLE)	10.38	0.13	13.24	0.34	0.01	0.003
2	No sampling (LS)	10.09	0.00	10.40	1.25	0.00	0.005
	Split sampling (LS)	10.69	0.00	10.64	0.13	0.00	0.008
	Bootstrapping (LS)	11.59	-0.06	12.69	0.15	0.01	0.004
	Bootstrapping (MLE)	10.55	0.22	16.78	0.22	0.01	0.003
3	No sampling (LS)	10.58	0.00	10.62	0.52	0.00	0.007
	Split sampling (LS)	10.60	0.33	17.76	0.15	0.01	0.002
	Bootstrapping (LS)	11.16	0.12	13.63	0.13	0.01	0.003
	Bootstrapping (MLE)	10.82	0.00	14.97	0.24	0.01	0.003

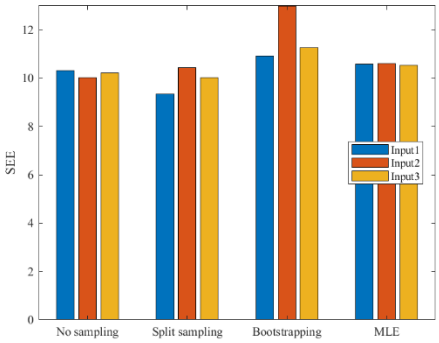

(a) SEE - new design

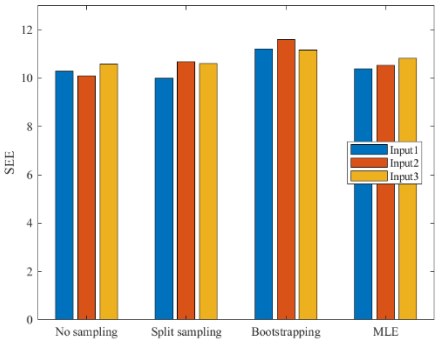

(b) SEE – overlay design

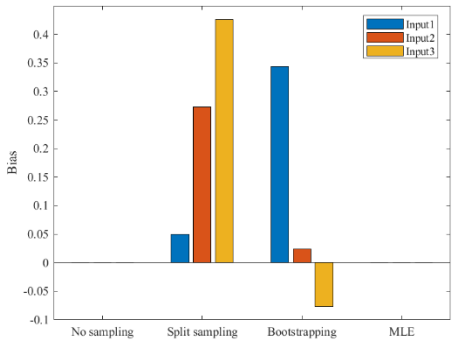

(c) Bias – new design

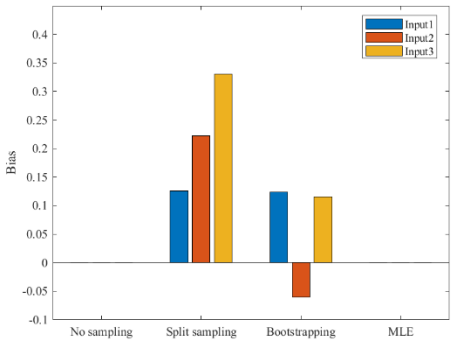

(d) Bias – overlay design

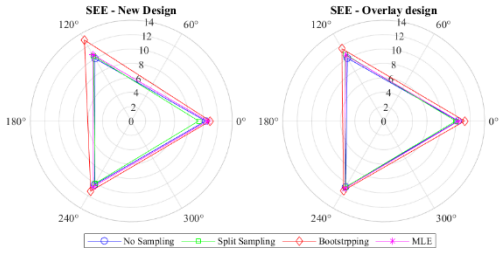

(e) SEE

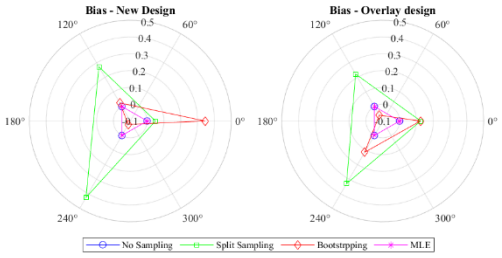

(f) Bias

Figure 6-17: SEE and bias comparison of new vs. overlay design

6.6 Reliability

The calibration process and the PMED predictions are obtained at a reliability of 50%. The concept and method are discussed in Chapter 5. The pavements are generally designed with a reliability of 90-95% based on desired usage. This section summarizes the results of reliability for each model.

6.6.1 Bottom-up Cracking

The measured and predicted cracking were sorted in bins based on the expected cracking. A relationship was developed between the standard deviation of the measured cracking and the mean predicted cracking. Tables 6-20 and 6-21 summarize the standard error equations for both approaches ing the bottom-up cracking model. Figure 6-18 compares the standard deviations of approaches 1 and 2 used to calibrate bottom-up cracking.

Table 6-20: Standard error equations summary – bottom-up cracking only (approach 1)

Design	Sampling technique	Global model equation	Local model equation
New	Level 1	$S_{e(Alligator)} = 1.13 + \frac{13}{1 + e^{7.57 - 15.5 \times log(D + 0.0001)}}$	$S_{e(Alligator)} = 0.9951 + \frac{2.3915}{1 + e^{0.1135 - 6.0511 \times log(D)}}$
	Level 2		$S_{e(Alligator)} = 0.6314 + \frac{2.9354}{1 + e^{0.00098 - 2.1243 \times log(D)}}$
	Level 3		$S_{e(Alligator)} = 1.055 + \frac{2.3813}{1 + e^{0.3771 - 3.1495 \times log(D)}}$
Overlay	Level 1		$S_{e(Alligator)} = 1.179 + \frac{2.383}{1 + e^{0.1721 - 4.096 \times log(D)}}$
	Level 2		$S_{e(Alligator)} = 0.7279 + \frac{2.7976}{1 + e^{0.0013 - 4.4145 \times log(D)}}$
	Level 3		$S_{e(Alligator)} = 1.0256 + \frac{2.4828}{1 + e^{0.0046 - 5.2091 \times log(D)}}$

Table 6-21: Standard error equations summary – bottom-up + top-down cracking (approach 2)

Design	Sampling technique	Global model equation	Local model equation
New	Level 1	$S_{e(Alligator)} = 1.13 + \frac{13}{1 + e^{7.57 - 15.5 \times log(D + 0.0001)}}$	$S_{e(Alligator)} = 1.0332 + \frac{3.3329}{1 + e^{0.0003 - 1.7523 \times log(D)}}$
	Level 2		$S_{e(Alligator)} = 0.9264 + \frac{3.4358}{1 + e^{0.0002 - 1.5021 \times log(D)}}$
	Level 3		$S_{e(Alligator)} = 1.0414 + \frac{3.3069}{1 + e^{0.0097 - 1.5147 \times log(D)}}$
Overlay	Level 1		$S_{e(Alligator)} = 1.1179 + \frac{3.5761}{1 + e^{0.0008 - 3.4492 \times log(D)}}$
	Level 2		$S_{e(Alligator)} = 1.0532 + \frac{3.2628}{1 + e^{0.0006 - 4.3429 \times log(D)}}$
	Level 3		$S_{e(Alligator)} = 1.0742 + \frac{3.3675}{1 + e^{0.007 - 3.2995 \times log(D)}}$

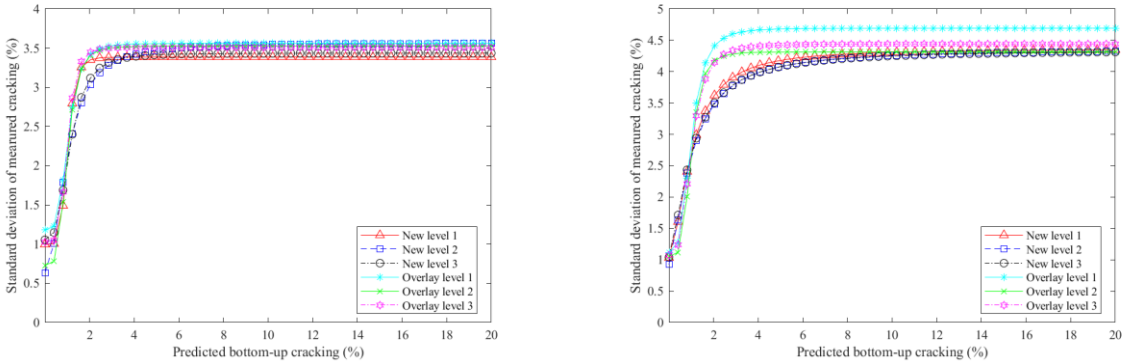

(a) Approach 1: Bottom-up only

(b) Approach 2: Bottom-up + top-down

Figure 6-18: Bottom-up cracking reliability comparison

6.6.2 Top-down Cracking

The reliability of the top-down cracking model is estimated by developing a relationship between the standard deviation of the measured cracking and the mean predicted cracking. It is noted that predictions of top-down cracking for new and overlay designs are the same, so reliability was estimated for one of the design options. Table 6-22 outlines the standard error equations for the top-down cracking model. Figure 6-19 graphically represents the comparison between standard errors of each input level.

Table 6-22: Top-down cracking standard error equations

Design	Sampling technique	Global model equation	Local model equation
New/ Overlay	Level 1	$S_{e(Top-down)} = 0.3657 \times TOP + 3.6563$	$S_{e(Top-down)} = 0.2846 \times TOP + 2.8188$
	Level 2		$S_{e(Top-down)} = 0.5658 \times TOP + 1.8088$
	Level 3		$S_{e(Top-down)} = 0.5534 \times TOP + 1.9319$

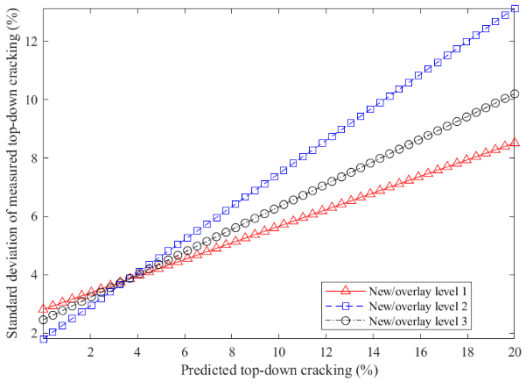

Figure 6-19: Top-down cracking reliability comparison

6.6.3 Rutting Model

The rutting predictions using the calibrated model are at 50% reliability. The standard error equations were formulated using the standard deviation of the measured rutting and mean predicted rutting to incorporate reliability in the model. The reliability of the rutting model was estimated for individual layer models. Tables 6-23 show the standard error equation for AC and unbound layer's rutting models for new and overlay designs at each input level. Figure 6-20 shows the graphical comparison between the reliabilities of rutting models at different input levels for new and overlay designs.

Table 6-23: Standard error equations comparison of rutting model

Design/ Level	Pavement layer	Global model equation	Local model equation
HMA rutting	New Level 1	$s_{e(HMA)} = 0.24(Rut_{HMA})^{0.8026} + 0.001$	$s_{e(HMA)} = 0.0971(Rut_{HMA})^{0.3506}$
	New Level 2		$s_{e(HMA)} = 0.0913(Rut_{HMA})^{0.3423}$
	New Level 3		$s_{e(HMA)} = 0.0644(Rut_{HMA})^{0.202}$
	Overlay Level 1		$s_{e(HMA)} = 0.089(Rut_{HMA})^{0.4613}$
	Overlay Level 2		$s_{e(HMA)} = 0.0732(Rut_{HMA})^{0.3073}$
	Overlay Level 3		$s_{e(HMA)} = 0.0672(Rut_{HMA})^{0.2352}$
Base Rutting	New Level 1	$s_{e(base)} = 0.1477(Rut_{base})^{0.6711} + 0.001$	$s_{e(base)} = 0.0204(Rut_{base})^{0.3438}$
	New Level 2		$s_{e(base)} = 0.0346(Rut_{base})^{0.4769}$
	New Level 3		$s_{e(base)} = 0.0154(Rut_{base})^{0.4522}$
	Overlay Level 1		$s_{e(base)} = 0.0306(Rut_{base})^{0.3879}$
	Overlay Level 2		$s_{e(base)} = 0.0363(Rut_{base})^{0.4066}$
	Overlay Level 3		$s_{e(base)} = 0.0128(Rut_{base})^{0.2804}$
Subgrade Rutting	New Level 1	$s_{e(subgrade)} = 0.1235\left(Rut_{subgrade}\right)^{0.5012} + 0.001$	$s_{e(subgrade)} = 0.0097\left(Rut_{subgrade}\right)^{0.7809}$
	New Level 2		$s_{e(subgrade)} = 0.008\left(Rut_{subgrade}\right)^{0.7101}$
	New Level 3		$s_{e(subgrade)} = 0.0054\left(Rut_{subgrade}\right)^{0.6123}$
	Overlay Level 1		$s_{e(subgrade)} = 0.0121\left(Rut_{subgrade}\right)^{0.8892}$
	Overlay Level 2		$s_{e(subgrade)} = 0.0069\left(Rut_{subgrade}\right)^{0.506}$
	Overlay Level 3		$s_{e(subgrade)} = 0.0056\left(Rut_{subgrade}\right)^{0.6628}$

6.6.4 Transverse (Thermal) Cracking

The standard error equations were developed using the standard deviation of the measured cracking and mean predicted cracking, as explained in Chapter 5. Table 6-24 summarizes the standard error equations for all input levels and design options. Figure 6-21 shows the standard error equation plots for transverse (thermal) cracking.

Table 6-24: Standard error equations summary of thermal cracking model

Design	Sampling technique	Global model equation	Local model equation
Level 1	New	$s_e = 0.14(TC) + 168$	$s_e = 0.015(TC) + 238.84$
	Overlay		$s_e = 0.0653(TC) + 167.75$
Level 2	New	$s_e = 0.20(TC) + 168$	$s_e = 0.0375(TC) + 194.34$
	Overlay		$s_e = 0.0653(TC) + 167.75$
Level 3	New	$s_e = 0.289(TC) + 168$	$s_e = 0.0325(TC) + 213.53$
	Overlay		$s_e = 0.0394(TC) + 184.48$

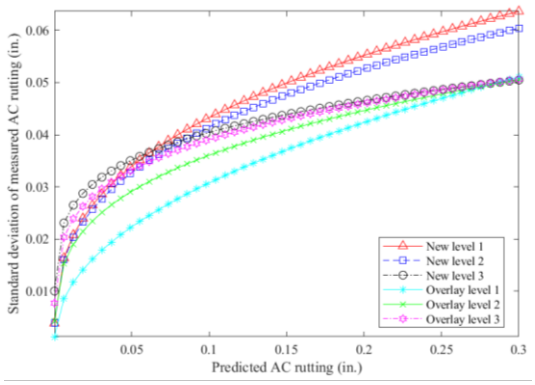

(a) AC rutting

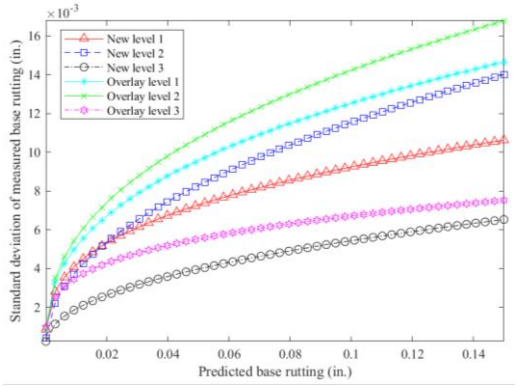

(b) Base rutting

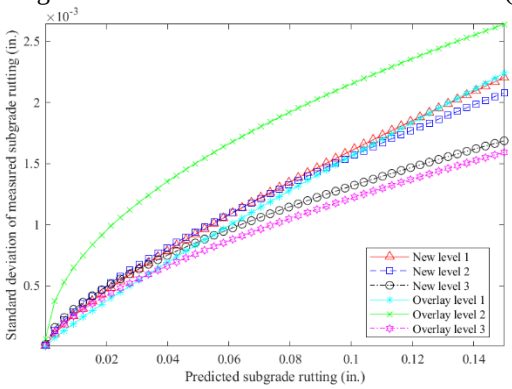

(c) Subgrade rutting

Figure 6-20: Reliability comparison of rutting models

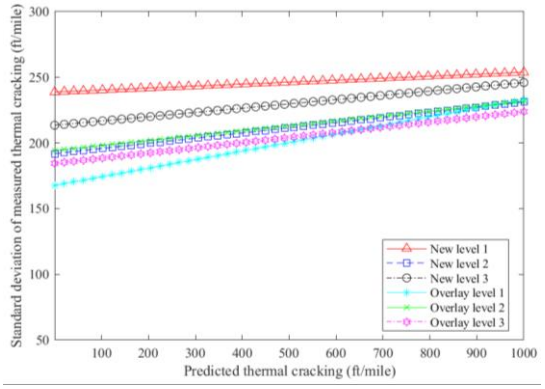

Figure 6-21: Reliability comparison of the thermal cracking model

6.7 Impact of Calibration

The accuracy in PMED design is subjected to an optimum solution of transfer function coefficients by reliable local calibration results by minimizing the error between measured and predicted performance. In this section, rubblized pavement sections with variable traffic and different climatic regions were designed using locally calibrated transfer function coefficients. Eleven random sections were designed as new and overlaid using PMED to analyze the impact of local calibration. MDOT recommends a minimum of 6.5-inch HMA thickness over rubblized PCC with a maximum of ± 1 inch from the original thickness achieved from AASHTO93. Table 6-25 shows selected sections' traffic, climate region, and other layer properties.

Table 6-25: Summary of selected sections used for design

No.	Region	Traffic (ADT)	Unbound layers				
			Base		Subbase		Subgrade
			Thickness (in.)	Modulus (psi)	Thickness (in.)	Modulus (psi)	Modulus (psi)
1	North	1081	4	30000	10	13500	4400
2	North	847	6	30000	14	13500	7000
3	University	2492	7	30000	10	13500	5000
4	North	1398	-	30000	11	13500	4400
5	Bay	2619	3	30000	11	13500	5000
6	Bay	2844	3	30000	11	13500	5000
7	Bay	1917	3	30000	11	13500	5000
8	North	972	3	30000	11	13500	4400
9	University	715	7.5	30000	10	13500	4400
10	University	318	7.5	30000	10	13500	4400
11	North	399	3	30000	13	13500	7000

These sections were designed at PMED input Level 1 using both design options for HMA over rubblized PCC, i.e., new flexible and an overlay design. The local calibration coefficients of

the bottom-up cracking model were based on approach 2 (measured bottom-up + top-down cracking in wheel path). Table 6-26 compares the design thickness between the new and overlay designs. It is pertinent to mention that these design thicknesses are directly obtained from PMED to compare AASHTO and PMED design options. However, MDOT recommends not deviating +-1 inches from the original AASHTO93 design thickness (4). Figure 6-22 shows the thickness comparison and average thickness along with the standard deviation.

Table 6-26: Designed thicknesses comparison for HMA overlay over rubblized PCC

Section no.	AASHTO93 thickness (in.)	PMED thickness (in.)	
		New Design	Overlay Design
1	6.7	5	4.5
2	6.5	5	6
3	7	5	5
4	6.5	6.5	6
5	6.5	6	5.25
6	6.5	6	5.25
7	6.5	6	5.25
8	8.5	7	7
9	6.5	4.5	4.5
10	6.5	5	4.5
11	6.5	5.25	4.5
Average	6.745	5.568	5.250
Standard Deviation	0.602	0.775	0.806

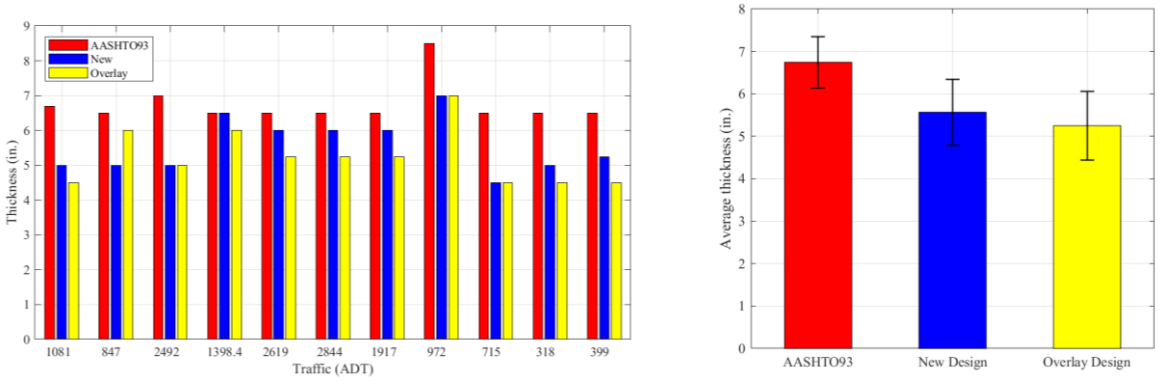

(a) Design thicknesses comparison (b) Average thicknesses

Figure 6-22: Design thicknesses comparison between AASHTO93 and PMED designs

6.8 Summary of Findings

This chapter outlines the calibration comparison for an overlay and new design approaches of rubblized pavements using different calibration techniques. The fatigue bottom-up, total rutting and IRI models are calibrated using all four calibration techniques discussed earlier. Three

distributions are used in MLE, and the most suitable distribution is selected based on NLL, AIC, and BIC values. The top-down and thermal cracking models are calibrated using no sampling technique only. PMED predicted the distresses and roughness at 50% reliability. Standard error equations for all distress models were developed to design the pavement sections at the desired reliability level (90%).

Once all the models are locally calibrated and validated, each model's final model statistics and coefficients are summarized. The following are the recommended final results for the locally calibrated models for Michigan conditions. It was found that there is no significant difference between the new and overlay design of rubblized pavement, and the input levels 1 produced better results; however, Level 3 results are acceptable where Level 1 data is not available. The bootstrapping technique led to the most robust calibration with minimum standard error and bias.

Table 6-27 summarizes the new design's global and locally calibrated model coefficients using input Level 3.

Table 6-27: Summary - locally calibrated model coefficients

Performance prediction model	Global coefficient	Local coefficient	Selected distribution	Statistical parameters	Global model	Local model
Approach 1: Fatigue cracking – Bottom-up only	$C_1 = 1.31$ $C_2 =$ 2.1585 (hac <5 in.) $C_2 = (0.867 + 0.2583 * hac) * 1$ (5 in. <= hac <=12 in.)	$C_1 = 0.20$ $C_2 =$ 1.07 (hac <5 in.) $C_2 = (0.867 + 0.2583 * hac) * 0.28$ (5 in. <= hac <=12 in.)	Exponential	SEE	7.17	5.69
				Bias	-4.77	0.00
				NLL	-	142
				AIC	-	286
				BIC	-	288
Approach 2: Fatigue cracking – Bottom-up + top-down		$C_1 = 0.24$ $C_2 =$ 0.60 (hac <5 in.) $C_2 = (0.867 + 0.2583 * hac) * 0.20$ (5 in. <= hac <=12 in.)		SEE	7.59	6.72
				Bias	-4.29	0.00
				NLL	-	242
				AIC	-	486
				BIC	-	489
Top-down cracking	$K_{L2} = 0.286$ $K_{L3} = 0.011$ $K_{L4} = 0.015$ $K_{L5} = 3.266$ $C_1 = 2.522$ $C_2 = 0.807$	$K_{L2} = 0.657$ $K_{L3} = 0.100$ $K_{L4} = 0.092$ $K_{L5} = 2.044$ $C_1 = 0.097$ $C_2 = 2.416$	-	SEE	4.402	3.672
				Bias	0.310	0.000
Rutting	$\beta_{1r} = 0.4$ $\beta_{s1} = 1$ $\beta_{sg1} = 1$	$\beta_{1r} = 0.576$ $\beta_{s1} = 0.569$ $\beta_{sg1} = 0.659$	Exponential	SEE	0.096	0.079
				Bias	0.055	0.000
				NLL	-	383
				AIC	-	768
				BIC	-	771
Transverse (thermal) cracking	$K = 1.0$	$K = 0.65$	-	SEE	1517.6	704.48
				Bias	-1323.9	145.38
IRI	$C_1 = 40.026$ $C_2 = 0.40$ $C_3 = 0.008$ $C_4 = 0.015$	$C_1 = 13.51$ $C_2 = 0.28$ $C_3 = 0.01$ $C_4 = 0.003$	Normal	SEE	15.79	10.59
				Bias	10.92	0.05
				NLL	-	1182
				AIC	-	2368
				BIC	-	2375

CHAPTER 7 CONCLUSIONS AND RECOMMENDATIONS

The study's first objective was to compare the performance predictions of the two design approaches for rubblized pavements, i.e., new and overlay, at three hierarchical input levels. Forty-eight rubblized sections were available throughout the different climate regions of Michigan state. In option 1, these sections were designed as new flexible pavement, modeling rubblized PCC layer as unbound aggregate base material with a modulus of 70,000 psi. Design option 2 modeled the rubblized pavement as an HMA overlay over fractured JPCP with a minimum modulus of 150,000 psi for the fractured JPCP layer. Chapter 3 discusses the selection process of the pavement sections and other inputs used in the evaluation of rubblized pavement performance predictions.

The study's second objective was to calibrate the performance prediction models locally at three hierarchical input levels and recommend a suitable option for MDOT design practices. Various calibration and sampling techniques minimize the local model's SEE and bias. For fatigue bottom-up cracking, the study used no sampling, traditional split sampling, and bootstrapping techniques, while for total rutting and IRI models, least square regression and maximum likelihood estimation (MLE) approaches are adopted. Only least square regression is used to calibrate the top-down cracking model. However, transverse thermal cracking is calibrated by running the PMED multiple times at a range of *K*-values.

The next objective was to perform a sensitivity analysis of transfer function coefficients using SSCs over the entire range of available sections and independent variables. The sensitivity analysis used various distresses and roughness while not changing the material inputs. The SSC-based ranking was compared with NSI values reported by Kim et al. (2014).

7.1 Conclusions

The following conclusions can be drawn based on the work performed.

a. The global model under-predicted the bottom-up fatigue cracking for new and overlay designs at all hierarchical input levels. Fatigue bottom-up cracking was calibrated using two different approaches; approach 1 uses bottom-up measured cracking only, and in approach 2, the bottom-up and top-down measured cracking in the wheel path was assumed as bottom-up cracking. Local calibration of an overlay and new design at input

Level 1 produced acceptable results with minimum SEE and bias using exponential distribution in MLE.

b. No difference was observed in top-down global prediction for new and overlay designs. No sampling technique using least square regression was adopted for local calibration of top-down cracking—the local calibration of top-down cracking at hierarchical input level 1 produced minimum SEE and bias. The SEE was reduced from 4.657 to 3.672, and the bias was improved from -1.097 to 0.00.
c. The global model for new and overlay design approaches slightly over-predicted the total rutting. The local calibration used all sampling techniques. The MLE using exponential distribution produced acceptable results for the new design at input Level 1; however, the difference between the new and overlay design after local calibration at hierarchical input levels 1 and 3 was insignificant. The SEE was reduced from 0.096 to 0.079, and the bias was reduced from 0.055 to 0.00.
d. Transverse thermal cracking was over-predicted at input Levels 1 and 2, whereas Level 3 under-predicted thermal cracking. The local calibration of an overlay design at input Levels 1 and 2 produced acceptable results per MDOT's practices. The K value for input Level 3 through local calibration exceeded 2 in both design approaches, which is not aligned with MDOT practices. As a result, it was rejected. Overall, the input Level 1 of the new design produced minimum SEE and bias. The SEE was reduced from 1517.62 to 704.48, and the bias was reduced from -1323.93 to 145.38.
e. IRI was slightly over-predicted by the global model for new and overlay design. No sampling, split sampling, or bootstrapping sampling techniques were used in the least square regression analysis, and only bootstrapping was used in the MLE analysis of the IRI model. The normal distribution using the MLE approach for new designs at input Level 1 produced better results; however, the difference between an overlay and new designs at input Level 1 is insignificant. The SEE was reduced from 21.48 to 10.59, and the bias was reduced from 19.02 to 0.05.
f. The standard error equations were obtained based on the predicted and measured performance to design the pavement sections at the desired reliability level. No significant difference was noted between standard error equations at three hierarchical input levels.

g. Eleven (11) random sections with varying traffic and climate regions were designed at 90% reliability to validate the impact of calibration for designed thicknesses. All these sections were designed as new and overlay to get the optimum thickness of the AC layer and then compared with AASHTO93 design thicknesses. The overlay design yielded minimum thickness compared to the new design and AASHTO93 design. The average difference between the AASHTO93 design and the PMED overlay design was around 1.5 inches, and the average difference between the new and overlay design using PMED was about 0.32 inches.
h. Sensitivity analysis using SSCs is a forward problem and does not require actual data; only a mathematical model is needed to analyze the sensitivity of coefficients over the range of the independent variables.
i. SSCs provide a visual representation of the variability in the sensitivity of the coefficient at a continuous range of independent variables. Unlike NSI, a point estimate, SSCs make it easier for users to understand and interpret the sensitivity results.
j. For a wide range of damage in the bottom-up cracking model, C_1 is more sensitive than C_2, and both are not correlated. Moreover, C_1 and C_2 are large enough to be confidently estimated. However, for a narrow range of damage, the sensitivity of the calibration coefficients is the same, i.e., C_2 is as sensitive as C_1 if the damage is less than 18 %. Coefficients with negative SSCs indicate that an increase in the coefficient will decrease predicted performance. Therefore, an increase in C_1 or C_2 will reduce bottom-up cracking.
k. The sensitivity of coefficients changes with the independent variables *t* (analysis time in days) and t_0 (time to crack initiation). Overall, C_3 is the most sensitive coefficient, followed by C_2 and C_1. C_1 and C_2 are correlated, indicating that only one can be confidently estimated. All coefficients have negative SSC values, which means an increase in any of the coefficients will reduce the predicted top-down cracking.
l. Subgrade rutting coefficient (β_{sg1}) is the most sensitive, followed by the AC rutting coefficient (β_{1r}). The base rutting coefficient (β_{s1}) is the least sensitive. All coefficients are not correlated, and the magnitude of SSCs is large enough to be estimable with confidence. SSC values are positive for all coefficients, which indicates an increase in individual layer rutting with an increase in coefficient value.

m. Likewise, the rutting model, the IRI for flexible pavements, is linear. The site factor coefficient C_4 is the most sensitive, followed by the total rutting coefficient C_1 and thermal cracking coefficient C3. Meanwhile, the fatigue cracking coefficient C_2 is the least sensitive. All coefficients have positive values for SSCs, which means that with an increase in coefficient value, the IRI-predicted performance will increase.

7.2 Recommendations

The following recommendations would improve the design and calibration methodology of rubblized pavements.

a. It is recommended for sensitivity analysis to use SSCs, as it is a convenient way of visual representation. Coefficients are ranked over a continuous range of independent variables. Visualizing the sensitivity of the model's coefficients through SSCs is a more practical approach for straightforward interpretation.
b. The local calibration of an overlay design and a new design has no significant difference after calibration. Therefore, MDOT's existing practices of designing rubblized pavement as new flexible pavement is recommended.
c. The global performance prediction and local calibration results of new and overlay designs at input Level 1 are not significantly different. Level 1 input is recommended to design rubblized pavement using any design approach accurately.
d. Overall, PMED resulted in a thinner AC layer than AASHTO93 designs. It is recommended to use PMED design as compared to AASHTO93.
e. A total of 48 sections were used in this study. It is recommended to include more sections of rubblized pavement in the MDOT database with additional performance data points.
f. Resampling techniques provide more robust results; hence, these techniques can improve local calibration.
g. Local calibration using the MLE approach is recommended for bottom-up cracking and rutting models.

7.3 Future Work

The study recommends the following future work.

a. The default properties of the existing rubblized PCC layer were used in this study. It is recommended for future work to characterize the in situ properties of the existing layer.

b. The modulus, crack spacing, and LTE directly affect the predicted performance. For example, if rubblization is not done correctly, it could lead to reflective cracking in the HMA overlay of rubblzied pavements. The actual data on the existing layer will further improve the design of rubblized pavements.
c. This study did not include the reflection cracking model of an overlay design. The reflection cracking model in future studies may be included to observe the rubblized pavement response.
d. Different distributions can be used to improve the calibration results further using MLE.

REFERENCES

1. Huang YH. Pavement analysis and design: Pearson Prentice Hall Upper Saddle River, NJ; 2004.

2. Guide ND. Guide 1-37a, guide for mechanistic-empirical design of new and rehabilitated pavement structures, national cooperative highway research program. Transportation Research Board, National Research Council: Washington, DC, USA. 2004.

3. Li Q, Xiao DX, Wang KC, Hall KD, Qiu Y. Mechanistic-empirical pavement design guide (MEPDG): a bird's-eye view. Journal of Modern Transportation. 2011;19:114-33.

4. MDOT. Michigan DOT User Guide for Mechanistic-Empirical Pavement Design. Michigan Department of Transportation Lansing, MI, USA; 2021.

5. Haider SW, Buch N, Brink W, Chatti K, Baladi G. Preparation for implementation of the mechanistic-empirical pavement design guide in Michigan, part 3: local calibration and validation of the pavement-ME performance models.; 2014. Report No.: RC-1595.

6. Von Quintus HL, Lee H, Bonaquist R. Practitioner's guide: part 2—determining properties of resource responsible asphalt mixtures for Use in the mechanistic empirical pavement design guide. US Department of Transportation. 2020.

7. Kang M, Adams TM, editors. Local calibration for fatigue cracking models used in the Mechanistic-empirical pavement design guide. Proceedings of the 2007 mid-continent transportation research symposium; 2007.

8. AASHTO. Mechanistic-empirical pavement design guide: A manual of practice; 2nd Edition: AASHTO; 2015 2015.

9. Haider SW, Musunuru G, Buch N, Brink WC. Local Recalibration of JPCP Performance Models and Pavement-ME Implementation Challenges in Michigan. Journal of Transportation Engineering, Part B: Pavements. 2020;146(1):04019037.

10. Tabesh M, Sakhaeifar MS. Local calibration and Implementation of AASHTOWARE Pavement ME performance models for Oklahoma pavement systems. International Journal of Pavement Engineering. 2021:1–12.

11. Buch N, Chatti K, Haider SW, Baladi G, Brink W, Harsini I. Preparation for implementation of the mechanistic-empirical pavement design guide in Michigan : part 2 - evaluation of rehabilitation fixes.; 2013. Report No.: RC-1594.

12.Buch N, Jahangirnejad S. Quantifying coefficient of thermal expansion values of typical hydraulic cement concrete paving mixtures. Michigan. Dept. of Transportation. Construction and Technology Division; 2008.

13. Buch N, Haider SW, Brown J, Chatti K. Characterization of truck traffic in Michigan for the new mechanistic empirical pavement design guide.: Michigan. Dept. of Transportation. Construction and Technology Division; 2009.

14. Haider SW, Musunuru G, Buch N, Selezneva OI, Desaraju P, Li JQ. Updated analysis of Michigan traffic inputs for pavement-ME design. Michigan State University. Dept. of Civil and Environmental Engineering; 2018.

15. Baladi G, Dawson T, Sessions C. Pavement subgrade MR design values for michigan's seasonal changes, final report. Michigan Department of Transportation, Construction and Technology Division, PO Box. 2009;30049.

16. Baladi GY, Thottempudi A, Dawson T. Backcalculation of unbound granular layer moduli. 2011.

17. Kutay ME, Jamrah A. Preparation for Implementation of the Mechanistic-Empirical Pavement Design Guide in Michigan: Part 1 – HMA Mixture Characterization.; 2013. Report No.: RC-1593.

18. Harsini I, Haider SW, Brink WC, Buch N, Chatti K. Investigation of significant inputs for pavement rehabilitation design in the Pavement-ME. Canadian Journal of Civil Engineering. 2018;45(5):386-92.

19. Harsini I, Brink WC, Haider SW, Chatti K, Buch N, Baladi GY, et al. Sensitivity of input variables for flexible pavement rehabilitation strategies in the ME PDG. Airfield and Highway Pavement 2013: Sustainable and Efficient Pavements2013. p. 539-50.

20. Brink WC, Harsini I, Haider SW, Buch N, Chatti K, Baladi GY, et al. Sensitivity of input variables for rigid pavement rehabilitation strategies in the MEPDG. Airfield and Highway Pavement 2013: Sustainable and Efficient Pavements2013. p. 528-38.

21. Islam S, Hossain M, Jones C, Gao Y, Wu X, Romanoschi S. Implementation of the AASHTO Mechanistic-Empirical Design Guide (AASHTOWare Pavement ME Design) for Pavement Rehabilitation. Kansas Department of Transportation. Bureau of Research; 2023.

22. VDOT. AASHTOWare Pavement ME User Manual 2018 .

23. Williams RC, Shaidur R. Mechanistic-empirical pavement design guide calibration for pavement rehabilitation.: Oregon. Dept. of Transportation. Research Section; 2013.

24. ARA I, ERES Consultants Division. Guide for Mechanistic–Empirical Design of New and Rehabilitated Pavement Structures. Final Rep, NCHRP Project 1-37A. 2004.

25. Titus-Glover L, Rao C, Sadasivam S. Local Calibration of the Pavement ME for Missouri. Missouri. Department of Transportation. Construction and Materials Division; 2020 2020.

26. Mallela J, Titus-Glover L, Von Quintus H, Darter MI, Stanley M, Rao C. Implementing the AASHTO Mechanistic-Empirical Pavement Design Guide for Missouri. Vol. II, MEDPG Model Validation and Calibration. 2009.

27. Wu Z, Xiao DX, Zhang Z. Research Implementation of AASHTOWare Pavement ME Design in Louisiana. Transportation Research Record. 2016;2590(1):1-9.

28. Mallela J, Titus-Glover L, Sadasivam S, Bhattacharya B, Darter M, Von Quintus H. Implementation of the AASHTO mechanistic-empirical pavement design guide for Colorado. Colorado. Dept. of Transportation. Research Branch; 2000.

29. Darter MI, Titus-Glover L, Von Quintus HL. Draft user's guide for UDOT mechanistic-empirical pavement design. Utah. Dept. of Transportation. Research Division; 2009.

30. Schwartz CW, Li R. Catalog of Material Properties for Mechanistic-Empirical Pavement Design. 2011.

31. Fick SB. Evaluation of the AASHTO empirical and mechanistic-empirical pavement design procedures using the AASHO road test: University of Maryland, College Park; 2010 2010.

32. AASHTO. Guide for the Local Calibration of the Mechanistic-Empirical Pavement Design Guide2010 2010.

33. Ceylan H, Kim S, Gopalakrishnan K, Smadi O. Validation of pavement performance curves for the mechanistic-empirical pavement design guide. 2009.

34. Ceylan H, Kim S, Gopalakrishnan K, Ma D. Iowa calibration of MEPDG performance prediction models. Iowa. Dept. of Transportation; 2013.

35. Kaya O. Investigation of AASHTOWare Pavement ME Design/Darwin-ME TM performance prediction models for Iowa pavement analysis and design: Iowa State University; 2015.

36. Mallela J, Titus-Glover L, Von Quintus H, Darter MI, Stanley M, Rao C, et al. Implementing the AASHTO Mechanistic-Empirical Pavement Design Guide for Missouri. Vol. I, Study Findings, Conclusions and Recommendations. 2009.

37. Nair H, Saha B, Merine G. Developing an Implementation Strategy for Virginia Department of Transportation Pavement Rehabilitation Design Using Mechanistic-Empirical Concepts. Virginia Transportation Research Council (VTRC); 2022.

38. Wu Z, Xiao DX, Zhang Z, Temple WH. Evaluation of AASHTO Mechanistic-Empirical Pavement Design Guide for designing rigid pavements in louisiana. International Journal of Pavement Research and Technology. 2014;7(6):405.

39. Wu Z, Yang X. Evaluation of current Louisiana flexible pavement structures using PMS data and new mechanistic-empirical pavement design guide. Louisiana Transportation Research Center; 2012.

40. Huang B, Gong H, Shu X. Local Calibration of Mechanistic-Empirical Pavement Design Guide in Tennessee. Tennessee. Department of Transportation; 2016 2016.

41. Zhou C, Huang B, Shu X, Dong Q. Validating MEPDG with Tennessee pavement performance data. Journal of Transportation Engineering. 2013;139(3):306-12.

42. Gong H, Huang B, Shu X, Udeh S. Local calibration of the fatigue cracking models in the mechanistic-empirical pavement design guide for Tennessee. Road Materials and Pavement Design. 2017;18(sup3):130-8.

43. Miner MA. Cumulative damage in fatigue. 1945.

44. AASHTO. AASHTOWare [Internet]2020. [2023-03-16 05:24:06].

45. Ling M, Luo X, Chen Y, Gu F, Lytton RL. Mechanistic-empirical models for top-down cracking initiation of asphalt pavements. International Journal of Pavement Engineering. 2020;21(4):464–73.

46. Titus-Glover L, Bhattacharya BB, Raghunathan D, Mallela J, Lytton RL. Adaptation of NCHRP project 1-41 reflection cracking models for semirigid pavement design in AASHTOWare pavement ME design. Transportation Research Record. 2016;2590(1):122-31.

47. Lytton RL, Tsai FL, Lee SI, Luo R, Hu S, Zhou F. Models for predicting reflection cracking of hot-mix asphalt overlays. NCHRP report. 2010;669:48-56.

48. You Z, Yang X, Hiller J, Watkins D, Dong J. Improvement of Michigan climatic files in pavement ME design. Michigan. Dept. of Transportation; 2015.

49. Buch N, Chatti K, Haider SW, Manik A. Evaluation of the 1-37A Design Process for New and Rehabilitated JPCP and HMA Pavements-Appendix. 2008.

50. Mallela J, Titus-Glover L, Bhattacharya B, Darter M, Von Quintus H. Idaho AASHTOWare pavement ME design user's guide, version 1.1. Idaho. Transportation Dept.; 2014.

51. Schwartz C, Li R, Ceylan H, Kim S, Gopalakrishnan K. Sensitivity evaluation of MEPDG performance prediction. 2011.

52. Ceylan H, Gopalakrishnan K, Kim S, Schwartz CW, Li R. Global sensitivity analysis of jointed plain concrete pavement mechanistic–empirical performance predictions. Transportation research record. 2013;2367(1):113-22.

53. Hall KD, Beam S. Estimating the sensitivity of design input variables for rigid pavement analysis with a mechanistic–empirical design guide. Transportation Research Record. 2005;1919(1):65-73.

54. Kim S, Ceylan H, Ma D, Gopalakrishnan K. Calibration of pavement ME design and mechanistic-empirical pavement design guide performance prediction models for Iowa pavement systems. Journal of Transportation Engineering. 2014;140(10):04014052.

55. Dong S, Zhong J, Tighe SL, Hao P, Pickel D. Approaches for local calibration of mechanistic-empirical pavement design guide joint faulting model: a case study of Ontario. International Journal of Pavement Engineering. 2020;21(11):1347-61.

56. Beck JV. K. J. Arnold, Parameter Estimation in Engineering and Science. Wiley, New York; 1977.

57. Geeraerd A, Valdramidis V, Van Impe J. GInaFiT, a freeware tool to assess non-log-linear microbial survivor curves. International journal of food microbiology. 2005;102(1):95-105.

58. Dolan KD, Mishra DK. Parameter estimation in food science. Annual review of food science and technology. 2013;4:401-22.

APPENDIX

A.1 Top-down Cracking Model

A.1.1 No Sampling

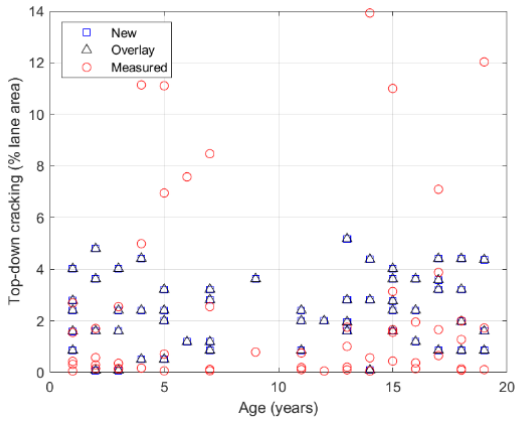

(a) New vs. overlay - level 1

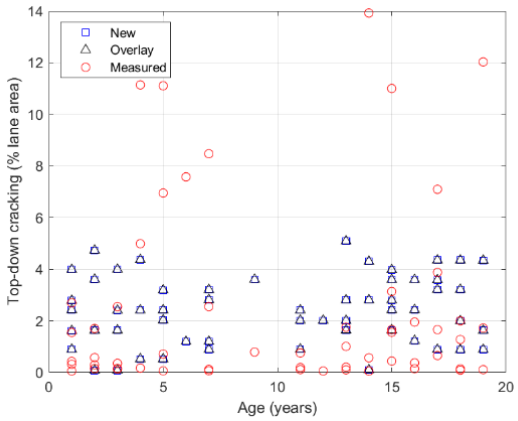

(b) New vs. overlay - level 2

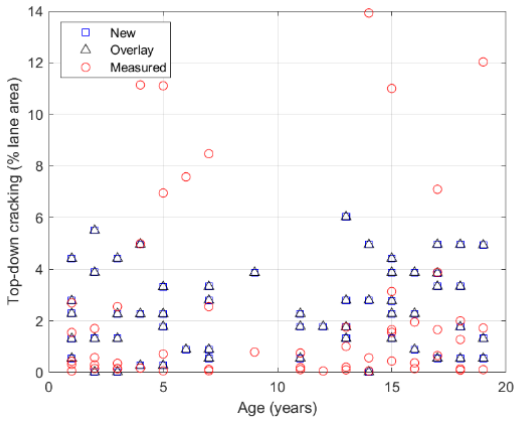

(c) New vs. overlay - level 3

Figure A- 1: Measured and predicted top-down-cracking (time series)

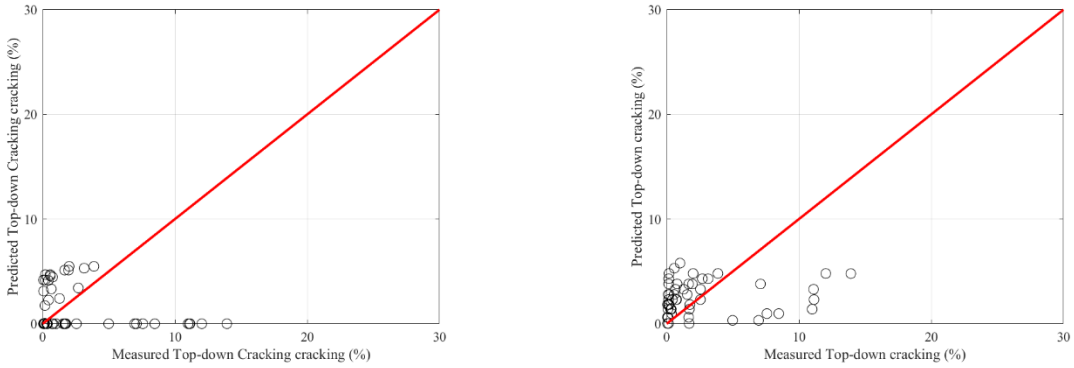

(a) Global model (level 1)

(b) Local model (level 1)

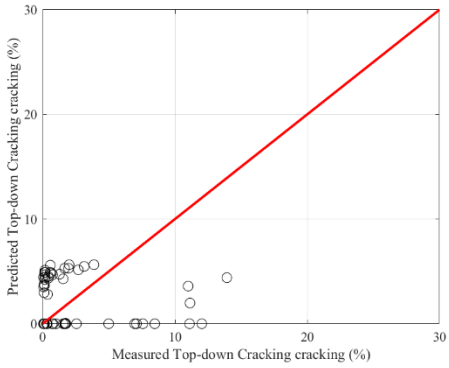

(c) Global model (level 2)

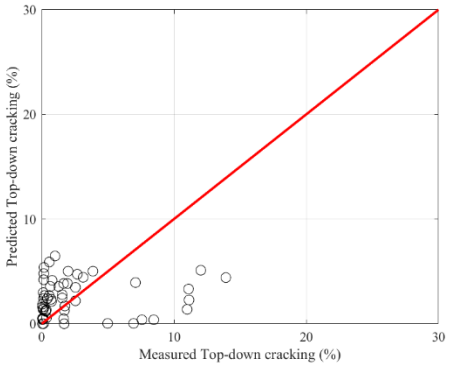

(d) Local model (level 2)

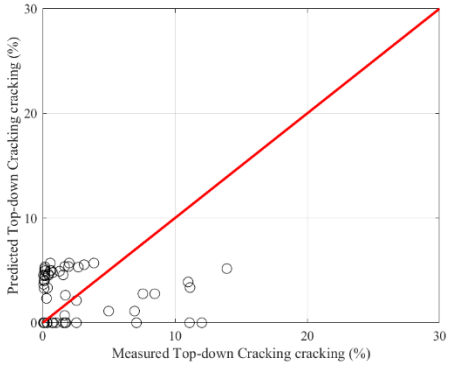

(e) Global model (level 3)

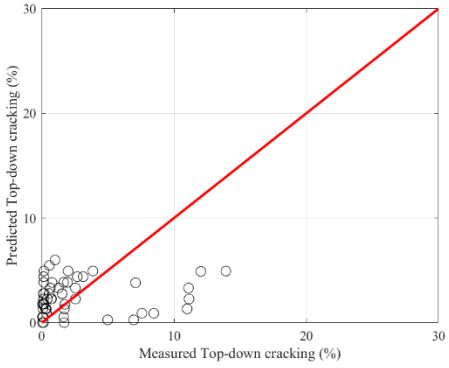

(f) Local model (level 3)

Figure A- 2: Predicted vs. measured top-down cracking (No sampling)

A.2 Total Rutting Model

A.2.1 No Sampling

Total predicted rutting is simply the sum of rutting predictions for individual layers. Figure A-3 shows the measured and predicted total rutting with time. Figures A-4 and A-5 simultaneously show the predicted vs. measured total rutting for both design approaches at global and local models. Table A-1 shows the calibration results for the global and local models. The SEE and

bias are minimal for calibrating overlay design predictions at Level 3. However, a negligible difference is noted between Levels 2 and 3 values. The predictions are close to the measured values for most of the rutting range.

Table A- 1: Local calibration summary for total rutting (No sampling)

Parameter	Level 1				Level 2				Level 3			
	New		Overlay		New		Overlay		New		Overlay	
	Global	Local	Global	Local	Global	Local	Global	Local	Global	Local	Global	Local
Br1	0.400	0.445	0.400	0.580	0.400	0.057	0.400	0.233	0.400	0.176	0.400	0.248
Bs1	1.000	0.101	1.000	2.245	1.000	2.173	1.000	0.930	1.000	0.926	1.000	0.392
Bsg1	1.000	0.851	1.000	0.351	1.000	0.200	1.000	0.676	1.000	0.626	1.000	0.830
SEE	0.099	0.079	0.088	0.082	0.122	0.081	0.103	0.077	0.111	0.077	0.095	0.076
Bias	0.057	-0.002	0.038	-0.005	0.089	-0.004	0.065	-0.001	0.076	-0.001	0.054	-0.002

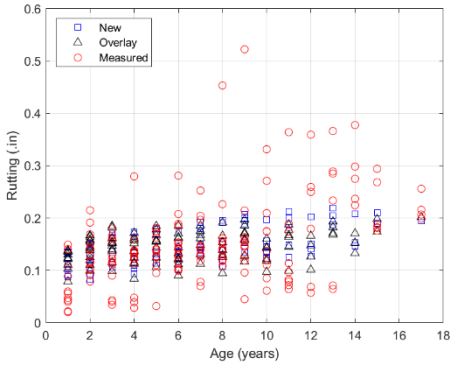

(a) New vs. overlay - level 1

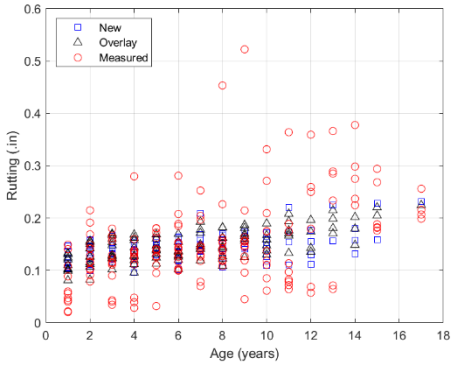

(b) New vs. overlay - level 2

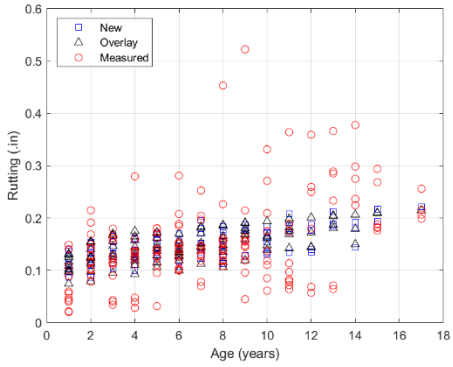

(c) New vs. overlay - level 3

Figure A- 3: Measured vs. predicted with time series for total rutting

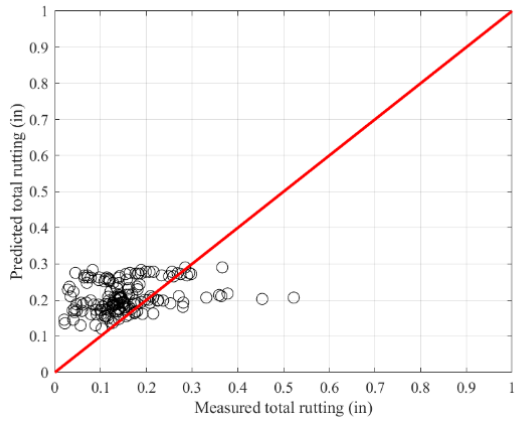

(a) Global model (level 1)

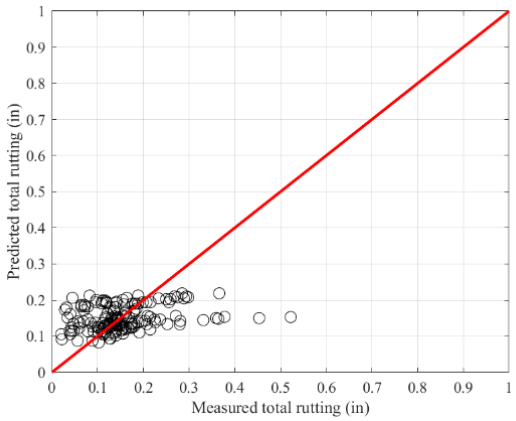

(b) Local model (level 1)

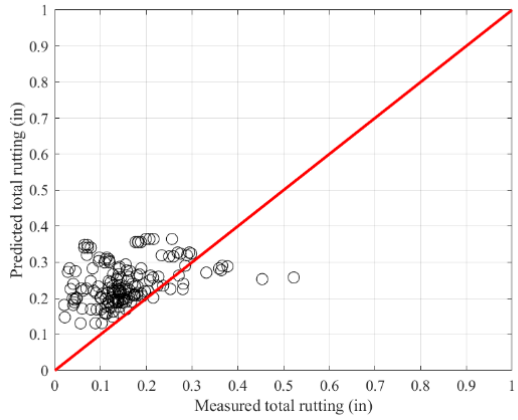

(c) Global model (level 2)

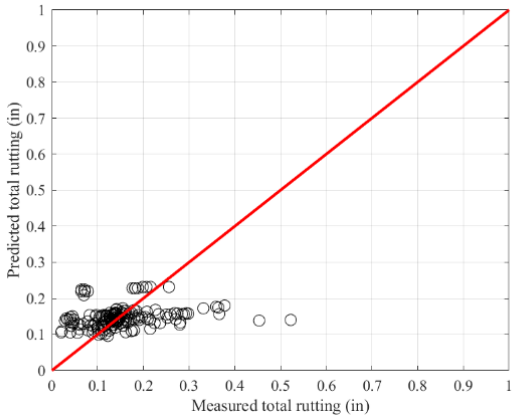

(d) Local model (level 2)

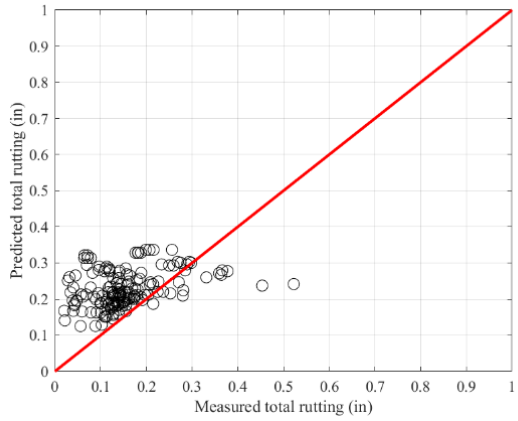

(e) Global model (level 3)

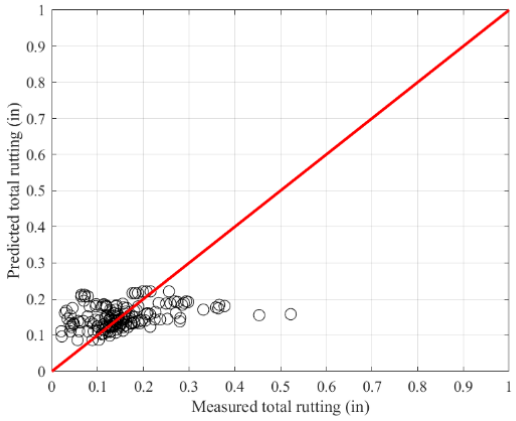

(f) Local model (level 3)

Figure A- 4: Predicted vs. measured total rutting (No sampling) – New design

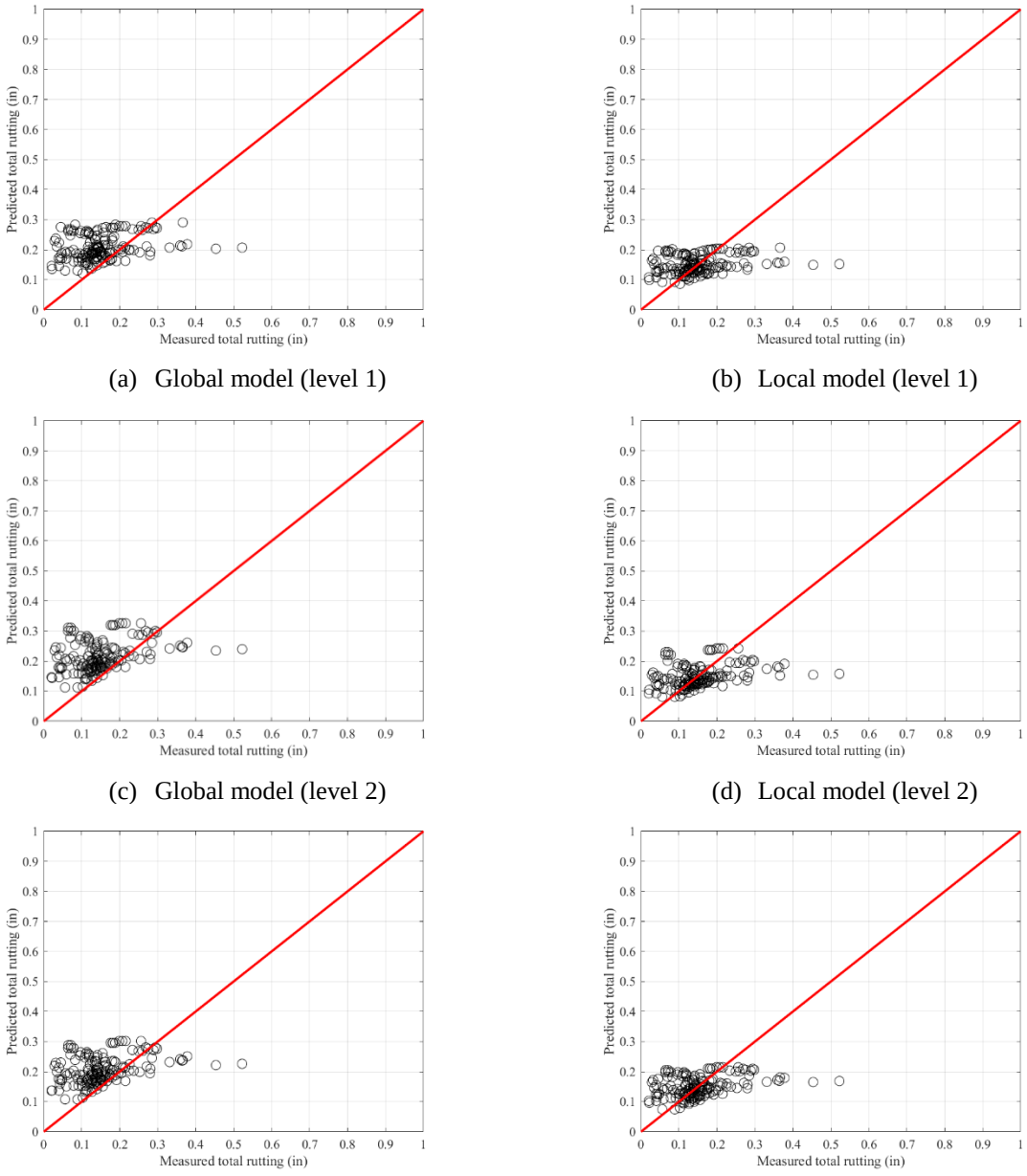

(a) Global model (level 1)

(b) Local model (level 1)

(c) Global model (level 2)

(d) Local model (level 2)

(e) Global model (level 3)

(f) Local model (level 3)

Figure A- 5: Predicted vs measured total rutting (No sampling) – Overlay design

A.2.2 Split Sampling

Split sampling was performed on 70% of the sections for the calibration set and 30% for the validation set. Figures A-6 and A-7 show the predicted vs. measured for calibration and validation set for both design approaches. Tables A-2 and A-3 show the calibration and validation results. Both SEE and bias significantly improved. Validations results are also satisfactory.

Table A- 2: Local calibration summary for total rutting (calibration set)

Parameter	Level 1				Level 2				Level 3			
	New		Overlay		New		Overlay		New		Overlay	
	Global	Local	Global	Local	Global	Local	Global	Local	Global	Local	Global	Local
Br1	0.40	0.15	0.40	0.33	0.40	0.17	0.40	0.15	0.40	0.13	0.40	0.13
Bs1	1.00	0.36	1.00	0.30	1.00	0.31	1.00	0.37	1.00	0.33	1.00	0.33
Bsg1	1.00	0.90	1.00	0.95	1.00	0.84	1.00	0.92	1.00	0.96	1.00	0.96
SEE	0.10	0.08	0.09	0.08	0.12	0.08	0.11	0.08	0.12	0.08	0.10	0.08
Bias	0.06	0.00	0.04	0.00	0.08	0.00	0.06	0.00	0.08	0.02	0.05	0.00

Table A- 3: Local calibration summary for total rutting (validation set)

Parameter	Level 1				Level 2				Level 3			
	New		Overlay		New		Overlay		New		Overlay	
	Global	Local	Global	Local	Global	Local	Global	Local	Global	Local	Global	Local
Br1	0.40	0.15	0.40	0.33	0.40	0.17	0.40	0.15	0.40	0.13	0.40	0.13
Bs1	1.00	0.36	1.00	0.30	1.00	0.31	1.00	0.37	1.00	0.33	1.00	0.33
Bsg1	1.00	0.90	1.00	0.95	1.00	0.84	1.00	0.92	1.00	0.96	1.00	0.96
SEE	0.10	0.08	0.08	0.11	0.13	0.08	0.10	0.06	0.10	0.08	0.09	0.07
Bias	0.06	-0.01	0.03	-0.08	0.10	0.00	0.08	0.01	0.06	-0.01	0.06	0.01

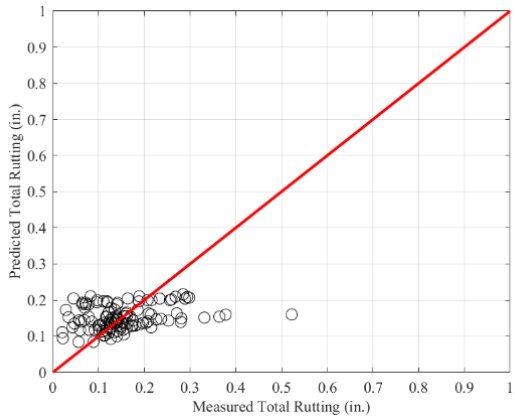

(a) Level 1 – local model (new design)

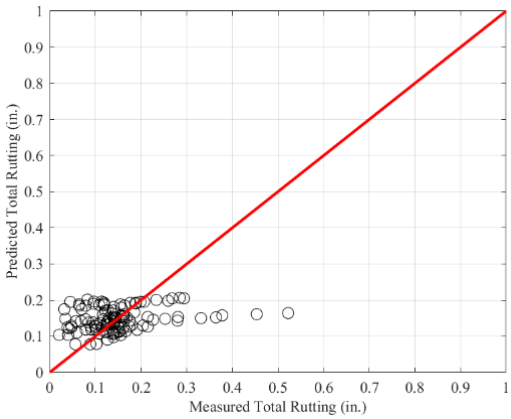

(b) Level 1 – local model (overlay design)

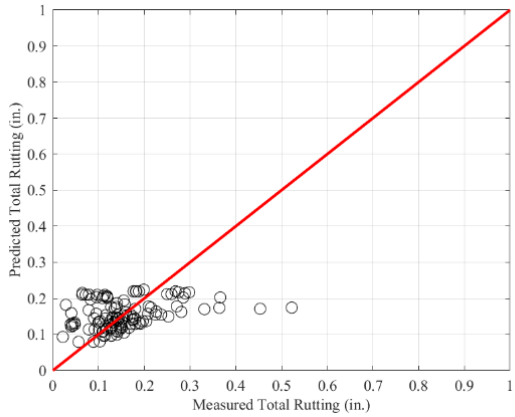

(c) Level 2 – local model (new design)

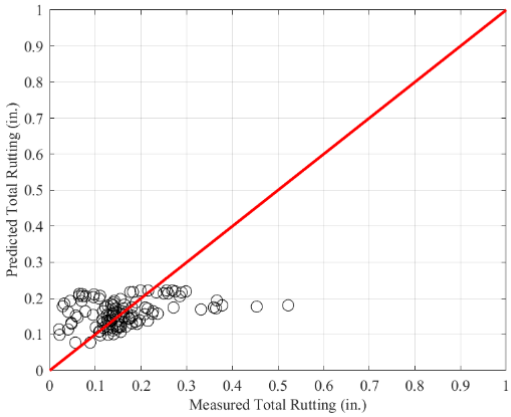

(d) Level 2 – local model (overlay design)

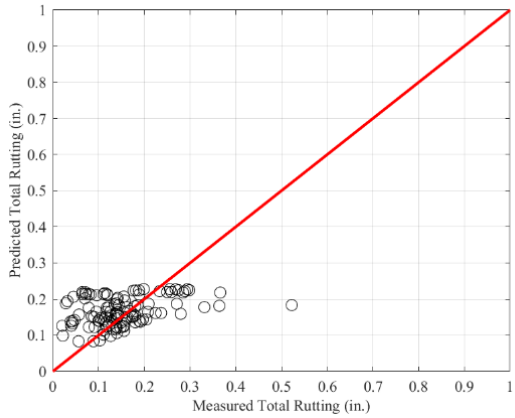

(e) Level 3 – local model (new design)

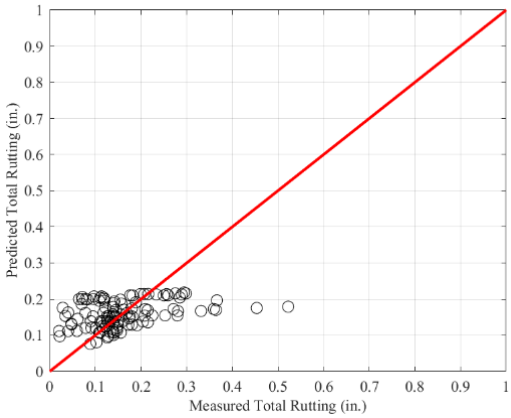

(f) Level 3 – local model (overlay design)

Figure A- 6: Predicted vs. measured total rutting (split sampling) – calibration set

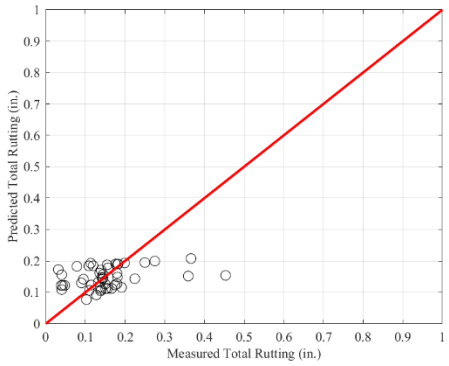

(a) Level 1 – local model (new design)

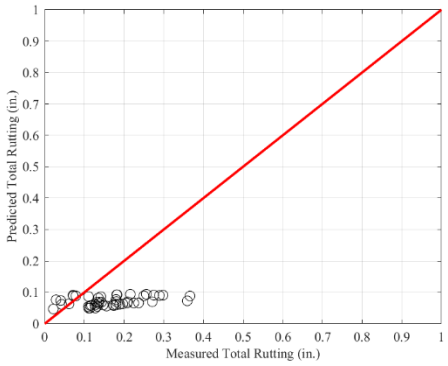

(b) Level 1 – local model (overlay design)

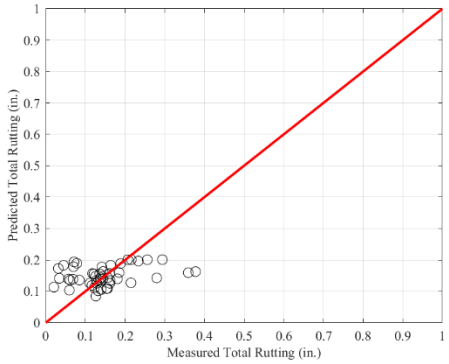

(c) Level 2 – local model (new design)

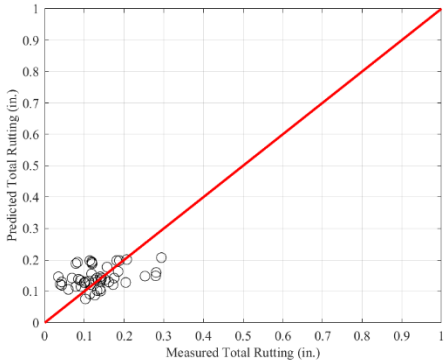

(d) Level 2 – local model (overlay design)

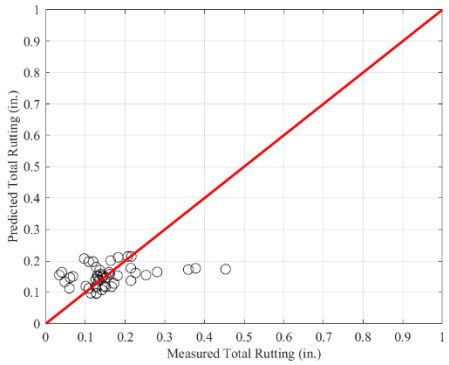

(e) Level 3 – local model (new design)

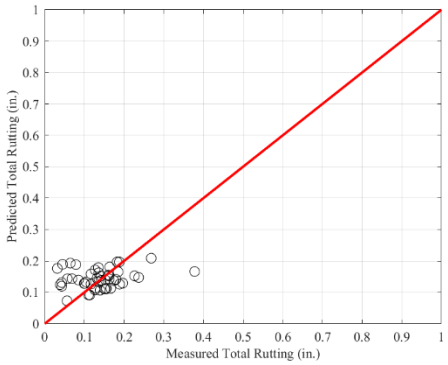

(f) Level 3 – local model (overlay design)

Figure A- 7: Predicted vs. measured total rutting (split sampling) – validation set

A.2.3 Bootstrapping

Bootstrapping was performed with 1000 bootstrap samples with replacement. Tables A-4 and A-5 summarize the calibration results for the global and local models. SEE and bias significantly improved for all models. Overall, an overlay design at Level 3 input produced better results. Figures A-8 and A-9 show the local model's measured versus predicted and residual distribution plots for the 1000 bootstrap samples, respectively.

Table A- 4: Bootstrapping global model summary

Parameters	Levels	1		2		3	
	Design	New	Overlay	New	Overlay	New	Overlay
Br1	Mean	0.40					
	Median						
Bs1	Mean	1.00					
	Median						
Bsg1	Mean	1.00					
	Median						
SEE	Mean	0.099	0.088	0.122	0.104	0.111	0.096
	Median	0.099	0.088	0.122	0.104	0.111	0.096
Bias	Mean	0.057	0.038	0.088	0.065	0.076	0.055
	Median	0.057	0.038	0.088	0.065	0.077	0.055

Table A- 5: Bootstrapping local calibration results summary

Parameters	Levels	1		2		3	
	Design	New	Overlay	New	Overlay	New	Overlay
Br1	Mean	0.598	0.361	0.378	0.386	0.413	0.463
	Median	0.592	0.361	0.342	0.305	0.329	0.383
Bs1	Mean	0.536	0.504	0.865	1.312	0.894	1.27
	Median	0.554	0.512	0.776	0.956	0.801	0.94
Bsg1	Mean	0.647	0.51	0.422	0.455	0.471	0.489
	Median	0.659	0.508	0.386	0.461	0.467	0.522
SEE	Mean	0.079	0.077	0.079	0.079	0.078	0.078
	Median	0.078	0.077	0.079	0.079	0.078	0.078
Bias	Mean	-0.001	-0.002	-0.004	-0.004	-0.003	-0.003
	Median	-0.001	-0.002	-0.004	-0.003	-0.003	-0.002

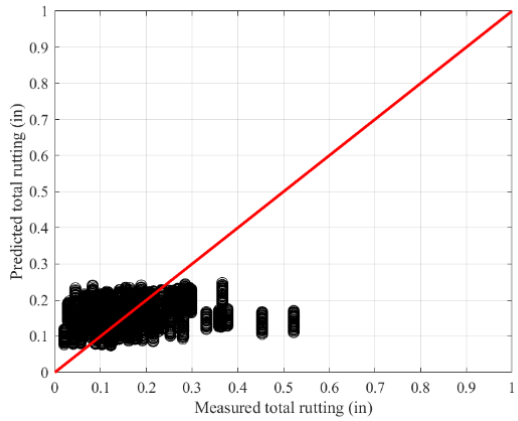

(a) Level 1 – local model (new design)

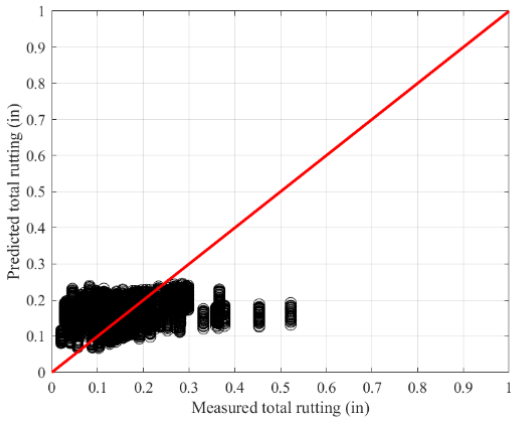

(b) Level 1 – local model (overlay design)

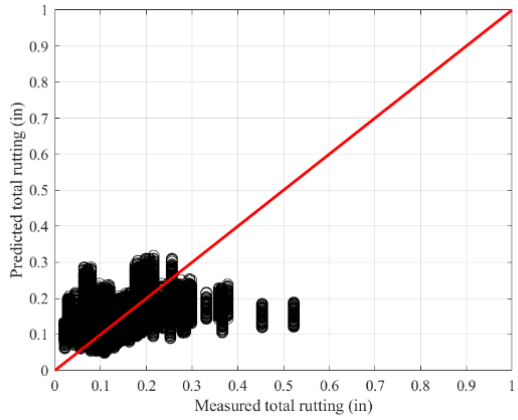

(c) Level 2 – local model (new design)

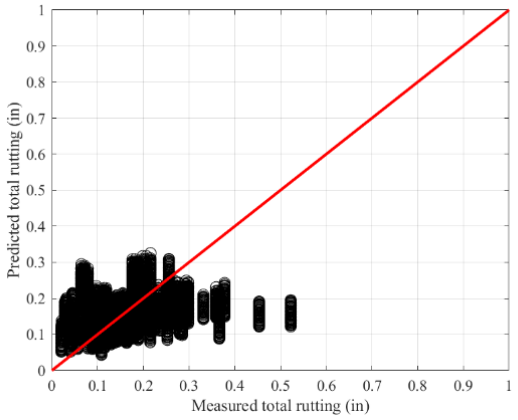

(d) Level 2 – local model (overlay design)

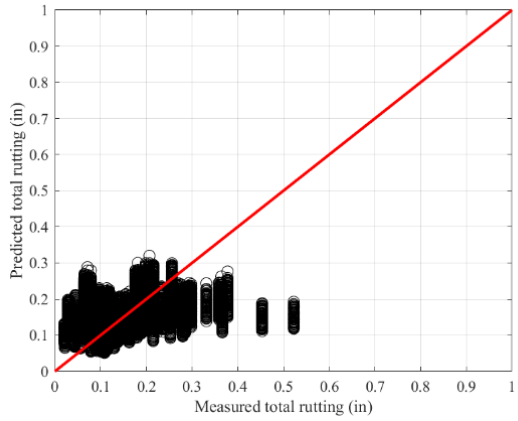

(e) Level 3 – local model (new design)

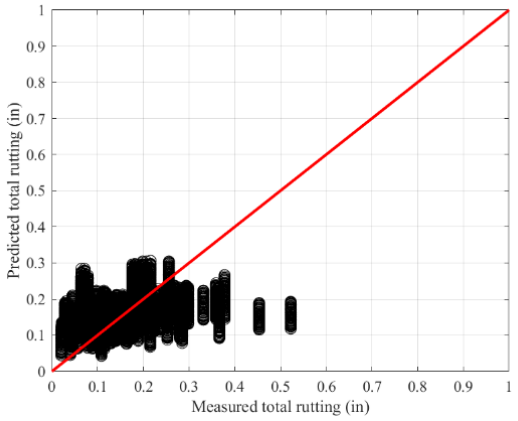

(f) Level 3 – local model (overlay design)

Figure A- 8: Measured vs. predicted for local model (bootstrapping)

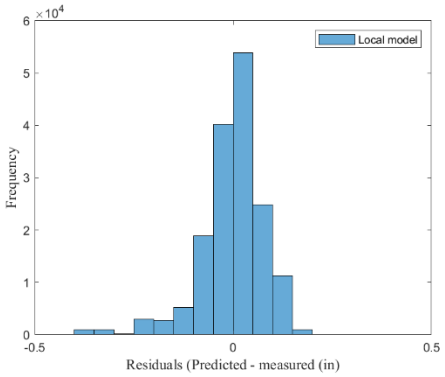

(a) Level 1 – local model (new design)

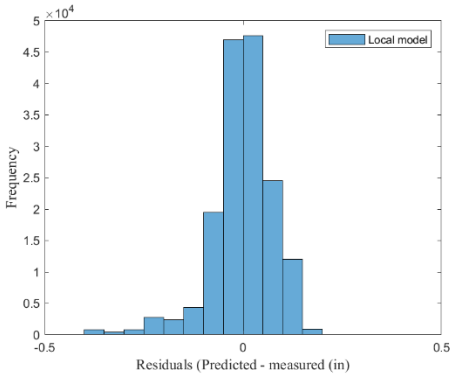

(b) Level 1 – local model (overlay design)

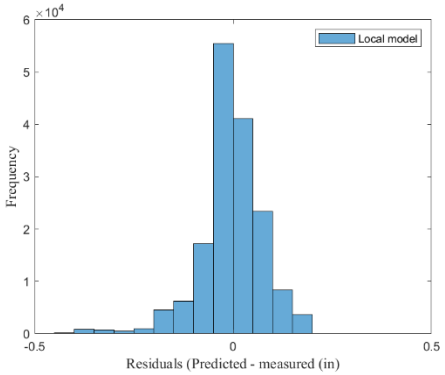

(c) Level 2 – local model (new design)

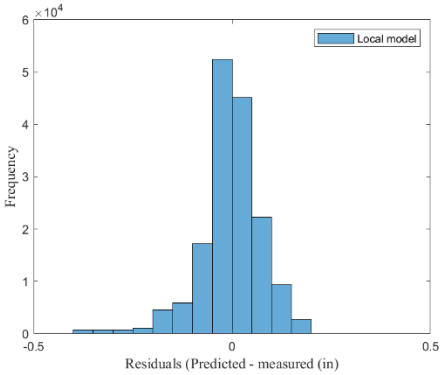

(d) Level 2 – local model (overlay design)

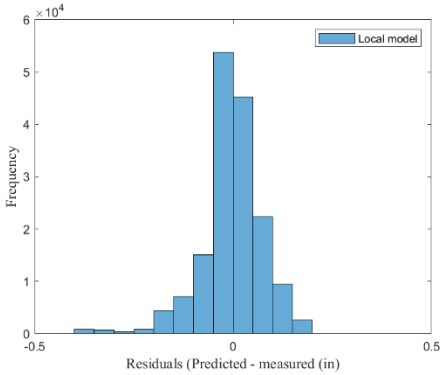

(e) Level 3 – local model (new design)

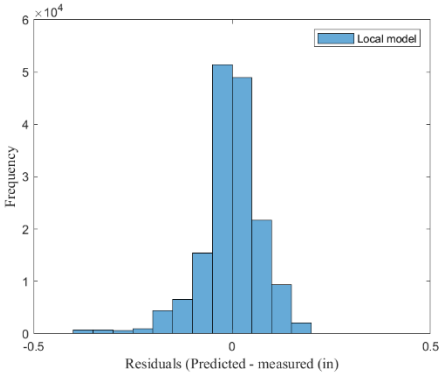

(f) Level 3 – local model (overlay design)

Figure A- 9: Residual distribution (bootstrapping)

A.2.4 Maximum Likelihood Estimation (MLE)

The exponential distribution significantly improved the bias; however, a negligible difference in SEE is noted for least square and MLE. Tables A-6 and A-7 show exponential distribution calibration summary results. Figures A-10 and A-11 present the measured vs. predicted and residual distribution, respectively. Table A-8 compares statistical parameters between least squares and MLE.

Table A- 6: Global model summary - bootstrapping using MLE (exponential distribution)

Parameters	Levels	1		2		3	
	Design	New	Overlay	New	Overlay	New	Overlay
Br1	Mean	0.40					
	Median						
Bs1	Mean	1.00					
	Median						
Bsg1	Mean	1.00					
	Median						
SEE	Mean	0.099	0.088	0.122	0.104	0.111	0.096
	Median	0.099	0.088	0.122	0.104	0.111	0.096
Bias	Mean	0.057	0.038	0.088	0.065	0.076	0.055
	Median	0.057	0.038	0.088	0.065	0.077	0.055

Table A- 7: Local model summary - bootstrapping using MLE (exponential distribution)

Parameters	Levels	1		2		3	
	Design	New	Overlay	New	Overlay	New	Overlay
Br1	Mean	0.576	0.359	0.313	0.322	0.779	0.816
	Median	0.573	0.36	0.31	0.319	0.779	0.813
Bs1	Mean	0.569	0.542	0.54	0.546	0.519	0.258
	Median	0.574	0.524	0.532	0.548	0.52	0.257
Bsg1	Mean	0.66	0.552	0.617	0.704	0.391	0.52
	Median	0.665	0.551	0.622	0.705	0.392	0.527
SEE	Mean	0.079	0.078	0.078	0.077	0.077	0.076
	Median	0.079	0.078	0.077	0.077	0.077	0.076
Bias	Mean	0	0	0	0	0	0
	Median	0	0	0	0	0	0

Table A- 8: Local model statistics

Levels	Design	Parameters					
		MLE			Least square		
		NLL	AIC	BIC	NLL	AIC	BIC
1	New	383.29	768.59	771.68	928.96	1861.93	1868.11
	Overlay	383.12	768.25	771.34	4540.59	9085.17	9091.36
2	New	382.93	767.87	770.96	952.45	1908.90	1915.09
	Overlay	383.04	768.09	771.18	1005.40	2014.80	2020.99
3	New	383.12	768.24	771.33	958.98	1921.95	1928.14
	Overlay	383.09	768.18	771.27	1014.25	2032.51	2038.70

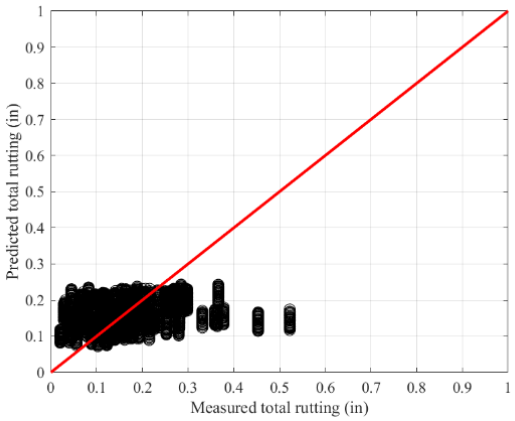

(a) Level 1 – local model (new design)

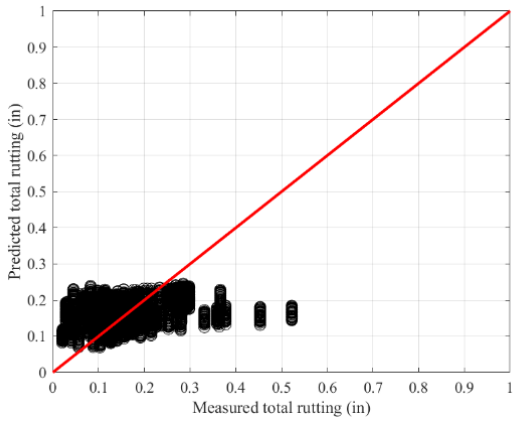

(b) Level 1 – local model (overlay design)

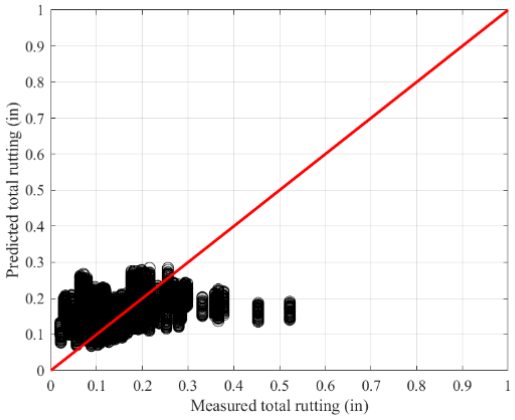

(c) Level 2 – local model (new design)

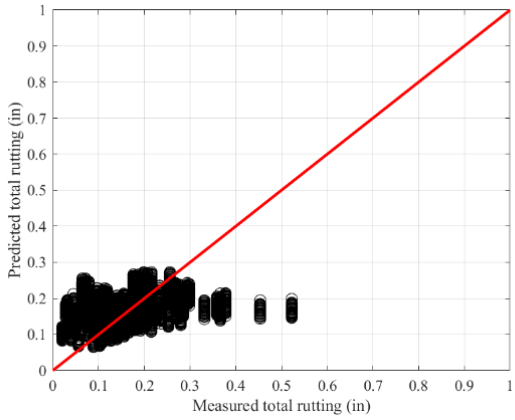

(d) Level 2 – local model (overlay design)

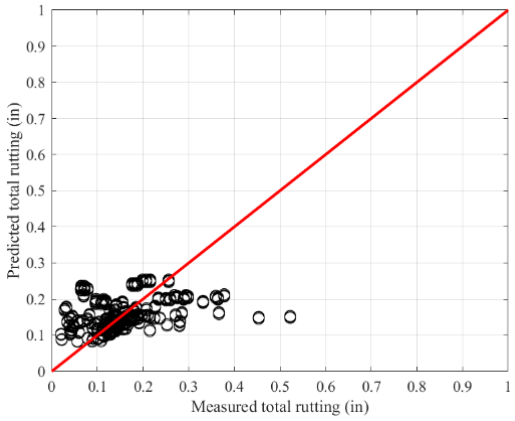

(e) Level 3 – local model (new design)

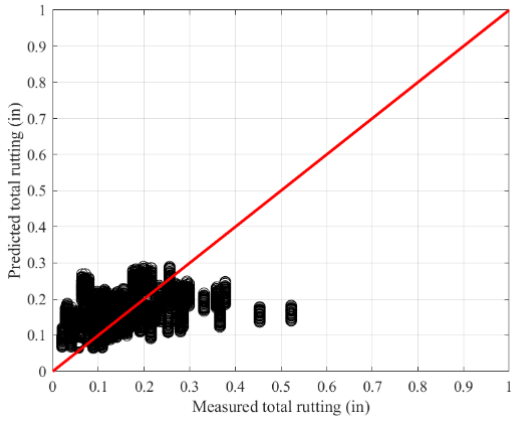

(f) Level 3 – local model (overlay design)

Figure A- 10: Local models' measured vs. predicted using MLE (exponential distribution)

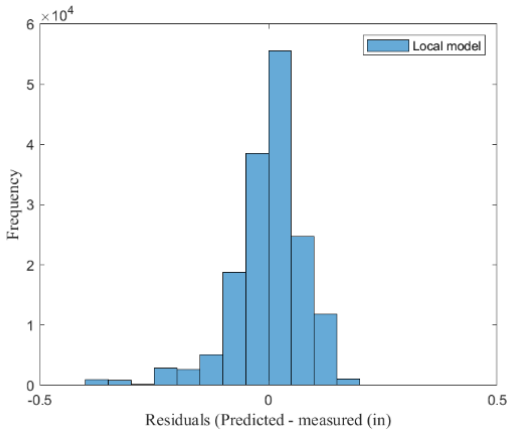

(a) Level 1 – local model (new design)

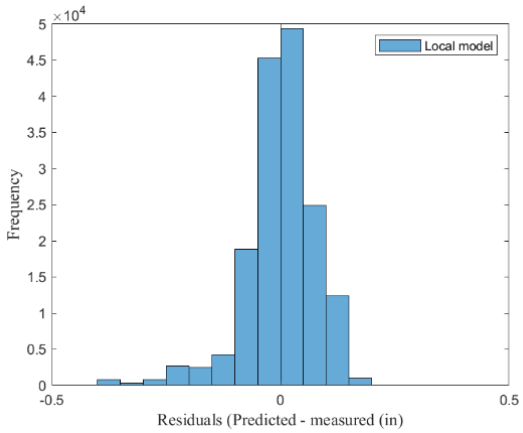

(b) Level 1 – local model (overlay design)

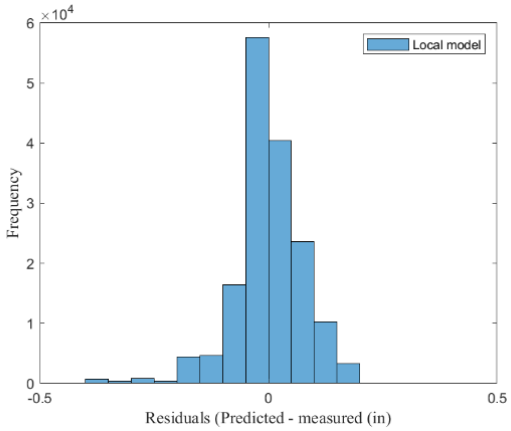

(c) Level 2 – local model (new design)

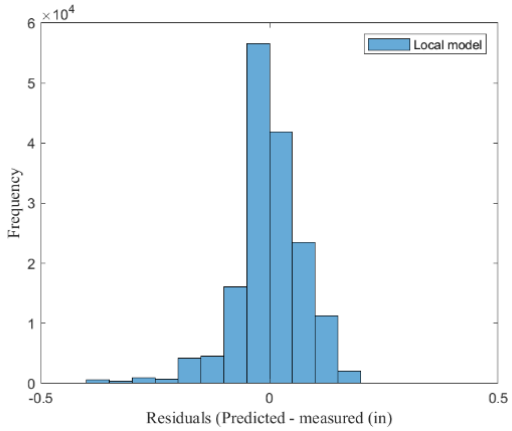

(d) Level 2 – local model (overlay design)

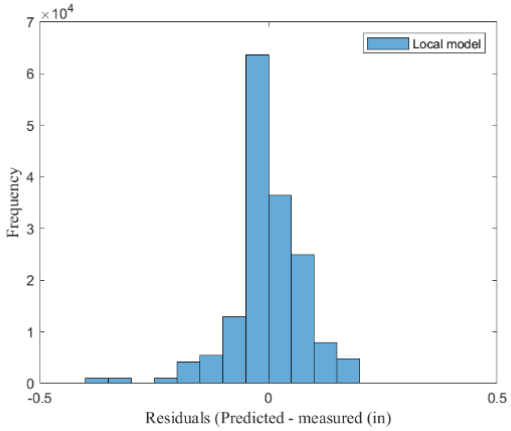

(e) Level 3 – local model (new design)

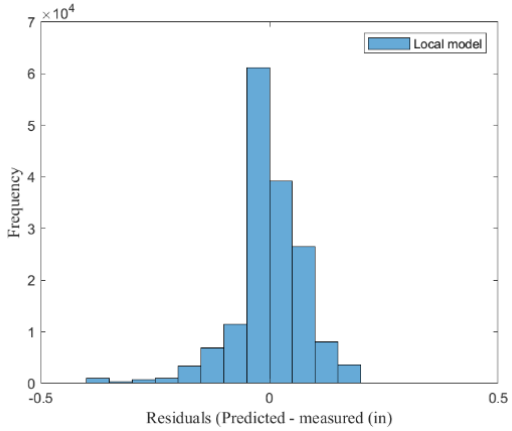

(f) Level 3 – local model (overlay design)

Figure A- 11: Residual distribution using MLE (exponential distribution)

A.3 Transverse Thermal Cracking

A.3.1 No Sampling

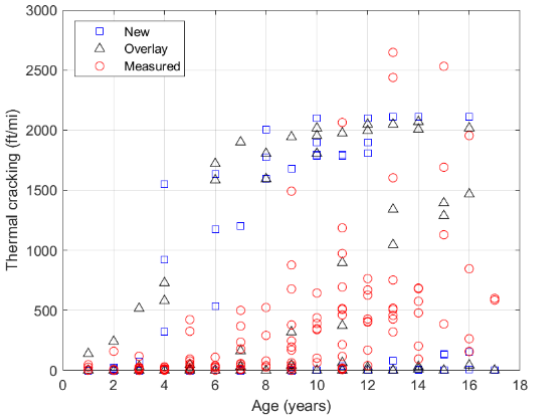

(a) New vs. overlay - level 1

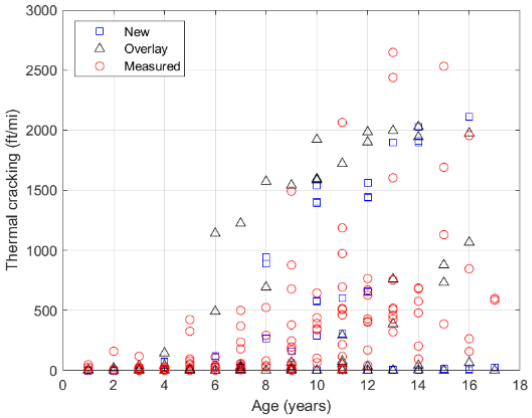

(b) New vs. overlay - level 2

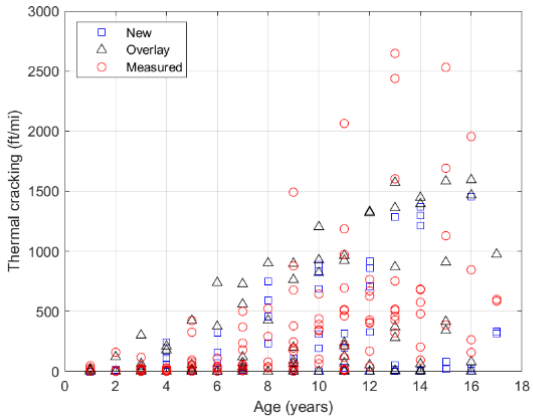

(c) New vs. overlay - level 3

Figure A- 12: Measured vs. predicted thermal cracking with time

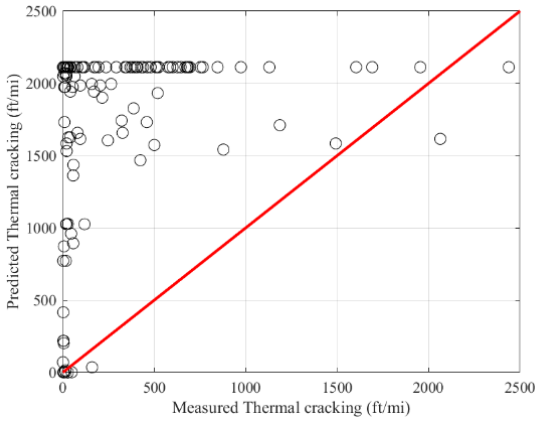

(a) Global model (level 1)

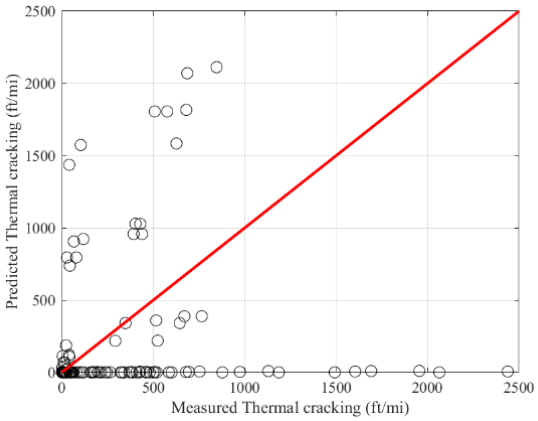

(b) Local model – K = 0.65 (level 1)

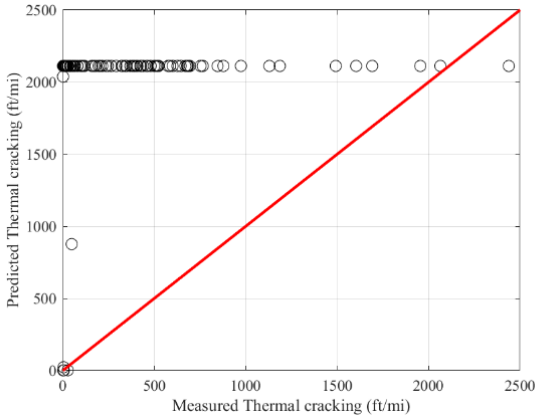

(c) Global model (level 2)

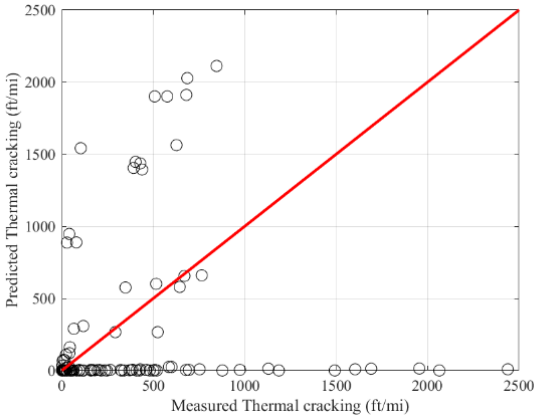

(d) Local model – K = 0.55 (level 2)

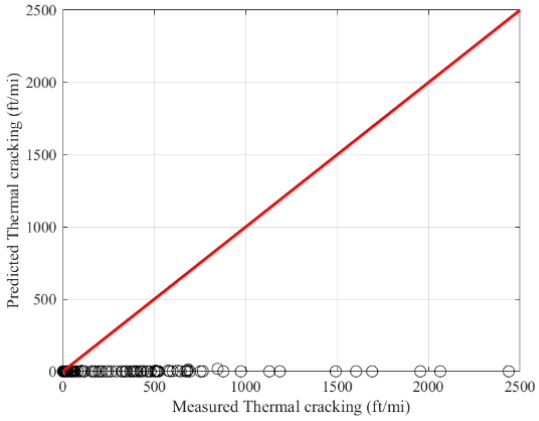

(e) Global model (level 3)

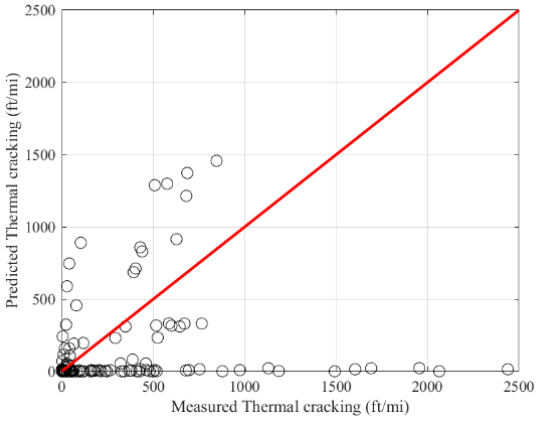

(f) Local model – K = 2.0 (level 3)

Figure A- 13: Predicted vs measured thermal cracking (No sampling) – New design

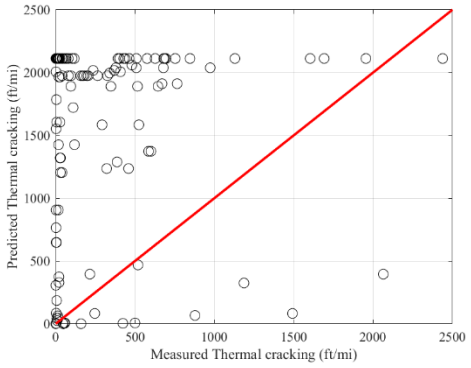

(a) Global model (level 1)

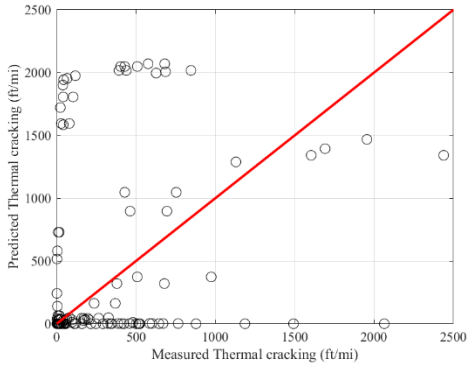

(b) Local model – K = 0.85 (level 1)

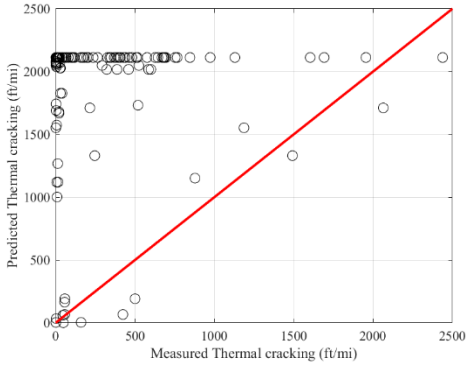

(c) Global model (level 2)

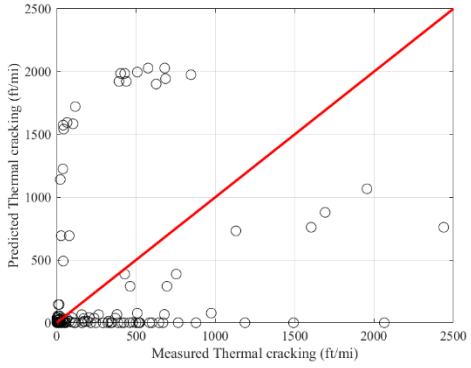

(d) Local model – K = 0.65 (level 2)

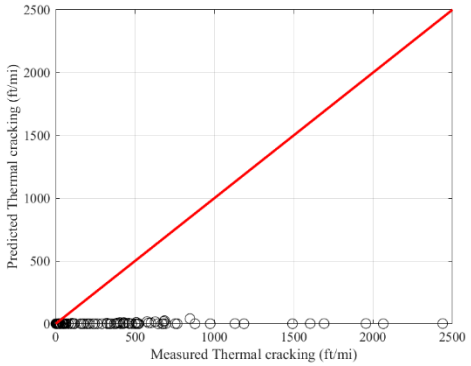

(e) Global model (level 3)

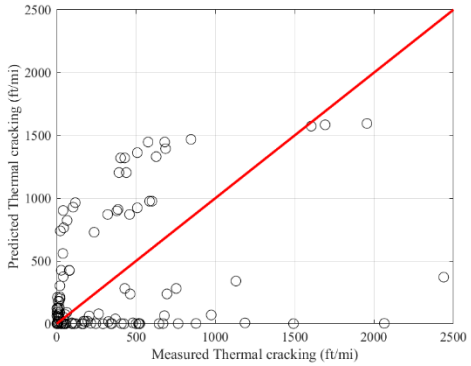

(f) Local model – K = 2.2 (level 3)

Figure A- 14: Predicted vs measured thermal cracking (No sampling) – Overlay design

A.4 IRI Model

A.4.1 No Sampling

This method used the entire dataset to calibrate the predicted IRI against the total measured performance. Figures A-15 and A-16 show the predicted vs. measured IRI for the global and local models for new and an overlay design, respectively. Table A-9 shows the summary of

model parameters using no sampling technique. SEE and bias are significantly enhanced from local calibration. Figure A-17 shows the measured and predicted IRI with time.

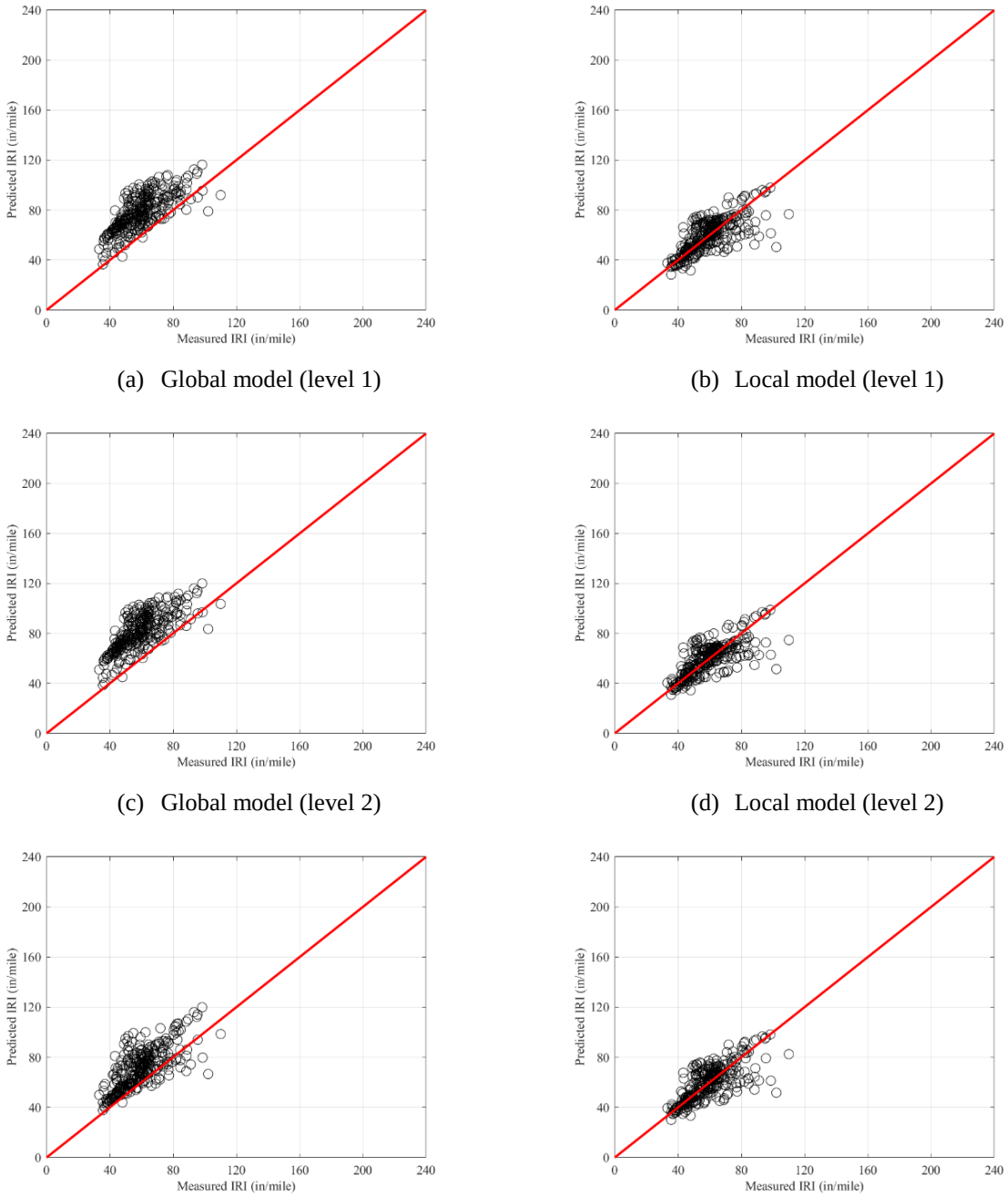

(a) Global model (level 1)

(b) Local model (level 1)

(c) Global model (level 2)

(d) Local model (level 2)

(e) Global model (level 3)

(f) Local model (level 3)

Figure A- 15: Predicted vs. measured IRI (No sampling) – New design

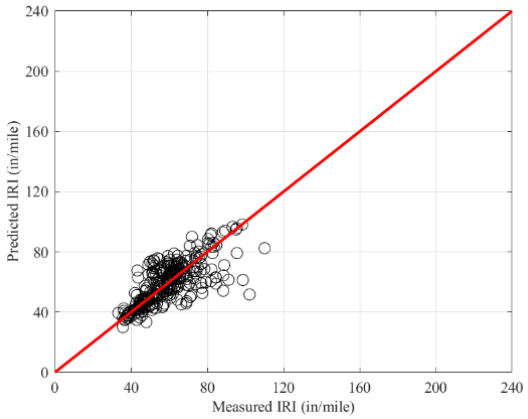

(a) Global model (level 1)

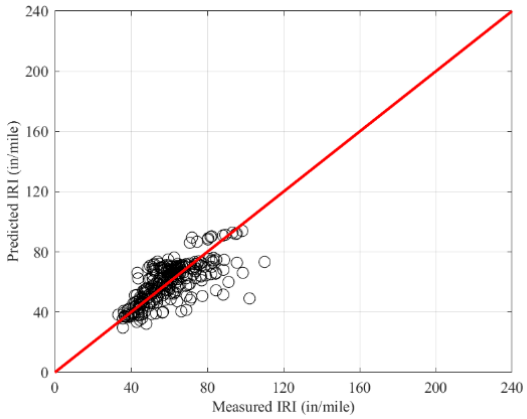

(b) Local model (level 1)

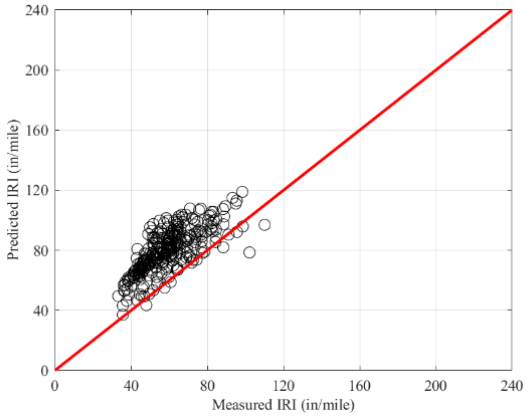

(c) Global model (level 2)

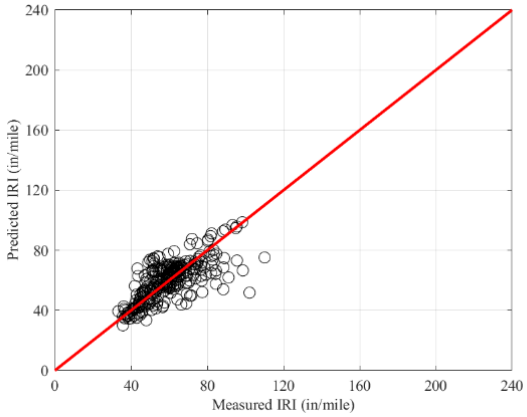

(d) Local model (level 2)

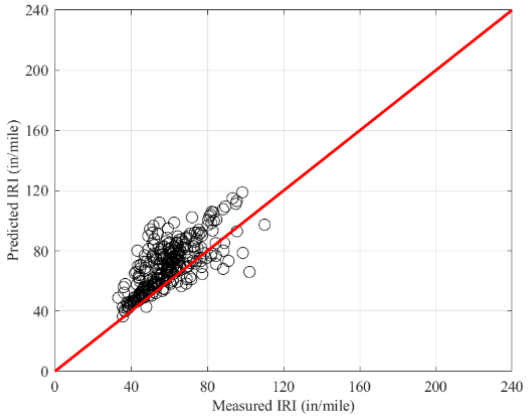

(e) Global model (level 3)

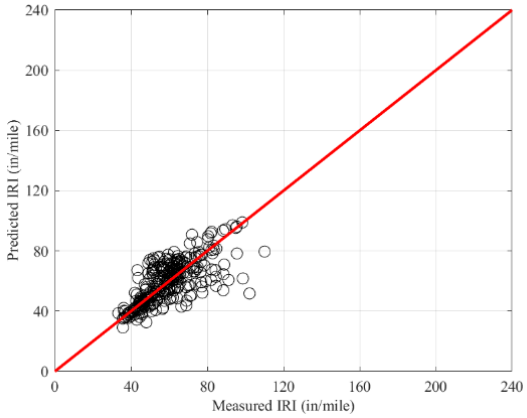

(f) Local model (level 3)

Figure A- 16: Predicted vs. measured IRI (No sampling) – Overlay design

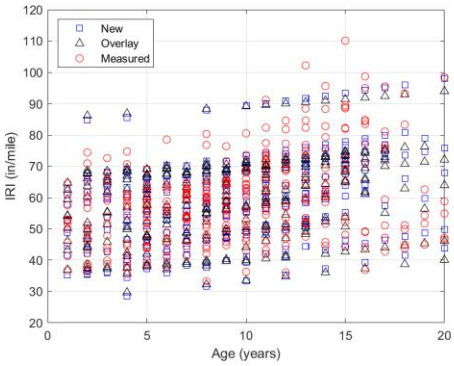

(a) New vs. overlay - level 1

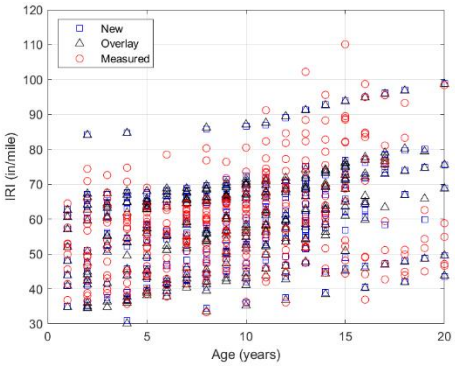

(b) New vs. overlay - level 2

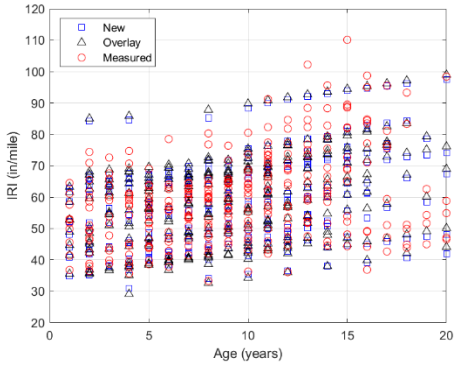

(c) New vs. overlay - level 3

Figure A- 17: Measured vs. predicted IRI with time

Table A- 9: Local calibration summary for IRI (No sampling)

Parameter	Level 1				Level 2				Level 3			
	New		Overlay		New		Overlay		New		Overlay	
	Global	Local	Global	Local	Global	Local	Global	Local	Global	Local	Global	Local
C1	40.00	14.05	40.00	28.19	40.00	9.86	40.00	10.40	40.00	7.30	40.00	10.62
C2	0.40	0.36	0.40	0.61	0.40	1.93	0.40	1.25	0.40	1.30	0.40	0.52
C3	0.01	0.00	0.01	0.00	0.01	0.00	0.01	0.00	0.01	0.00	0.01	0.00
C4	0.02	0.01	0.02	0.00	0.02	0.00	0.02	0.01	0.02	0.00	0.02	0.01
SEE	21.27	10.31	20.54	10.29	24.41	10.02	23.05	10.09	16.33	10.21	15.76	10.58
Bias	18.45	0.00	17.38	0.00	21.99	0.00	20.45	0.00	11.67	0.00	10.87	0.00

A.4.2 Split Sampling

The entire dataset was split into two parts, with 70% of the sections used for calibration and 30% for validation using a split sampling approach. Figures A-18 and A-19 show the predicted vs. measured IRI for calibration and validation. Tables A-10 and A-11 summarize the model parameters for the calibration and validation set.

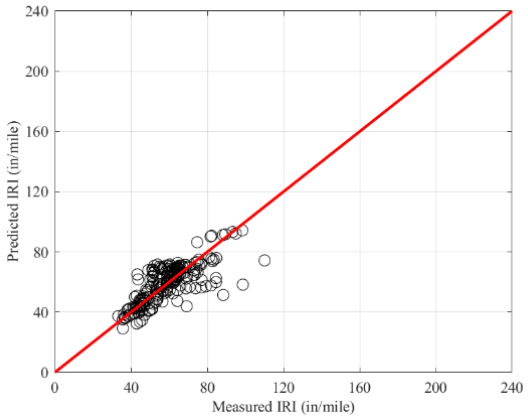

(a) Level 1 – local model (new design)

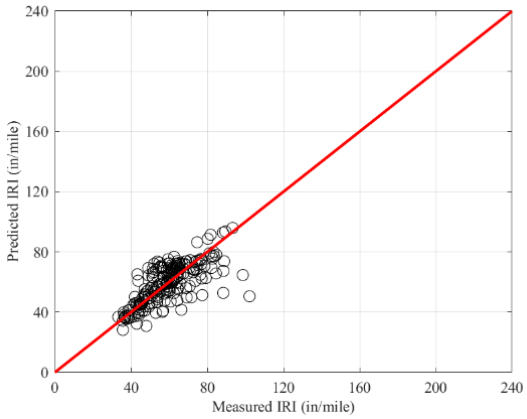

(b) Level 1 – local model (overlay design)

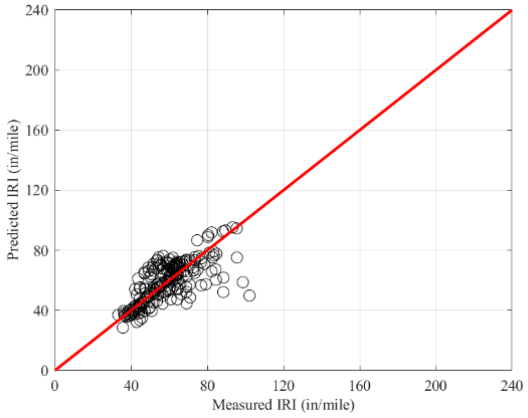

(c) Level 2 – local model (new design)

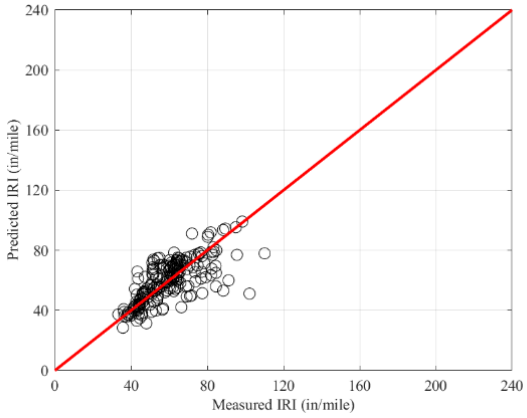

(d) Level 2 – local model (overlay design)

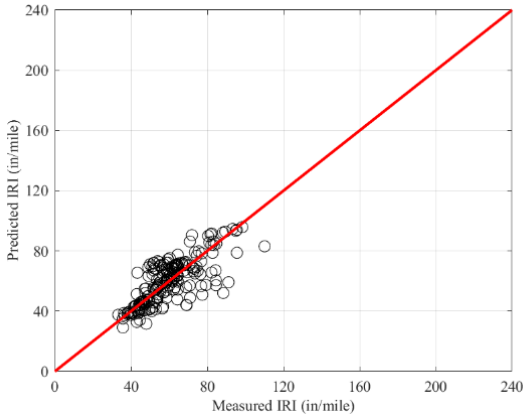

(e) Level 3 – local model (new design)

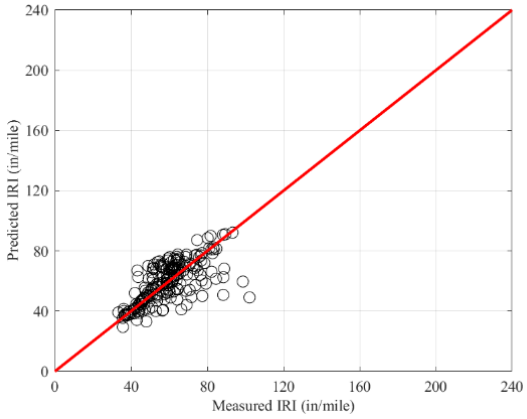

(f) Level 3 – local model (overlay design)

Figure A- 18: Predicted vs. measured IRI (split sampling) – calibration set

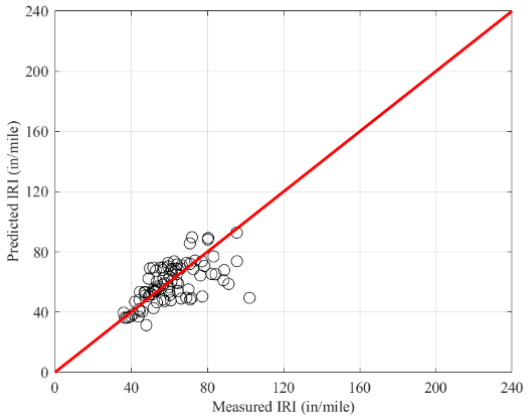

(a) Level 1 – local model (new design)

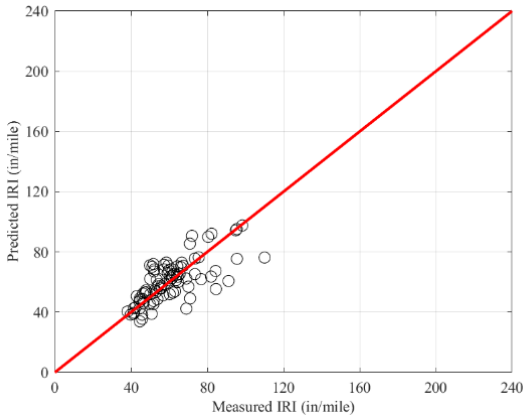

(b) Level 1 – local model (overlay design)

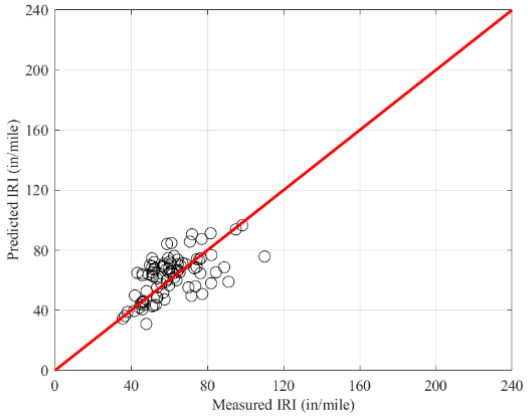

(c) Level 2 – local model (new design)

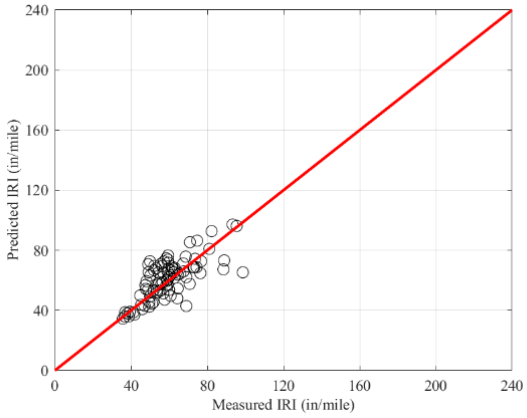

(d) Level 2 – local model (overlay design)

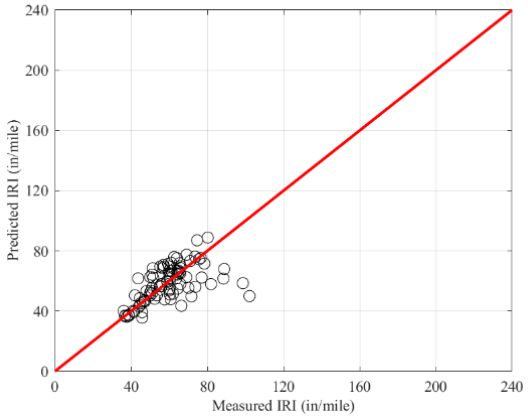

(e) Level 3 – local model (new design)

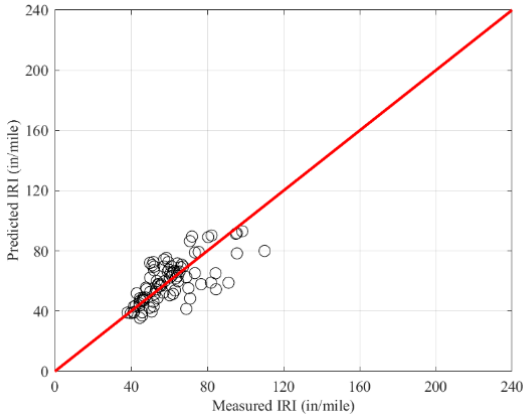

(f) Level 3 – local model (overlay design)

Figure A- 19: Predicted vs measured IRI (split sampling) – validation set

Table A- 10: Local calibration summary for IRI (calibration set)

Parameter	Level 1				Level 2				Level 3			
	New		Overlay		New		Overlay		New		Overlay	
	Global	Local	Global	Local	Global	Local	Global	Local	Global	Local	Global	Local
C1	40.00	10.22	40.00	12.59	40.00	10.01	40.00	10.64	40.00	19.39	40.00	17.76
C2	0.40	0.42	0.40	0.20	0.40	0.45	0.40	0.13	0.40	0.32	0.40	0.15
C3	0.01	0.00	0.01	0.00	0.01	0.02	0.01	0.00	0.01	0.01	0.01	0.01
C4	0.02	0.00	0.02	0.01	0.02	0.00	0.02	0.01	0.02	0.00	0.02	0.00
SEE	21.48	9.34	20.21	9.99	24.07	10.43	22.54	10.69	16.80	10.03	15.80	10.60
Bias	19.02	0.05	16.99	0.13	21.74	0.27	19.92	0.22	12.26	0.43	10.93	0.33

Table A- 11: Local calibration summary for IRI (validation set)

Parameter	Level 1				Level 2				Level 3			
	New		Overlay		New		Overlay		New		Overlay	
	Global	Local	Global	Local	Global	Local	Global	Local	Global	Local	Global	Local
C1	40.00	10.22	40.00	12.59	40.00	10.01	40.00	10.64	40.00	19.39	40.00	17.76
C2	0.40	0.42	0.40	0.20	0.40	0.45	0.40	0.13	0.40	0.32	0.40	0.15
C3	0.01	0.00	0.01	0.00	0.01	0.02	0.01	0.00	0.01	0.01	0.01	0.01
C4	0.02	0.00	0.02	0.01	0.02	0.00	0.02	0.01	0.02	0.00	0.02	0.00
SEE	21.01	12.51	21.51	11.01	25.46	12.80	24.48	10.17	15.34	11.76	15.87	11.41

A.4.3 Bootstrapping

Tables A-12 and A-13 summarize the calibration results for the global and local models. Figures A-20 and A-21 show the local model's measured versus predicted and residual distribution plots for the 1000 bootstrap samples, respectively. The SEE and bias improved in after local calibration.

Table A- 12: Bootstrapping global model summary

Parameters	Levels	1		2		3	
	Design	New	Overlay	New	Overlay	New	Overlay
C1	Mean	40.00					
	Median						
C2	Mean	0.40					
	Median						
C3	Mean	0.01					
	Median						
C4	Mean	0.02					
	Median						
SEE	Mean	21.28	20.5	24.37	23.03	16.34	15.79
	Median	21.26	20.48	24.37	23.03	16.35	15.81
Bias	Mean	18.47	17.34	21.95	20.44	11.71	10.92
	Median	18.48	17.34	21.96	20.46	11.7	10.94

Table A- 13: Bootstrapping local calibration results summary

Parameters	Levels	1		2		3	
	Design	New	Overlay	New	Overlay	New	Overlay
C1	Mean	13.98	13.43	12.68	12.69	13.15	13.63
	Median	11.08	11.14	11.07	11.03	11.1	11.07
C2	Mean	0.25	0.24	0.33	0.15	0.32	0.13
	Median	0.18	0.1	0.14	0.08	0.13	0.06
C3	Mean	0.01	0.01	0.02	0.01	0.01	0.01
	Median	0.01	0.01	0.01	0.01	0.01	0.01
C4	Mean	0.003	0.004	0.004	0.004	0.003	0.003
	Median	0.003	0.003	0.002	0.003	0.002	0.002
SEE	Mean	10.93	11.22	12.99	11.59	11.25	11.16
	Median	10.59	10.84	11.37	11.03	10.95	10.99
Bias	Mean	0.34	0.12	0.02	-0.06	-0.08	0.12
	Median	0.24	0.05	-0.03	-0.16	-0.24	-0.13

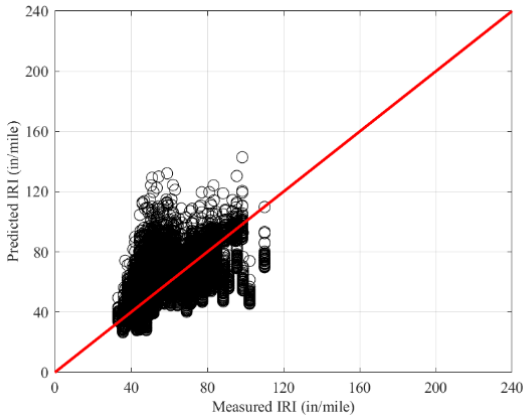

(a) Level 1 – local model (new design)

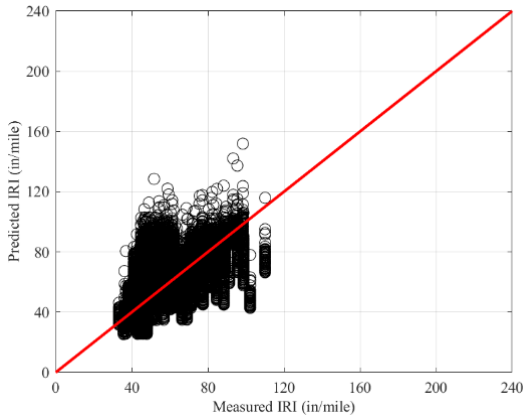

(b) Level 1 – local model (overlay design)

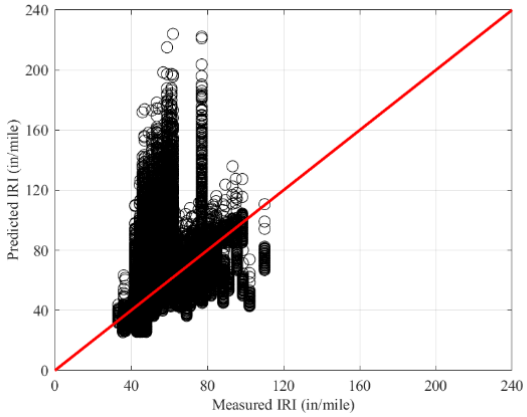

(c) Level 2 – local model (new design)

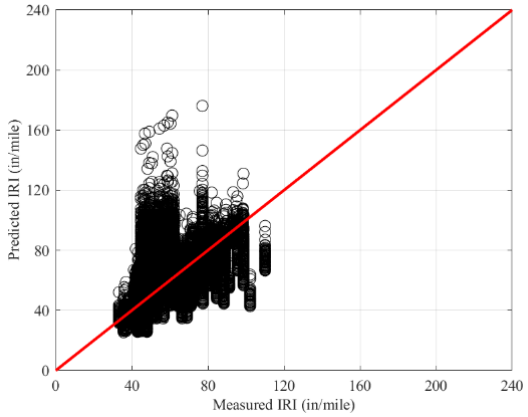

(d) Level 2 – local model (overlay design)

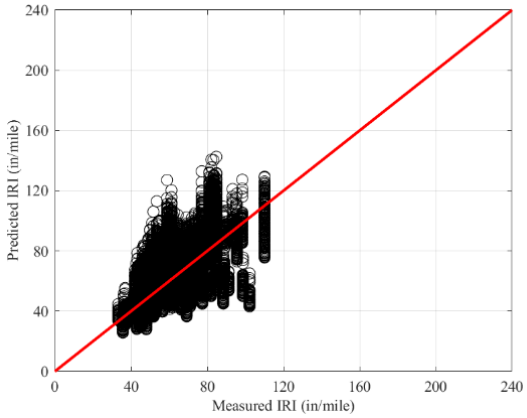

(e) Level 3 – local model (new design)

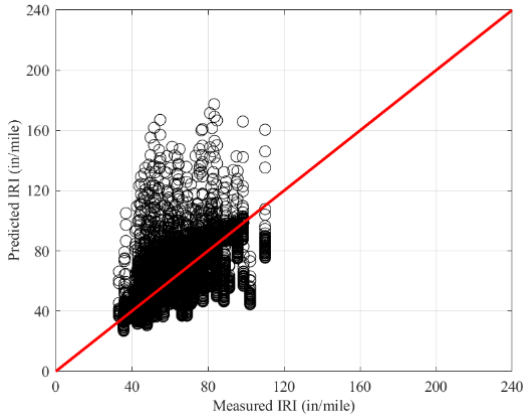

(f) Level 3 – local model (overlay design)

Figure A- 20: Measured vs. predicted for local model (bootstrapping)

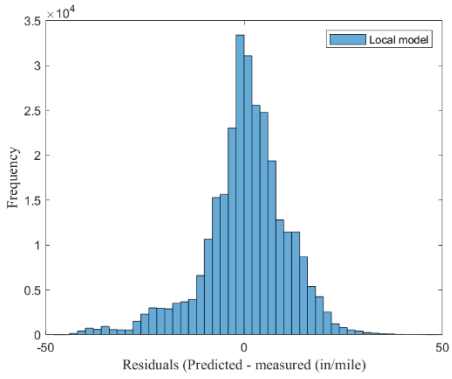

(a) Level 1 – local model (new design)

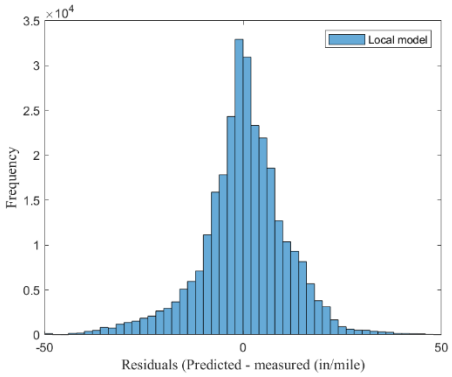

(b) Level 1 – local model (overlay design)

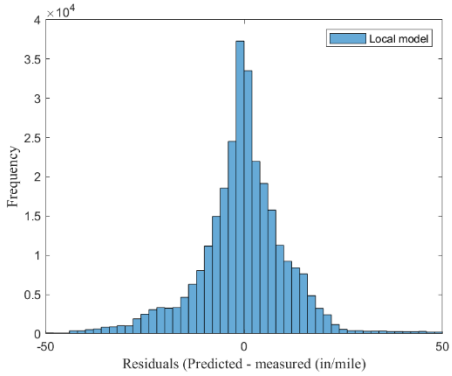

(c) Level 2 – local model (new design)

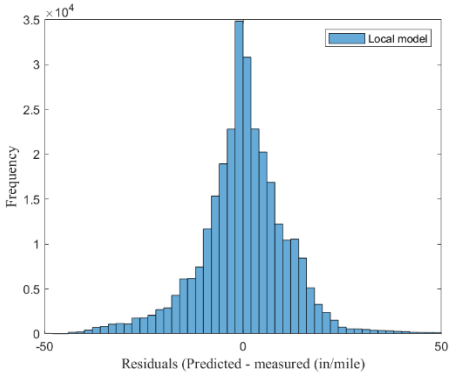

(d) Level 2 – local model (overlay design)

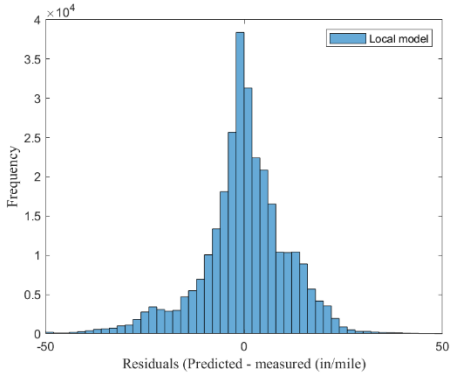

(e) Level 3 – local model (new design)

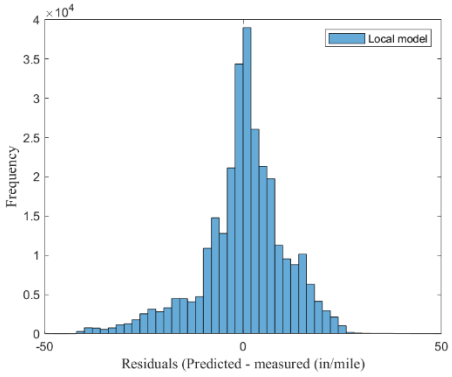

(f) Level 3 – local model (overlay design)

Figure A- 21: Residual distribution (bootstrapping)

A.4.4 Maximum Likelihood Estimation (MLE)

Tables A-14 and A-15 show the global and local calibration results using exponential distribution. Figures A-22 and A-23 present the measured vs. predicted and residual distribution, respectively. Table A-16 compares statistical parameters between least squares and MLE.

Table A- 14: Global model summary (bootstrapping using MLE)

Parameters	Levels	1		2		3	
	Design	New	Overlay	New	Overlay	New	Overlay
C1	Mean	40.00					
	Median						
C2	Mean	0.40					
	Median						
C3	Mean	0.01					
	Median						
C4	Mean	0.02					
	Median						
SEE	Mean	21.28	20.5	24.37	23.03	16.34	15.79
	Median	21.26	20.48	24.37	23.03	16.35	15.81
Bias	Mean	18.47	17.34	21.95	20.44	11.71	10.92
	Median	18.48	17.34	21.96	20.46	11.7	10.94

Table A- 15: Local model summary (bootstrapping using MLE)

Parameters	Levels	1		2		3	
	Design	New	Overlay	New	Overlay	New	Overlay
C1	Mean	13.51	13.24	14.33	16.78	19.56	14.97
	Median	11.38	11.07	12.52	14.14	18.28	12.81
C2	Mean	0.28	0.34	0.51	0.22	0.44	0.24
	Median	0.25	0.34	0.56	0.22	0.43	0.21
C3	Mean	0.01	0.01	0.01	0.01	0.01	0.01
	Median	0.01	0.01	0.01	0.01	0.01	0.01
C4	Mean	0.003	0.003	0.003	0.003	0.003	0.002
	Median	0.003	0.003	0.002	0.002	0.003	0.001
SEE	Mean	10.59	10.38	10.61	10.55	10.52	10.82
	Median	10.46	10.32	10.55	10.51	10.49	10.83
Bias	Mean	0	0	0	0	0	0
	Median	-0.03	-0.05	-0.03	-0.02	0	0

Table A- 16: Local model statistics

Levels	Design	Parameters					
		MLE			Least square		
		NLL	AIC	BIC	NLL	AIC	BIC
1	New	1180.54	2365.08	2372.46	2945.26	5894.53	5901.90
	Overlay	1182.19	2368.38	2375.75	2939.89	5883.79	5891.16
2	New	1182.20	2368.40	2375.77	2775.31	5554.62	5562.00
	Overlay	1181.86	2367.72	2375.10	2857.42	5718.85	5726.22
3	New	1182.07	2368.13	2375.51	2745.05	5494.10	5501.48
	Overlay	1181.90	2367.79	2375.17	2862.76	5729.53	5736.90

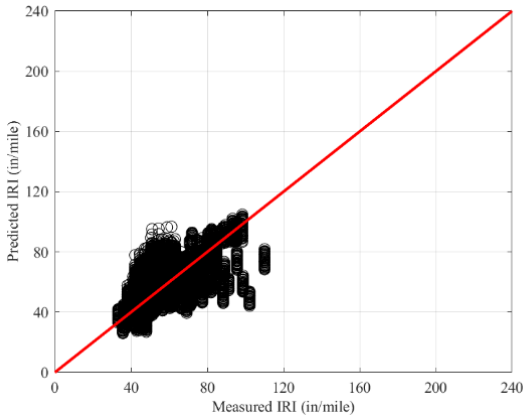

(a) Level 1 – local model (new design)

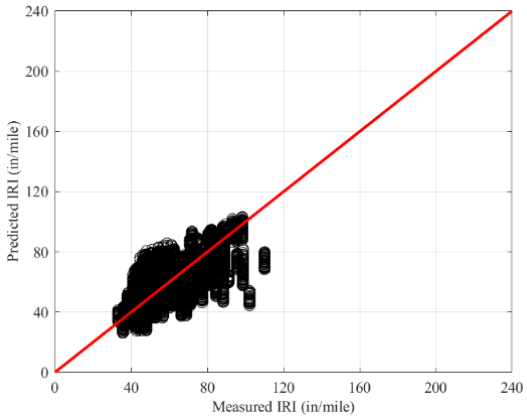

(b) Level 1 – local model (overlay design)

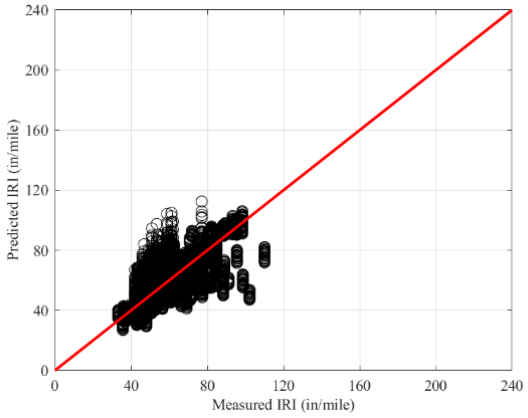

(c) Level 2 – local model (new design)

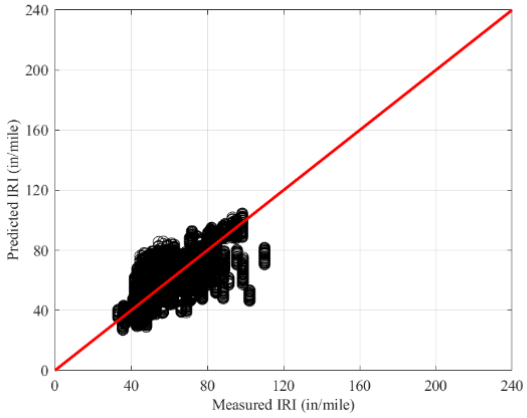

(d) Level 2 – local model (overlay design)

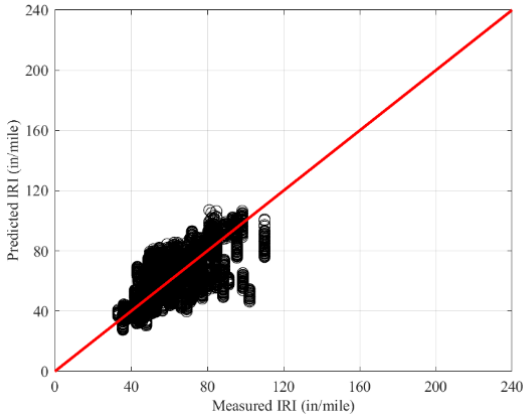

(e) Level 3 – local model (new design)

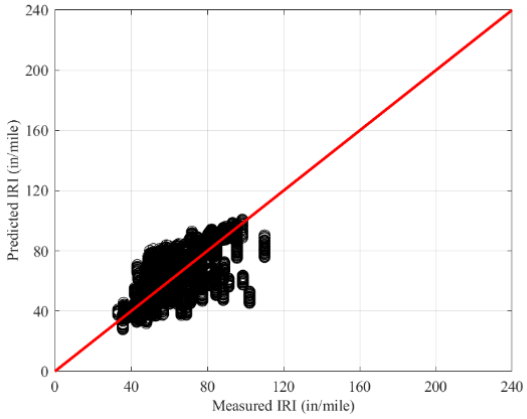

(f) Level 3 – local model (overlay design)

Figure A- 22: Local models' measured vs. predicted using MLE (log-normal distribution)

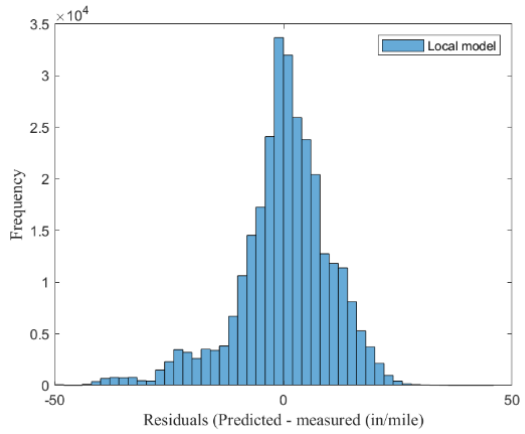

(a) Level 1 – local model (new design)

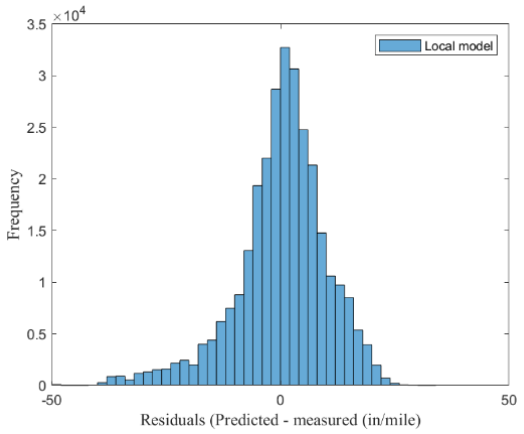

(b) Level 1 – local model (overlay design)

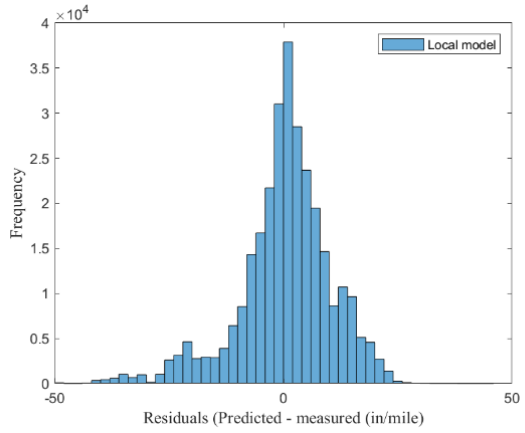

(c) Level 2 – local model (new design)

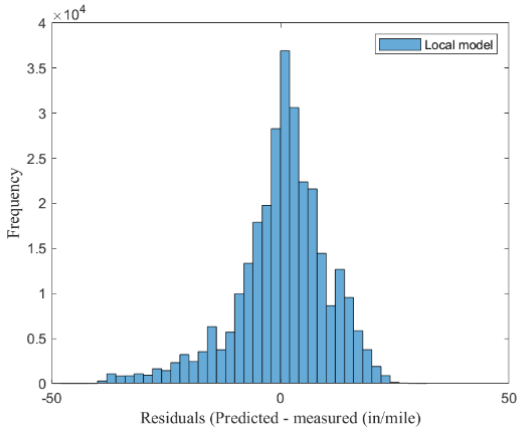

(d) Level 2 – local model (overlay design)

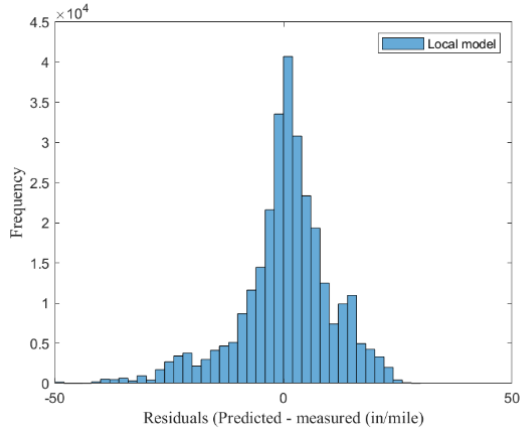

(e) Level 3 – local model (new design)

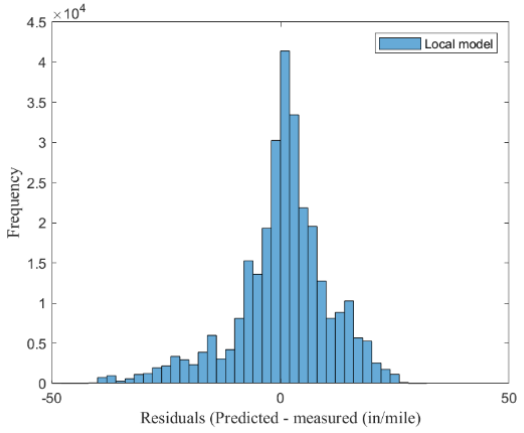

(f) Level 3 – local model (overlay design)

Figure A- 23: Residual distribution using MLE (log-normal distribution)